VOL. 16 NO. 2 FEBRUARY 1968
PUBLISHED MONTHLY

JOURNAL OF

ELECTROANALYTICAL CHEMISTRY

AND INTERFACIAL ELECTROCHEMISTRY

International Journal devoted to all Aspects of Electroanalytical Chemistry, Double Layer Studies, Electrokinetics, Colloid Stability, and Electrode Kinetics.

ELSEVIER

GENERAL INFORMATION

See also Suggestions and Instructions to Authors which will be sent free, on request to the Publishers.

Types of contributions

(a) Original research work not previously published in other periodicals.
(b) Reviews on recent developments in various fields.
(c) Short communications.
(d) Bibliographical notes and book reviews.

Languages

Papers will be published in English, French or German.

Submission of papers

Papers should be sent to one of the following Editors:
Professor J. O'M. Bockris, John Harrison Laboratory of Chemistry, University of Pennsylvania, Philadelphia 4, Pa. 19104, U.S.A.
Dr. R. H. Ottewill, Department of Chemistry, The University, Bristol 8, England.
Dr. R. Parsons, Department of Chemistry, The University, Bristol 8, England.
Professor C. N. Reilley, Department of Chemistry, University of North Carolina, Chapel Hill, N.C. 27515, U.S.A.

Authors should preferably submit two copies in double-spaced typing on pages of uniform size. Legends for figures should be typed on a separate page. The figures should be in a form suitable for reproduction, drawn in Indian ink on drawing paper or tracing paper, with lettering etc. in thin pencil. The sheets of drawing or tracing paper should preferably be of the same dimensions as those on which the article is typed. Photographs should be submitted as clear black and white prints on glossy paper. Standard symbols should be used in line drawings, the following are available to the printers:

All references should be given at the end of the paper. They should be numbered and the numbers should appear in the text at the appropriate places.
A summary of 50 to 200 words should be included.

Reprints

Fifty reprints will be supplied free of charge. Additional reprints (minimum 100) can be ordered at quoted prices. They must be ordered on order forms which are sent together with the proofs.

Publication

The *Journal of Electroanalytical Chemistry and Interfacial Electrochemistry* appears monthly and has four issues per volume and three volumes per year.
Subscription price: $ 52.50 or Sfr. 228.00 per year; $ 17.50 or Sfr. 76.00 per volume; plus postage. Additional cost for copies by air mail available on request. For advertising rates apply to the publishers.

Subscriptions

Subscriptions should be sent to:

ELSEVIER SEQUOIA S.A., P.O. Box 851, 1001 Lausanne 1, Switzerland

ELECTROANALYTICAL CHEMISTRY AND INTERFACIAL ELECTROCHEMISTRY
Elsevier Sequoia S.A., Lausanne – Printed in The Netherlands

THE POTENTIAL-DEPENDENCE OF ELECTROCHEMICAL RATE CONSTANTS

KEITH B. OLDHAM
North American Aviation Science Center, Thousand Oaks, Calif. 91360 (U.S.A.)
(Received April 28th, 1967)

If the electrode reaction

$$\mathrm{Ox(soln.)} + ne^- \rightleftarrows \mathrm{Rd(soln.)} \tag{1}$$

proceeds by a simple unimolecular mechanism, the rate constants for the forward and reverse processes depend on the electrode potential, E, and may be defined by

$$\vec{k}(E) = \frac{\overrightarrow{\text{rate}}}{[\mathrm{Ox}]} \tag{2}$$

and

$$\overleftarrow{k}(E) = \frac{\overleftarrow{\text{rate}}}{[\mathrm{Rd}]} \tag{3}$$

Here $\overrightarrow{\text{rate}}$ and $\overleftarrow{\text{rate}}$ denote the number of Rd moles formed from Ox, and *vice versa*, unit electrode area/unit time. The concentrations, [Ox] and [Rd], and the potential, E, are particularly well-defined terms when the electrode is at equilibrium, being then the concentrations at the reaction site and the potential between the electrode metal and the reaction site, measured with respect to any chosen reference. In practice, the bulk concentrations and the measured cell potential (less "iR drop" when this is a significant correction) are often close-enough approximations to [Ox], [Rd], and E. Otherwise, the procedures devised by Frumkin and Gierst and reported by Delahay[1] may be employed to calculate [Ox], [Rd], and E from measurable quantities.

At equilibrium, $\overrightarrow{\text{rate}}$ and $\overleftarrow{\text{rate}}$ are equal and therefore

$$\vec{k}(E)/\overleftarrow{k}(E) = [\mathrm{Rd}]/[\mathrm{Ox}] \tag{4}$$

If E_s is the standard potential of the Ox/Rd couple measured with respect to the chosen reference electrode, the thermodynamic Nernst relationship gives

$$\exp\left\{\frac{nF}{RT}(E - E_s)\right\} = \frac{[\mathrm{Ox}]}{[\mathrm{Rd}]}\,\frac{f_{ox}}{f_{rd}} \tag{5}$$

where F, R, and T have their usual significance. Ignoring the activity coefficients, f_{ox} and f_{rd}, in eqn. (5) and combining it with eqn. (4), we obtain

$$\overleftarrow{k}(E)/\vec{k}(E) = \exp\{(nF/RT)(E - E_s)\} \tag{6}$$

This equation is obeyed whatever individual potential-dependences $\overleftarrow{k}(E)$ and $\overrightarrow{k}(E)$ may have, and whether or not the electrode reaction is at equilibrium.

The absolute reaction rate theory[2] suggests that the rate constants depend on potential according to

$$\overleftarrow{k}(E) = k_s \exp\{(1-\alpha)(nF/RT)(E-E_s)\} \tag{7}$$

and

$$\overrightarrow{k}(E) = k_s \exp\{-\alpha(nF/RT)(E-E_s)\} \tag{8}$$

where

$$k_s = \overleftarrow{k}(E_s) = \overrightarrow{k}(E_s) \tag{9}$$

and α, the dimensionless transfer coefficient, takes some value between zero and unity. There is nothing in the absolute reaction rate theory that implies that the transfer coefficient should not itself be potential-dependent, but experimental evidence indicates that usually α is nearly constant over the potential ranges studied.

Equation (8) predicts that $\overrightarrow{k}(E)$ should increase without limit as E becomes increasingly negative. However, a finite limit must exist since, *even in the complete absence of any transport control*, the reaction rate cannot exceed the collision frequency of solute species with the electrode surface. According to Reiss[3], the number of solute collisions with each side of a plane of unit area immersed in a solution of solute concentration C is $3DC/2\lambda$ where D is the diffusion coefficient of the solute and λ is a mean jump length. The latter may be set equal to the "lattice" spacing of the solvent, say about 1.5 Å for water. A diffusion coefficient of 10^{-5} $cm^2 sec^{-1}$ is typical for a monomeric solute in aqueous solution and hence, for such a system, the maximum possible cathodic heterogeneous rate constant is

$$\overrightarrow{k}(E \to -\infty) = \overrightarrow{k}_m = \frac{3D}{2\lambda} \approx \frac{3}{2}\left(\frac{10^{-5}\ cm^2\,sec^{-1}}{1.5\times 10^{-8}\ cm}\right) = 1000\ cm\ sec^{-1} \tag{10}$$

This magnitude of rate constant is, of course, much too large to be measurable by any existing or projected electrochemical technique. The existence of an upper limit to electrochemical rate constants has been predicted earlier[4,5] by arguments which parallel the foregoing.

Analogously, an upper limit $\overleftarrow{k}_m$ will exist for $\overleftarrow{k}(E)$. The anodic and cathodic limits, $\overleftarrow{k}_m$ and $\overrightarrow{k}_m$, will be of similar magnitude but the two may differ numerically somewhat on account of different values of D and, in cases where Ox and Rd are dissolved in different solvents, of λ.

To exemplify the above argument, consider the electrode reaction

$$Cd^{2+}(aq.) + 2e^- \rightleftarrows Cd(Hg) \tag{11}$$

at equilibrium at a potential, E, positive of the cadmium ion/cadmium amalgam standard electrode potential. A small uniform concentration, C, of cadmium atoms will exist throughout the amalgam. Any plane of unit area within the amalgam, for example one parallel to the electrode surface, will be traversed in each direction by $3NDC/2\lambda$ cadmium atoms in unit time, N being Avogadro's constant. If we assume the amalgam remains homogeneous right up to its surface, $3\ NDC/2\lambda$ also gives the rate of collision of cadmium atoms with unit area of the surface. However, only a

certain fraction, φ, of the colliding atoms will be successful in traversing the electrode surface and entering the solution phase, the complementary fraction $(1-\varphi)$ being "reflected" back into the amalgam. Since we have prescribed equilibrium, the number of Cd atoms traversing the electrode plane to become ions will equal the number of ions being discharged to produce newly amalgamated atoms. Now, consider the potential to be made progressively more positive, equilibrium being maintained by a simultaneous increase in the cadmium ion concentration. The backward member of reaction pair (11) becomes progressively favored, corresponding to a steady increase in the fraction φ. Since φ cannot exceed unity, the rate of oxidation of cadmium atoms must eventually reach a limit given by the collision rate $3\,NDC/2\lambda$. The only alternative possibility would be for an inhomogeneity to develop close to the amalgam/solution surface, with an enhanced cadmium concentration there; however, it is difficult to see how this could fail to produce a chemical potential gradient, which is forbidden by our equilibrium postulate.

In the light of these considerations, it may be postulated that as the potential becomes increasingly negative, eqn. (8) ceases to apply, being gradually supplanted by the potential-independent relation (10). Moreover, the need to satisfy eqn. (6) at all potentials means that as $\overleftarrow{k}(E)$ approaches its $\overleftarrow{k}_m$-limit, $\vec{k}(E)$ must acquire the behavior given by

$$\vec{k}(E\rightarrow+\infty)=\overleftarrow{k}_m\exp\{-(nF/RT)(E-E_s)\} \tag{12}$$

In view of eqns. (10) and (12), eqn. (8) may be regarded as applicable only in an intermediate potential range, *i.e.*,

$$\vec{k}(E\approx E_s)=k_s\exp\{-\alpha(nF/RT)(E-E_s)\} \tag{13}$$

Thus, in different regions of potential, $\vec{k}(E)$ is given successively by eqns. (10), (13), and (12). A theorem[6] applicable in this circumstance combines these three relations such that

$$\frac{1}{\vec{k}(E)}=\frac{1}{\vec{k}(E\rightarrow-\infty)}+\frac{1}{\vec{k}(E\approx E_s)}+\frac{1}{\vec{k}(E\rightarrow+\infty)} \tag{14}$$

whence, at *any* potential

$$\vec{k}(E)=\frac{k_s\vec{k}_m\overleftarrow{k}_m}{k_s\overleftarrow{k}_m+\vec{k}_m\overleftarrow{k}_m\exp\left\{\alpha\frac{nF}{RT}(E-E_s)\right\}+k_s\vec{k}_m\exp\left\{\frac{nF}{RT}(E-E_s)\right\}} \tag{15}$$

By a similar argument

$$\overleftarrow{k}(E)=\frac{k_s\vec{k}_m\overleftarrow{k}_m}{k_s\overleftarrow{k}_m\exp\left\{-\frac{nF}{RT}(E-E_s)\right\}+\vec{k}_m\overleftarrow{k}_m\exp\left\{-(1-\alpha)\frac{nF}{RT}(E-E_s)\right.+\left.k_s\vec{k}_m\right\}} \tag{16}$$

Figure 1 shows graphs of eqns. (16) and (15) based on the values $T=298°K$, $n=2$ equiv. mole^{-1}, $\vec{k}_m=\overleftarrow{k}_m=k_m=10^3$ cm sec^{-1}, $k_s=10^{-1}$ cm sec^{-1} and $\alpha=0.30$. The last two values are close to those recently reported[7] for reaction (11). It will be

noted that there is no significant deviation from eqns. (7) and (8) over a potential range extending from about 150 mV more positive to about 350 mV more negative, than the standard potential. Notice also, that whereas the upper branches of the two curves ($k \rightarrow k_m$) are not experimentally accessible with present day techniques, the lower "abnormal" branches correspond to rate constant values that are easily measured. Although it is difficult to measure, for example $\vec{k}(E)$ at a potential at which $\overleftarrow{k}(E)$ is several orders of magnitude greater, this author believes that such a measurement is feasible.

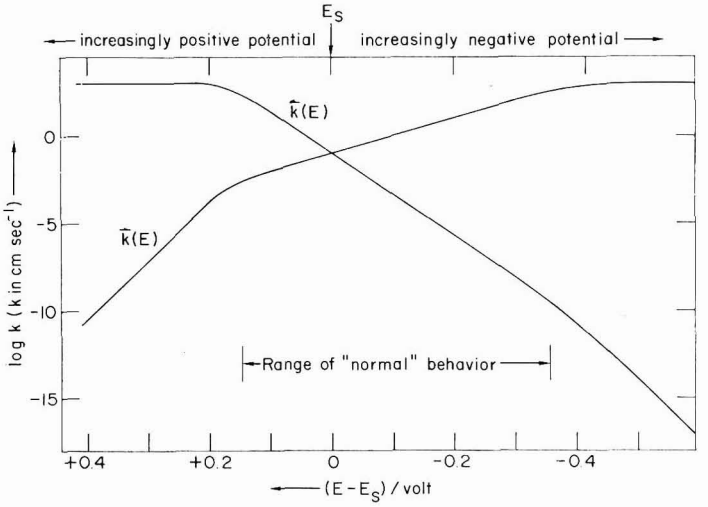

Fig. 1. Graphs of eqns. (15) and (16). k_m, 10^3 cm sec^{-1}; k_s, 10^{-1} cm sec^{-1}; α, 0.30; n, 2 equiv. mole^{-1}.

It may be asked why curvature of the type indicated in Fig. 1 has not been observed in Tafel studies of inherently slower electrode reactions. It is easily demonstrated that the range of "normal" behavior embraces a potential span of about

$$\Delta E = (RT/\alpha(1-\alpha)nF) \ln(k_m/k_s) \tag{17}$$

This means that for a one-electron reaction, "normal" behavior could fill the entire 2-V range of most electrode/solvent systems for k_s-values of 10^{-5} cm sec^{-1} or less.

Equation (15) predicts that as $(E-E_s)$ changes progressively from large positive to large negative values, the quantity $\alpha(E)$ defined by

$$-\frac{RT}{nF}\frac{\mathrm{d}}{\mathrm{d}E}\ln \vec{k}(E) = 1 + \frac{RT}{nF}\frac{\mathrm{d}}{\mathrm{d}E}\ln \overleftarrow{k}(E) = \alpha(E) \tag{18}$$

changes in a stepwise fashion from 0 to α to 1. Such behaviour is unnatural and it may be surmised that $\alpha(E)$ is actually a continuously (but gradually) varying function of potential such that α is the value that $\alpha(E)$ happens to acquire in the vicinity of the standard potential, *i.e.*, $\alpha(E_s) = \alpha$.

There is an infinity of equations that produce a sigmoid variation in $\alpha(E)$ from zero through α to unity as E passes from $+\infty$ through E_s to $-\infty$. Correspondingly,

there is an infinity of smooth curves of $\ln \vec{k}(E)/k_s$ *vs.* $(E-E_s)$ that pass through the origin and which have eqns. (12) and (10) as asymptotes at the $E=\pm\infty$ limits. One such possibility is the hyperbola

$$\ln \frac{\overleftarrow{k}_m}{\vec{k}(E)} - \frac{nF}{RT}(E-E_s) = \ln \frac{\overleftarrow{k}_m}{k_s} \ln \frac{\vec{k}_m}{k_s} \Big/ \ln \frac{\vec{k}_m}{\vec{k}(E)} \tag{19}$$

Another is the relation

$$\vec{k}(E) = \frac{k_s \overleftarrow{k}_m + k_s \vec{k}_m \exp\left\{-\frac{nF}{RT}(E-E_s)\right\}}{\vec{k}_m + \overleftarrow{k}_m + 4k_s \sinh^2\left\{\frac{nF}{2RT}(E-E_s)\right\}} \tag{20}$$

It must be emphasized that there is no basis for either of these equations, except their reduction to the correct limiting forms. However, it is to be noted that either equation predicts a parabolic dependence of $\ln \vec{k}(E)$ upon potential in the vicinity of E_s, in accordance with the theories of Hush and Marcus[8].

Equations such as (19) and (20) enable α to be expressed as functions of the three rate constants k_s, $\vec{k}_m$, and $\overleftarrow{k}_m$. Thus, according to eqn. (19)

$$\alpha = \ln\{\vec{k}_m/k_s\}/\ln\{\vec{k}_m \overleftarrow{k}_m/k_s^2\} \tag{21}$$

whereas by eqn. (20)

$$\alpha = \vec{k}_m/(\vec{k}_m + \overleftarrow{k}_m) \tag{22}$$

Either of these equations implies that departure of the transfer coefficient from the symmetrical value of $\frac{1}{2}$ arises because of the inequality of $\overleftarrow{k}_m$ and $\vec{k}_m$ and should therefore be greater for electrode reactions such as (11) in which Ox and Rd are in different phases. Published α-values[9] are insufficiently reliable for this conclusion to be tested.

SUMMARY

Two consequences of the concept of a maximum value for heterogeneous electrochemical rate constants are presented. First, it is suggested that the approach to the limit is reflected in the rate constant of the reverse reaction. Secondly, it is speculated that the transfer coefficient may be determined by the magnitudes of the limiting rate constants.

REFERENCES

1 P. DELAHAY, *Double-Layer and Electrode Kinetics*, Interscience Publishers, Inc., New York, 1965, ch. 3.
2 H. EYRING, S. GLASSTONE AND K. J. LAIDLER, *J. Chem. Phys.*, 7 (1939) 1053.
3 H. REISS, *J. Chem. Phys.*, 18 (1950) 996.
4 J. E. B. RANDLES, *Trans. Faraday Soc.*, 48 (1952) 828.
5 H. RUBIN AND F. C. COLLINS, *J. Phys. Chem.*, 58 (1954) 958.
6 K. B. OLDHAM, *J. Am. Chem. Soc.*, 77 (1955) 4697.

7 G. LAUER AND R. A. OSTERYOUNG, *Anal. Chem.*, 38 (1966) 1106.
8 R. A. MARCUS, *Ann. Rev. Phys. Chem.*, 15 (1964) 155.
9 N. TANAKA AND R. TAMAMUSHI, *Electrochim. Acta*, 9 (1964) 963.

ELECTROANALYTICAL CHEMISTRY AND INTERFACIAL ELECTROCHEMISTRY
Elsevier Sequoia S.A., Lausanne – Printed in The Netherlands

COUPLING OF CHARGING AND FARADAIC PROCESSES

ELECTRODE ADMITTANCE FOR REVERSIBLE PROCESSES

PAUL DELAHAY AND KAREL HOLUB
Department of Chemistry, New York University, Washington Square, New York, N.Y. 10003, (U.S.A.)
(Received May 4th, 1967)

The admittance of an electrode with a single charge transfer reaction was previously derived[1] for any value of the exchange current, on the basis of recently developed ideas[2-3]. This derivation supersedes a previous treatment[4] in which inadequate time-derivatives of surface excesses were used. Both charging and faradaic currents were considered in setting up the boundary value problem, and the *total* electrode impedance was thus obtained. The resulting equation was given in a compact form but is in fact very involved for a finite exchange current different from zero. The admittance for an infinite exchange current, *i.e.*, for a reversible process, can easily be deduced as a limiting case of the general result. This was done as was mentioned in our previous paper[1], but details were not given. Since the admittance for reversible processes may possibly be useful, a formula for it is derived directly here (SLUYTERS *et al.*[5] mention that REINMUTH also derived this result recently). The derivation is preceded by a discussion of the separation of charging and faradaic currents from a very general point of view.

COUPLING BETWEEN CHARGING AND FARADAIC PROCESSES

We shall examine the effect of a perturbation, from initial equilibrium conditions, upon the charge density and the faradaic current for an electrode of constant area. We first consider equilibrium and note that the charge density on the electrode, q_e, at the equilibrium potential, is a function of the following variables for a given solvent: the equilibrium potential E_e; the bulk concentrations a^s, b^s ... of all the species involved in the electrode reaction; the bulk concentrations u^s, v^s ... of other ions present in solution (supporting electrolyte). The variables are not independent because E_e is related to the concentrations a^s, b^s ... by the Nernst equation and the activity coefficients depend on all ionic concentrations.

If the potential is changed by δE by some external device, either directly (potentiostatic control) or indirectly (*e.g.*, galvanostatic control), the concentrations just outside the double layers (in solution and also in the metallic phase for amalgams) are different from their bulk values because of some mass transfer control. These local concentrations are designated by a, b ... and u, v ... Thus, the change, δq, resulting from the outside perturbation is a function of δE, δa, δb ..., δu, δv ... where $\delta E = E - E_e$, $\delta a = a - a^s$ ..., $\delta u = u - u^s$ ...

We now examine the effect of the external perturbation on the faradaic current

density, i_f. Thus i_f is a function of δE, δa ..., δu ... and of some kinetic parameters characterizing the kinetics of the charge transfer reaction (exchange current, stoichiometric number, etc.).

The same variables appear in the functions representing δq and i_f and, consequently, the mass transfer problem leading to explicit forms of δE (if not forced upon the system), a ..., u ... must be solved by *simultaneous* consideration of the effect of the perturbation on δq and i_f. This can be done, for instance, by using the three general equations previously advanced[2] with the proper explicit forms of the time-derivative of the surface excesses[3]. General equations involving even fewer assumptions could be advanced, but the mathematical analysis, already quite laborious, would rapidly become hopelessly complicated.

In principle, one is not justified in solving the mass transfer problem for i_f alone on the assumption that δq is solely dependent on δE, as has generally been done. Such *a priori* separation of charging and faradaic processes is not justified in principle, as was previously pointed out[2]. The error resulting from this simplified approach is serious only when δq is significantly affected by the changes δa ... and δu ... resulting from the perturbation. This seems to be the case when the following three conditions are fulfilled: (a) there is strong adsorption (specific or non-specific) of reactant and product; (b) adsorption is strongly potential-dependent because of the rapid variation of the equilibrium concentrations a^s, b^s ... (Nernst equation); (c) the charge transfer reaction is sufficiently fast (high exchange current density).

The above analysis, based on the general forms of the functions, δq and i_f, does not require the introduction of charge separation or recombination without external current. This concept was introduced initially[2] in the examination of charging of an electrode of variable area at constant potential. There is indeed charge separation or recombination in that particular case but transposition of this type of intuitive analysis to more general cases is *not essential*. Analysis can proceed more safely from the three general starting equations.

The above analysis, based on the general forms of the functions δq and i_f could be generalized to interfacial processes involving storage of some species at an interface and transfer of one or several of these species through the interface. In the particular case we consider, the excess (positive or negative) electrons are stored in the metallic phase and they "cross" the interface *via* the electrode reaction. More generally, coupling of the type considered here results from the description of two processes in terms of some time-dependent variables the values of which are determined by a third process (mass transfer here).

TOTAL ELECTRODE ADMITTANCE

We consider an electrode reaction, $O + z\,e = R$, for the usual conditions of mass transfer controlled by semi-infinite linear diffusion in presence of a large excess of supporting electrolyte. Species O and R are soluble in solution or, for R, in the electrode (*e.g.*, amalgam). The electrode reaction may also involve other species present in such a large excess that mass transfer of these species need not be considered. The total electrode admittance is derived for an infinite exchange current and for small amplitudes. Limitations on the amplitude are stated more precisely below.

The first boundary condition is the same as in the general treatment[1], namely

$$D_O(\partial c_O/\partial x)_{x=0} - D_R(\partial c_R/\partial x)_{x=0} = \mathrm{d}(\Gamma_O + \Gamma_R)/\mathrm{d}t \tag{1}$$

where c is the concentration, Γ the surface excess, D the diffusion coefficient, and x and t represent the distance from the electrode, and time, respectively. Equation (1) is valid for any amplitude but can be written in a linearized form, valid only for small amplitudes. Thus, by selecting the potential E and one of the concentrations of O or R as independent variables

$$\mathrm{d}\Gamma/\mathrm{d}t = \Gamma^{(c^s)}(\partial c/\partial t)_{x=0} + \Gamma^{(E)}\,\mathrm{d}E/\mathrm{d}t \tag{2}$$

with

$$\Gamma^{(c^s)} = (\partial\Gamma/\partial c^s)_{E_e}\,, \qquad \Gamma^{(E)} = (\partial\Gamma/\partial E)_{c^s} \tag{3}$$

c^s being the bulk concentration of O or R and E_e the equilibrium potential corresponding to $c_R{}^s$ and $c_O{}^s$. Equation (2) is valid provided the other terms in the series expansion of $\mathrm{d}\Gamma/\mathrm{d}t$ are negligible.

The second boundary condition expresses the Nernst equation. For small amplitude we use the Taylor-series expansion truncated after the first derivatives, and this simplification determines the maximum permissible amplitude of the overvoltage. Thus

$$\begin{aligned}(c_R)_{x=0} &= c_R{}^s + (\partial c_R{}^s/\partial c_O{}^s)_{E_e}(c_O - c_O{}^s) + (\partial c_R{}^s/\partial E)_{c_O{}^s}\ (E - E_e)\\ &= c_O{}^s + A\,(c_O - c_O{}^s) + B\,(E - E_e)\end{aligned} \tag{4}$$

with

$$A = c_R{}^s/c_O{}^s \tag{5}$$

$$B = -(zF/RT)\,c_R{}^s \tag{6}$$

where F, R and T have their usual significance. Moreover, as usual $c_O \to c_O{}^s$ and $c_R \to c_R{}^s$ for $x \to \infty$ ($x \to -\infty$ if R is a metal in an amalgam).

The overvoltage η ($\equiv E - E_e$) is

$$\eta = \eta_a \exp(j\omega t) \tag{7}$$

where η_a is the amplitude, $j = (-1)^{\frac{1}{2}}$, and $\omega = 2\pi f$, f being the frequency.

The concentrations at the electrode obeying Fick's equation for O and R are for the steady state

$$(c_O)_{x=0} = c_O{}^s\{1 - P\exp[-x(1+j)(\omega/2D_O)^{\frac{1}{2}} + j\omega t]\} \tag{8}$$

$$(c_R)_{x=0} = c_R{}^s\{1 + N\exp[x(1+j)(\omega/2D_R)^{\frac{1}{2}} + j\omega t]\} \tag{9}$$

where N and P are such that the boundary conditions are satisfied. Once N and P have been determined (only algebra), the amplitude of the current is expressed by the third general equation previously advanced[1,2], and one determines the element of the equivalent circuit for the electrode. The corresponding resistance and capacity in a parallel configuration are:

$$R = (c_R{}^s/\lambda B)[(\xi_r{}^2 + \xi_i{}^2)/(K\xi_r + H\xi_i)] \tag{10}$$

$$C = (\lambda B/c_R{}^s\omega)\{[(H\xi_r - K\xi_i)/(\xi_r{}^2 + \xi_i{}^2)] + w\} \tag{11}$$

where

$$\xi_r = \varrho_0 \tag{12}$$

$$\xi_i = \varrho_0 + \varrho_1 \omega^{\frac{1}{2}} \tag{13}$$

$$H = H_0 + H_1 \omega^{\frac{1}{2}} \tag{14}$$

$$K = K_1 \omega^{\frac{1}{2}} + K_2 \omega \tag{15}$$

$$w = [\Gamma_O^{(E)} + (q^{(E)}/zF)](1/B)(2\omega/D_O)^{\frac{1}{2}} \tag{16}$$

with the symbols of Appendix 1. Note that the quantities between brackets in eqn. (10) and between braces in eqn. (11) are dimensionless. It can be verified that eqns. (10) and (11) reduce to the classical form for the parallel circuit of the faradaic impedance when the terms involving Γ and q-derivatives are set equal to zero. Some limiting values are listed in Appendix 2.

The explicit forms of R and C contain six double-layer parameters, *viz.*, the first derivatives of Γ_O, Γ_R and q with respect to E and c_R^s (or c_O^s). Thus analysis of a reversible process poses a problem in the *unambiguous* of double layer parameters.

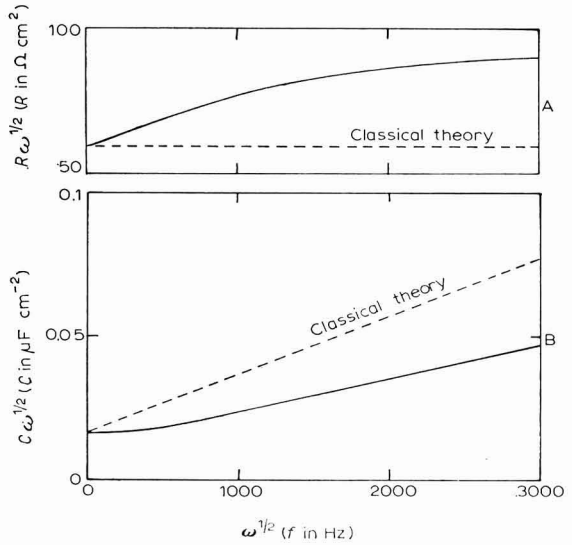

Fig. 1. A. Plot of $R\omega^{\frac{1}{2}}$ *vs.* $\omega^{\frac{1}{2}}$ with R computed from eqn. (10). Data: $z = 2$, $T = 25°$, $c_O^s = c_R^s = 10^{-6}$ mole cm^{-3}, $D_O = D_R = 10^{-5}$ cm^2 sec^{-1}, $\Gamma_O^{(c_O^s)} = 1.4 \times 10^{-5}$ cm, $\Gamma_O^{(E)} = -5.4 \times 10^{-11}$ mole cm^{-2} V^{-1}, $\Gamma_R^{(c_O^s)} = 0$, $\Gamma^{(E)} = 0$ (no adsorption of R), $q^{(c_O^s)} = -1.974$ C cm mole^{-1}, $q^{(E)} = 20$ μF cm^{-2}. B. Plot of $C\omega^{\frac{1}{2}}$ *vs.* $\omega^{\frac{1}{2}}$ for the same data as Fig. 1A.

Simultaneous use of data from electrocapillary curves should make matters somewhat easier.

The departure from classical behavior is shown in Fig. 1 (the plot of Fig. 1A was recently used by SLUYTERS and co-workers[6] to show departure from the classical

* Except for $q^{(c_O^s)}$ which was previously set equal to zero. This derivative is obtained as follows: One sets $q = -\sum z_i F \Gamma_i$ where i is taken for all ions, z_i being taken with its sign. Γ_i is expressed by means of the diffuse double-layer theory for mixed electrolytes and then q is differentiated with respect to c_+^s.

behaviour). Data were those previously used* in a theoretical calculation[1] and correspond *approximately* to the discharge of a divalent cation in 0.1 *M* supporting electrolyte at −0.5 V against the point of zero charge in the absence of specific adsorption for all ions and without metal adsorption.

ACKNOWLEDGEMENT

This work was supported by a grant from the National Science Foundation.

APPENDIX I. SYMBOLS IN EQNS. (10)–(17)

$$\lambda = zFc_O^s(\omega D_O/2)^{\frac{1}{2}}$$

$$\varrho_0 = S + AQ$$

$$\varrho_1 = (Sg + Am)\omega^{-\frac{1}{2}}$$

$$H_0 = -2Q$$

$$H_1 = -K_1 = -[Q(g+u) + Sn + m]\omega^{-\frac{1}{2}}$$

$$K_2 = (Sn+m)(g+u)\omega^{-1}$$

$$g = \Gamma_O^{(c_O^s)}(2\omega/D_O)^{\frac{1}{2}}$$

$$m = \Gamma_R^{(c_R^s)}(2\omega/D_O)^{\frac{1}{2}}$$

$$n = [\Gamma_R^{(E)} + \Gamma_O^{(E)}](1/B)(2\omega/D_R)^{\frac{1}{2}}$$

$$q^{(c_O^s)} = (\partial q/\partial c_O^s)_E \qquad (q = \text{charge density on electrode})$$

$$q^{(E)} = (\partial q/\partial E)_{c_O^s}$$

$$Q = (c_R^s/c_O^s)(D_R/D_O)^{\frac{1}{2}}$$

$$S = c_R^s/c_O^s$$

$$u = (1/zF)q^{(c_O^s)}(2\omega/D_O)^{\frac{1}{2}}$$

APPENDIX 2. LIMITING VALUES OF R AND C

$\omega \to 0$

$R \to [RT/(zF)^2 c_R^s](2/\omega D_R)^{\frac{1}{2}} \to \infty$

$C \to (\lambda B/c_O^s\omega)[(H_0/2\varrho_0) + w] \to \infty$

$\omega \to \infty$

$R \to (c_O^s/\lambda B)[\varrho_1^2/(\varrho_0 K_2 + \varrho_1 H_1)] \to 0$

$C \to (\lambda B/c_O^s\omega)[-(K_2/\varrho_1)\omega^{\frac{1}{2}} + w]$

SUMMARY

Coupling between double-layer charging and a faradaic process is examined in a very general way for an electrode at which a charge transfer reaction takes place. It is shown that coupling follows directly from the *general* forms of the equations describing the effect of an external perturbation on the charging and faradaic processes. It is not necessary to introduce the concept of charge separation or recombination at the interface.

The electrode admittance is derived and discussed for reversible processes (infinite exchange current). Six double-layer parameters are required in the analysis.

REFERENCES

1 K. HOLUB, G. TESSARI AND P. DELAHAY, *J. Phys. Chem.*, 71 (1967) 2612.
2 P. DELAHAY, *ibid.*, 70 (1966) 2067, 2373.
3 P. DELAHAY, K. HOLUB, G. G. SUSBIELLES AND G. TESSARI, *ibid.*, 71 (1967) 779.
4 P. DELAHAY AND G. G. SUSBIELLES, *ibid.*, 70 (1966) 3150.
5 B. TIMMER, M. SLUYTERS-REHBACH AND J. H. SLUYTERS, *J. Electroanal. Chem.*, 15 (1967) 343.
6 M. SLUYTERS-REHBACH, B. TIMMER AND J. H. SLUYTERS, *J. Electroanal. Chem.*, 15 (1967) 151.

ELECTROANALYTICAL CHEMISTRY AND INTERFACIAL ELECTROCHEMISTRY
Elsevier Sequoia S.A., Lausanne – Printed in The Netherlands

CONSECUTIVE OVERALL STABILITY CONSTANTS OF METAL COMPLEXES IN SOLUTION FROM DIFFUSION CURRENT DATA

D. R. CROW
Department of Chemistry, The Woolwich Polytechnic, London (England)
(Received March 17th, 1967)

INTRODUCTION

Polarography has for some time proved to be a valuable technique for determining the stability constants of metal ion complexes in solution. The method devised by DEFORD AND HUME[1] has proved particularly useful in that it enables the consecutive overall and step stability constants to be found in systems characterised by a series of metal–ligand step-equilibria. Measured shifts in half-wave potential of a metal aquo ion with increasing ligand concentration, can be used for the determination of stability constants by graphical extrapolation methods, provided that reductions at the dropping mercury electrode proceed reversibly. Precise determinations of these shifts can be rather laborious as complete polarograms need to be plotted manually at small potential intervals for a number of solutions containing the ligand over a fairly wide concentration range. Other methods based on the measurement of diffusion currents have been devised, *e.g.*, the indicator method of SCHWARZENBACH AND ACKERMANN[2] and the methods of KACENA AND MATOUSEK[3] and ZABRANSKY[4]. These, however, are only applicable to systems containing a single complex species. The techniques described here may be applied to systems of several species in equilibrium.

THEORETICAL

Suppose that a hydrated metal ion has the formula $M(H_2O)_n$ in solution; let the volume of M be v_1 and that of H_2O, v_2. Then the total volume of the aquo ion may be expressed approximately as (v_1+nv_2). Let the n water molecules now be replaced successively by ligand molecules each of volume v_3. When one water molecule has been replaced by one molecule of ligand, the volume of the resulting species becomes $(v_1+(n-1)\,v_2+v_3)$. The change in volume that has occurred, Δv_1, is then (v_3-v_2) and the ligand number with respect to the added complexing agent is 1. Similarly, when j water molecules are replaced by j ligand molecules, the volume of the species becomes $(v_1+(n-j)\,v_2+jv_3)$. The change in volume, Δv_j, is now $j(v_3-v_2)$ and the ligand number is j. When, finally, n ligand molecules replace the n water molecules the final volume becomes (v_1+nv_3). The maximum change in volume, Δv_n, is $n\,(v_3-v_2)$ with n the maximum coordination number. Thus, the change in volume is directly proportional to the ligand number, $\bar{n}$. By extending this idea to a large assemblage of hydrated

metal ions, it is seen that the average volume change/ion produced by a given excess of ligand is proportional to the average number of ligands coordinated/ion, *i.e.*, the ligand number.

The Stokes–Einstein[5] equation relates the diffusion coefficient, D, of a spherical particle to its radius, r, by

$$D = \frac{RT}{N} \frac{1}{6\pi\eta r} \tag{1}$$

where η is the coefficient of viscosity of the solvent and N is the Avogadro number.

The diffusion coefficient is also related to the polarographic diffusion current by the Ilkovič[6] equation,

$$i_d = 607nD^{\frac{1}{2}}m^{\frac{2}{3}}t^{\frac{1}{6}}C \tag{2}$$

where i_d is the mean diffusion current produced by reduction of the metal ion at concentration C, m is the rate of mercury flow, t the drop time and n the number of electrons transferred in the reduction process.

Thus,

$$i_d \propto \sqrt{1/r}, \quad \text{or} \quad i_d^2 \propto 1/r$$

Therefore, the change in mean diffusion current caused by a change in particle radius from r_1 to r_2 ($r_2 > r_1$) is given by,

$$(i_{d_1} - i_{d_2}) = k\{1/\sqrt{r_1} - 1/\sqrt{r_2}\} \tag{3}$$

where k is a constant.

Or,

$$i_{d_1}^2 - i_{d_2}^2 = k\{1/r_1 - 1/r_2\} \tag{4}$$

Therefore,

$$(i_{d_1} + i_{d_2})(i_{d_1} - i_{d_2}) = k\,\frac{r_2 - r_1}{r_1 r_2} \tag{5}$$

that is,

$$(i_{d_1} + i_{d_2})\Delta i_d = k\Delta r/r_1 r_2 \tag{6}$$

where

$$\Delta i_d = i_{d_1} - i_{d_2} \quad \text{and} \quad \Delta r = r_2 - r_1$$

Or, since

$$(i_{d_1} + i_{d_2}) = 2i_{d_1} - \Delta i_d \tag{7}$$

$$2i_{d_1}\Delta i_d - \Delta i_d^2 = k\Delta r/r_1 r_2 \tag{8}$$

When no ligand is present, the radii of all hydrated ions in solution may be regarded as being the same. When ligand is present, several types of particle co-exist, having relatively different proportions of ligand to water molecules attached to the central ion. If the introduction of some ligand species in place of water does not cause undue departure from spherical shape, the average diffusion behaviour may be explained in terms of a large assemblage of particles of different size the radii of which are, on average, slightly greater than r_1.

The small difference in volume between two spheres of radius r_1 and r_2 may be written as,

$$4\pi r_1^2 \Delta r = \Delta v \tag{9}$$

i.e.

$$\Delta r = \Delta v / 4\pi r_1^2 \tag{10}$$

Therefore, substituting for Δr in eqn. (8) gives the following relation:

$$(2i_{d_1}\Delta i_d - \Delta i_d^2) = [k/4\pi r_1^3 r_2]\, \Delta v \tag{11}$$

Since r_1 is only slightly less than r_2,

$$r_1^3 r_2 \cong r_1^4 = \text{constant.}$$

Therefore,

$$(2i_{d_1}\Delta i_d - \Delta i_d^2) = k'\Delta v \tag{12}$$

where k' is another constant.
Now, Δi_d is for most cases considerably less than i_{d_1}, so that the term Δi_d^2 is very small in comparison with the term $2i_{d_1}\Delta i_d$.
Thus,

$$2i_{d_1}\Delta i_d = k'\Delta v \tag{13}$$

or

$$\Delta i_d \propto \Delta v \tag{14}$$

i.e.,

$$\Delta i_d \propto \bar{n} \tag{15}$$

It must be assumed that the presence of ligand does not significantly alter the viscosity of the solvent medium.

EXPERIMENTAL

The cadmium solutions were prepared with AnalaR cadmium sulphate. Pyrazole, imidazole and benzimidazole were of commercially available reagent-grade, and 3,5-dimethylpyrazole was prepared as described previously[7]. AnalaR potassium nitrate was used as supporting electrolyte in all determinations.

The concentration of Cd^{2+} used was $5 \cdot 10^{-4}\,M$ in all cases and the ligand concentrations were varied over as wide a range as was compatible with solubility. Water was used as solvent for pyrazole and imidazole complexes, and 50% methanol/water (v/v) was used for 3,5-dimethylpyrazole and benzimidazole.

All polarographic waves were plotted manually by means of a Pye Universal Potentiometer and an accurately calibrated microammeter. In determining half-wave potentials by logarithmic analysis of the waves, correction was made for the iR drop through the cell and reference electrode system. All potential measurements were made with respect to the saturated calomel electrode at 25°.

Changes in diffusion coefficients of the complexed cadmium ion with change in ligand concentration, were determined in terms of, either the change in diffusion current (Δi_d) determined from the manual plots, or the change in peak current (ΔI_p)

obtained with the aid of a Southern cathode ray polarograph. It was found that shifts in peak current could be measured quite well with this instrument by using high sensitivity and adjusting the Y-shift control so as to accommodate only the apex of the peak on the screen.

RESULTS AND DISCUSSION

Stability constant data for the cadmium complexes of pyrazole[8], 3,5-dimethylpyrazole[7] and imidazole[9] have been reported previously. Data for the benzimidazole complexes were determined by the method of DEFORD AND HUME, the various derived functions being given in Table 1.

TABLE 1

DEFORD-HUME DERIVED FUNCTIONS FOR THE CADMIUM–BENZIMIDAZOLE SYSTEM

$[BIm]$ (M)	$\Delta E_{\frac{1}{2}}$	F_0	F_1	F_2	F_3
0.00	0.0000	1.00	—	—	—
0.01	0.0094	2.09	109	—	—
0.02	0.0176	3.94	147	3,100	15,000
0.03	0.0241	6.49	183	3,267	15,567
0.04	0.0293	9.80	220	3,375	14,375
0.05	0.0337	13.80	256	3,420	12,400
0.06	0.0383	19.77	313	3,800	16,667
0.07	0.0417	25.76	354	3,843	14,900
0.08	0.0452	33.81	410	4,062	15,775

Overall constants: $\beta_1 = 85$; $\beta_2 = 2{,}800$; $\beta_3 = 15{,}500$.
Step constants: $K_1 = 85$; $K_2 = 33.1$; $K_3 = 6.92$.

TABLE 2

STABILITY CONSTANT DATA FOR THE CADMIUM COMPLEXES OF PYRAZOLE, 3,5-DIMETHYLPYRAZOLE, IMIDAZOLE AND BENZIMIDAZOLE

Ligand	β_1	β_2	β_3	β_4
pyrazole[8]	14	45	90	42
3,5-dimethylpyrazole[7]	14	4	76	—
imidazole[8]	6.3×10^2	8.0×10^4	2.8×10^6	3.8×10^7
benzimidazole	85	2.8×10^3	15.5×10^3	—

The consecutive overall constants for the four systems are given in Table 2.

From the values of the various overall stability constants, it was possible to calculate, for each system, the ligand number, $\bar{n}$, at each ligand concentration. Observed values of Δi_d or ΔI_p are plotted against calculated values of $\bar{n}$ in Fig. 1.

It can be seen that, in each case, the plots are satisfactorily linear, in agreement with eqn. (15). For curve III, however, there is a tendency for some curvature at higher $\bar{n}$-values. This is to be expected since the largest shifts in diffusion and peak current were observed for the dimethylpyrazole system and departures from the rela-

tion for small Δi_d-values begin to become significant. In this case, the Δi_d-values should have the correction term $\Delta i_d^2/2i_{d_1}$ subtracted in accordance with eqn. (8). Figure 2 shows the uncorrected and corrected curves; the latter shows good linearity.

In principle, therefore, it should be possible to obtain stability constant data, for certain metal–ligand systems, from measurements of the change in diffusion current of the hydrated metal ion as it is increasingly complexed with ligand. This would necessitate a knowledge of a reliable value of $\bar{n}$ for at least one value of ligand concen-

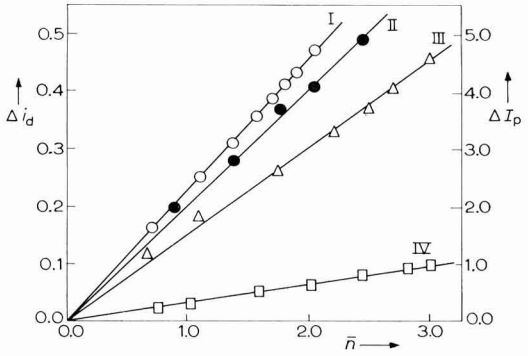

Fig. 1. Shifts, Δi_d or ΔI_p, as functions of calcd. ligand number, $\bar{n}$, for systems containing cadmium complexes. (I), Δi_d *vs.* $\bar{n}$, cadmium–benzimidazole; (II), as I, cadmium–pyrazole; (III), ΔI_p *vs.* $\bar{n}$, cadmium–3,5-dimethylpyrazole; (IV), as III, cadmium–imidazole.

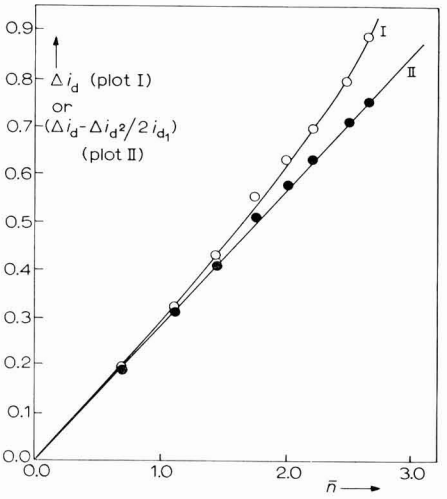

Fig. 2. Corrected and uncorrected plots of Δi_d *vs.* $\bar{n}$ for cadmium–3,5-dimethylpyrazole system. (o), uncorrected points; (●), corrected points obtained by subtraction of term, $\Delta i_d^2/2i_{d_1}$.

tration. Values of $\bar{n}$ over the whole concentration range then follow by simple proportion. The polarographic indicator-ion method of RINGBOM AND ERIKSSON[10] provides ligand number data. This technique is based on the competitive complexing reactions of an indicator metal ion, and an ion under study, with a chosen ligand. The shift in

half-wave potential of the indicator ion, for a particular ligand concentration, is smaller in the presence of the added metal ion than in its absence, the difference between the two shifts being directly related to[11] $\bar{n}$. The method is tedious and gives rather unreliable data for lower and higher values of $\bar{n}$, but can be used, however, to give a reliable estimate of $\bar{n}$ at intermediate values. Thus, if one value of $\bar{n}$ is obtained in this way, the rest follow from the values of Δi_d.

Alternatively, if the Δi_d-data show an approach to a measurable limiting value at the highest ligand concentrations, ligand number data may be obtained over the whole range if the maximum coordination number of the system is known or can be inferred. Figure 3 shows plots of Δi_d and $\bar{n}$ *versus* concentration of 3,5-dimethylpyrazole, the $\bar{n}$-values being calculated on the assumption that the maximum coordination number is three. The formation curve for this system is presented in Fig. 4.

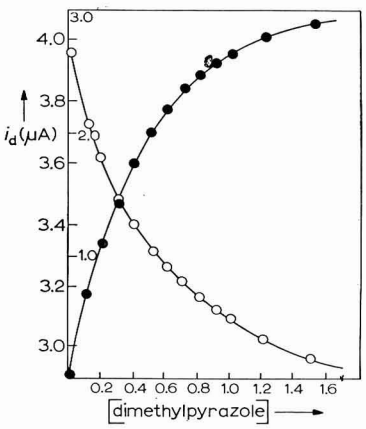

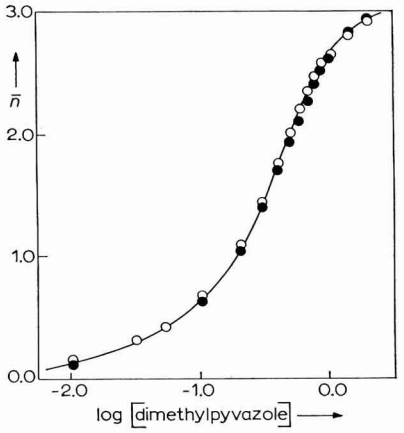

Fig. 3. Plots of i_d and $\bar{n}$ *vs.* concn. 3,5-dimethylpyrazole.

Fig. 4. Formation curve of cadmium–3,5-dimethylpyrazole system. (○), points obtained from previously determined data; (●), points obtained from diffusion current measurements.

TABLE 3

STABILITY CONSTANT DATA FOR THE CADMIUM–3,5-DIMETHYLPYRAZOLE SYSTEM OBTAINED BY THE DEFORD–HUME AND THE CURRENT METHODS

Method	β_1	β_2	β_3
DeFord–Hume	14	4	75
Crow	12	4	60

In Figure 4 one set of points is calculated from the known stability constant data, the other being determined from Δi_d measurements. Integration of the directly determined $\bar{n}$ *versus* log[ligand] curve by the method of Fronaeous[12], gave values of stability constants agreeing closely with those found previously. The two sets of data are given for comparison in Table 3.

CONCLUSIONS

The results obtained provide the basis for a new polarographic method for determining stability constants in metal–ligand systems characterised by a set of step-equilibria.

Advantages of such a method are: (1) Values of Δi_d may be determined fairly rapidly without the necessity of plotting complete polarograms. Since diffusion current measurements are made at a fixed applied potential, as the ligand concentration is varied the residual current contribution is a constant quantity in each value of the current determined. This fixed potential must be sufficiently negative in order that full development of the diffusion current is obtained, even at the highest ligand concentration. (2) The method is applicable to both reversible and irreversible reductions at the dropping electrode and depends only on the polarographic wave being diffusion-controlled and hence obeying the Ilkovič equation. The results in the present paper refer only to the behaviour of neutral ligands, so that the charge residing on all species in a solution of metal ions and ligand is the same. Changes in the electrostatic interaction between the complex species and ions of the supporting electrolyte will thus be neglible. It might be expected that in the case of a charged ligand, where the charge varies from complex to complex, this may not necessarily be the case. However, from preliminary work using charged ligands in a medium of constant ionic strength, early results indicate that the proportionality between Δi_d and $\bar{n}$ is maintained reasonably well.

ACKNOWLEDGEMENT

The author wishes to express sincere thanks to Mr. J. V. WESTWOOD (Sir John Cass College, London) for helpful discussions during the preparation of this study.

SUMMARY

It is shown theoretically that the change in polarographic diffusion current of a metal ion in solution, produced by the presence of excess coordinating ligand, is directly proportional to the ligand number, $\bar{n}$, of the system. The relationship is confirmed by the observed behaviour of the cadmium ion when complexed with four different heterocyclic ligand species for which stability constant data were determined by conventional means. The formation curve for a particular metal–ligand system may be constructed provided that a reliable assessment of the ligand number may be made at one or (preferably) two values of the free ligand concentration. Since a diffusion-controlled polarographic wave-height is given by the Ilkovič equation, regardless of the degree of reversibility of the electrode process, the method may be used to determine the stabilities of complexes of metal ions that behave irreversibly at the dropping mercury electrode.

REFERENCES

1 D. D. DEFORD AND D. N. HUME, *J. Am. Chem. Soc.*, 73 (1951) 5321.
2 G. SCHWARZENBACH AND H. ACKERMANN, *Helv. Chim. Acta*, 35 (1952) 485.
3 V. KAČENA AND L. MATOUŠEK, *Collection Czech. Chem. Commun.*, 18 (1953) 294.

4 Z. ZABRANSKY, *Collection Czech. Chem. Commun.*, 24 (1959) 3075.
5 A. EINSTEIN, *Ann. Physik*, 17 (1905) 549; 19 (1906) 371. *Z. Elektrochem.*, 14 (1908) 235.
6 D. ILKOVIČ, *Collection Czech. Chem. Commun.*, 6 (1934) 498. *J. Chim. Phys.*, 35 (1938) 129.
7 D. R. CROW, *J. Polarog. Soc.*, 11 (1965) 22.
8 D. R. CROW, *J. Polarog. Soc.*, 11 (1965) 67.
9 C. TANFORD AND M. L. WAGNER, *J. Am. Chem. Soc.*, 75 (1953) 434.
10 A. RINGBOM AND L. ERIKSSON, *Acta Chem. Scand.*, 7 (1953) 1105.
11 D. R. CROW AND J. V. WESTWOOD, *Quart. Rev. London*, 19 (1965) 57.
12 S. FRONAEOUS, *Acta Chem. Scand.*, 4 (1950) 72.

ELECTROANALYTICAL CHEMISTRY AND INTERFACIAL ELECTROCHEMISTRY
Elsevier Sequoia S.A., Lausanne – Printed in The Netherlands

A METHOD BASED ON POLYNOMIAL APPROXIMATIONS FOR NUMERICAL SOLUTION OF VOLTERRA INTEGRAL EQUATIONS

MICHAEL L. OLMSTEAD AND RICHARD S. NICHOLSON
Chemistry Department, Michigan State University, East Lansing, Mich. (U.S.A.)
(Received March 21st, 1967)

INTRODUCTION

A number of electrochemical techniques are described by boundary value problems that do not yield analytical solutions, but which usually can be formulated as Volterra integral equations. This fact has led some authors to rely on approximate numerical methods for solution of these integral equations (see ref. 1 for a recent review). The numerical techniques most generally used may be classified according to the type of approximate function employed on successive integration intervals. The approximate functions in three of these methods are: (1) a constant[1] (step function technique); (2) a straight line[2] (HUBER's method); and (3) a parabola[3] (WAGNER's method). In principle, the third method should provide solutions that are more accurate than those obtained from the first two methods. However, for some integral equations, solutions resulting from application of WAGNER's method become unstable, especially for large values of the independent variable[3]. In such cases this technique may not be a suitable method of solution.

We have developed a method of numerical analysis based on a polynomial approximate function of any desired degree. This technique is apparently convergent for all values of the independent variable. When the approximate function is a parabola, the results are as accurate, or more accurate, than WAGNER's method under its best conditions of stability. Relationships necessary for use of this method and results of calculations for a specific example are presented here.

DEVELOPMENT OF THE METHOD

Generalized kernels

A Volterra integral equation of the second kind may be written

$$F(x) = bf(x) + \int_0^x f(z)K(x,z)\mathrm{d}z \qquad (1)$$

Here $f(x)$ is the unknown function, and $F(x)$ and the kernel, $K(x,z)$, are expressions of known form. If the constant, b, is zero, eqn. (1) is a Volterra integral equation of the first kind.

The domain of x for which a solution of eqn. (1) is required is divided into N equal intervals of width, $k\delta$. On each interval the approximate function is defined as a polynomial of degree k. Each interval $k\delta$ wide is serialized by the integer, n.

For purposes of discussion the interval, $k\delta$, will be referred to as the *interval of definition* and δ as the *interval of integration*. The serial number, l, will be used to identify a particular interval of integration on the interval of definition being considered, *i.e.*, l will take on values $l=1,2,\ldots,k$ on the n-th interval of definition.

For values of the independent variable in eqn. (1) on the n-th interval of definition

$$(n-1)k\delta \leq x \leq nk\delta \tag{2}$$

the polynomial approximation is

$$f_n(x) = \sum_{j=1}^{k}[x-(n-1)k\delta]^j a_j^{(n)} + \sum_{i=1}^{n-1}\sum_{j=1}^{k}(k\delta)^j a_j^{(i)} + f(0) \tag{3}$$

The coefficients, $a_j^{(n)}$, once determined, permit calculation of the approximate function on the interval defined by eqn. (2). It is assumed that the coefficients, $a_j^{(i)}$, $(i<n)$ have been determined previously. The value of $f(0)$ may be obtained from eqn. (1).

To specify the extent of integration, the following substitution is made in eqn. (1)

$$x = m\delta \tag{4}$$

where

$$m = (n-1)k + l \tag{5}$$

The integer m is introduced only as a worthwhile construction to simplify notation in the remainder of the text. Equation (1) can then be written

$$F(m\delta) = bf_n(m\delta) + \sum_{i=1}^{n-1}\int_{(i-1)k\delta}^{ik\delta} f_i(z)K(m\delta,z)\mathrm{d}z + \int_{(m-l)\delta}^{m\delta} f_n(z)K(m\delta,z)\mathrm{d}z \tag{6}$$

Combination of eqns. (3) and (6) accompanied by a lengthy but straightforward algebraic manipulation leads to the matrix equation:

$$\boldsymbol{A}^{(n)}\boldsymbol{a}^{(n)} = \boldsymbol{g}^{(n)} \tag{7}$$

Equation (7) describes a system of k linear algebraic equations in the unknown column matrix, $\boldsymbol{a}^{(n)}$, whose elements are the k coefficients, $a_j^{(n)}$. The column matrix, $\boldsymbol{g}^{(n)}$, and the $k\times k$ coefficient matrix, $\boldsymbol{A}^{(n)}$, are determined by relationships given in Appendix A. Equation (7) may be solved for $\boldsymbol{a}^{(n)}$ provided that $\boldsymbol{A}^{(n)}$ is a non-singular matrix. The resultant column matrix, $\boldsymbol{a}^{(n)}$, is subsequently used in eqn. (3) to calculate values of the unknown function. Repeated solution of eqn. (7) for $n=1,2,\ldots,N$ results in complete description of the unknown function on the interval $0 \leq x \leq Nk\delta$.

Convolution kernels

For the special case in which eqn. (1) is of the convolution type

$$K(x,z) = K(x-z) \tag{8}$$

eqn. (7) and the auxiliary expressions in Appendix A can be simplified. In this case the matrix equation becomes

$$\boldsymbol{\alpha}\boldsymbol{a}^{(n)} = \boldsymbol{\gamma}^{(n)} \tag{9}$$

Auxiliary expressions for calculation of terms in eqn. (9) are given in Appendix B.

Volterra integral equations having convolution kernels are more easily solved than those having more general kernel functions. This fact is easily illustrated by comparing the number of numerical terms each auxiliary expression generates in the two cases. These comparisons are presented in Table 1 for three of the auxiliary expressions.

TALE 1

COMPARISON OF NUMBER OF NUMERICAL TERMS REQUIRED FOR SOLUTION OF EQUATIONS (7) AND (9) ON THE INTERVAL $[O,Nk\delta]$

Auxiliary term	*No. of numerical terms*
$A_{ij}^{(n)}$	Nk^2
$B_{ij}^{(n,i)}$	$N(N-1)k^2/2$
$V_{pq}^{(m)}$	$N(N+1)k(k+1)/2$
α_{ij}	k^2
$\beta_{ij}^{(i)}$	$(N-1)k^2$
ψ_{pq}	$Nk(k+1)$

It should be noted that terms in Table 1 taken from Appendix B are independent of the serial number of the interval of definition. This loss of dependence on n accounts for the significant reduction in the number of terms in Table 1 for convolution kernels. This feature simplifies solution of eqn. (9) for $\boldsymbol{a}^{(n)}$ because the inverse of the matrix, $\boldsymbol{\alpha}$, need be determined only once[4].

DISCUSSION OF THE METHOD

The present technique may be viewed as a method that produces polynomials that satisfy the integral equation on each interval of definition. Polynomials generated in this manner accurately approximate the unknown function. The complete approximate function is a piece-wise smooth curve[5] consisting of these polynomial segments. The approximate function is restricted by the relationship (see eqn. (3)):

$$f_{n+1}(nk\delta) = f_n(nk\delta) \tag{10}$$

This restriction states that the approximate function possesses a common limit from the right and left at the end-point of each interval of definition.

Comparison with previous methods

The method described here for polynomials of degree, $k=1$, reduces to the method of HUBER. Thus HUBER's method may be regarded as a particular case of this general treatment.

The present method with $k=2$, however, is not the same as the parabolic method of WAGNER, because of differences in definition of the parabolic approximations. WAGNER's definition is restricted by the condition that the parabola must satisfy the last two calculated function values, and the unknown function value being determined. Therefore, the parabolic approximate function possesses only one undetermined parameter which may be strongly influenced by prior calculations. These restrictions are in sharp contrast to the single restriction (eqn. (10)) placed

on the present method. Furthermore, initiation of calculation by WAGNER's method always requires an independent technique to determine the function value at the mid-point of the first integration interval. Both techniques require numerical evaluation of the same number of auxiliary terms. All these considerations indicate that when the accuracy of a parabolic approximation is desired, the present method is preferable to WAGNER's method.

Non-linear integral equations

Polynomial approximations also can be used to solve non-linear Volterra integral equations. It is not possible, however, to develop a general procedure like the one for solution of eqn. (1). The present technique may be applied if the non-linearity does not occur in the integrand of the integral equation. In such cases application of a polynomial approximation on each interval of definition results in a system of non-linear algebraic equations, which can be solved numerically for the unknown coefficients in eqn. (3). When the non-linearity occurs within the integrand, difficulties may be encountered in development of auxiliary numerical terms. In these cases it may be desirable to employ the step functional technique which has been applied recently to equations of this type[6].

Additional considerations

An important practical consideration in using this method is evaluation of the definite integrals in eqns. (A-6) or (B-5). For many kernel functions, these integrals will be integrable directly to algebraic forms and no serious difficulties are presented. When this is not the case, some approximate numerical method of integration must be used. If the number of integrals is large (large N in Table 1), the number of computations required for numerical integration consistent with good accuracy may impose limitations on the method. In these cases application may be restricted to use of the quadratic approximate function.

ILLUSTRATION OF THE METHOD

To illustrate the method developed above, we have applied it to calculation of the unknown function in the following equation:

$$\frac{1-\exp(-x)}{1+\exp(c-x)} = \frac{1}{\sqrt{\pi}} \int_0^x \frac{f(z)\mathrm{d}z}{\sqrt{x-z}} \tag{11}$$

Equation (11) is a singular Volterra integral equation of the first kind, which appears in the theory of stationary electrode polarography[1]. Equation (11) also is an Abel integral equation, and its solution can be written directly

$$f(x) = \frac{(1+\exp(-c))}{4\sqrt{\pi}} \int_0^x \frac{\mathrm{d}z}{\sqrt{x-z}\cosh^2(\frac{1}{2}c-\frac{1}{2}z)} \tag{12}$$

Equation (12) was used to check the results of approximate numerical calculations.

Equation (11) was solved numerically with a digital computer by successive application of eqn. (9) for polynomial approximations of degree one, two, three, and four, with $c=7.0$. Preliminary calculations were performed for a number of values

of $Nk\delta$ ($5 \leq Nk\delta \leq 10$). Results of these calculations showed that for a given polynomial approximation, $f_N(Nk\delta)$ converged to the correct value of the unknown function at a rate very nearly independent of $Nk\delta$. Therefore, results of these calculations are summarized in Fig. 1 for only one particular value of $Nk\delta$ (=8.1094). This point very nearly corresponds to a maximum in $f(x)$ which is of polarographic interest[1]. In Fig. 1, $f_N(Nk\delta)$ is plotted *versus* the size of the interval of definition used in the calculation. For purposes of comparison Fig. 1 also includes results of calculations for the step function method and WAGNER's method. To make a valid comparison between our parabolic method and WAGNER's method, $k\delta$ for WAGNER's method was chosen as twice the integration interval originally defined by WAGNER.

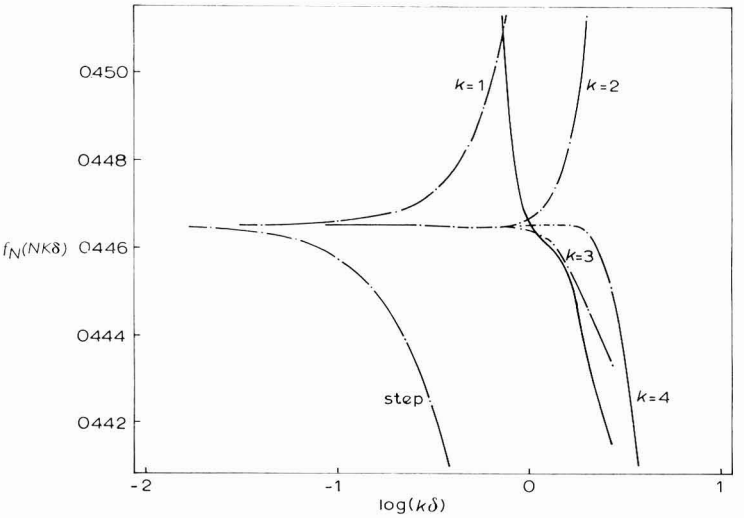

Fig. 1. Variation of $f_N(Nk\delta)$ with $k\delta$. $Nk\delta = 8.1094$; correct value of $f_N(Nk\delta) = 0.44653$. (—) Wagner's method.

Several interesting conclusions can be drawn from the data of Fig. 1. For example, as δ is decreased, all the results converge to the correct answer, except for WAGNER's method. In this case answers correct within 1% are obtained only for δ on the interval, $0.37 < \delta < 1.25$. For large δ on this interval, WAGNER's method gives results of accuracy comparable with our parabolic method. However, for values of δ outside this interval results of WAGNER's method rapidly become uncertain because of instability. In the case of eqn. (11), for values of $Nk\delta$ greater than 8.1, the uncertainty resulting from instability becomes more severe. Thus, with WAGNER's method accurate results are obtained only by fortuitous choice of an optimum value of δ, and an indication of the correct answer cannot be obtained simply by decreasing δ. It should be pointed out, however, that these conclusions apply only for the particular integral equation considered (eqn. (11)). Nevertheless, as WAGNER has indicated[3], similar conclusions may result in other cases when the independent variable becomes large.

APPENDIX A

Equation (7) is the matrix form for the k linear equations produced by

$$\sum_{j=1}^{k} A_{lj}{}^{(n)} a_j{}^{(n)} = g_l{}^{(n)} \tag{A-1}$$

One equation results for each value of l, $l=1,2,\ldots,k$. The l-th row and j-th column element of $\boldsymbol{A}^{(n)}$ is:

$$A_{lj}{}^{(n)} = \sum_{q=0}^{j} \binom{j}{q} [(l-m)\delta]^{j-q} [V_{mq}{}^{(m)} - V_{m-l,q}{}^{(m)}] + b(l\delta)^j \tag{A-2}$$

Elements of the column vector $\boldsymbol{g}^{(n)}$, are:

$$g_l{}^{(n)} = F(m\delta) - f(0)[V_{m0}{}^{(m)} + b] - \sum_{i=1}^{n-1} \sum_{j=1}^{k} B_{lj}{}^{(n,i)} a_j{}^{(i)} \tag{A-3}$$

where

$$B_{lj}{}^{(n,i)} = T_{mj}{}^{(i)} + (k\delta)^j [V_{m0}{}^{(m)} - V_{ik,0}{}^{(m)} + b] \tag{A-4}$$

$$T_{mj}{}^{(i)} = \sum_{q=0}^{j} \binom{j}{q} [(1-i)k\delta]^{j-q} [V_{ik,q}{}^{(m)} - V_{(i-1)k,q}{}^{(m)}] \tag{A-5}$$

$$V_{pq}{}^{(m)} = \int_0^{p\delta} z^q K(m\delta, z)\mathrm{d}z \tag{A-6}$$

The notation $\binom{j}{q}$ represents the binomial coefficient

$$\binom{j}{q} = \frac{j!}{q!(j-q)!} \tag{A-7}$$

When $m=l$ and $q=j$ in the expression for $A_{lj}{}^{(1)}$, we adopt the convention that $0^0=1$; the same applies to the term $T_{mj}{}^{(1)}$ when $q=j$.

APPENDIX B

Matrix elements of $\boldsymbol{\alpha}$ in eqn. (9) are:

$$\alpha_{lj} = \sum_{q=0}^{j} \binom{j}{q} (-1)^q (l\delta)^{j-q} \Psi_{lq} + b(l\delta)^j \tag{B-1}$$

The k elements of $\boldsymbol{\gamma}^{(n)}$ are calculated according to:

$$\gamma_l{}^{(n)} = F(m\delta) - f(0)[\Psi_{m0} + b] - \sum_{i=1}^{n-1} \sum_{j=1}^{k} \beta_{lj}{}^{(i)} a_j{}^{(n-i)} \tag{B-2}$$

where

$$\beta_{lj}{}^{(i)} = \Phi_{ik+l,j} + (k\delta)^j [\Psi_{(i-1)k+l,0} + b] \tag{B-3}$$

$$\Phi_{ik+l,j} = \sum_{q=0}^{j} \binom{j}{q} (-1)^q [(ik+l)\delta]^{j-q} [\Psi_{ik+l,q} - \Psi_{(i-1)k+l,q}] \tag{B-4}$$

$$\Psi_{pq} = \int_0^{p\delta} y^q K(y)\mathrm{d}y \tag{B-5}$$

ACKNOWLEDGEMENT

Support of this work by the National Science Foundation is gratefully acknowledged.

SUMMARY

A general treatment based on polynomial approximations is presented for numerical solution of Volterra integral equations. The method is developed with a formalism that permits use of polynomials of any degree. In general, as the degree of the polynomial is increased, accuracy of solutions also is improved. The new procedure is illustrated by solving an integral equation of stationary electrode polarographic interest. The same equation also is solved by other numerical methods used previously, and it is concluded that the new method is preferable when accurate solutions are required.

The new method also is capable of providing accurate solutions of integral equations even when the independent variable is very large. This fact should make it possible to treat mathematically techniques such as cyclic voltammetry under conditions approaching the steady state.

REFERENCES

1 R. S. NICHOLSON AND I. SHAIN, *Anal. Chem.*, 36 (1964) 706.
2 A. HUBER, *Monatsh. Mathemat. Phys.*, 47 (1939) 240.
3 C. WAGNER, *J. Math. Phys.*, 32 (1954) 289.
4 A. H. FOX, *Fundamentals of Numerical Analysis*, Ronald Press, New York, 1963, p. 17.
5 T. M. APOSTOL, *Mathematical Analysis*, Addison Wesley, Reading, Mass., 1957, p. 233.
6 R. S. NICHOLSON, *Anal. Chem.*, 37 (1965) 667.

ELECTROANALYTICAL CHEMISTRY AND INTERFACIAL ELECTROCHEMISTRY
Elsevier Sequoia S.A., Lausanne – Printed in The Netherlands

ZUR THEORIE DER ELEKTROLYSE MIT ZWEI ENG BENACHBARTEN ELEKTRODEN IN STRÖMUNGSANORDNUNGEN. ALLGEMEINE FORMEL FÜR DIE ÜBERTRAGUNGSAUSBEUTE

HIROAKI MATSUDA
Government Chemical Industrial Research Institute, Tokyo, Hon-machi, Shibuya-ku, Tokio (Japan)
(Eingegangen den 4. April, 1967)

EINLEITUNG

Für die Bestätigung des Reaktionsmechanismus von Elektrodenvorgängen ist die direkte Erfassung der Reaktions- oder Zwischenprodukte ausserordentlich wertvoll. Frumkin und Mitarbeiter[1] haben zuerst ein elegantes Verfahren für solche direkte Erfassung vorgeschlagen, bei dem eine rotierende Scheibenelektrode als erzeugende Elektrode verwendet wird, die von einem konzentrischen Ring als Indikatorelektrode umgeben ist. Bei diesem Verfahren lassen sich die Reaktionsprodukte, die an der Oberfläche der Scheibenelektrode entstehen, durch radiale Abströmung von der Rotationsachse zur Ringelektrode überführen und an deren Oberfläche analysieren. Um die hohe Empfindlichkeit zu erhalten, ist es notwendig, für die möglichst schnelle und vollständige Überführung der Reaktionsprodukte von der erzeugenden Elektrode zur Indikatorelektrode zu sorgen. Diese Bedingung lässt sich dann erfüllen, wenn die Reaktionsprodukte in engster Benachbarschaft zur Indikatorelektrode erzeugt und ferner durch die möglichst schnelle Strömung zur Indikatorelektrode transportiert werden. Unter Berücksichtigung dieser Verhältnisse haben Gerischer und Mitarbeiter[2] in den letzteren Jahren eine Kanalanordnung vorgeschlagen, bei der sich die Versuchslösung an zwei eng benachbarten, flach in der Wand liegenden Elektroden vorüberströmen lässt.

Der wichtige Faktor für die Verfahren mit zwei eng benachbarten Elektroden ist die Übertragungsausbeute, d.h. die Effektivität der Überführung zur Indikatorelektrode, für die das Verhältnis N zwischen dem Indikatorstrom I_2 und dem Erzeugerstrom I_1 charakteristisch ist. Für das Ring-Scheibensystem ist die theoretische Behandlung über N bereits näherungsweise von Lewitsch und Iwanow[3] und später in exakter Weise von Albery und Bruckenstein[4] durchgeführt worden. Anderseits haben Gerischer und Mitarbeiter in der oben benannten Arbeit[2] die Grösse von N für die Kanalanordnung näherungsweise abgeschätzt.

Unter Berücksichtigung der Wichtigkeit der Verfahren mit zwei eng benachbarten Elektroden in dem Bereich der Elektrodenkinetik wollen wir in der vorliegenden Arbeit den allgemeinen Ausdruck für das Verhältnis N ableiten, der für verschiedene Strömungsanordnungen gilt. Als Beispiele der praktischen Anwendung sollen einige Strömungsanordnungen behandelt und diskutiert werden.

(1) Beziehung zwischen der Konzentration und dem Konzentrationsgradient an der Elektrodenoberfläche

Zuerst wollen wir die allgemeine Beziehung zwischen der Konzentration und dem Konzentrationsgradient an der Elektrodenoberfläche ermitteln, mit deren Hilfe die nachfolgenden Rechnungen durchgeführt werden können.

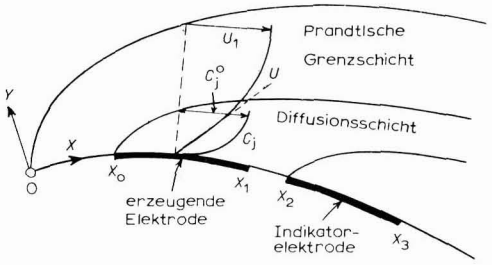

Abb. 1. Koordinatensystem und Zeichen bei zweidimensionalen Strömungen.

Wenn man die in Abb. 1 gegebenen krummlinigen Koordinaten (x, y) benützt, so erhält man folgende Differentialgleichung für die Konzentrationsverteilung des Depolarisators S_j in der Nähe der Elektrodenoberfläche im stationären Zustand:

$$u\frac{\partial C_j}{\partial x} + v\frac{\partial C_j}{\partial y} = D_j\frac{\partial^2 C_j}{\partial y^2}, \tag{1}$$

mit

$$u = \frac{\partial \psi}{\partial y}, \qquad v = -\frac{\partial \psi}{\partial x}. \tag{2}$$

Hierbei bedeuten:

x = Abstand, gemessen längs der Oberfläche des Festkörpers vom Anfang der Prandtlschen Grenzschicht

y = Abstand von der Oberfläche des Festkörpers

u, v = x- bzw. y-Komponenten der Strömungsgeschwindigkeit in der Prandtlschen Grenzschicht

C_j, D_j = Konzentration bzw. Diffusionskoeffizient des Depolarisators S_j

ψ = Stokessche Stromfunktion

Wir nehmen ferner an, dass die Prandtlsche Grenzschicht und die Diffusionsschicht an $x=0$ bzw. an $x=x_0$ beginnen, wie in Abb. 1 gezeigt ist. Dabei lässt sich die Randbedingung unmittelbar ausserhalb der Diffusionsschicht angeben durch

$$\left.\begin{array}{l} x<x_0\,, \quad y>0 \\ x>x_0\,, \quad y\to\infty \end{array}\right\}: \quad C_j = C_j^0 \tag{3}$$

wobei C_j^0 die Konzentration des Depolarisators S_j im Innern der Lösung ist. Anderseits kann die Randbedingung an der Elektrodenoberfläche folgendermassen ausgedrückt werden:

$$x > x_0\,, \quad y = 0: \quad D_j(\partial C_j/\partial y) = f_j(x)\,, \tag{4}$$

wobei $f_j(x)$ eine beliebige Funktion von x ist.

Bei Flüssigkeiten ist im allgemeinen die Prandtlsche Zahl von der Grössenordnung 10^3. Wie in der früheren Arbeit[5] gezeigt worden ist, lässt sich damit die Strömungskomponente u innerhalb der Diffusionsschicht durch erstes Glied der Taylorschen Reihe in bezug auf y approximieren. Wir erhalten

$$u = (\partial u/\partial y)_{y=0}\, y = [\tau(x)/\mu]y\,, \tag{5}$$

wobei $\tau(x)$ die Wandschubspannung bedeutet und μ die innere Reibung ist. Daher ergibt sich aus Gl. (2)

$$\psi = \int_0^y u\,\mathrm{d}y = [\tau(x)/2\mu]y^2 \tag{6}$$

und also folgt aus Gln. (5) und (6)

$$u = [2\tau(x)/\mu]^{\frac{1}{2}}\psi^{\frac{1}{2}}\,. \tag{7}$$

Wenn man an stelle von x und y die Stromfunktion ψ und

$$t = \int_{x_0}^{x} [2\tau(x)/\mu]^{\frac{1}{2}}\,\mathrm{d}x \tag{8}$$

als neue unabhängige Variablen benützt, so kann die Differentialgleichung (1) unter Berücksichtigung der Gln. (6) und (7) transformiert werden in

$$\frac{\partial C_j}{\partial t} = D_j \frac{\partial}{\partial \psi}\left(\psi^{\frac{1}{2}} \frac{\partial C_j}{\partial \psi}\right) \tag{9}$$

mit den transformierten Randbedingungen:

$$\left.\begin{array}{ll} \left.\begin{array}{l} t=0 \\ \psi\to\infty \end{array}\right\}: & C_j = C_j^0 \\ \psi = 0 \quad : & f_j = D_j(2\tau/\mu)^{\frac{1}{2}}\psi^{\frac{1}{2}}\left(\dfrac{\partial C_j}{\partial \psi}\right) \end{array}\right\} \tag{10}$$

Dieses Differentialgleichungssystem ist bereits in der früheren Arbeit[5] durch Anwendung der Laplace-Transformation aufgelöst worden. Nach unserem Ergebnis lautet die Oberflächenkonzentration

$$(C_j)_{y=0} = C_j^0 - \frac{(\frac{2}{3})^{\frac{1}{3}}}{\Gamma(\frac{2}{3})} D_j^{-\frac{2}{3}} \int_0^t \frac{(2\tau/\mu)^{-\frac{1}{2}} f_j\,\mathrm{d}t'}{(t-t')^{\frac{2}{3}}} \tag{11}$$

oder unter Berücksichtigung der Gl. (8)

$$(C_j)_{y=0} = C_j^0 - \frac{(\frac{1}{3})^{\frac{1}{3}}}{\Gamma(\frac{2}{3})} D_j^{-\frac{2}{3}} \mu^{\frac{1}{3}} \int_{x_0}^{x} \frac{f_j(x')\mathrm{d}x'}{\left\{\int_{x'}^{x} [\tau(x'')]^{\frac{1}{2}}\,\mathrm{d}x''\right\}^{\frac{2}{3}}} \tag{12}$$

Gln. (11) oder (12) sind die zu erhaltende Beziehung zwischen $(C_j)_{y=0}$ und $f_j(x)$ bei zweidimensionalen Strömungen.

(2) *Ermittelung des Ausdruckes für den Erzeugerstrom*

Zunächst soll der Erzeugerstrom I_1 ermittelt werden. Wir nehmen hier an,

dass an der Oberfläche der erzeugenden Elektrode der Stoff S_1 elektrochemisch in den Stoff S_2 reduziert oder oxydiert wird nach dem Schema:

$$S_1 \pm n_1 e \rightleftarrows S_2 , \tag{13}$$

wobei n_1 die Zahl der Elektronen bedeutet, die bei der Elektrodenreaktion aufgenommen bzw. angegeben werden. Darin gilt ferner das obere Vorzeichen (+) für die Reduktion und das untere (−) für die Oxydation. Bei der Bedingung des Grenzstromes in bezug auf S_1 gilt $(C_1)_{y=0}=0$. Aus Gl. (11) für S_1 ergibt sich damit folgende Abelsche Integralgleichung:

$$\int_0^t \frac{(2\tau/\mu)^{-\frac{1}{2}} f_1}{(t-t')^{\frac{2}{3}}}\,dt' = \frac{\Gamma(\frac{2}{3})}{(\frac{2}{3})^{\frac{1}{3}}} C_1^0 D_1^{\frac{2}{3}} . \tag{14}$$

Diese Integralgleichung lässt sich folgendermassen auflösen. Ersetzt man t in Gl. (14) durch t'', multipliziert dann die beiden Seiten der erhaltenen Gleichung mit

$$(t-t'')^{-\frac{1}{3}}$$

und integriert von Null bis t, so erhält man

$$\Gamma(\tfrac{1}{3}) \int_0^t (2\tau/\mu)^{-\frac{1}{2}} f_1\,dt' = (\tfrac{2}{3})^{-\frac{4}{3}} C_1^0 D_1^{\frac{2}{3}} t^{\frac{2}{3}} ,$$

wobei folgende Rechnung zur Anwendung gelangte:

$$\int_0^t \left\{ \int_0^{t''} \frac{(2\tau/\mu)^{-\frac{1}{2}} f_1}{(t''-t')^{\frac{2}{3}}}\,dt' \right\} \frac{dt''}{(t-t'')^{\frac{1}{3}}}$$

$$= \int_0^t \left\{ \int_{t'}^t \frac{dt''}{(t-t'')^{\frac{1}{3}}(t''-t')^{\frac{2}{3}}} \right\} (2\tau/\mu)^{-\frac{1}{2}} f_1\,dt'$$

$$= \Gamma(\tfrac{1}{3})\Gamma(\tfrac{2}{3}) \int_0^t (2\tau/\mu)^{-\frac{1}{2}} f_1\,dt' .$$

Nach Differentiation der obigen Gleichung in bezug auf t folgt

$$f_1 = \{(\tfrac{2}{3})^{\frac{1}{3}} \Gamma(\tfrac{1}{3})\}^{-1} C_1^0 D_1^{\frac{2}{3}} (2\tau/\mu)^{\frac{1}{2}} t^{-\frac{1}{3}} . \tag{15}$$

Die Stromdichte i_1 ist proportional zu dem Konzentrationsgradient von S_1 an der Elektrodenoberfläche. Damit erhalten wir für die Erzeugerstromdichte i_1 unter Berücksichtigung der Gl. (8)

$$i_1 = \pm n_1 F f_1 = \pm \frac{3^{\frac{1}{3}}}{\Gamma(\frac{1}{3})} n_1 F C_1^0 D_1^{\frac{2}{3}} \mu^{-\frac{1}{3}} \frac{\tau^{\frac{1}{2}}}{\left[\int_{x_0}^{x} \tau^{\frac{1}{2}}\,dx\right]^{\frac{1}{3}}} \tag{16}$$

wobei das obere und untere Vorzeichen der Reduktions- bzw. Oxydationselektrodenreaktion entspricht.

Die Gesamterzeugerstromstärke I_1 lässt sich durch Integration über die gesamte Oberfläche der erzeugenden Elektrode erhalten. Wenn sich die erzeugende Elektrode von x_0 bis x_1 erstreckt, wie in Abb. 1 gezeigt ist, so erhalten wir

$$I_1 = \int_{x_0}^{x_1} i_1 \, dx = \pm \frac{3^{\frac{4}{3}}}{2\Gamma(\frac{1}{3})} n_1 F C_1^0 D_1^{\frac{2}{3}} \mu^{-\frac{1}{3}} \left[\int_{x_0}^{x_1} \tau^{\frac{1}{2}} dx \right]^{\frac{2}{3}} . \tag{17}$$

(3) *Ermittelung der Ausdrücke für den Indikatorstrom und für N*

Im folgenden wollen wir den Ausdruck des Indikatorstromes I_2 ermitteln. Wir nehmen an, dass das Reaktionsprodukt S_2, das an der Oberfläche der ersten Elektrode (x_0---x_1) erzeugt worden ist, ferner an der Oberfläche der Indikatorelektrode (x_2---x_3) in den Stoff S_3 (der mit den Stoff S_1 identisch sein mag) reduziert oder oxydiert wird nach dem Schema:

$$S_2 \pm n_2 e \rightleftarrows S_3 \tag{18}$$

wobei n_2 die Zahl der Elektronen bedeutet, die bei der Elektrodenreaktion (18) aufgenommen bzw. abgegeben werden. Für die Reduktion gilt das obere (+) und für die Oxydation das untere (−) Vorzeichen der Gl. (18).

Bei der Bedingung des Grenzstromes in bezug auf S_2 erhalten wir folgende Bedingung für den Stoff S_2:

$$\left.\begin{aligned} &x_0 < x < x_1: \quad f_2 = -f_1 \\ &x_1 < x < x_2: \quad f_2 = 0 \\ &x_2 < x: \qquad (C_2)_{y=0} = 0 . \end{aligned}\right\} \tag{19}$$

Führen wir die obige Bedingung in Gl. (11) für S_2 ein, so erhalten wir damit unter Berücksichtigung der Gl. (15)

$$\frac{C_1^0 D_1^{\frac{2}{3}}}{(\frac{2}{3})^{\frac{1}{3}} \Gamma(\frac{1}{3})} \int_0^{t_1} \frac{dt'}{(t')^{\frac{1}{3}}(t-t')^{\frac{2}{3}}} = \int_{t_2}^{t} \frac{(2\tau/\mu)^{-\frac{1}{2}} f_2}{(t-t')^{\frac{2}{3}}} dt' \tag{20}$$

mit

$$t_j = \int_{x_0}^{x_j} [2\tau(x)/\mu]^{\frac{1}{2}} dx \qquad (j = 1, 2) . \tag{21}$$

Hierbei ist es angenommen, dass die Konzentration von S_2 im Innern der Lösung gleich Null ist. Das Integral auf der linken Seite der Gl. (20) lässt sich durch Einführung von $\xi = t'/(t-t')$ als neue Integrationsvariable ermitteln. Wir erhalten

$$\int_{t_2}^{t} \frac{(2\tau/\mu)^{-\frac{1}{2}} f_2}{(t-t')^{\frac{2}{3}}} dt' = \frac{\Gamma(\frac{2}{3})}{(\frac{2}{3})^{\frac{1}{3}}} C_1^0 D_1^{\frac{2}{3}} G\left(\frac{t_1}{t-t_1}\right)$$

mit

$$\begin{aligned} G(\theta) &= \frac{3^{\frac{1}{2}}}{2\pi} \int_0^{\theta} \frac{d\xi}{\xi^{\frac{1}{3}}(1+\xi)} \\ &= \frac{3^{\frac{1}{2}}}{4\pi} \ln \frac{1+\theta}{(1+\theta^{\frac{1}{3}})^3} + \frac{3}{2\pi} \tan^{-1}\left(\frac{2\theta^{\frac{1}{3}}-1}{3^{\frac{1}{2}}}\right) + \tfrac{1}{4} \end{aligned} \tag{22}$$

Die obige Gleichung ist die Abelsche Integralgleichung, deren Lösung mit Hilfe des gleichen Rechnungsverfahrens erhalten werden kann, wie bei der Ermittelung der Erzeugerstromdichte i_1 benützt worden ist. Für $x > x_2$ ergibt sich damit

$$f_2 = \frac{1}{(\frac{2}{3})^{\frac{1}{3}}\Gamma(\frac{1}{3})} C_1^0 D_1^{\frac{2}{3}} (2\tau/\mu)^{\frac{1}{2}} \frac{\mathrm{d}}{\mathrm{d}t} \int_{t_2}^{t} G\left(\frac{t_1}{t'-t_1}\right) \frac{\mathrm{d}t'}{(t-t')^{\frac{1}{3}}} \tag{23}$$

Das Integral in Gl. (23) ist im Anhang (S. 163) ermittelt. Wir erhalten daraus

$$f_2 = \{(\tfrac{2}{3})^{\frac{1}{3}}\Gamma(\tfrac{1}{3})\}^{-1} C_1^0 D_1^{\frac{2}{3}} (2\tau/\mu)^{\frac{1}{2}} \times \left\{(t-t_2)^{-\frac{1}{3}} G\left(\frac{t_1}{t_2-t_1}\right) - t^{-\frac{1}{3}} G\left(\frac{t_1}{t}\,\frac{t-t_2}{t_2-t_1}\right)\right\} . \tag{24}$$

Die Indikatorstromdichte i_2 ist proportional zu dem Konzentrationsgradient von S_2 an der Oberfläche der Indikatorelektrode. Daraus ergibt sich unter Berücksichtigung der Beziehungen (8) und (21)

$$\begin{aligned} i_2 &= \pm n_2 F f_2 \\ &= \pm \frac{3^{\frac{1}{3}}}{\Gamma(\frac{1}{3})} n_2 F C_1^0 D_1^{\frac{2}{3}} \mu^{-\frac{1}{3}} \tau^{\frac{1}{2}} \\ &\quad \times \left\{ \left(\int_{x_2}^{x} \tau^{\frac{1}{2}}\,\mathrm{d}x\right)^{-\frac{1}{3}} G\left(\frac{\int_{x_0}^{x_1} \tau^{\frac{1}{2}}\,\mathrm{d}x}{\int_{x_1}^{x_2} \tau^{\frac{1}{2}}\,\mathrm{d}x}\right) - \left(\int_{x_0}^{x} \tau^{\frac{1}{2}}\,\mathrm{d}x\right)^{-\frac{1}{3}} G\left(\frac{\int_{x_0}^{x_1} \tau^{\frac{1}{2}}\,\mathrm{d}x}{\int_{x_0}^{x} \tau^{\frac{1}{2}}\,\mathrm{d}x}\,\frac{\int_{x_2}^{x} \tau^{\frac{1}{2}}\,\mathrm{d}x}{\int_{x_1}^{x_2} \tau^{\frac{1}{2}}\,\mathrm{d}x}\right) \right\} \end{aligned} \tag{25}$$

wobei das obere und untere Vorzeichen der Reduktions- bzw. Oxydationselektrodenreaktion entspricht. Für die Gesamtindikatorstromstärke I_2 erhalten wir

$$I_2 = \int_{x_2}^{x_3} i_2\,\mathrm{d}x = \pm n_2 F \int_{t_2}^{t_3} f_2 [2\tau/\mu]^{-\frac{1}{2}}\,\mathrm{d}t \tag{26}$$

Setzen wir den Ausdruck (23) für f_2 in Gl. (26) ein, so erhalten wir nach Durchführung der angegebenen Integration

$$\begin{aligned} I_2 = \pm \frac{3^{\frac{4}{3}}}{2\Gamma(\frac{1}{3})} n_2 F C_1^0 D_1^{\frac{2}{3}} \mu^{-\frac{1}{3}} \\ \times \left\{ \left(\int_{x_2}^{x_3} \tau^{\frac{1}{2}}\,\mathrm{d}x\right)^{\frac{2}{3}} G\left(\frac{\int_{x_0}^{x_1} \tau^{\frac{1}{2}}\,\mathrm{d}x}{\int_{x_1}^{x_2} \tau^{\frac{1}{2}}\,\mathrm{d}x}\right) + \left(\int_{x_0}^{x_1} \tau^{\frac{1}{2}}\,\mathrm{d}x\right)^{\frac{2}{3}} G\left(\frac{\int_{x_2}^{x_3} \tau^{\frac{1}{2}}\,\mathrm{d}x}{\int_{x_1}^{x_2} \tau^{\frac{1}{2}}\,\mathrm{d}x}\right) \right. \\ \left. - \left(\int_{x_0}^{x_3} \tau^{\frac{1}{2}}\,\mathrm{d}x\right)^{\frac{2}{3}} G\left(\frac{\int_{x_0}^{x_1} \tau^{\frac{1}{2}}\,\mathrm{d}x}{\int_{x_0}^{x_3} \tau^{\frac{1}{2}}\,\mathrm{d}x}\,\frac{\int_{x_2}^{x_3} \tau^{\frac{1}{2}}\,\mathrm{d}x}{\int_{x_1}^{x_2} \tau^{\frac{1}{2}}\,\mathrm{d}x}\right) \right\} \end{aligned} \tag{27}$$

Daher ergibt sich aus Gln. (17) und (27) für das Verhältnis N

$$N = |I_2/I_1|$$

$$= \frac{n_2}{n_1}\left\{\left(\frac{\int_{x_2}^{x_3}\tau^{\frac{1}{2}}\,dx}{\int_{x_0}^{x_1}\tau^{\frac{1}{2}}\,dx}\right)^{\frac{2}{3}} G\left(\frac{\int_{x_0}^{x_1}\tau^{\frac{1}{2}}\,dx}{\int_{x_1}^{x_2}\tau^{\frac{1}{2}}\,dx}\right) + G\left(\frac{\int_{x_2}^{x_3}\tau^{\frac{1}{2}}\,dx}{\int_{x_1}^{x_2}\tau^{\frac{1}{2}}\,dx}\right)\right.$$

$$\left. - \left(\frac{\int_{x_0}^{x_3}\tau^{\frac{1}{2}}\,dx}{\int_{x_0}^{x_1}\tau^{\frac{1}{2}}\,dx}\right)^{\frac{2}{3}} G\left(\frac{\int_{x_0}^{x_1}\tau^{\frac{1}{2}}\,dx}{\int_{x_0}^{x_3}\tau^{\frac{1}{2}}\,dx}\,\frac{\int_{x_2}^{x_3}\tau^{\frac{1}{2}}\,dx}{\int_{x_1}^{x_2}\tau^{\frac{1}{2}}\,dx}\right)\right\} \tag{28}$$

Gl. (28) ist der allgemeine Ausdruck für N bei zweidimensionalen Strömungen.

BEI DREIDIMENSIONALEN ROTATIONSSYMMETRISCHEN STRÖMUNGEN

Wie in der früheren Arbeit[5] gezeigt worden ist, lässt sich die Beziehung zwischen der Konzentration und dem Konzentrationsgradient des Depolarisators an der Elektrodenoberfläche bei den dreidimensionalen rotationssymmetrischen Strömungen ausdrücken durch

$$(C_j)_{y=0} = C_j^0 - \frac{(\frac{2}{3})^{\frac{1}{3}}}{\Gamma(\frac{2}{3})} D_j^{-\frac{2}{3}} \int_0^t \frac{(2r_0\tau/\mu)^{-\frac{1}{2}} f_j}{(t-t')^{\frac{2}{3}}}\,dt' \tag{29}$$

mit

$$t = \int_{x_0}^{x} [2r_0(x)^3\,\tau(x)/\mu]^{\frac{1}{2}}\,dx \tag{30}$$

Hierbei bedeuten:

x = Abstand, gemessen längs der Meridiankurve des Rotationskörpers von dem Anfang der Prandtlschen Grenzschicht

y = Abstand von der Oberfläche des Rotationskörpers

r_0 = Abstand des Punktes $(x, 0)$ an der Oberfläche des Rotationskörpers von der Rotationsachse

Infolgedessen können wir mit Hilfe der ganz gleichen Rechnungsverfahren die Ausdrücke für die Erzeuger- und Indikatorstromdichte ermitteln, wie bei den zweidimensionalen Strömungen benützt worden ist. Die Ergebnisse lauten

$$i_1 = \pm \frac{3^{\frac{1}{3}}}{\Gamma(\frac{1}{3})} n_1 F C_1^0 D_1^{\frac{2}{3}} \mu^{-\frac{1}{3}} \frac{(r_0\tau)^{\frac{1}{2}}}{\left[\int_{x_0}^{x}(r_0^3\tau)^{\frac{1}{2}}\,dx\right]^{\frac{1}{3}}} \tag{31}$$

$$i_2 = \pm \frac{3^{\frac{1}{3}}}{\Gamma(\frac{1}{3})} n_2 F C_1^0 D_1^{\frac{2}{3}} \mu^{-\frac{1}{3}} (r_0\tau)^{\frac{1}{2}} \times \left\{\left(\int_{x_2}^{x}[r_0^3\tau]^{\frac{1}{2}}\,dx\right)^{-\frac{1}{3}} G\left(\frac{\int_{x_0}^{x_1}[r_0^3\tau]^{\frac{1}{2}}\,dx}{\int_{x_1}^{x_2}[r_0^3\tau]^{\frac{1}{2}}\,dx}\right)\right.$$

$$\left. - \left(\int_{x_0}^{x}[r_0^3\tau]^{\frac{1}{2}}\,dx\right)^{-\frac{1}{3}} G\left(\frac{\int_{x_0}^{x_1}[r_0^3\tau]^{\frac{1}{2}}\,dx}{\int_{x_0}^{x}[r_0^3\tau]^{\frac{1}{2}}\,dx}\,\frac{\int_{x_2}^{x}[r_0^3\tau]^{\frac{1}{2}}\,dx}{\int_{x_1}^{x_2}[r_0^3\tau]^{\frac{1}{2}}\,dx}\right)\right\} \tag{32}$$

Damit ergeben sich für die gesamte Erzeuger- und Indikatorstromstärke

$$I_1 = 2\pi \int_{x_0}^{x_1} i_1 r_0 \mathrm{d}x = \pm \frac{3^{\frac{4}{3}}\pi}{\Gamma(\frac{1}{3})} n_1 F C_1^0 D_1^{\frac{2}{3}} \mu^{-\frac{1}{3}} \left(\int_{x_0}^{x_1} [r_0^3 \tau]^{\frac{1}{2}} \mathrm{d}x \right)^{\frac{2}{3}} \tag{33}$$

$$\begin{aligned} I_2 &= 2\pi \int_{x_2}^{x_3} i_2 r_0 \mathrm{d}x \\ &= \pm \frac{3^{\frac{4}{3}}\pi}{\Gamma(\frac{1}{3})} n_2 F C_1^0 D_1^{\frac{2}{3}} \mu^{-\frac{1}{3}} \\ &\quad \times \left\{ \left(\int_{x_2}^{x_3} [r_0^3 \tau]^{\frac{1}{2}} \mathrm{d}x \right)^{\frac{2}{3}} G\left(\frac{\int_{x_0}^{x_1} [r_0^3 \tau]^{\frac{1}{2}} \mathrm{d}x}{\int_{x_1}^{x_2} [r_0^3 \tau]^{\frac{1}{2}} \mathrm{d}x} \right) + \left(\int_{x_0}^{x_1} [r_0^3 \tau]^{\frac{1}{2}} \mathrm{d}x \right)^{\frac{2}{3}} G\left(\frac{\int_{x_2}^{x_3} [r_0^3 \tau]^{\frac{1}{2}} \mathrm{d}x}{\int_{x_1}^{x_2} [r_0^3 \tau]^{\frac{1}{2}} \mathrm{d}x} \right) \right. \\ &\quad \left. - \left(\int_{x_0}^{x_3} [r_0^3 \tau]^{\frac{1}{2}} \mathrm{d}x \right)^{\frac{2}{3}} G\left(\frac{\int_{x_0}^{x_1} [r_0^3 \tau]^{\frac{1}{2}} \mathrm{d}x}{\int_{x_0}^{x_3} [r_0^3 \tau]^{\frac{1}{2}} \mathrm{d}x} \frac{\int_{x_2}^{x_3} [r_0^3 \tau]^{\frac{1}{2}} \mathrm{d}x}{\int_{x_1}^{x_2} [r_0^3 \tau]^{\frac{1}{2}} \mathrm{d}x} \right) \right\} \end{aligned} \tag{34}$$

Für das Verhältnis N erhalten wir daraus

$$\begin{aligned} N &= |I_2/I_1| \\ &= \frac{n_2}{n_1} \left\{ \left(\frac{\int_{x_2}^{x_3} [r_0^3 \tau]^{\frac{1}{2}} \mathrm{d}x}{\int_{x_0}^{x_1} [r_0^3 \tau]^{\frac{1}{2}} \mathrm{d}x} \right)^{\frac{2}{3}} G\left(\frac{\int_{x_0}^{x_1} [r_0^3 \tau]^{\frac{1}{2}} \mathrm{d}x}{\int_{x_1}^{x_2} [r_0^3 \tau]^{\frac{1}{2}} \mathrm{d}x} \right) + G\left(\frac{\int_{x_2}^{x_3} [r_0^3 \tau]^{\frac{1}{2}} \mathrm{d}x}{\int_{x_1}^{x_2} [r_0^3 \tau]^{\frac{1}{2}} \mathrm{d}x} \right) \right. \\ &\quad \left. - \left(\frac{\int_{x_0}^{x_3} [r_0^3 \tau]^{\frac{1}{2}} \mathrm{d}x}{\int_{x_0}^{x_1} [r_0^3 \tau]^{\frac{1}{2}} \mathrm{d}x} \right)^{\frac{2}{3}} G\left(\frac{\int_{x_0}^{x_1} [r_0^3 \tau]^{\frac{1}{2}} \mathrm{d}x}{\int_{x_0}^{x_3} [r_0^3 \tau]^{\frac{1}{2}} \mathrm{d}x} \frac{\int_{x_2}^{x_3} [r_0^3 \tau]^{\frac{1}{2}} \mathrm{d}x}{\int_{x_1}^{x_2} [r_0^3 \tau]^{\frac{1}{2}} \mathrm{d}x} \right) \right\} \end{aligned} \tag{35}$$

BEISPIELE

In den vorangehenden Abschnitten sind die allgemeinen Ausdrücke für N ermittelt worden. Für die Strömungen, bei den die Wandschubspannung $\tau(x)$ bekannt ist, können wir damit den Wert von N sehr leicht ausrechnen. Im folgenden wollen wir als Beispiele einige Strömungsanordnungen behandeln.

(1) *Strömungen an rotierenden Scheiben*

Für die Strömungen an der rotierenden Scheibe ergeben sich[6]

$$\left.\begin{aligned}\tau(x) &= 0.510(\mu\rho)^{\frac{1}{2}}\Omega^{\frac{3}{2}}x\\ r_0(x) &= x\end{aligned}\right\} \tag{36}$$

wobei ρ die Dichte der Flüssigkeit ist und Ω die Winkelgeschwindigkeit der rotierenden Scheibe bedeutet. Führen wir die obigen Beziehungen in Gl. (35) ein, so erhalten wir nach Durchführung der angegebenen Integrationen

$$N = \frac{n_2}{n_1}\left\{\left(\frac{x_3^3-x_2^3}{x_1^3-x_0^3}\right)^{\frac{2}{3}} G\left(\frac{x_1^3-x_0^3}{x_2^3-x_1^3}\right) + G\left(\frac{x_3^3-x_2^3}{x_2^3-x_1^3}\right) - \left(\frac{x_3^3-x_0^3}{x_1^3-x_0^3}\right)^{\frac{2}{3}} G\left(\frac{x_1^3-x_0^3}{x_3^3-x_0^3}\,\frac{x_3^3-x_2^3}{x_2^3-x_1^3}\right)\right\} \tag{37}$$

Diese Gleichung gilt für die konzentrische 2-fache Ringelektrode.

Bei der Ring-Scheibenelektrode ist $x_0=0$. Damit ergibt sich unmittelbar aus Gl.(37)

$$N = \frac{n_2}{n_1}\left\{\left(\frac{x_3^3-x_2^3}{x_1^3}\right)^{\frac{2}{3}} G\left(\frac{x_1^3}{x_2^3-x_1^3}\right) + G\left(\frac{x_3^3-x_2^3}{x_2^3-x_1^3}\right) - \left(\frac{x_3^3}{x_1^3}\right)^{\frac{2}{3}} G\left(\frac{x_1^3}{x_3^3}\,\frac{x_3^3-x_2^3}{x_2^3-x_1^3}\right)\right\}. \tag{38}$$

Diese Beziehung ist bereits von Albery und Bruckenstein[4] abgeleitet und diskutiert worden.

(2) *Kanal- und Rohrströmungen*

Für das Poiseuillesche Profil der Kanal- und Rohrströmung ergeben sich[7]

$$\left.\begin{aligned}\tau(x) &= 3\mu U_m/b \quad \text{(für Kanalströmung)}\\ \tau(x) &= 4\mu U_m/R \quad \text{(für Rohrströmung)}\end{aligned}\right\} \tag{39}$$

wobei bedeuten:

U_m = mittlere Strömungsgeschwindigkeit
b = halber Kanalquerschnitt
R = Halbmesser des Rohrs

Daher erhalten wir nach Einsetzen der Gl. (39) in Gl. (28) für beide Strömungen

$$N = \frac{n_2}{n_1}\left\{\left(\frac{x_3-x_2}{x_1-x_0}\right)^{\frac{2}{3}} G\left(\frac{x_1-x_0}{x_2-x_1}\right) + G\left(\frac{x_3-x_2}{x_2-x_1}\right) - \left(\frac{x_3-x_0}{x_1-x_0}\right)^{\frac{2}{3}} G\left(\frac{x_1-x_0}{x_3-x_0}\,\frac{x_3-x_2}{x_2-x_1}\right)\right\}. \tag{40}$$

Für die Kanalanordnung, bei der die zwei ebenen Bleche mit gleicher Länge l zur Erzeuger- und Indikatorelektrode dienten, haben Gerischer und Mitarbeiter[2] die Übertragungsausbeute als Funktion des Elektrodenabstandes d gemessen. Bei der Gerischerschen Anordnung lautet Gl. (40) mit $n_1=n_2$

$$N = 2G\left(\frac{1}{[d/l]}\right) - (2+[d/l]^{\frac{2}{3}}G)\left(\frac{1}{2[d/l]+[d/l]^2}\right). \tag{41}$$

Der Verlauf von N in Abhängigkeit von (d/l), der nach Gl. (41) numerisch ausgerechnet

worden ist, ist in Abb. 2 wiedergegeben. Wenn man die experimentellen Daten nach Gerischer und Mitarbeiter in derselben Abbildung einträgt, so ersieht man eine Nichtübereinstimmung zwischen den theoretischen und experimentellen Werten, insbesondere für grösseren Elektrodenabstand. Dies scheint davon zu stammen, dass die Einlaufstörung auch an den Elektroden wirksam ist, da bei der Gerischerschen Anordnung die Elektroden nur etwa einen 40-fachen Abstand von der Kanaleinmündung haben.

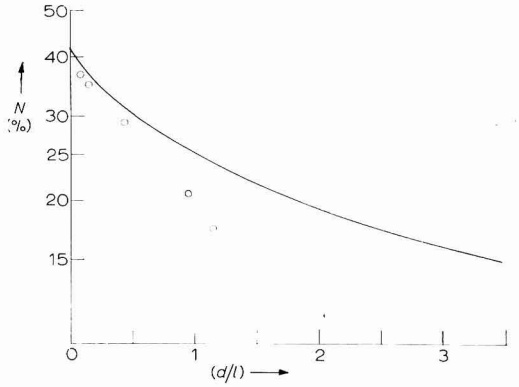

Abb. 2. Verlauf von N in Abhängigkeit von (d/l) bei der Gerischerschen Kanalströmung. (———) berechnet nach Gl. (41); (○) Messwerte nach Gerischer und Mitarbeiter[2].

(3) *Keilströmungen*

Die Wandschubspannung $\tau(x)$ für die Keilströmung lässt sich folgendermassen darstellen[8]:

$$\tau(x) = f_m\{(m+1)/2\}^{\frac{1}{3}}(\mu\rho)^{\frac{1}{2}}(U/L^m)^{\frac{1}{2}}x^{(3m-1)/2} \tag{42}$$

mit

$$m = \beta/(2-\beta)\,,$$

wobei bedeuten:

x = Abstand, gemessen längs der Keilfläche von der Spitze
$\beta\pi$ = Winkel zwischen den zwei Flächen des Keils
f_m = Konstante, die von m abhängig ist
U = Geschwindigkeit der Grundströmung
L = charakteristische Länge

Einsetzen der Gl. (42) in Gl. (28) liefert damit für N

$$N = \frac{n_2}{n_1}\left\{\left(\frac{x_3^{3(m+1)/4}-x_2^{3(m+1)/4}}{x_1^{3(m+1)/4}-x_0^{3(m+1)/4}}\right)^{\frac{2}{3}} G\left(\frac{x_1^{3(m+1)/4}-x_0^{3(m+1)/4}}{x_2^{3(m+1)/4}-x_1^{3(m+1)/4}}\right)\right.$$
$$+G\left(\frac{x_3^{3(m+1)/4}-x_2^{3(m+1)/4}}{x_2^{3(m+1)/4}-x_1^{3(m+1)/4}}\right)-\left(\frac{x_3^{3(m+1)/4}-x_0^{3(m+1)/4}}{x_1^{3(m+1)/4}-x_0^{3(m+1)/4}}\right)^{\frac{2}{3}}$$
$$\left.\times G\left(\frac{x_1^{3(m+1)/4}-x_0^{3(m+1)/4}}{x_3^{3(m+1)/4}-x_0^{3(m+1)/4}}\,\frac{x_3^{3(m+1)/4}-x_2^{3(m+1)/4}}{x_2^{3(m+1)/4}-x_1^{3(m+1)/4}}\right)\right\} \tag{43}$$

Die Fälle: $m=0$ ($\beta=0$) und $m=1$ ($\beta=1$) entsprechen der linearen Strömung längs der ebenen Platte bzw. der zweidimensionalen Staupunktströmung.

(4) *Kreiskegelströmungen*
Für die Kreiskegelströmung ergeben sich[9]

$$\left.\begin{aligned} r_0(x) &= x \sin\theta_0 \\ \tau(x) &= f_{m'}\{(m'+3)/2\}^{\frac{1}{2}}(\mu\rho)^{\frac{1}{2}}(U/L^{m'})^{\frac{1}{2}}x^{(3m'-1)/2} \end{aligned}\right\} \tag{44}$$

wobei bedeuten:

x = Abstand, gemessen längs der Kegeloberfläche von der Spitze
θ_0 = Winkel zwischen der Achse und einem beliebigen Generator des Kreiskegels
m' = Index, dessen Wert in Abhängigkeit von θ_0 durch Leuteritz und Mangler[10] ermittelt worden ist
$f_{m'}$ = Konstante, die von m' abhängig ist

Wenn man die Beziehungen (44) in Gl. (35) einsetzt und dann die angegebenen Integrationen durchführt, so erhält man für N

$$\begin{aligned} N = \frac{n_2}{n_1}\Bigg\{&\left(\frac{x_3^{3(m'+3)/4}-x_2^{3(m'+3)/4}}{x_1^{3(m'+3)/4}-x_0^{3(m'+3)/4}}\right)^{\frac{2}{3}} G\left(\frac{x_1^{3(m'+3)/4}-x_0^{3(m'+3)/4}}{x_2^{3(m'+3)/4}-x_1^{3(m'+3)/4}}\right) \\ &+ G\left(\frac{x_3^{3(m'+3)/4}-x_2^{3(m'+3)/4}}{x_2^{3(m'+3)/4}-x_1^{3(m'+3)/4}}\right) \\ &- \left(\frac{x_3^{3(m'+3)/4}-x_0^{3(m'+3)/4}}{x_1^{3(m'+3)/4}-x_0^{3(m'+3)/4}}\right)^{\frac{2}{3}} G\left(\frac{x_1^{3(m'+3)/4}-x_0^{3(m'+3)/4}}{x_3^{3(m'+3)/4}-x_0^{3(m'+3)/4}}\,\frac{x_3^{3(m'+3)/4}-x_2^{3(m'+3)/4}}{x_2^{3(m'+3)/4}-x_1^{3(m'+3)/4}}\right)\Bigg\} \end{aligned} \tag{45}$$

Der Fall: $m'=1$ ($\theta_0=\pi/2$) entspricht der dreidimensionalen Staupunktströmung.

ANHANG

Es ist folgendes Integral zu ermitteln:

$$F = \int_{t_2}^{t} G\left(\frac{t_1}{t'-t_1}\right)\frac{\mathrm{d}t'}{(t-t')^{\frac{1}{3}}}$$

Durch Anwendung der partiellen Integration auf das obige Integral erhält man

$$F = \tfrac{3}{2}(t-t_2)^{\frac{2}{3}}G\left(\frac{t_1}{t_2-t_1}\right) - \tfrac{3}{2}t_1^{\frac{2}{3}}\int_{t_2}^{t}\left(\frac{t-t'}{t'-t_1}\right)^{\frac{2}{3}}\frac{\mathrm{d}t'}{t'}$$

Führt man als neue Integrationsvariable $\xi=(t-t')/(t'-t_1)$ ein, so erhält man daraus

$$F = \tfrac{3}{2}(t-t_2)^{\frac{2}{3}}G\left(\frac{t_1}{t_2-t_1}\right) + \tfrac{3}{2}t_1^{\frac{2}{3}}G\left(\frac{t-t_2}{t_2-t_1}\right) - \tfrac{3}{2}t_1^{\frac{2}{3}}t\int_0^{(t-t_2)/(t_2-t_1)}\frac{\mathrm{d}\xi}{\xi^{\frac{2}{3}}(t+t_1\xi)}$$

Nach Einführung der neuen Integrationsvariable $\xi'=(t_1/t)\xi$ in das Integral der obigen Gleichung erhalten wir folgenden endgültigen Ausdruck:

$$F = \tfrac{3}{2}\left\{(t-t_2)^{\frac{2}{3}} G\left(\frac{t_1}{t_2-t_1}\right) + t_1^{\frac{2}{3}} G\left(\frac{t-t_2}{t_2-t_1}\right) - t^{\frac{2}{3}} G\left(\frac{t_1}{t}\ \frac{t-t_2}{t_2-t_1}\right)\right\} .$$

ZUSAMMENFASSUNG

Ein grundsätzlicher Faktor für das Elektrolysenverfahren mit zwei eng benachbarten Elektroden in Strömungsanordnungen ist die Übertragungsausbeute N. Ein allgemeiner Ausdruck für N, der für verschiedene Strömungen gilt, wird in exakter Weise durch Auflösen der konvektiven Diffusionsgleichung abgeleitet. Als Beispiele der praktischen Anwendung wird die allgemeine Formel auf einige Strömungen, d.h. Strömung an der rotierenden Scheibe, Kanal- und Rohrströmung und Keil- und Kreiskegelströmung, angewandt.

SUMMARY

A fundamental factor for the electrolysis technique with two closely-spaced electrodes in flow systems is the collection efficiency N. A general expression for N, which is valid for various types of flow, is derived by rigorously solving the convective diffusion equation. As examples of practical application, the general formula is applied to several types of flow, i.e., flow due to a rotating disk, flow in a channel and a circular pipe and flow along a wedge and a circular cone.

LITERATUR

1 A. FRUMKIN, L. NEKRASSOW, V. G. LEWITSCH UND JU. IWANOW, *J. Electroanal. Chem.*, 1 (1959) 84; A. FRUMKIN UND L. NEKRASSOW, *Dokl. Akad. Nauk SSSR*, 126 (1959) 115.
2 H. GERISCHER, I. MATTES UND R. BRAUN, *J. Electroanal. Chem.*, 10 (1965) 553.
3 V. G. LEWITSCH UND JU. IWANOW, *Dokl. Akad. Nauk SSSR*, 126 (1959) 1029.
4 W. J. ALBERY UND S. BRUCKENSTEIN, *Trans. Faraday Soc.*, 62 (1966) 1920.
5 H. MATSUDA, *J. Electroanal. Chem.*, 15 (1967) 109.
6 V. G. LEWITSCH, *Physicochemical Hydrodynamics*, übersetzt aus dem Russischen (2. Aufl., 1959), Prentice-Hall, Inc., Englewood Cliffs, N.J., 1962, S. 60.
7 H. MATSUDA, *J. Electroanal. Chem.*, 15 (1967) 325.
8 L. ROSENHEAD (Ed.), *Laminar Boundary Layers*, Oxford University Press, London E.C. 4, 1963, S. 234.
9 *Ibid.*, S. 428.
10 R. LEUTERITZ UND W. MANGLER, *Untersuch. Mitt. Deut. Luftfahrf.*, Nr. 3226 (1945); siehe ferner Ref. 8, S. 429.

ELECTROANALYTICAL CHEMISTRY AND INTERFACIAL ELECTROCHEMISTRY
Elsevier Sequoia S.A., Lausanne – Printed in The Netherlands

ELECTRODE KINETICS AND DOUBLE-LAYER STRUCTURE. THE $Zn^{2+}/Zn(Hg)$ ELECTRODE REACTION IN MIXED POTASSIUM HALIDE SOLUTIONS

P. TEPPEMA, M. SLUYTERS-REHBACH AND J. H. SLUYTERS
Laboratory of Analytical Chemistry, State University, Utrecht (The Netherlands)
(Received April 12th, 1967)

INTRODUCTION

Specific rate constants of electrode reactions are strongly influenced by the nature and concentration of the base electrolyte used. In some cases (see for example, DELAHAY[1]) the concentration effect has been interpreted quantitatively by taking into account the potential difference across the diffuse double layer (Frumkin-theory). The effect of the nature of the supporting electrolyte has only qualitatively been correlated to the specific adsorption of the anions, especially in the case of halide solutions. For example, GIERST AND CORNELISSEN[2] measured the half-wave potentials of the Eu^{3+}/Eu^{2+} couple as a function of composition in 1 M mixtures of perchlorate and halides. They found the reaction rate to increase in the series $Cl^- < Br^- < I^-$ in the presence of perchlorate. Specific adsorption on mercury, exhibited by the anions, varies in the same sequence. TAMAMUSHI *et al.*[3] observed the same trend for the $Zn^{2+}/Zn(Hg)$ electrode in mixtures of $NaClO_4$ with halides. On the other hand, BLACKLEDGE AND HUSH[4] ascribed the results of their experiments on the same electrode in similar base electrolyte mixtures to a mechanism in which complexes of Zn^{2+} with the added anions take part.

In this connection it seemed worthwhile to make a quantitative study of the relation between the rate constant and the specifically adsorbed amount of anions in mixtures of base electrolytes. We chose the $Zn^{2+}/Zn(Hg)$ reaction in mixtures of KCl, KBr and KI with a total concentration of 1 M, for the following reasons: (a) the rate constant values of the zinc reaction in the pure base electrolytes differ greatly[5]; (b) the rates can easily be measured with an alternating current method; (c) double-layer data of at least chloride and iodide are known from the literature[6,7]; (d) the $Zn^{2+}/Zn(Hg)$ reaction mechanism has been investigated many times; it appears that the rate-determining step is likely to be a two-electron transfer[8]. In addition, the presence of Zn^{2+} ions in millimolar concentration has no detectable effect upon the double-layer capacity in 1 M solution[9], and it may therefore be assumed that the double-layer structure is not significantly changed by the addition of Zn^{2+}.

EXPERIMENTAL

The measurements of the kinetic parameters were made using the oscilloscopic

square-wave method developed in this laboratory[10,11], which allows the direct reading of the activation overvoltage from the screen of an oscilloscope at the moment of zero diffusion polarization, t_0, occurring in each half period of the applied square-wave current. The effect of the double-layer capacity is minimized by measuring at frequencies sufficiently low to allow an accurate extrapolation to zero frequency. Recently, we discussed the applicability and the limitations of this method[11] and in that communication it is erroneously stated that the upper limit depends on the error in the activation overvoltage measured at low frequency (16 Hz).

However, if k_{sh} is large, the application of much higher frequencies is permissible, as the effect of the double-layer capacity is smaller in this case*. The highest frequencies at which the double-layer charging current is negligible have been estimated earlier as a function of k_{sh} for the oscilloscopic sine-wave method[12]. Approximately the same frequency limits will be valid for the square-wave method and it can be calculated that both methods are now limited by the ohmic resistance and the double-layer capacity to k_{sh}-values of *ca.* 0.2 cm sec^{-1}.

Solutions were made from analytical-grade salts dissolved in doubly-distilled tap-water. The cell solutions consisted of mixtures of KCl, KBr, KI and KNO_3 with a total concentration of 1 M, and 5 mM $ZnSO_4$. It was necessary to acidify the solutions (with perchloric acid) to pH 3 in order to avoid precipitation of zinc hydroxide on the electrode. Solutions were de-aerated with nitrogen which had been passed through vanadous sulphate solution.

Zinc amalgam was prepared electrolytically and kept in a nitrogen atmosphere. An amalgam pool could not be used as a counter electrode—the indicator electrode being an amalgam drop—because of spontaneous dissolution of zinc from the pool in the acid solution. Therefore *two amalgam drops* served as electrodes; they were *both* renewed before a new measurement. A mercury pool was placed at the bottom of the cell in order to minimize dissolution of zinc from the discarded drops on strong dilution.

The surface area of the electrodes was determined by the usual drop weight method. The radius of the drops was about 0.05 cm, which allows the application of the current–voltage relation in terms of linear diffusion. An electrode distance of 1.2–1.3 cm was adopted. With distances down to 1 cm, no deviations were noticed as a result of distortion of the lines of force between the drops.

Capacitance–potential curves of mercury in mixtures of 1 M KCl and 1 M KI were carried out using the impedance bridge described earlier[9]. Electrocapillary curves of the same mixtures were recorded with the drop-time method.

The kinetic parameters of the zinc reaction in various supporting electrolytes

From the measured charge transfer resistances, θ, apparent formal rate constants, $k_{sh}{}^a$, were calculated using RANDLES' equation[13]

$$k_{sh}{}^a = (RT/n^2F^2)\{(C_{ox}{}^*)^\alpha (C_{red}{}^*)^\beta \theta\}^{-1}$$

in which $C_{ox}{}^* = C_{red}{}^* = 5 \cdot 10^{-6}$ mole cm^{-3} was introduced for the bulk concentrations. In Fig. 1, the rate constants thus obtained, have been plotted against composition for 1 M mixtures of KCl + KI, and KNO_3 + KI, with almost identical results. Similar curves were obtained for KCl + KBr, and KBr + KI mixtures (Fig. 2).

* This fact was brought to our attention by Mr. D. J. KOOIJMAN.

Our $k_{sh}{}^{a}$-values are in good agreement with literature data[3-5]. The transfer coefficient, β, of the zinc reaction has frequently been found to be close to 0.3, regardless of the nature of the base electrolyte, except for the value 0.00 in 1 M KI, observed by BLACKLEDGE AND HUSH[4]. However, we found $\beta = 0.32 \pm 0.08$ for the zinc reaction in 1 M KI, which is quite close to the values in the other media. In 0.5 M KCl + 0.5 M KI a similar result, $\beta = 0.27 \pm 0.06$, was obtained (Fig. 4).

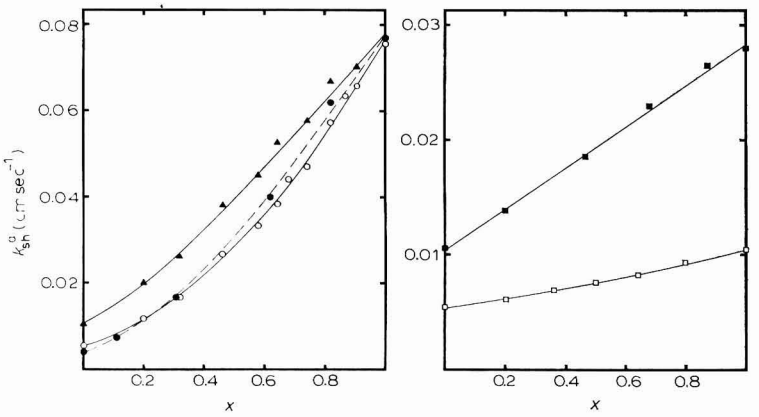

Figs. 1 and 2. Apparent rate constants, $k_{sh}{}^{a}$, of Zn^{2+}/Zn(Hg) electrode reaction as a function of x in mixed solns. (○), (1 − x) M KCl + x M KI; (●), (1 − x) M KNO_3 + x M KI (dashed curve); (▲), (1 − x) M KBr + x M KI; (□), (1 − x) M KCl + x M KBr; (■), (1 − x) M KBr + 0.5 x M KCl + 0.5 x M KI.

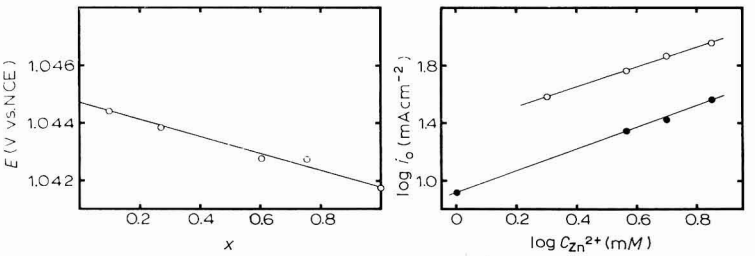

Fig. 3. Equilibrium potentials of Zn^{2+}/Zn(Hg) electrode ($C_{Zn} = C_{Zn^{2+}} = 5$ mM) in (1 − x) M KCl + x M KI solutions.

Fig. 4. Determination of the transfer coefficient, α, of Zn^{2+}/Zn(Hg) electrode reaction, in (○), 1 M KI; (●), 0.5 M KCl + 0.5 M KI. $C_{Zn} = 5$ mM. The slopes are $\alpha = 0.68$ and $\alpha = 0.73$, respectively.

In order to evaluate the double-layer parameters, the equilibrium potential of a 5 mM zinc amalgam electrode in 5 mM Zn^{2+} solution was measured as a function of the molar ratio in KCl + KI mixtures. The results are shown in Fig. 3.

Specific adsorption and ϕ_2-potentials in halides at the equilibrium potential of the zinc reaction

The double-layer parameters needed for our investigation are not directly

available in the literature. We can use only the data on pure KCl and KI solutions of varying ionic strength reported by GRAHAME AND PARSONS[6], from which we obtained the specifically adsorbed quantities, $q_{Cl}{}^1 = -0.5\ \mu C\ cm^{-2}$ and $q_I{}^1 = -5.9\ \mu C\ cm^{-2}$ in 1 M solution at the equilibrium potentials given in Fig. 3. The ϕ_2-potentials are -0.046 V and -0.056 V in KCl and KI, respectively. For 1 M KBr we applied GRAHAME's procedure to the interfacial tension data given by DEVANATHAN AND PERIES[14], which resulted in an approximate value for $q_{Br}{}^1 = -1 \pm 0.5\ \mu C\ cm^{-2}$ and $\phi_2 = -0.047 \pm 0.001$ V.

Specific adsorption studies in mixed electrolytes have, to our knowledge, been carried out only with mixtures of one specifically adsorbing anion (*e.g.*, KI[7] or NH_4NO_3[15]) with fluoride, which is assumed to be not specifically adsorbed. On this assumption, the specifically adsorbed charge is obtained by an elegant method developed by DUTKIEWICZ AND PARSONS[7]. These authors showed also that a plot of the specifically adsorbed charge against the salt activity of KI at constant surface charge density, q, for KF + KI solutions is identical with the same plot for pure KI solutions at the same q. This means that values of $q_I{}^1$ pertaining to the mixtures can be derived from the data available[6] on pure KI solutions.

When both anions of a binary electrolyte, *e.g.*, KCl + KI, are subject to specific adsorption, the separate values of $q_{Cl}{}^1$ and $q_I{}^1$ can be determined, in principle, by a combination of the procedures of GRAHAME[6] and DUTKIEWICZ AND PARSONS[7]. However, at the potential of interest, -1.04 V *vs.* NCE, chloride is only slightly adsorbed in the inner layer and, as a first approximation, the structure of the double layer in $(1-x)$ M KCl + x M KI may be assumed to be identical with that of $(1-x)$ M KF + x M KI. This is supported by the fact that the capacity–potential curves for KCl + KI, measured by us for $x = 0$, 0.01 and 0.1, proved to be identical with the corresponding curves in KF + KI at potentials below -1.0 V *vs.* NCE.

We therefore used GRAHAME's data on pure KI solution to prepare plots of

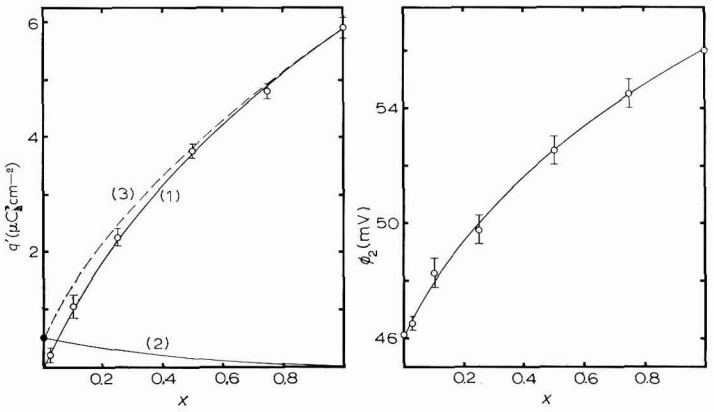

Fig. 5. (Curve 1), charge due to specific adsorption of anions at the equilibrium potential of $Zn^{2+}/Zn(Hg)$ electrode ($C_{Zn} = C_{Zn^{2+}} = 5$ mM) in solns. of $(1-x)$ M KF + x M KI; (curve 2), analogous plot, estimated for $(1-x)$ M KCl + x M KF; (curve 3), sum of 1 and 2 (see text).

Fig. 6. Potentials of the outer Helmholtz plane at the equilibrium potential of $Zn^{2+}/Zn(Hg)$ electrode ($C_{Zn} = C_{Zn^{2+}} = 5$ mM) in mixed solns. of $(1-x)$ M KCl + x M KI.

q_I^1 *vs.* the salt activity, $a_{K^+}a_{I^-}$, at some integral values of q (-10 to $-12\ \mu C\ cm^{-2}$). Following DUTKIEWICZ AND PARSONS[7], such plots are easily transformed into plots of q_I^1 *vs.* x, the mole fraction of KI in KF + KI mixtures, after calculation of $a_{K^+}a_{I^-}$ in 1 M solutions as a function of x (the mean activity coefficient is taken as constant). Then, only the proper values of q are needed to obtain q_I^1 at the equilibrium potential of the zinc reaction as a function of x. These values were calculated from the above-mentioned capacity–potential curves by back integration from -1.54 V *vs.* NCE, where $q = -20\ \mu C\ cm^{-2}$ for both 1 M KI and 1 M KCl[6]. The resulting "specific adsorption isotherm at the zinc equilibrium potential" is shown in Fig. 5 (curve 1). In addition, a curve is given, that represents an estimation of the variation of q_{Cl}^1 with x, calculated in a similar way from Grahame's data on pure KCl solutions (curve 2). It seems reasonable to assume that the presence of chloride in the inner layer has only a minor effect on the total specifically adsorbed charge, except for low values of x. The attribution of Cl^- might be accounted for by adding together curves 1 and 2 (curve 3), although this is a rather debatable procedure.

However, as will be shown in the discussion, Fig. 5 is sufficiently useful for the comparison of k_{sh}-values with q^1. Since the specific adsorption of NO_3^- is of the same order of magnitude as that of Cl^-, it may also be applicable to KNO_3–KI mixtures, in particular for $x > 0.2$.

Finally, the ϕ_2-potentials at the zinc equilibrium potential can be calculated as a function of x in the usual way[6] from q and q^1 (Fig. 6).

DISCUSSION

The data represented in Figs. 1 and 2 are "apparent" rate constants, $k_{sh}{}^a$, calculated from the measured exchange current density, i_0, by

$$i_0 = nFk_{sh}{}^a[Zn^{2+}]_a{}^\alpha[Zn]^\beta \tag{1}$$

in which $n = 2$, $[Zn]$ is the concentration of zinc in the amalgam, and $[Zn^{2+}]_a$ the concentration of the total amount of zinc ions introduced into the solution. A "true" rate constant, k_{sh}, may be defined in the usual way by introduction of the Frumkin correction and activities instead of concentrations:

$$i_0 = nFk_{sh}f[Zn^{2+}]_t{}^\alpha[Zn]^\beta \exp\{-(\alpha nF/RT)\phi_2\} \tag{2}$$

where $[Zn^{2+}]_t$ is the true concentration of non-complexed Zn^{2+} present in the solution, and the exponential term represents the Frumkin correction ($z = n$). In a first approximation, the "activity factor", $f = (f_{Zn^{2+}})^\alpha(f_{Zn})^\beta$, may be considered as a constant in solutions of varying composition at constant ionic strength, and we will therefore calculate a "true formal rate constant" $k_{sh}{}^f$, given by

$$k_{sh}{}^f = fk_{sh} = k_{sh}{}^a \frac{[Zn^{2+}]_a{}^\alpha}{[Zn^{2+}]_t{}^\alpha} \exp\left(\frac{\alpha nF}{RT}\phi_2\right) \tag{3}$$

Among the anions concerned in our investigation, NO_3^- and I^- are known to show little tendency to complex formation[16], so that we may take $[Zn^{2+}]_t \approx [Zn^{2+}]_a$ for solutions of these ions. If chloride is present, however, complex formation is appreciable[17], the dominant species being probably $ZnCl^+$ and $ZnCl_3^-$. Unfortunately, unambiguous evaluation of the correction factor $[Zn^{2+}]_a/[Zn^{2+}]_t$ is hardly feasible,

because the study of complex formation involves variation of the composition of the solution, which also causes changes in other quantities. For example, SILLÉN AND LILJEQUIST[17] measured the e.m.f.'s of the cell

$$Hg|Hg_2Cl_2|4M\ NaCl||a\ (1-x)\ M\ NaClO_4,\ ax\ M\ NaCl,\ Zn(ClO_4)_2|Zn(Hg)$$

$a = 3$ or 0.5

from which the stability constants of the zinc–chloride complexes can be derived if one neglects the changes in the activity coefficients and in the liquid junction potential. In 3 M solution they found $K_{Cl,1}=0.65$ and $K_{Cl,3}=1.4$ for the complexes $ZnCl^+$ and $ZnCl_3^-$, respectively. In 0.5 M solution, only the first constant could be obtained: $K_{Cl,1}=0.45$.

The equilibrium potential measurements in KCl + KI mixtures, described in the present paper, are similar to SILLÉN's experiments and, again neglecting the changes in $f_{Zn^{2+}}$ and the liquid junction potential, the observed change in e.m.f. can be interpreted as the consequence of the presence of $ZnCl^+$ and $ZnCl_3^-$ with stability constants $K_{Cl,1}=0.5$ and $K_{Cl,3}=0.08$. As this is in reasonable agreement with SILLÉN's results, it seems justified to use the e.m.f. values of Fig. 3 for the estimation of the correction factor from

$$\Delta E = E_{x=1} - E_x = 29.58 \log [Zn^{2+}]_a/[Zn^{2+}]_t \qquad (4)$$

The error introduced by the approximation, will not be very serious, because the correction itself is of minor importance compared to the large variation of $k_{sh}{}^a$ with composition in KCl + KI mixtures. This can be seen in Fig. 7 where the effects

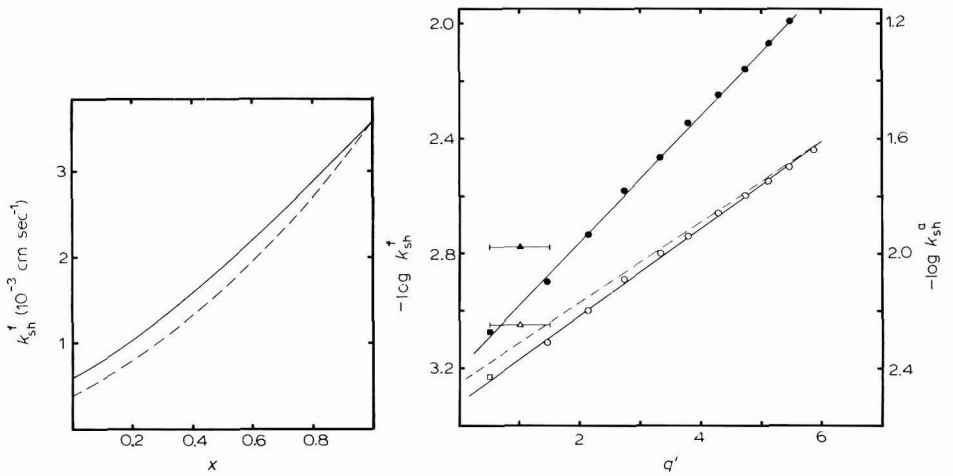

Fig. 7. Formal "true" rate constants of $Zn^{2+}/Zn(Hg)$ electrode reaction in $(1-x)$ M KCl + x M KI solns. (---), $k_{sh}{}^a$ (from curve in Fig. 1) corrected only for the Frumkin effect; (—), *idem*, corrected also for existing complexes (see text).

Fig. 8. Relation between the rate constant of $Zn^{2+}/Zn(Hg)$ electrode reaction and amount of specifically adsorbed anions. White symbols, log $k_{sh}{}^f$, black symbols, log $k_{sh}{}^a$, both *vs.* q^1 from curve 3 in Fig. 5. Dashed line: log $k_{sh}{}^f$ *vs.* q^1 from curve 1 in Fig. 5. (○, ●), $(1-x)$ M KCl + x M KI; (□, ■), 1 M KCl; (△, ▲), 1 M KBr.

of this correction and of the Frumkin correction are demonstrated separately. The latter has been calculated with the aid of the ϕ_2-potentials given above, together with $\alpha = 0.70$.

The "true" rate constant obtained still appears to depend strongly on x. It should be realized, however, that with the definition of $k_{sh}{}^f$ in eqn. (2), it is implicitly assumed that the exchange reaction proceeds *via* the Zn^{2+} ion. That this assumption is not *a-priori* correct, follows, for example, from the work of GERISCHER[18], in which it was shown that in a number of cases a certain zinc complex is the reacting species, although its concentration can be quite low compared to the dominant zinc species.

Relation between $k_{sh}{}^f$ and x on the assumption of complex reactants

A model may be adopted, in which, in principle, all zinc species, $ZnX_\nu^{2-\nu}$, take part in the electrode reaction, each with its own exchange current density, which according to GERISCHER is given by

$$i_{0,X,\nu} = nF\, k_{X,\nu} [Zn]^\beta [ZnX_\nu^{2-\nu}]^\alpha [X^-]^{\nu\beta} \exp[(\nu - \alpha n)(F/RT)\phi_2] \quad (5)$$

where according to the absolute rate theory, $k_{X,\nu}$ is the formal exchange rate under hypothetical standard conditions ($[Zn][X^-]^\nu = [ZnX_\nu^{2-\nu}]$ and $\phi_2 = 0$). Let $K_{X,\nu}$ be the formal stability constant of the νth complex, defined as

$$[ZnX_\nu^{2-\nu}]/[Zn^{2+}]_t [X^-]^\nu = K_{X,\nu} \quad (6)$$

Then

$$i_{0,X,\nu} = nF\, k_{X,\nu} [Zn]^\beta [Zn^{2+}]_t^\alpha [X^-]^\nu K_{X,\nu}^\alpha \exp[(\nu - \alpha n)(F/RT)\phi_2] \quad (7)$$

In the case of KCl + KI mixtures, this equation pertains to all possible chloride and iodide complexes of zinc and to the aquo-zinc ion ($\nu = 0$). The measured exchange current density will be the sum of all individual $i_{0,X,\nu}$ values, so

$$i_0 = nF[Zn]^\beta [Zn^{2+}]_t^\alpha \exp\left(-\frac{\alpha n F}{RT}\phi_2\right) \times$$

$$\left\{k_{aq} + \sum_{\nu=1,2,\ldots} k_{I,\nu} K_{I,\nu}^\alpha [I^-]^\nu \exp\left(\frac{\nu F}{RT}\phi_2\right) + \sum_{\nu=1,2} k_{Cl,\nu} K_{Cl,\nu}^\alpha [Cl^-]^\nu \exp\left(\frac{\nu F}{RT}\phi_2\right)\right\} \quad (8)$$

This expression is, in fact, a simplification, as α is assumed to be the same for all partial exchange processes. Since, experimentally, α appears to be independent of composition, this seems at least a good approximation.

With eqns. (2) and (3) and $[I^-] = x$ and $[Cl^-] = 1 - x$, it follows that

$$k_{sh}{}^f = k_{aq} + \sum_{\nu=1,2,\ldots} \{k_{I,\nu} K_{I,\nu}^\alpha x^\nu + k_{Cl,\nu} K_{Cl,\nu}^\alpha (1-x)^\nu\} \exp\left(\frac{\nu F}{RT}\phi_2\right)$$

$$= A + Bx + Cx^2 + \ldots \quad (9)$$

The curves drawn in Fig. 7 can be fitted to eqn. (9) with the following coefficients for KCl + KI mixtures:

$$A = 0.58 \times 10^{-3}, \quad B = 2.1 \times 10^{-3}, \quad C = 0.9 \times 10^{-3},$$

the higher-order terms being negligibly small. The same reasoning can, of course, be applied to KNO_3 + KI mixtures if Cl is replaced by NO_3. Assuming that for the

calculation of $k_{sh}{}^f$ in these mixtures the ϕ_2 *vs.* x plot of Fig. 6 can be used, we calculate for $KNO_3 + KI$ mixtures:

$$A = 0.33 \times 10^{-3}, \quad B = 2.2 \times 10^{-3}, \quad C = 1.1 \times 10^{-3}.$$

In the simplest interpretation, these results imply that the dominant reactants are $Zn^{2+}(aq)$, $ZnCl^+$, ZnI^+ and ZnI_2.

A similar theory is supported by BLACKLEDGE AND HUSH[4] for explaining the relation between i_0 and I^- or Cl^- in solutions of 2 M $NaClO_4 + y$ M NaI or NaCl. The interpretation of their results leads to the same conclusion as regards the reacting species. Note that the parameter, k_c, determined by these authors, is equivalent to $k_{X,\nu}K_{X,\nu}{}^{\alpha}$ in our notation.

Although the model described seems to be confirmed by the experimental facts, it still leaves the most interesting question unanswered, *i.e.*, what makes the rate constants of the iodide complexes so large, despite the instability of the latter? As their concentration in the solution is extremely small, the complex formation, preceding charge transfer, must take place at the reaction site in the double layer. In eqns. (5)–(9) this is accounted for by the Frumkin correction terms, which imply that the reaction site is identified with the outer Helmholtz plane and that the reaction rate is influenced only by the structure of the diffuse double layer. However, it seems to be equally—or even more—realistic to take into account the iodide ions present in the *non-diffuse part* of the double layer.

Relation between $k_{sh}{}^f$ and the amount of specific adsorption

TAMAMUSHI *et al.*[3] postulate that the electrode surface can be divided into a "naked" part $(1-\vartheta)$ at which the electrode reaction proceeds with a rate constant k_1, and a part, ϑ, covered with halide ions, at which the reaction proceeds with a higher rate constant, k_2. The overall rate constant is given by

$$k_{sh}{}^f = (1-\vartheta)k_1 + \vartheta k_2 \tag{10}$$

From this model we infer that $k_{sh}{}^f$ should be a linear function of the specifically adsorbed charge. A comparison of Fig. 7 and Fig. 5 shows, however, that this is not the case. Instead, the data suggest that $k_{sh}{}^f$ increases exponentially with q^1.

We therefore plotted the logarithm of the $k_{sh}{}^f$-values of $KCl + KI$ mixtures against q^1 and obtained, in fact, a surprisingly straight line, see Fig. 8. The plot of log $k_{sh}{}^a$ in the same figure demonstrates that the corrections for existing complexes and ϕ_2-potentials have only a minor effect on the slope of the line. Furthermore, it makes little difference, whether q^1 is taken from curve 1 or curve 3 in Fig. 5. Note that the points for 1 M KCl and 1 M KBr fit reasonably well on the lines. Also the k_{sh}-data for $KBr + KI$ and $KCl + KBr$ mixtures (Figs. 1 and 2) qualitatively indicate that the increase of k_{sh} with the amount of specific adsorption is—at least to a first approximation—not dependent on the nature of the anion.

This result can be interpreted in a very simple way with the aid of the definition of k_{sh} in the absolute rate theory[1]

$$k_{sh} = \frac{kT}{h} \exp\left[\frac{-\overrightarrow{\Delta G}^{\neq 0} + \alpha n F \phi_M{}^0}{RT}\right] = \frac{kT}{h} \exp\left[\frac{-\overleftarrow{\Delta G}^{\neq 0} - \beta n F \phi_M{}^0}{RT}\right] \tag{11}$$

where $\phi_M{}^0$ is the inner potential of the electrode at the standard potential of the redox couple and $\Delta G^{\neq 0}$ is the chemical standard free energy of activation ($\rightarrow$ and $\leftarrow$

pertain to oxidation and reduction, respectively). As all the other symbols in eqn. (11) represent constants, Fig. 8 can be explained on the basis of a single exchange mechanism with an activation energy that decreases linearly with the specifically adsorbed charge (μC cm^{-2}), according to

$$\Delta G_{+}^{0} = (\Delta G_{+}^{0})_{q^1=0} - 205\ q^1 \text{ cal mole}^{-1} \qquad (12)$$

Although the experimental facts described in this paper, do not lead to a definite decision between the "complex reactant model" and the "specific adsorption model", we believe that the latter is fairly plausible. SCHMIDT AND MARK[19] presented a quantum chemical theory on the mechanism of charge transfer at an electrode, in which the solvation sheath adjacent to the electrode plays an important part. In this connection, it seems logical that the presence of polarizable anions like halides may change the energy level of the activated state. In any case, there is some evidence in the literature to support the idea that specific adsorption of anions is essential for their accelerating effect on electrode reactions. For example, the anomalous polarograms of In(III) in SCN^- and halide solutions[20,21] indicate that the rate constants of these systems depend on the potential qualitatively in the same way as the inner-layer charge. Moreover, the experiments of GERISCHER[19], which convincingly support the "complex reactant" model, do not conflict with our views, although they were mostly performed at rather negative potentials where no significant specific adsorption of anions exists. In most cases it is observed that the reacting species is an uncharged particle, *e.g.*, $Zn(OH)_2$ or $Zn(COO)_2$, so that the low activation energy apparently pertaining to these complexes may be due also to adsorption in the double layer.

It may be noticed that, if our model holds, one should be very cautious in the determination of parameters of electrode reactions requiring variations in the experimental conditions that may be accompanied by a change in the amount of specific adsorption (*e.g.*, potential or temperature variation for the determination of the transfer coefficient and the heat of activation, respectively). On the other hand, anomalous results observed in such experiments, may supply more evidence in favour of the model, and may eventually be used for its refinement. This will be further investigated.

ACKNOWLEDGEMENT

The present investigations have been carried out under the auspices of the Netherlands Foundation of Chemical Research (S.O.N.) with financial aid from the Netherlands Organization for the Advancement of Pure Research (Z.W.O.).

The authors gratefully acknowledge the work of Mr. J. S. M. C. BREUKEL in carrying out the double-layer capacity measurements.

SUMMARY

The $Zn^{2+}/Zn(Hg)$ electrode in binary 1 M potassium halide solutions has been studied using the oscilloscopic method for the determination of the kinetic parameters. The apparent standard heterogeneous rate constant, k_{sh}, is found to be a non-linear function of the mole fraction, x, of the components of the base electrolyte.

Taking into account the Frumkin correction and the occurrence of complex formation, the measured k_{sh}-values in $(1-x)$ *M* KCl $+x$ *M* KI are compared with the amount of specific adsorbed anions, q^1. A linear relation is found between log k_{sh} and q^1 (Fig. 8), from which it is inferred that the energy of activation decreases linearly with q^1. This model is preferred to the assumption of complex reactants.

REFERENCES

1 P. DELAHAY, *Double-Layer and Electrode Kinetics*, Interscience Publishers Inc., New York, 1965.
2 L. GIERST AND P. CORNELISSEN, *Collection Czech. Chem. Commun.*, 25 (1960) 3004.
3 R. TAMAMUSHI, R. ISHIBASHI AND N. TANAKA, *Z. Physik. Chem. N.F.*, 35 (1962) 209; 39 (1963) 117.
4 J. BLACKLEDGE AND N. S. HUSH, *J. Electroanal. Chem.*, 5 (1963) 435.
5 J. E. B. RANDLES AND K. W. SOMERTON, *Trans. Faraday Soc.*, 48 (1952) 951.
6 D. C. GRAHAME AND R. PARSONS, *J. Am. Chem. Soc.*, 83 (1961) 1548. D. C. GRAHAME, *ibid.*, 80 (1958) 4201. Dr. R. PARSONS kindly supplied additional data not given in the paper.
7 E. DUTKIEWICZ AND R. PARSONS, *J. Electroanal. Chem.*, 11 (1966) 100.
8 B. TIMMER, M. SLUYTERS-REHBACH AND J. H. SLUYTERS, *J. Electroanal. Chem.*, 14 (1967) 181.
9 M. SLUYTERS-REHBACH AND J. H. SLUYTERS, *Rec. Trav. Chim.*, 82 (1963) 535.
10 M. D. WIJNEN AND W. M. SMIT, *Rec. Trav. Chim.*, 79 (1960) 22, 289.
11 P. TEPPEMA, M. SLUYTERS-REHBACH AND J. H. SLUYTERS, *Rec. Trav. Chim.*, 85 (1966) 303, 1161.
12 J. H. SLUYTERS, *Rec. Trav. Chim.*, 81 (1962) 297.
13 J. E. B. RANDLES, *Discussions Faraday Soc.*, 1 (1947) 11.
14 M. A. V. DEVANATHAN AND P. PERIES, *Trans. Faraday Soc.*, 50 (1954) 1236.
15 R. PAYNE, *J. Phys. Chem.*, 69 (1965) 4113.
16 L. G. SILLÉN AND A. E. MARTELL, *Stability Constants of Metal-Ion Complexes*, The Chemical Society, London, 1964.
17 L. G. SILLÉN AND B. LILJEQUIST, *Svensk Kem. Tidskr.*, 56 (1944) 85.
18 H. GERISCHER, *Z. Physik. Chem.*, 202 (1953) 292, 302.
19 P. P. SCHMIDT AND H. B. MARK JR., *J. Chem. Phys.*, 43 (1965) 3291.
20 (a) N. TANAKA, T. TAKEUCHI AND R. TAMAMUSHI, *Bull. Chem. Soc. Japan*, 37 (1964) 1435; (b) A. G. STROMBERG AND KH. Z. BRAININA, *Zh. Fiz. Khim. (English Transl.)*, 35 (1961) 989.
21 M. SLUYTERS-REHBACH, B. TIMMER AND J. H. SLUYTERS, *Z. Physik. Chem. N.F.*, 52 (1967) 89.

ELECTROANALYTICAL CHEMISTRY AND INTERFACIAL ELECTROCHEMISTRY
Elsevier Sequoia S.A., Lausanne – Printed in The Netherlands

ELECTRIC DOUBLE LAYER ON PLATINUM-GROUP METALS AND THE ESIN–MARKOV EFFECT

A. FRUMKIN, O. PETRY, A. KOSSAYA, V. ENTINA AND V. TOPOLEV

Moscow State University, Institute of Electrochemistry, Academy of Sciences of the USSR, Moscow (U.S.S.R.)

(Received May 15th, 1967)

* See Erratum : U 14. Pages 2HH 1968

THERMODYNAMICAL RELATIONS

The thermodynamics of surface phenomena on platinum-group metals (Pt, Rh) electrodes was considered in refs. 1–7 where some of the thermodynamical relations derived were also confirmed by experiment. In these studies, however, use was made of the chemical potential of the H^+ ion, μ_{H^+}, *i.e.*, of a quantity that cannot be determined from experimental data in the general case. This partly limits the applicability of the results to dilute solutions. In the present communication we want, primarily, to eliminate this limitation.

Let us consider a solution containing a neutral salt, CA, and an acid, HA. Let μ_{HA} and μ_{CA} be the chemical potentials of HA and CA, Γ_{HA} and Γ_{CA} the surface densities of these components which are understood to mean the amounts of HA and CA to be introduced into the system for the solution composition to remain unchanged with an increase in the interface by 1 cm^2 ($\Gamma_{H_2O}=0$), μ_H and Γ_H the chemical potential and surface density of hydrogen, respectively, φ_r the electrode potential measured against the hydrogen electrode in the same solution in equilibrium with H_2 at atmospheric pressure and σ the surface density of free energy. As in refs. 3–5, Γ and μ are expressed in electrical units.

It is evident that

$$\Gamma_{HA}=\Gamma_{H^+};\quad \Gamma_{CA}=\Gamma_{C^+};\quad \Gamma_{A^-}=\Gamma_{HA}+\Gamma_{CA};\quad \Gamma_{H^+}=\Gamma_{A^-}-\Gamma_{C^+} \tag{1}$$

Subsequent conclusions are based on the equation

$$d\sigma=-\Gamma_H d\mu_H-\Gamma_{HA}d\mu_{HA}-\Gamma_{CA}d\mu_{CA} \tag{2}$$

derived from Gibbs thermodynamics or, since

$$d\mu_H=-d\varphi_r \tag{3}$$

$$d\sigma=\Gamma_H d\varphi_r-\Gamma_{HA}d\mu_{HA}-\Gamma_{CA}d\mu_{CA} \tag{4}$$

It follows from eqn. (4) that

$$\left(\frac{\partial \Gamma_H}{\partial \mu_{HA}}\right)_{\varphi_r,\mu_{CA}} = -\left(\frac{\partial \Gamma_H}{\partial \varphi_r}\right)_{\mu_{HA},\mu_{CA}} \left(\frac{\partial \varphi_r}{\partial \mu_{HA}}\right)_{\Gamma_H,\mu_{CA}} = -\left(\frac{\partial \Gamma_{HA}}{\partial \varphi_r}\right)_{\mu_{HA},\mu_{CA}} \tag{5}$$

$$\left(\frac{\partial \varphi_r}{\partial \mu_{HA}}\right)_{\Gamma_H,\mu_{CA}} = \left(\frac{\partial \Gamma_{HA}}{\partial \varphi_r}\right)_{\mu_{HA},\mu_{CA}} : \left(\frac{\partial \Gamma_H}{\partial \varphi_r}\right)_{\mu_{HA},\mu_{CA}} =$$

$$= \left(\frac{\partial \Gamma_{H^+}}{\partial \varphi_r}\right)_{\mu_{HA},\mu_{CA}} : \left(\frac{\partial \Gamma_H}{\partial \varphi_r}\right)_{\mu_{HA},\mu_{CA}} \tag{6}$$

As was shown in refs. 3–5, the change in Γ_H is related to the quantity of electricity, Q, imparted to the electrode from outside by the equation

$$\Delta \Gamma_H = -\Delta Q \tag{7}$$

provided the electrode is not accessible to any substances which, in the potential range under consideration, can act as oxidizing or reducing agents, and molecular H_2 is not evolved in the bulk of the solution in measurable quantities. Thus, eqn. (6) can be written as:

$$\left(\frac{\partial \varphi_r}{\partial \mu_{HA}}\right)_{Q,\mu_{CA}} = -\left(\frac{\partial \Gamma_{HA}}{\partial \varphi_r}\right)_{\mu_{HA},\mu_{CA}} : \left(\frac{\partial Q}{\partial \varphi_r}\right)_{\mu_{HA},\mu_{CA}}$$

$$= -\left(\frac{\partial \Gamma_{H^+}}{\partial \varphi_r}\right)_{\mu_{HA},\mu_{CA}} : \left(\frac{\partial Q}{\partial \varphi_r}\right)_{\mu_{HA},\mu_{CA}} \tag{8}$$

For the practical use of eqn. (8) it is important that the effect of dissolved H_2 upon μ_{HA} and μ_{CA} can be neglected. Therefore, with HA and CA constant, and φ_r (and hence, μ_H) changing, μ_{HA} and μ_{CA} remain constant.

Two particular cases of eqn. (8) are of especial interest.

1. Pure acid solution, [CA] = 0.

In this case eqn. (8) is simplified

$$\left(\frac{\partial \varphi_r}{\partial \mu^{\pm}_{HA}}\right)_{Q} = -2\left(\frac{\partial \Gamma_{H^+}}{\partial \varphi_r}\right)_{\mu^{\pm}_{HA}} : \left(\frac{\partial Q}{\partial \varphi_r}\right)_{\mu^{\pm}_{HA}} \tag{9}$$

where $\mu^{\pm}_{HA}$ is the mean chemical potential of HA ions.

2. Acidified neutral salt solution in which [CA] $\gg$ [HA]. In this case, μ_{A^-} remains practically constant with changing [HA], if [CA] is constant, and, hence

$$d\mu_{HA} = d\mu_{H^+} + d\mu_{A^-} = d\mu_{H^+}$$

where $d\mu_{H^+}$ can be determined from the change in the hydrogen electrode potential with [CA] remaining constant. Under these conditions, the introduction of the quantity, μ_{H^+}, is justified. In this case, it follows from eqn. (8) that

$$\left(\frac{\partial \varphi_r}{\partial \mu_{H^+}}\right)_{Q,\mu_{CA}} = -\left(\frac{\partial \Gamma_{H^+}}{\partial \varphi_r}\right)_{\mu_{H^+},\mu_{CA}} : \left(\frac{\partial Q}{\partial \varphi_r}\right)_{\mu_{H^+},\mu_{CA}} \tag{10}$$

Equations (9) and (10) express the same relations as those derived earlier. It is easy to show that eqn. (10) holds also in the case of an acid with a bivalent anion, H_2A.

The situation is somewhat more complicated in the case of changing concentration of CA with [HA] constant (see Appendix).

In some cases it is more convenient to refer the potential being measured to a constant reference electrode the potential of which does not change with μ_{HA}, rather than to a hydrogen electrode in the same solution. Let us denote the potential measured against such an electrode, by φ. If the condition [CA] $\gg$ [HA] is fulfilled and μ_{CA} is constant, it is evident that

$$d\varphi = d\varphi_r + d\mu_{H^+} \tag{11}$$

It follows from eqns. (10) and (11) that

$$\left(\frac{\partial\varphi}{\partial\mu_{H^+}}\right)_{Q,\mu_{CA}} = 1 - \left(\frac{\partial\Gamma_{H^+}}{\partial\varphi}\right)_{\mu_{H^+},\mu_{CA}} : \left(\frac{\partial Q}{\partial\varphi}\right)_{\mu_{H^+},\mu_{CA}} \tag{12}$$

In solutions with varying concentration of HA, if the latter exceeds the applicability limits of the laws of dilute solutions, the reference of the measured potential to an electrode of constant potential is a problem lying beyond the scope of a thermodynamical treatment. However, as was shown in ref. 8, when the potential is referred to an imaginary reference electrode the potential of which differs from that of an electrode reversible with respect to the cation (in our case with respect to the H^+ ion) by the quantity $-\mu^{\pm}_{HA}$, the thermodynamical relations of electrocapillarity theory in concentrated solutions are of the same form as in dilute solutions. Therefore, such an electrode can be conditionally regarded as a constant reference electrode; in dilute solutions this definition becomes identical with the generally accepted one. Thus, for pure acid solutions with varying concentration we shall assume

$$d\varphi = d\varphi_r + d\mu^{\pm}_{HA} \tag{13}$$

It follows from eqns. (13) and (10) that

$$\left(\frac{\partial\varphi}{\partial\mu^{\pm}_{HA}}\right)_{Q} = 1 - 2\left(\frac{\partial\Gamma_{H^+}}{\partial\varphi}\right)_{\mu^{\pm}_{HA}} : \left(\frac{\partial Q}{\partial\varphi}\right)_{\mu^{\pm}_{HA}} \tag{14}$$

It was shown in refs. 4–7 how the dependence of Γ_{H^+} upon φ_r could be determined from the experimentally-obtained values of the dependence of the potential upon the solution acidity at constant Q and from the slope of the charging curve, $\partial\varphi_r/\partial Q$, and then compared with the experimental Γ_{H^+}–φ_r-curve. In refs. 3–6 the prerequisites for an experimental realization of the isoelectricity condition, *i.e.*, Q = constant, were also considered.

In the case when [CA] $\gg$ [HA], the H^+ cations can be assumed to be completely displaced from the ionic side of the double layer by the C^+ cations. Under these conditions, Γ_{H^+} can be equated with the electrode charge density, ε. In this case,

as was explained in refs. 4–5, it is assumed that the charge of the C^+ and A^- ions belongs to the ionic side of the double layer and the possibility of its being partly redistributed between the adsorbed particle and the metal is not taken into consideration, whether this corresponds to the real structure of the double layer or not. Under these assumptions, it follows from eqn. (10) that

$$\left(\frac{\partial \varepsilon}{\partial \varphi_r}\right)_{\mu_{H^+},\mu_{CA}} = -\left(\frac{\partial \varphi_r}{\partial \mu_{H^+}}\right)_{Q,\mu_{CA}} \left(\frac{\partial Q}{\partial \varphi_r}\right)_{\mu_{H^+},\mu_{CA}} \tag{15}$$

The quantity in the left-hand side of eqn. (15) is the equilibrium value of the differential capacity of the double layer at the electrode–solution interface. In principle, it would be possible to obtain this value by differentiation of the experimental Γ_{H^+}–φ_r-curve. This is, however, impracticable owing to the insufficiently accurate determination of Γ_{H^+}. Another possible method for determining the value of $\partial\varepsilon/\partial\varphi_r$ is to make a.c. measurements of the electrode differential capacity at high enough frequencies, at which the pseudocapacity of the reaction

$$H^+ + \bar{e} \rightleftarrows H_{ads.}$$

can be neglected. Apart from the experimental difficulties encountered in this case (compare for example, ref. 4), one cannot be certain that the value of $\partial\varepsilon/\partial\varphi_r$ thus found is the equilibrium value of the differential capacity of the double layer, owing to the slowness of the processes leading to the establishment of equilibrium in the ion adsorption on the surface of the platinum-group metals[4]. Thus, at the present time, the use of eqn. (15) seems to be the only possible method of determining the equilibrium value of the differential capacity of the double layer for this kind of electrode.

In solutions without an excess of the foreign cation C^+, Γ_{H^+} cannot be equated with ε since some of the H^+ ions, the surface density of which we shall denote by $\Gamma^i_{H^+}$, can take part in the formation of the ionic side of the double layer. It is evident that

$$\Gamma_{H^+} = \varepsilon + \Gamma^i_{H^+} \tag{16}$$

It follows from eqns. (9) and (16) that

$$\left(\frac{\partial \varphi_r}{\partial \mu^{\pm}_{HA}}\right)_Q = -2\left(\frac{\partial(\varepsilon + \Gamma^i_{H^+})}{\partial \varphi_r}\right)_{\mu^{\pm}_{HA}} : \left(\frac{\partial Q}{\partial \varphi_r}\right)_{\mu^{\pm}_{HA}} \tag{17}$$

and from the thermodynamical theory of electrocapillarity[8] that at small surface charges, *i.e.*, near the point of zero charge (p.z.c.), in the absence of specific adsorption, the excess amounts of cation and anion on the surface, which are opposite in sign, are equal in their absolute value to half the charge density. Assuming that this conclusion can be extended to the case under consideration, we obtain

$$\Gamma^i_{H^+} = -\Gamma_{A^-} = -\tfrac{1}{2}\varepsilon \tag{18}$$

It follows from eqns. (17) and (18) that

$$\left(\frac{\partial\varepsilon}{\partial\varphi_r}\right)_{\mu^{\pm}_{HA}} = -\left(\frac{\partial\varphi_r}{\partial\mu^{\pm}_{HA}}\right)_{Q}\left(\frac{\partial Q}{\partial\varphi_r}\right)_{\mu^{\pm}_{HA}} \tag{19}$$

It is evident from a comparison of eqns. (19) and (15) that, near the p.z.c., the same potential change with changing acidity under isoelectric conditions can be expected to occur in pure acid solutions as in the presence of an excess of neutral salt.

A relation can be readily derived from eqn. (17), that enables the Esin–Markov coefficient to be determined for platinum-group electrodes. Let us substitute Γ_H, as in refs. 1 and 2, by $A_H-\varepsilon$, where A_H is the amount of atomic hydrogen adsorbed on 1 cm^2 of surface, expressed in electrical units. Thus, taking into consideration that in an acid solution

$$\varepsilon=\Gamma_{A^-}-\Gamma^{i}_{H^+} \tag{20}$$

we find

$$dQ=-d\Gamma_H=d\varepsilon-dA_H=d\Gamma_{A^-}-d\Gamma^{i}_{H^+}-dA_H \tag{21}$$

It follows from eqns. (13), (17), (20) and (21) that

$$\left(\frac{\partial\varphi}{\partial\mu^{\pm}_{HA}}\right)_{Q} = 1+2\left(\frac{\partial\Gamma_{A^-}}{\partial\varphi}\right)_{\mu^{\pm}_{HA}}:\left[\frac{\partial(A_H-\Gamma_{A^-}+\Gamma^{i}_{H^+})}{\partial\varphi}\right]_{\mu^{\pm}_{HA}}$$

$$= \left[\frac{\partial(A_H+\Gamma_{A^-}+\Gamma^{i}_{H^+})}{\partial(A_H-\Gamma_{A^-}+\Gamma^{i}_{H^+})}\right]_{\mu^{\pm}_{HA}} \tag{22}$$

At $A_H=0$, the condition $Q=$constant becomes $\varepsilon=$constant and eqn. (22) can be presented in the form

$$\left(\frac{\partial\varphi}{\partial\mu^{\pm}_{HA}}\right)_{\varepsilon} = -\left(\frac{\partial\Gamma^{i}_{H^+}}{\partial\varepsilon}\right)_{\mu^{\pm}_{HA}}-\left(\frac{\partial\Gamma_{A^-}}{\partial\varepsilon}\right)_{\mu^{\pm}_{HA}} \tag{23}$$

Equation (23) coincides with the thermodynamical expression for the Esin–Markov effect known from electrocapillarity theory[8,10]. In contrast to mercury, however, it is inapplicable at $\varepsilon=0$, since the condition $A_H=0$ is realized only in solutions of halogen acids within a certain range of positive values of φ_r[1,5–7].

The above treatment can be readily extended to alkaline solutions, COH, and alkaline solutions of a neutral salt, CA + COH (assuming as above [CA] $\gg$ [COH] and [CA] $\approx$ constant, which justifies the introduction of the quantity μ_{OH^-}). It is evident that in alkaline solutions

$$\Gamma_{COH}=\Gamma_{OH^-};\quad \Gamma_{C^+}=\Gamma_{CA}+\Gamma_{COH};\quad \Gamma_{A^-}=\Gamma_{CA};\quad \Gamma_{OH^-}=\Gamma_{C^+}-\Gamma_{A^-} \tag{24}$$

The stoichiometry of the charging of a hydrogen electrode in alkaline solution is expressed by the reaction

$$H_{ads.}+OH^- \rightleftarrows H_2O+\bar{e}$$

Therefore, in the presence of an excess of neutral salt

$$\varepsilon = -\Gamma_{OH^-} \tag{25}$$

and in a pure alkali solution

$$\varepsilon = -\Gamma_{OH^-} + \Gamma^{i}_{OH^-} \tag{26}$$

where $\Gamma^{i}_{OH^-}$ is the surface density of OH^- ions in the ionic side of the electric double layer.

In the case of pure alkali solutions, we obtain in place of eqns. (9) and (14)

$$\left(\frac{\partial \varphi_r}{\partial \mu^{\pm}_{COH}}\right)_Q = -2\left(\frac{\partial \Gamma_{OH^-}}{\partial \varphi_r}\right)_{\mu^{\pm}_{COH}} : \left(\frac{\partial Q}{\partial \varphi_r}\right)_{\mu^{\pm}_{COH}} \tag{27}$$

$$\left(\frac{\partial \varphi}{\partial \mu^{\pm}_{COH}}\right)_Q = -1-2\left(\frac{\partial \Gamma_{OH^-}}{\partial \varphi}\right)_{\mu^{\pm}_{COH}} : \left(\frac{\partial Q}{\partial \varphi}\right)_{\mu^{\pm}_{COH}} \tag{28}$$

where $\mu^{\pm}_{COH}$ is the mean chemical potential of the C^+ and OH^- ions, and for alkaline neutral salt solutions the following two equations replace, respectively, eqns. (10) and (12)*:

$$\left(\frac{\partial \varphi_r}{\partial \mu_{OH^-}}\right)_{Q,\mu_{COH}} = -\left(\frac{\partial \Gamma_{OH^-}}{\partial \varphi_r}\right)_{\mu_{OH^-},\mu_{COH}} : \left(\frac{\partial Q}{\partial \varphi_r}\right)_{\mu_{OH^-},\mu_{CA}} \tag{29}$$

$$\left(\frac{\partial \varphi}{\partial \mu_{OH^-}}\right)_{Q,\mu_{COH}} = -1-\left(\frac{\partial \Gamma_{OH^-}}{\partial \varphi}\right)_{\mu_{OH^-},\mu_{COH}} : \left(\frac{\partial Q}{\partial \varphi_r}\right)_{\mu_{OH^-},\mu_{COH}} \tag{30}$$

The potential, φ, in alkaline solutions is referred to a reference electrode, that differs from an electrode in the solution under consideration reversible with respect to H_2 at atmospheric pressure, by the quantity μ_{OH^-} in the case of alkaline solutions of neutral salts, and by the quantity $\mu^{\pm}_{COH}$ in the case of pure alkali.

Finally, let us attempt to extend the above relations to the potentials at which adsorbed hydrogen on the electrode surface is substituted by adsorbed oxygen, *i.e.*, to the oxygen part of the charging curve. Assuming that under these conditions the system can still be treated as reversible (to what extent this is admissible will be shown in the experimental part of the present paper), eqns. (2), (3) and (7) should be substituted by the following equations:

$$d\mu_O = d\varphi_r \tag{31}$$

$$d\sigma = -\Gamma_O d\mu_O - \Gamma_{HA} d\mu_{HA} - \Gamma_{CA} d\mu_{CA} \tag{32}$$

$$\Delta\Gamma_O = \Delta Q \tag{33}$$

where μ_O and Γ_O are also expressed in electrical units. Since the changes of sign

* It is obvious that eqns. (10) and (12) can be used in the case of alkaline neutral salt solutions instead of eqns. (29) and (30) as well.

before $d\varphi_r$ in eqn. (31) compared to eqn. (3), and before ΔQ in eqn. (33) compared to eqn. (7), are mutually compensating, eqn. (8), and all the relations derived from it, remain valid. This holds also for eqns. (27)–(30) derived for alkaline solutions. Thus, if the assumption of reversibility of the ionization reaction of adsorbed oxygen is at least approximately justified, the experimental results can be treated alike whether there is adsorbed hydrogen or oxygen present on the electrode surface. This is already apparent for the reason that, taking into account the condition $\Gamma_{H_2O}=0$, oxygen adsorption can be considered as a negative hydrogen adsorption. The case when $H_{ads.}$ and $O_{ads.}$ are present simultaneously does not require special consideration, since their presence in equivalent quantities is indistinguishable thermodynamically from water chemisorption and, according to the condition $\Gamma_{H_2O}=0$, should not be taken into account. Only that fraction of Γ_O that exceeds the equivalent of Γ_H and *vice versa* is to be taken into consideration in the calculations.

EXPERIMENTAL RESULTS

Equation (14) has been experimentally verified for a 10^{-2} *N* HCl solution on a Pt/Pt electrode (the characteristics of the electrodes used and the experimental details are given in ref. 11. In Fig. 1, the dependence of $(\partial\varphi/\partial\mu^{\pm}_{HA})_Q$ upon φ_r for a 10^{-2} *N* HCl

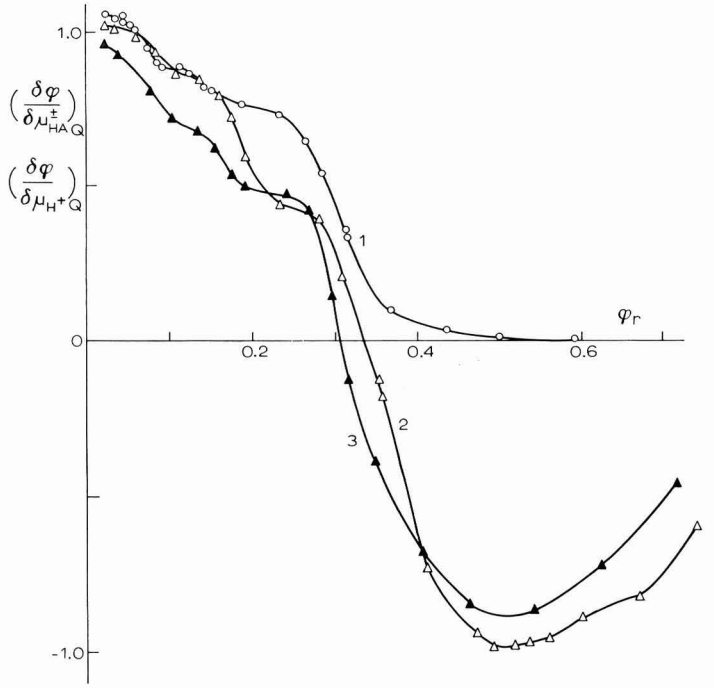

Fig. 1. Dependence of $(\partial\varphi/\partial\mu_{H^+})_Q$ upon φ_r for 0.01 *N* HCl + KCl (1) and of $(\partial\varphi/\partial\mu^{\pm}_{HA})$ upon φ_r for 0.01 *N* HCl (2) and 0.1 *N* HCl (3) on a Pt/Pt electrode.

solution (Curve 2) is compared with a similar dependence of $(\partial\varphi/\partial\mu_{H^+})_Q$ for a 10^{-2} N HCl + N KCl solution (Curve 1), which was determined previously[5,6]. The transition from experimental values of $(\partial\varphi_r/\partial\mu^{\pm}_{HA})_Q$ to $(\partial\varphi/\partial\mu^{\pm}_{HA})_Q$ was made on the basis of eqn. (13). At small φ_r the values of the derivatives for both solutions are close to unity. The reasons for this have already been discussed[5,6]. In the range of φ_r, 0.06–0.16 V, curves 1 and 2 practically coincide. Since the p.z.c. of a Pt/Pt electrode in a 10^{-2} N HCl + N KCl lies at $\varphi_r = 0.16$ V[1,5,6], the potentials, 0.06–0.16 V correspond to small negative surface charges. Therefore, the coincidence between the values of $(\partial\varphi/\partial\mu^{\pm}_{HA})_Q$ in pure acid solutions and of $(\partial\varphi/\partial\mu_{H^+})_Q$ in those with neutral salt addition appears to be due to the approximate validity of eqn. (18) for the case under consideration.

With increasing anodic potential, the values of the derivatives decrease for both solutions, but according to different laws. At $\varphi_r \gtrsim 0.5$ V in the case of a 10^{-2} N HCl + N KCl solution, $(\partial\varphi/\partial\mu_{H^+})_Q$ vanishes which, as was shown earlier, is the result of the disappearance of A_H. In a pure acid solution, in the range of values of φ_r at which $A_H = 0$, $(\partial\varphi/\partial\mu^{\pm}_{HA})_Q$ passes through a minimum, reaching a value close to -1. Thus, in the above range of φ_r, in an acid solution without a neutral salt addition, the Pt/Pt electrode under isoelectric conditions behaves approximately as a reversible chlorine electrode.

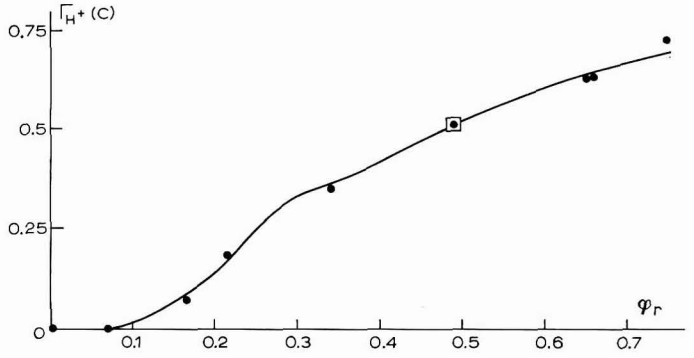

Fig. 2. Comparison of: (—), theoretically calcd. (by means of eqn. (9)) and (●), exptl. dependences of Γ_{H^+} upon φ_r for 0.01 N HCl on a Pt/Pt electrode. Γ_{H^+} is given in coulombs for the whole electrode surface. (⊡), Γ_{H^+}-value used in the determination of the integration constant.

In Fig. 2, the $\Gamma_{H^+}\varphi_r$-curve calculated from eqn. (9) is compared with the experimental curve. In Fig. 2 and in Figs. 5 and 6, the experimental values of Γ_{H^+}, which were used in the determination of the integration constant, are marked with a special symbol. A quantitative agreement between the theoretically-calculated curve and the experimental curve is observed over the whole potential range investigated.

Equations (10) and (29) were verified for the following systems: N KCl + 0.01 N HCl[7], N Na_2SO_4 + 0.01N H_2SO_4 and N KCl + 0.01 N KOH[12] on Pt coated with Rh black, and N KCl + 0.01 N HCl on Pt coated with Ru black[13]. The preparation of the electrodes and experimental details have already been described[7,12,13].

In Figs. 3 and 4 are shown the experimentally-determined dependences of $(\partial\varphi/\partial\mu_{H^+})_Q$ upon φ_r for the systems investigated.

As is evident from Fig. 3, the dependence of $(\partial\varphi/\partial\mu_{H^+})_Q$ upon φ_r for the Rh electrode in an acidified KCl solution has, on the whole, the same shape as the similar dependence for the Pt/Pt electrode. At small φ_r, the Rh electrode behaves as a reversible hydrogen electrode in equilibrium with hydrogen gas at constant pressure. At $\varphi_r \gtrsim 0.4$ V, $(\partial\varphi/\partial\mu_{H^+})_Q = 0$, from which it can be inferred that on a Rh electrode in acidified chloride solutions, A_H becomes zero. In contrast, in acidified sulfate and

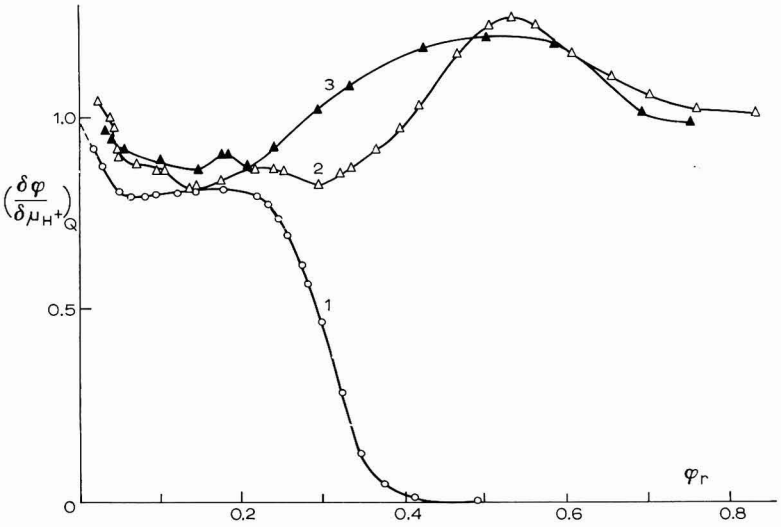

Fig. 3. Dependence of $(\partial\varphi/\partial\mu_{H^+})_Q$ upon φ_r for: (1), 0.01 N HCl + N KCl; (2), 0.01 N H_2SO_4 + N Na_2SO_4; (3), 0.01 N KOH + N KCl on Rh black electrode.

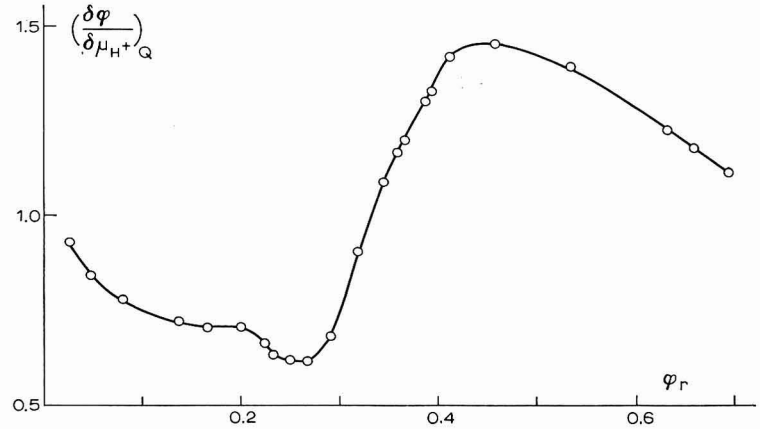

Fig. 4. Dependence of $(\partial\varphi/\partial\mu_{H^+})_Q$ upon φ_r for 0.01 N HCl + N KCl on a Ru black electrode.

alkaline chloride solutions in the potential range 0–0.8 V, the value of $(\partial\varphi/\partial\mu_{H^+})_Q$ remains close to unity. This phenomenon can be accounted for only by the absence in such solutions of a potential range in which $A_H=0$ owing to the overlapping of the hydrogen and oxygen adsorption regions. On the Ru electrode a similar situation obtains in acidified chloride solutions. Thus, on Ru, even at high concentrations of Cl^- ions, there is a continuous transition from the hydrogen adsorption region to that of oxygen adsorption.

At $\varphi_r > 0.4$ V in acidified sulfate solutions and at $\varphi_r > 0.3$ V in alkaline chloride solutions on Rh, and at $\varphi_r > 0.35$ V in an acidified chloride solution on Ru, $(\partial\varphi/\partial\mu_{H^+})_Q$

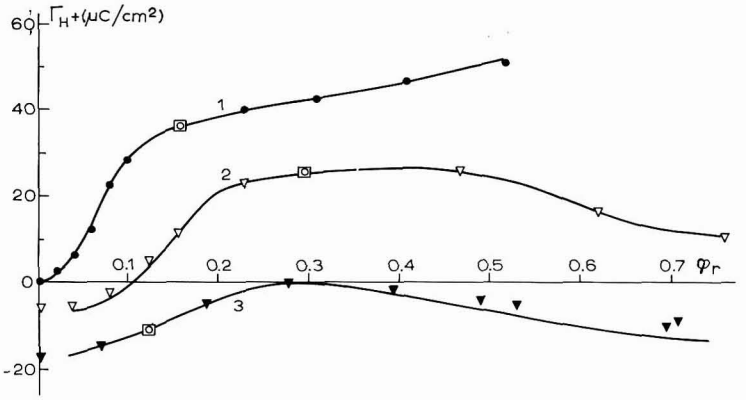

Fig. 5. Comparison of the calcd. (by means of eqn. (10)) (full drawn curve) and exptl. (dots) dependences of Γ_{H^+} upon φ_r for: (1), 0.01 N HCl + N KCl; (2), 0.01 N H_2SO_4 + N Na_2SO_4; (3), 0.01 N KOH + N KCl on a Rh black electrode.

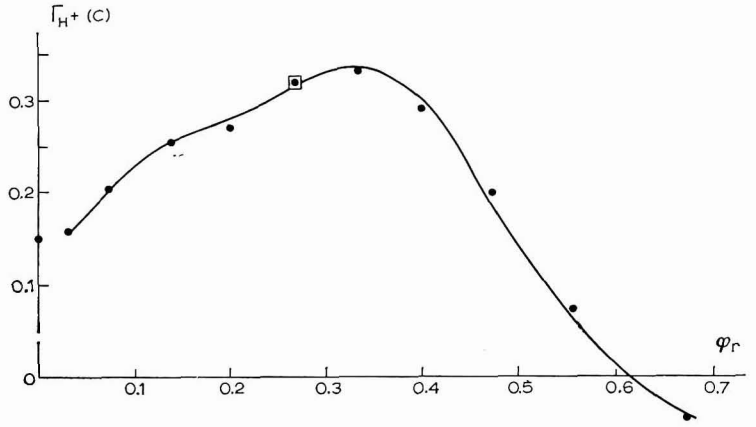

Fig. 6. Comparison of: (—), calcd. (by means of eqn. (10)) and (●), exptl. dependences of Γ_{H^+} upon φ_r for 0.01 N HCl + N KCl on a Ru black electrode. Γ_{H^+} is given in coulombs for the whole electrode surface.

is greater than unity. According to eqn. (12), this is possible owing to the value of $\partial\Gamma_{H^+}/\partial\varphi_r$ becoming negative, *i.e.*, the dependence of Γ_{H^+} upon φ_r must pass through a maximum.

In Figs. 5 and 6, the Γ_{H^+}–φ_r-curves theoretically-calculated from eqn. (10) are compared with the experimental curves*. The following should be noted. In the measurements of the slow charging curves of Rh and Ru by the usual method at the potentials of hydrogen adsorption (up to ~0.3 V) the anodic and cathodic charging curves coincide. However, when the measurements are performed up to 0.8 V, an appreciable hysteresis is observed. This introduces an uncertainty into the determination of the values of $\partial Q/\partial\varphi_r$, which are necessary for calculations by means of eqn. (10). The hysteresis is apparently due to slow establishment of equilibrium in oxygen adsorption. Therefore, the charging curves were determined as follows. A certain charge was supplied to the electrode, whereupon the polarizing circuit was opened. After the establishment of a constant potential, the electrode was again polarized, etc. The potentials established at open circuit were plotted against the amount of electricity passed. To distinguish these charging curves from those measured by the conventional method, we shall call them equilibrium curves. At the potential of hydrogen adsorption, the anodic and cathodic equilibrium charging curves coincide; at the potentials of oxygen adsorption (up to 0.8 V) only a slight hysteresis is observed, so that the choice of the direction of potential change in the charging curve measurements has little effect upon the calculation of the Γ_{H^+}–φ_r-curves[12,13]. The anodic charging curve was used in the calculations presented.

It can be seen from Figs. 5 and 6, that there is a quantitative agreement between the theoretically-calculated and experimental Γ_{H^+}–φ_r-curves for acid solutions. On the Rh electrode in an alkaline solution, a quantitative agreement is observed only up to $\varphi_r \sim 0.3$ V, which is possibly due to the difficulties in the establishment of equilibrium in alkaline solutions at the potentials of oxygen adsorption. However, at more anodic potentials also, there is a great similarity between the calculated and experimental curves.

According to Fig. 5, the p.z.c. of a Rh electrode in N Na_2SO_4 + 0.01 N H_2SO_4 solution lies at $\varphi_r \gtrsim 0.10$ V, and in N KCl + 0.01 N HCl solution, at $\varphi_r \gtrsim 0$ V, *i.e.*, $\varphi_{z.c.}$ is −0.04 and −0.12 V, respectively. The value of the p.z.c. of a Rh electrode in a sulfate solution coincides with that determined by the tracer method[15]. As was shown earlier[1,16,17] also for a Pt/Pt electrode, no p.z.c. in the usual sense is observed with a Rh electrode in alkaline solution. After passing through a minimum, the cation adsorption begins to increase again. At $\varphi_r = 0$, a marked acid adsorption is observed on a Ru electrode. In other words, the p.z.c. of Ru lies at a negative potential. The abcissa axis intersects with the Γ_{H^+}–φ_r-curve only at $\varphi_r \sim 0.61$ V. This potential can be considered as a p.z.c. of oxidized Ru.

Figure 7 shows the differential capacity curves of a Pt/Pt and Rh black electrodes in N KCl + 0.01 N HCl and N Na_2SO_4 + 0.01 N H_2SO_4 solutions, respectively.

* The values of Γ_{H^+} on the Rh electrode are given/cm² of true surface which was determined from the hydrogen section of the charging curve according to ref. 14.

The differential capacity curves were calculated from eqn. (15). The curves obtained have a feature in common, *viz.* at the potentials of hydrogen adsorption they pass through a pronounced maximum.

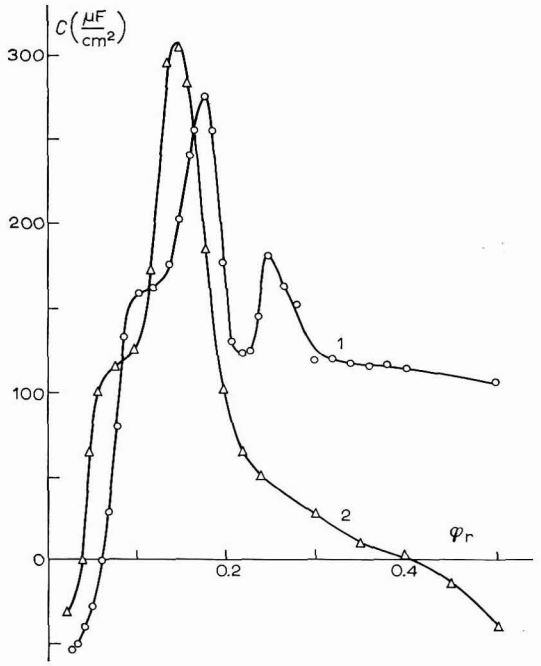

Fig. 7. Dependence of the differential capacity of the electric double layer upon φ_r on: (1), Pt/Pt electrode in 0.01 N HCl + N KCl; (2), Rh black electrode in 0.01 N H_2SO_4 + N Na_2SO_4. The capacity values are calcd./cm² of the true surface of the electrodes.

DISCUSSION OF RESULTS

The quantitative agreement between the theoretically-calculated and experimental Γ_{H^+}–φ_r-curves justifies treating the surface of the platinum-metals electrodes in solutions of varying composition as equilibrium systems, the state of which at μ_{CA}=constant is determined by the independent variables, μ_H and μ_{HA} or μ_{COH}. Especially interesting, and even somewhat surprising, is the fact that the assumption of reversibility holds not only for potentials of hydrogen adsorption, but to some extent also for those of oxygen adsorption, at least in acid solutions.

According to the Γ_{H^+}–φ_r-curves, the appearance of adsorbed oxygen on the surface of Rh and Ru electrodes brings about a decrease in anion adsorption, as was earlier observed on a Pt/Pt electrode[1,16,17]. Similar relationships appear to exist between the cation and hydrogen adsorptions*. Thus, the values of $(\partial\varphi/\partial\mu_{H^+})_Q$ on a

* A small maximum of cation adsorption had already been observed in ref. 1 in an approximate calculation of the adsorption curve.

Rh electrode in a 10^{-2} N $H_2SO_4 + N$ Na_2SO_4 solution at small φ_r are larger than unity, which should correspond to a decrease of Γ_{C^+} with decreasing φ_r. With direct adsorption measurements, however, a decrease in the cation adsorption could not be detected with certainty. Apparently, the method of measuring the dependence of the potential upon pH of the solution at constant Q (which gives directly the slope of the adsorption curve) permits a more accurate determination of the shape of the adsorption curve on approaching to $\varphi_r = 0$. At low φ_r, however, it becomes difficult to realize isoelectric conditions of the experiments and definite conclusions can be drawn only when the experimental technique is further refined, in accordance with the theory set out in ref. 5, to fit the case of the presence of dissolved H_2 in the solution in measurable concentrations.

As is evident from Fig. 1, on a Pt/Pt electrode in pure acid solutions at the potentials of the double-layer region $\partial\varphi/\partial\mu^{\pm}_{HA} = -1$. In other words, the electrode potential, φ, shifts by ~ 58 V when the HCl concentration is changed by one order of magnitude. Thus, the Esin–Markov effect associated with the discrete structure of the double layer is not observed with a Pt electrode in the case of Cl^- ions. In this respect, the Pt electrode differs from the Hg electrode. The absence of the effect of discreteness may be assumed to be due to a strong chemisorptive interaction between the adsorbed anions and the platinum surface, which results in the anions sharing their charges, to a considerable degree, with the metal*. According to eqn. (40)**, the absence of any appreciable super-equivalent adsorption of cations and anions[4,17] on platinum also points to the absence of a Esin–Markov effect. The high values of the electric double-layer capacity of the Pt/Pt electrode at the potentials of the double-layer region (~ 70–100 $\mu F/cm^2$) are an indication of a strong deformation of anions upon adsorption. The decrease of the capacity observed in the case of Rh in $H_2SO_4 + Na_2SO_4$ (Fig. 7, curve 2) is caused by the appearance of oxygen.

The differential capacity curves of the electric double layer of a Pt/Pt electrode, given in the present paper, show some interesting features. The decrease in the capacity on approaching to $\varphi_r = 0$, due to the surface coverage with adsorbed hydrogen, had already been observed and discussed in the literature[1,4]. The data obtained show that a similar phenomena is also observed on a Rh electrode. The decrease in the capacity on lowering φ_r is preceded by a strong increase up to values of the order of 300 $\mu F/cm^2$ in the region of hydrogen adsorption. In the case of the Pt/Pt electrode, the highest value of the capacity is observed near the p.z.c. of the electrode. This coincidence seems to be accidental, however, since on a Rh electrode the maximum is observed at potentials that are remote from the p.z.c. Thus, the capacity maximum cannot be explained by the change in the double-layer structure with changing sign of the surface charge. Nor can the capacity maximum be associated with the peculiarities of specific anion adsorption since it is also observed in the presence of weakly adsorbable SO_4^{2-} anions. The capacity maximum seems to be due to the displacement

* According to the theory developed by LEVICH, KIRYANOV AND KRYLOV[18], the Esin–Markov effect should disappear with decreasing distance between the inner Helmholtz plane and the metal surface.
** See Appendix.

of adsorbed anions by adsorbed hydrogen, forming dipoles turned with their negative ends towards the solution and at the same time decreasing the electric double-layer capacity. A more complete interpretation of this phenomenon necessitates further investigation involving a greater number of systems.

APPENDIX

Potential change under isoelectric conditions with changing concentration of neutral salt

It follows from eqns. (4) and (7) that

$$\left(\frac{\partial \Gamma_H}{\partial \mu_{CA}}\right)_{\varphi_r,\mu_{HA}} = -\left(\frac{\partial \Gamma_{CA}}{\partial \varphi_r}\right)_{\mu_{CA},\mu_{HA}} \tag{34}$$

$$\left(\frac{\partial \varphi_r}{\partial \mu_{CA}}\right)_{\Gamma_H,\mu_{HA}} = -\left(\frac{\partial \varphi_r}{\partial \Gamma_H}\right)_{\mu_{CA},\mu_{HA}} \left(\frac{\partial \Gamma_H}{\partial \mu_{CA}}\right)_{\varphi_r,\mu_{HA}}$$

$$= -\left(\frac{\partial \Gamma_{CA}}{\partial \varphi_r}\right)_{\mu_{CA},\mu_{HA}} : \left(\frac{\partial Q}{\partial \varphi_r}\right)_{\mu_{CA},\mu_{HA}} = -\left(\frac{\partial \Gamma_{CA}}{\partial Q}\right)_{\mu_{CA},\mu_{HA}} \tag{35}$$

It follows from eqns. (35) and (1) that

$$\left(\frac{\partial \varphi_r}{\partial \mu_{CA}^{\pm}}\right)_{Q,\mu_{HA}} = -2\left(\frac{\partial \Gamma_{C^+}}{\partial Q}\right)_{\mu_{CA},\mu_{HA}} \tag{36}$$

where $\mu_{CA}^{\pm}$ is the mean chemical potential of CA ions.

Let us introduce in place of φ_r, the potential φ_{C^+} measured against an electrode reversible with respect to the C^+ cation. Since

$$\varphi_{C^+} + \mu_{C^+} = \varphi_r + \mu_{H^+} + \text{const.}$$

and, hence, $\varphi_{C^+} + \mu_{CA} = \varphi_r + \mu_{HA} + \text{const.}$, we get, according to eqn. (35)

$$\left(\frac{\partial \varphi_{C^+}}{\partial \mu_{CA}}\right)_{Q,\mu_{HA}} = -\left(\frac{\partial \Gamma_{C^+}}{\partial Q}\right)_{\mu_{CA},\mu_{HA}} - 1 \tag{37}$$

At $A_H = 0$, $dQ = d\varepsilon = d\Gamma_{A^-} - d\Gamma_{C^+}$ and eqn. (37) becomes the well known equation of electrocapillarity theory[9]:

$$\left(\frac{\partial \varphi_{C^+}}{\partial \mu_{CA}}\right)_{\varepsilon,\mu_{HA}} = -\left(\frac{\partial \Gamma_{A^-}}{\partial \varepsilon}\right)_{\mu_{CA},\mu_{HA}} \tag{38}$$

If in place of φ_{C^+}, we introduce the potential, φ, referred to an imaginary reference electrode, which is by $\mu_{CA}^{\pm}$ more negative than the electrode reversible with respect

to C^+, and which in thermodynamical relations can serve as a constant reference electrode at any concentrations[8] (see above), we obtain from eqn. (37):

$$\left(\frac{\partial\varphi}{\partial\mu^{\pm}_{CA}}\right)_{Q,\mu_{HA}} = -2\left(\frac{\partial\Gamma_{C^+}}{\partial Q}\right)_{\mu_{HA},\mu^{\pm}_{CA}} - 1 \tag{39}$$

At $A_H=0$, eqn. (39) becomes

$$\left(\frac{\partial\varphi}{\partial\mu^{\pm}_{CA}}\right)_{\varepsilon,\mu_{HA}} = -\left(\frac{\partial\Gamma_{C^+}}{\partial\varepsilon}\right)_{\mu_{HA},\mu^{\pm}_{CA}} - \left(\frac{\partial\Gamma_{A^-}}{\partial\varepsilon}\right)_{\mu_{HA},\mu^{\pm}_{CA}} \tag{40}$$

Equation (40) is a thermodynamical expression for the Esin–Markov coefficient as applied to the change in neutral salt concentration; it is similar to the relation known from electrocapillarity theory. By means of this expression, it is possible to find the coefficient in question from the $(\partial\varphi/\partial\mu^{\pm}_{CA})_{\varepsilon,\mu_{HA}}$ value at any concentrations, whereas the relation derived earlier (eqn. (9a) in ref. 5), which can be written as:

$$\left(\frac{\partial\varphi}{\partial\mu^{\pm}_{CA}}\right)_{\varepsilon,\mu_{H^+}} = -\left(\frac{\partial\Gamma_{C^+}}{\partial\varepsilon}\right)_{\mu^{\pm}_{CA},\mu_{H^+}} - \left(\frac{\partial\Gamma_{A^-}}{\partial\varepsilon}\right)_{\mu^{\pm}_{CA},\mu_{H^+}} \tag{41}$$

is applicable only to dilute solution. It can be readily shown (see footnote on p. 190) that in the case of dilute solutions, it is possible to obtain eqn. (41) from eqn. (40).

It is more convenient, for use with experimental data, to have relations expressing the dependence of φ_r or φ upon $\mu^{\pm}_{CA}$ under isoelectric conditions, not at constant μ_{HA} as for example, in eqn. (36), but at constant [HA]. This dependence can be obtained from eqn. (36) using eqns. (6) or (8), *i.e.*, by superimposing upon the change of μ_{CA} a change of μ_{HA} to bring [HA] to its original value. Assuming [CA] $\gg$ [HA], it follows from eqns. (3) and (8) that

$$\left(\frac{\partial\varphi_r}{\partial\mu^{\pm}_{CA}}\right)_{Q,[HA]} = \left(\frac{\partial\varphi_r}{\partial\mu^{\pm}_{CA}}\right)_{Q,\mu_{HA}} + \left(\frac{\partial\varphi_r}{\partial\mu_{HA}}\right)_{Q,\mu^{\pm}_{CA}}\left(\frac{\partial\mu_{HA}}{\partial\mu^{\pm}_{CA}}\right)_{[HA]}$$

$$= -2\left(\frac{\partial\Gamma_{C^+}}{\partial Q}\right)_{\mu^{\pm}_{CA},\mu_{HA}} - \left(\frac{\partial\Gamma_{H^+}}{\partial Q}\right)_{\mu^{\pm}_{CA},\mu_{HA}}\left(\frac{\partial\mu_{HA}}{\partial\mu^{\pm}_{CA}}\right)_{[HA]} \tag{42}$$

It follows from eqns. (42) and (1) that

$$\left(\frac{\partial\varphi_r}{\partial\mu^{\pm}_{CA}}\right)_{Q,[HA]} =$$

$$= -\left[2 - \left(\frac{\partial\mu_{HA}}{\partial\mu^{\pm}_{CA}}\right)_{[HA]}\right]\left(\frac{\partial\Gamma_{C^+}}{\partial Q}\right)_{\mu^{\pm}_{CA},\mu_{HA}} - \left(\frac{\partial\mu_{HA}}{\partial\mu^{\pm}_{CA}}\right)_{[HA]}\left(\frac{\partial\Gamma_{A^-}}{\partial Q}\right)_{\mu^{\pm}_{CA},\mu_{HA}} \tag{43}$$

In an experimental verification of eqn. (43), $(\partial\mu_{HA}/\partial\mu^{\pm}_{CA})_{[HA]}$ can be found, for example, from the change of e.m.f. of a cell with electrodes reversible with respect to H^+ and A^- in an (HA+CA) solution on changing [CA] at constant [HA]. Since [CA] $\gg$ [HA], $\mu^{\pm}_{CA}$ can be taken from the data in the literature*.

SUMMARY

A derivation of the equations relating the potential change of an hydrogen adsorbing electrode with changing hydrogen ion activity under isoelectric conditions, to the dependence of the hydrogen ion adsorption upon the potential has been given, which can be applied to solutions of any concentration. Similar equations have been derived for alkaline solutions and for an oxygen adsorbing electrode. The calculated dependences of the hydrogen ion adsorption upon the potential have been compared with the experimental data for the following systems: Pt in 10^{-2} *N* HCl, Rh in *N* $Na_2SO_4 + 10^{-2}$ *N* H_2SO_4, Rh in *N* KCl + 10^{-2} *N* HCl, Rh in *N* KCl + 10^{-2} *N* KOH, Ru in *N* KCl + 10^{-2} *N* HCl. It has been found that in the case of Cl^- ions adsorption on Pt from HCl solutions, the Esin–Markov effect disappears; this seems to be due to the transfer of the charge of the adsorbed anions to the electrode surface. It has been shown that measurements of the dependence of the potential upon the hydrogen ion activity under isoelectric conditions in the presence of an excess of neutral salt, is a direct method for the determination of the double-layer differential capacity of a hydrogen adsorbing electrode.

REFERENCES

1 A. FRUMKIN AND A. ŠLYGIN, *Acta Physicochim. URSS*, 5 (1936) 819.
2 A. FRUMKIN, *Advan. Electrochem. Electrochem. Eng.*, Vol. 3, edited by P. Delahay, Interscience Publishers Inc., New York, 1963, p. 287.
3 A. FRUMKIN, *Elektrokhimiya*, 2 (1966) 387.
4 A. FRUMKIN, N. BALASHOVA AND V. KAZARINOV, *J. Electrochem. Soc.*, 113 (1966) 1011.
5 A. FRUMKIN, O. PETRY AND R. MARVET, *J. Electroanal. Chem.*, 12 (1966) 504.
6 O. PETRY, R. MARVET AND A. FRUMKIN, *Elektrokhimiya*, 3 (1967) 116.
7 O. PETRY, A. KOSSAYA-TSYBULEVSKAYA AND YU. TYURIN, *Elektrokhimiya*, 3 (1967) 617.
8 A. FRUMKIN, *Zh. Fiz. Khim.*, 30 (1956) 2066.
9 S. CRAXFORD, O. GATTY AND H. A. C. MCKAY, *Phil. Mag.*, 22 (1936) 359.

* In dilute solutions where the inequality [CA] $\gg$ [HA] is valid, μ_{A^-} can be equated with $\mu^{\pm}_{CA}$, and since $\mu_{HA} = \mu_{H^+} + \mu_{A^-}$

$$\left(\frac{\partial\mu_{HA}}{\partial\mu^{\pm}_{CA}}\right)_{[HA]} = 1 \tag{44}$$

In this case, the condition [HA] = constant coincides with μ_{H^+} = constant. Thus, for dilute solutions it follows from eqns. (43) and (44) that

$$\left(\frac{\partial\varphi_r}{\partial\mu^{\pm}_{CA}}\right)_{Q,\mu_{H^+}} = \left(\frac{\partial\varphi}{\partial\mu^{\pm}_{CA}}\right)_{Q,\mu_{H^+}} = -\left(\frac{\partial\Gamma_{C^+}}{\partial Q}\right)_{\mu^{\pm}_{CA},\mu_{H^+}} - \left(\frac{\partial\Gamma_{A^-}}{\partial Q}\right)_{\mu^{\pm}_{CA},\mu_{H^+}} \tag{45}$$

At $A_H = 0$, eqn. (45) becomes eqn. (41).

10 R. PARSONS, *Proc. IInd Congr. Surf. Activity, Electrical Phenomena, 1957*, Butterworths, London, 1957, p. 38.
11 O. PETRY AND V. TOPOLEV, *Elektrokhimiya*, in press.
12 A. FRUMKIN, O. PETRY AND A. KOSSAYA, *Elektrokhimiya*, in press.
13 O. PETRY AND V. ENTINA, *Elektrokhimiya*, in press.
14 M. TARASEVICH, K. RADYUSHKINA AND R. BURSHTEIN, *Elektrokhimiya*, 3 (1967) 455.
15 N. BALASHOVA, A. KOSSAYA AND N. GOROKHOVA, *Elektrokhimiya*, 3 (1967) 656.
16 A. ŠLYGIN, A. FRUMKIN AND V. MEDVEDOVSKY, *Acta Physicochim. URSS*, 4 (1936) 911.
17 N. BALASHOVA AND V. KASARINOV, *Usp. Khim.*, 34 (1965) 1721.
18 B. LEVICH, V. KIRYANOV AND V. KRYLOV, *Dokl. Akad. Nauk SSSR*, 135 (1960) 1425.

ELECTROANALYTICAL CHEMISTRY AND INTERFACIAL ELECTROCHEMISTRY
Elsevier Sequoia S.A., Lausanne – Printed in The Netherlands

ADSORPTION OF HALIDES AT THE MERCURY–WATER INTERFACE

JOHN LAWRENCE AND ROGER PARSONS*
Department of Physical Chemistry, The University, Bristol, 8 (England)
RICHARD PAYNE
Air Force Cambridge Research Laboratories, L. G. Hanscom Field, Bedford, Mass. (U.S.A.)
(Received May 10th, 1967)

INTRODUCTION

Recent discussions[1–3] of the measurement of adsorption of ions at the mercury–water interface have suggested that discrepancies exist between the two principal methods of obtaining these results: electrocapillary measurements and capacity measurements. It has been suggested that some of the discrepancies are due to inevitable inaccuracies in the computation of data by the different routes and that some arise from essential differences in the quantities measured.

In order to assesss the situation, existing capacity data on NaF[4], KCl[5], and KI[6], together with new data on KBr, are compared with electrocapillary data[7–10] with particular attention to the accuracy with which the required data can be obtained.

EXPERIMENTAL

Measurements of the double-layer capacity of mercury in aqueous KBr solution were made using the bridge previously described[11]. The balance point was usually taken just after the 8th second on a drop the total life of which was 10–12 sec, but the capacity was checked over the range between the 4th and 10th second to ensure independence of the drop age. Similar checks were made in the frequency range 600 c/sec–3 kc/sec. No frequency-dependence was observed and measurements were made at 1 kc/sec. Reproducibility of capacities was 0.05% within a given run and 0.15% from one run to another. The flow rate of Hg (normally about 0.2 mg sec^{-1}) was determined by collecting mercury over an accurately timed (1 kc/sec tuning fork + dekatron scaler) interval, drying and weighing. It remained constant within 0.2%. Thin-walled, tapering capillaries were drawn from 1-mm bore capillary tubing, selected by trial and siliconed by brief exposure to dichlorodimethylsilane vapour, followed by wet nitrogen. The tip was then recut to ensure that the solution should wet the horizontal surface of the tip. The potential of the electrocapillary maximum was determined by the streaming electrode method[12] and was reproducible to within 0.5 mV. All potentials were measured using a Croydon type P3 potentio-

* At present, Visiting Professor, Division of Chemistry and Chemical Engineering, California Institute of Technology, Pasadena, Calif. 91109.

meter and a Pye "Scalamp" 1400 Ω galvanometer. The reference electrode was a 0.1 *M* KCl calomel electrode joined to a reservoir containing 0.1 *M* KBr. This solution was then put in contact with the working solution of KBr, forming the junction in a tap. Both these liquid junctions were stable and potentials were reproducible to 0.1 mV. All measurements were made with the cell immersed in a water thermostat at 25°. Mercury was purified by a wet process followed by three distillations in a Hulett still[13]. Laboratory-distilled water was redistilled from dilute alkaline permanganate in a still with special splash traps. B.D.H. AnalaR KBr or once-recrystallized salt was dissolved in this water.

RESULTS AND ANALYSIS

Measurements were made of the capacity and potential of the electrocapillary maximum at ten concentrations of KBr from 0.005 to 5 *M*. The capacity curves are shown in Fig. 1. The interfacial tension at the electrocapillary maximum was obtained

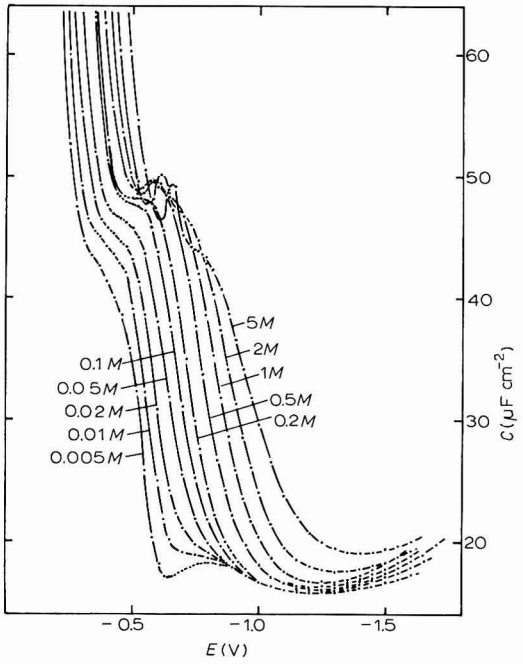

Fig. 1. Capacity of a mercury electrode in contact with aq. KBr at 25°. Concn. of KBr is indicated by each curve. Potential is measured with respect to a 0.1 *M* KCl calomel electrode dipping into a soln. containing 0.1 *M* KBr which made contact with the working soln.

by plotting the experimental values found by GOUY[7] and by DEVANATHAN AND PERIES[9] as a function of log activity, and interpolating. There are small differences between the two sets of electrocapillary data but it is unlikely that errors exceed 0.2 dyn cm^{-1} at concentrations below 1 *M*; at higher concentrations they may rise to 0.5 dyn cm^{-1}. The capacity–potential curves were integrated with the aid of a computer (Elliott 503) using a program written in Algol but similar to that described

TABLE 1

0.01 *M* KBr IN WATER AT 25°

q ($\mu C\ cm^{-2}$)	$-E$ (V)	C ($\mu F\ cm^{-2}$)	q_+ ($\mu C\ cm^{-2}$)	q_-^1 ($\mu C\ cm^{-2}$)	ϕ_2 (mV)	ϕ^{M-2} (mV)	γ ($dyn\ cm^{-1}$)
−18	1.592	17.59	16.0	1.4	−172	−958	329.8
−16	1.475	16.65	14.0	1.5	−165	−848	349.7
−14	1.353	16.04	12.1	1.4	−158	−733	368.0
−12	1.227	15.90	10.2	1.3	−150	−616	384.3
−10	1.102	16.16	8.3	1.1	−140	−500	398.1
−8	0.982	17.04	6.5	1.0	−128	−392	408.9
−6	0.868	18.24	4.5	1.0	−111	−295	416.9
−4	0.761	18.88	2.5	1.0	−86	−213	422.3
−2	0.656	19.76	+0.8	+0.8	−46	−149	425.4
0	0.572	29.08	0.0	0.0	0	−105	426.3
+2	0.512	37.75	−0.1	−1.8	+8	−58	425.7
4	0.463	42.74	+0.1	−4.1	−5	+4	424.3
6	0.417	43.75	0.3	−6.6	−23	69	422.0
8	0.371	45.09	0.7	−9.0	−41	131	418.8
10	0.328	46.40	1.2	−11.5	−56	190	414.9
12	0.286	51.51	1.7	−14.1	−69	245	410.3
14	0.250	60.00	2.2	−16.7	−81	293	405.6
16	0.220	72.20	2.9	−19.4	−92	334	401.1
18	0.191	95.88	3.5	−22.0	−100	371	396.3
20	0.173	130.9	4.0	−24.5	−106	395	392.9
22	0.160	165.1	4.6	−27.2	−112	415	390.0
24	0.144	231.0	5.2	−29.7	−118	436	386.7

TABLE 2

0.1 *M* KBr IN WATER AT 25°

q ($\mu C\ cm^{-2}$)	$-E$ (V)	C ($\mu F\ cm^{-2}$)	q_+ ($\mu C\ cm^{-2}$)	q_-^1 ($\mu C\ cm^{-2}$)	ϕ_2 (mV)	ϕ^{M-2} (mV)	γ ($dyn\ cm^{-1}$)
−18	1.543	17.79	17.6	−1.3	−121	−962	331.7
−16	1.428	16.87	15.5	−1.1	−115	−853	351.4
−14	1.307	16.24	13.3	−0.9	−108	−739	369.5
−12	1.182	16.03	11.0	−0.6	−100	−623	385.6
−10	1.059	16.40	8.9	−0.4	−90	−508	399.3
−8	0.940	17.57	6.9	−0.3	−80	−400	409.9
−6	0.833	20.17	5.3	−0.7	−69	−304	417.4
−4	0.745	25.87	4.2	−1.5	−61	−223	421.9
−2	0.678	33.90	3.8	−3.0	−57	−160	424.0
0	0.624	41.56	3.8	−5.1	−58	−107	424.5
+2	0.578	45.58	4.1	−7.4	−60	−59	424.1
4	0.536	47.56	4.5	−9.8	−63	−13	422.8
6	0.494	47.87	4.9	−12.2	−66	+33	420.7
8	0.452	48.20	5.4	−14.8	−70	78	417.8
10	0.411	50.29	5.9	−17.3	−74	122	414.1
12	0.373	56.50	6.5	−14.9	−77	164	404.9
14	0.341	65.56	7.0	−22.5	−81	200	405.7
16	0.312	73.86	7.6	−25.1	−84	232	401.4
18	0.285	87.43	8.2	−27.7	−87	262	396.9
20	0.265	105.7	8.8	−30.3	−90	285	392.9
22	0.242	144.4	9.3	−32.9	−92	310	388.5
24	0.230	189.5	9.8	−35.4	−95	324	385.7

previously[14] in the first routine where values of the function $\xi_{\pm}=\gamma+qE_{\pm}$ are calculated. Here γ is the interfacial tension, q the charge on the metal and $E_{\pm}$ the potential of the mercury electrode with respect to an electrode reversible to the cation (+subscripts) or anion (−subscripts). The new program further fits the pairs of values of $\xi_{\pm}$ and log activity at a given value of q, to a power series by the method of least-squares. The ionic surface excesses are then calculated according to the appropriate form of the electrocapillary equation[15]

$$(\partial\xi_{\pm}/RT\partial \ln a_{\pm}^{2})_q = -\Gamma_{\mp} = -q_{\mp}/z_{\mp}F$$

From the charge due to the cation, the program then uses Gouy–Chapman theory[16] to calculate the outer Helmholtz potential (ϕ_2) and the charge in the diffuse layer due to the anion. Finally, the charge (q_{-1}) due to specifically adsorbed anions and the potential drop (ϕ^{M-2}) across the inner layer are computed. Some typical results are shown in Tables 1, 2, and 3.

TABLE 3

1 *M* KBr IN WATER AT 25°

q ($\mu C\ cm^{-2}$)	$-E$ (V)	C ($\mu F\ cm^{-2}$)	q_{+} ($\mu C\ cm^{-2}$)	q_{-1} ($\mu C\ cm^{-2}$)	ϕ_2 (mV)	ϕ^{M-2} (mV)	γ ($dyn\ cm^{-1}$)
−18	1.488	18.09	13.0	0.9	−60	−969	334.0
−16	1.373	17.09	11.3	0.9	−55	−859	353.4
−14	1.254	16.71	9.7	0.6	−50	−746	371.2
−12	1.136	17.13	8.4	0.2	−46	−632	386.7
−10	1.025	19.28	7.4	−0.7	−42	−524	398.9
−8	0.931	24.10	7.0	−2.2	−40	−432	407.4
−6	0.858	30.94	7.1	−4.3	−41	−359	412.5
−4	0.799	37.50	7.6	−6.9	−43	−298	415.5
−2	0.750	43.16	8.4	−9.8	−46	−246	417.0
0	0.705	45.87	9.3	−12.8	−49	−198	417.4
+2	0.663	48.05	10.1	−15.8	−52	−153	417.0
4	0.621	48.80	10.9	−18.7	−54	−109	415.7
6	0.581	49.56	11.7	−21.6	−56	−66	413.7
8	0.540	48.48	12.5	−24.5	−59	−23	410.9
10	0.499	49.63	13.3	−27.4	−61	+20	407.2
12	0.460	53.67	14.1	−30.2	−63	61	402.9
14	0.425	60.42	14.9	−33.1	−65	98	398.3
16	0.394	69.34	15.6	−35.8	−67	131	393.6
18	0.367	80.57	16.3	−38.6	−68	160	389.1
20	0.343	94.77	17.0	−41.4	−70	186	384.5
22	0.323	113.1	17.7	−44.1	−71	206	380.5
24	0.307	132.2	18.3	−46.7	−73	224	376.7

DISCUSSION

(a) Comparison with other data

Direct comparison of the integrated capacity curves with the electrocapillary curves measured by DEVANATHAN AND PERIES[9] is possible at 0.01, 0.1, and 1 *M*. This is illustrated in Fig. 2(a), (b), and (c). Deviations between the two curves are never greater than 1 dyn cm^{-1} in the range +24 to −18 μC cm^{-2} and more often of the order of 0.1 dyn cm^{-1}. Thus, in this system there appears to be little doubt that the two methods of measurement are in agreement within experimental error.

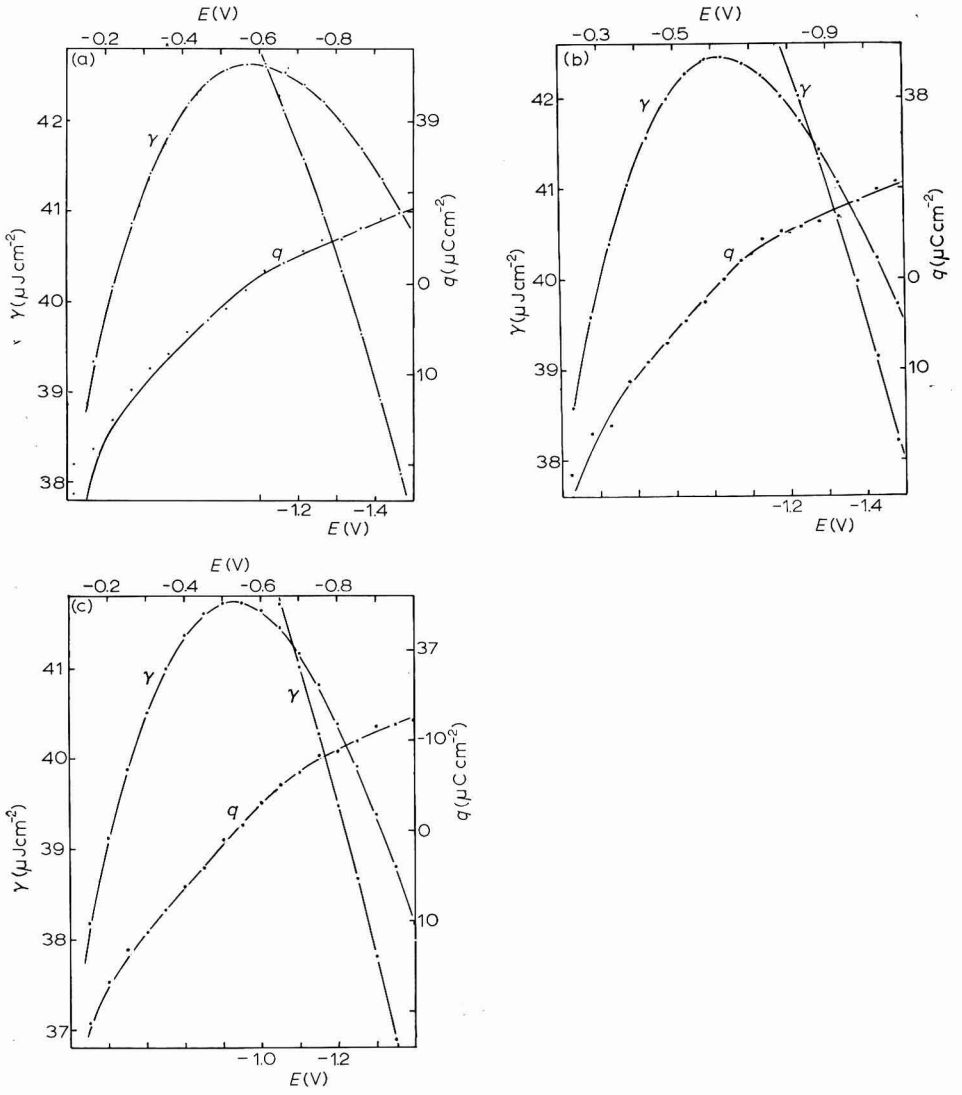

Fig. 2. Comparison of electrocapillary curves and charge–potential curves obtained from capacity measurements (full line) with those obtained from electrocapillary measurements of DEVANATHAN AND PERIES[9] (points). The extreme negative part of the electrocapillary curve is shown on a separate scale. (a), 0.01 *M*; (b), 0.1 *M*; (c), 1.0 *M* KBr.

Similar conclusions may be drawn from a comparison of the integral of GRAHAME's data[5,6] for 0.1 and 1 *M* KCl, 0.015, 0.1 and 1 *M* KI with electrocapillary results[7–10]. Agreement in dilute solutions of weakly adsorbed electrolytes is poorer, as already reported[1,4] for $H_2PO_4^-$ and Cl^-. The appearance of the diffuse-layer minimum in the capacity curve is an indication of conditions under which disagreement may be expected. In the case of $H_2PO_4^-$, where the disagreement is large, evidence was

presented[14] supporting the proposal that the electrocapillary data are in error under these conditions.

Similar results are obtained with fluoride solutions, as might be expected. In 0.1 *M* solution, as shown in Fig. 3, GRAHAME's capacity curves for NaF[4], when

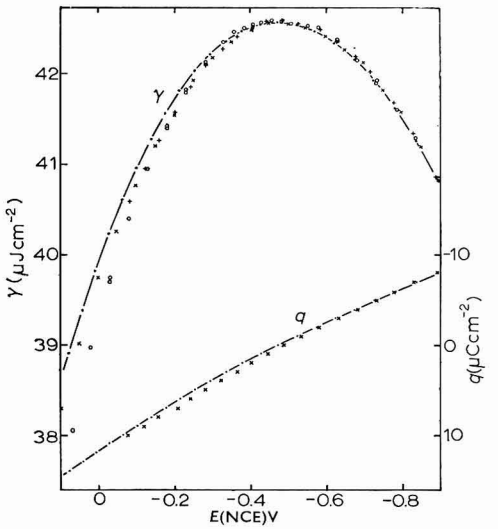

Fig. 3. Comparison of electrocapillary curves and charge–potential curves obtained from capacity measurements on 0.1 *M* NaF by GRAHAME (—·—) with those from electrocapillary measurements: (×), DUTKIEWICZ, KF; (+), DUTKIEWICZ, NH_4F; (○), PAYNE, NaF.

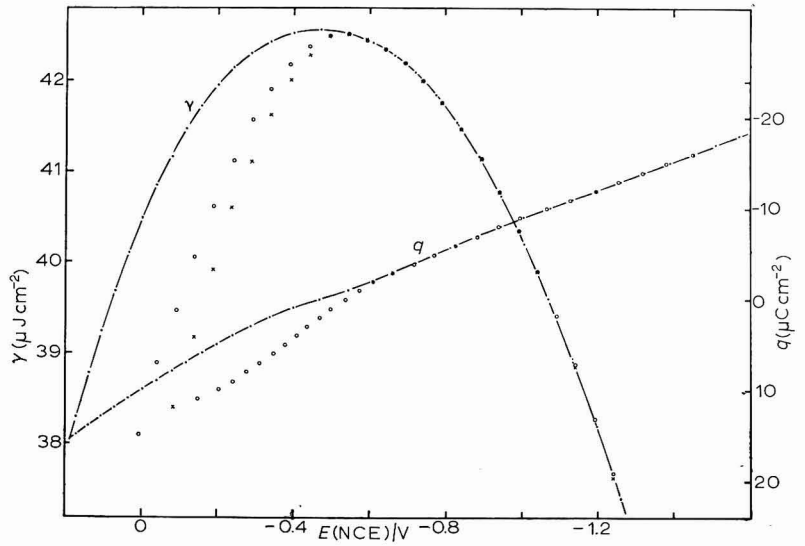

Fig. 4. Comparison of electrocapillary curves and charge–potential curves obtained from capacity measurements on 0.01 *M* NaF (—·—) with those obtained from electrocapillary measurement: (○), with an unsiliconed capillary; (×), with a siliconed capillary.

integrated agree well with electrocapillary curves measured in Bristol using NaF (PAYNE), KF (DUTKIEWICZ), and NH_4F (DUTKIEWICZ AND GARNISH) except for small divergences on the positive branch reaching 1.6 dyn cm^{-1} at $+10\,\mu C\ cm^{-2}$. However in 0.01 *M* NaF, the discrepancies become very large on the positive branch although the agreement on the negative branch is excellent (Fig. 4). In the electrocapillary measurements, "sticking" was observed at potentials (*vs.* NCE) > -0.25V and also < -1.25 V; in the former region the electrocapillary curve lies well below the integrated capacity curve while in the latter they agree well. Use of a siliconed capillary in the electrometer reduces the amount of "sticking" and confines it to the region of potentials > -0.1 V. As can be seen from Fig. 4, agreement with the integrated capacity is still excellent at potentials < -0.55 V. However, in the region where the electrocapillary curve diverges from the integrated capacity curve, the electrocapillary curve measured with the siliconed capillary lies markedly below that measured with the unsiliconed capillary; the divergences reach 10 dyn cm^{-1} at -0.1 V.

These results show that variation in the wetting properties of the glass affects the electrocapillary curve over the region in which divergences from the integrated capacity curve occur. This behaviour suggests that the phenomenon is related to the "de-wetting" process described by GOUY[7], and may be due to a change of the contact angle at the glass–mercury–solution contact. This is consistent with the lower apparent interfacial tension observed with the siliconed capillary, where the contact angle would be expected to be greater because water wets siliconed glass imperfectly. However, it appears that when the mercury is negatively charged, the contact angle is zero for both types of capillary.

Attempts have been made to study the drop-time curve in this system in the hope that these curves would be less affected by changes in the contact angle. The results were not very reproducible and showed an anomalous minimum in the drop-time curves at potentials more positive than the maximum. On the negative side, the correct qualitative behaviour was found but the curves were not in good agreement with the electrocapillary curves.

Comparison of charge–potential curves derived from the two types of measurement confirms that they are usually in good agreement within the errors to be expected from graphical differentiation of electrocapillary curves. This accuracy will depend on the spacing of experimental points; 50-mV intervals have been usual in recent studies[9,14,17]. Comparison of the present results with those of DEVANATHAN AND PERIES[9] (Fig. 2(a), (b), and (c)) suggests that the general trend is in good agreement although a scatter of $1\,\mu C\ cm^{-2}$ in individual points is fairly frequent. At the far anodic end, when the charge is greater than $20\,\mu C\ cm^{-2}$ and both the electrocapillary curve and the capacity curve are very steep, the errors may be much larger Electrocapillary curves were also differentiated using a computer following a procedure based on an unpublished suggestion by GRAHAME. From the set of γ–E points, a new set of points, y–E, was computed where $y = \gamma + q^*E$, q^* being a constant. The curve y–E now has a maximum at the value of E for which q^* is the slope of the original γ–E curve. Thus, by repeating this procedure a set of values of E corresponding to given values of q^* may be found. The value of y at the maximum of the y–E curve is, of course, the value of ξ corresponding to q^* and the fact that the y–E curve has a flat maximum shows that ξ may be obtained with an accuracy comparable to

the original values of γ. In fact, the calculation of ξ does not depend upon an accurate differentiation of the electrocapillary curve, in contrast to the remark of DEVANATHAN AND TILAK[2]. This procedure is thus excellent for converting from γ to ξ but does not produce charge–potential curves of any greater accuracy than those from graphical differentiation.

Direct comparison of twice-differentiated electrocapillary curves with capacity curves again confirms, qualitatively, the agreement between the two types of measurement, but the inaccuracies introduced by differentiation are too great to allow more quantitative conclusions.

The most important information obtained from capacity and electrocapillary measurements concerns the ionic composition of the double layer. This is obtained by the application of Gibbs adsorption equation in one form or another and necessarily involves a differentiation step, although this may be carried out by fitting integrated theoretical isotherms to the experimental data[15] and then differentiating analytically. Such a procedure has particular advantages if the isotherm constants are independent of charge, but there is a risk in imposing this condition on a set of data since the surface–pressure curve is not very sensitive to variations in isotherm constants. A more direct procedure might therefore have advantages. The computer program described above is an attempt to solve this problem in a simple way. In fitting a polynomial to the $\xi_{\pm}$–ln $a_{\pm}$ points, different degrees of polynomial were examined. High-order polynomials produce results that are too sensitive to experimental error

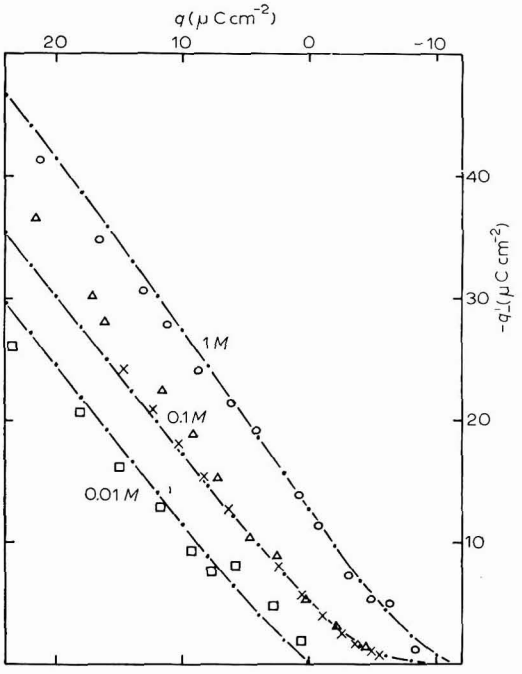

Fig. 5. Plot of charge due to specifically adsorbed Br^- (q_{-}^{-1}) *vs.* charge on the mercury electrode: (—·—), present results; (×), data of GRAHAME AND SODERBERG[18] at 0.1 *M* KBr; data of DEVANATHAN AND PERIES[9] at: (○), 1 *M*; (△), 0.1 *M*; (□), 0.01 *M* KBr.

and are consequently meaningless. The criterion adopted was that of comparing the results of an n-th order fit, with that of an $(n+1)$-th order fit. Best agreement was obtained when $n=3$. Even so, the end-points produced large variations, the results being less plausible for the 4th- than for the 3rd-order fit. It is, therefore, recommended that a 3rd-order polynomial provides the most satisfactory simple route to the differentiation of $\xi_{\pm}$–ln $a_{\pm}$ curves. Agreement with graphical differentiation for the KBr system was found to be within 0.3 μC cm^{-2} except at extreme concentrations or charges. The curves of q_-^{-1} against q can be compared directly (Fig. 5) with the results of GRAHAME AND SODERBERG[18] at 0.1 M and of DEVANATHAN AND PERIES[9] at 0.01, 0.1, and 1 M. With the former, no deviation is greater than 0.7 μC cm^{-2}, while with the latter discrepancies of greater than 1 μC cm^{-2} are found, undoubtedly as a result of errors introduced by graphical differentiation to obtain both q_-^{-1} and q.

As a further check, the data of GRAHAME[6] for aqueous KI was put through the computer program using integration constants based on electrocapillary data[7–10]. In this case, the agreement between the 3rd- and 4th-order fits was much better and at the lower concentrations good agreement with the published data[6] was obtained. The results obtained from this system are undoubtedly better, primarily because the concentration points are more closely spaced. GRAHAME[6] measured capacities at 17 concentrations between 0.015 and 1.2 M; *i.e.*, over 8 points/decade. The present KBr results are based on 3 points/decade and must be correspondingly less accurate. This must be considered as the main weakness of much recent work on the electrical double layer[14,19] especially that based on 2 points/decade[9,17].

At concentrations of the order of 1 M and higher, the computed KI results differ from the published data[6] owing to the effect of the thickness of the inner layer previously discussed[5]. In spite of contrary assertions[2], there seems good reason to suppose that the correction for this effect is charge-dependent[14]. Since no way of measuring this effect in the presence of specific adsorption has been devised, values of q_-^{-1} for solutions of higher concentrations are subject to error from this cause as well as from defects in diffuse-layer theory.

Data from the dilute solutions calculated from capacity measurements with the aid of electrocapillary integration constants, also appear to deviate by a microcoulomb or two from the expected value at negative charge, as commented upon recently[19]. It is possible that this may be the result of the slow transport of ions to the double layer[20,21] but a clear proof that this is the cause is at present lacking.

(b) Specific adsorption of bromide ion

Adsorption isotherms at constant charge for bromide ion are shown in Fig. 6. The shape of the isotherm changes quite markedly with potential in a similar way to that observed previously[5] with KCl. At high positive charges, the slope becomes quite low even at amounts adsorbed of between 20 and 30 μC cm^{-2}. This curvature would be accentuated if a correction were applied for the thickness of the inner layer[5,14] since this would increase the specifically adsorbed charge at the higher concentrations. It is possible that, as suggested previously[5], the results at low concentration are in error because of the inaccuracy of the diffuse-layer correction[14]. However, this inaccuracy should be less here than for KCl because bromide ion is more strongly adsorbed and, in fact, at charges of greater than 10 μC cm^{-2}, the cation is positively adsorbed at all concentrations studied. The plot of potential

across the inner layer against specifically adsorbed charge (Fig. 7) shows deviations from linearity at the lower concentrations, but these change sign as the charge on the metal changes, unlike the previous results for KCl. The linearity of these plots is supported by the fact that the straight lines through the points at moderate concentrations extrapolates at $q_-^{-1}=0$ to the points given by integration of the inner-layer capacity of mercury in NaF solutions. Hence, there may be some justification in using the straight lines of Fig. 7 to obtain corrected values of the specifically adsorbed charge at high charge on the mercury, and low concentrations. The results of such a correction are shown in Fig. 6 as dotted lines. Partial capacities and the thickness ratio derived from Fig. 7 are shown in Fig. 8.

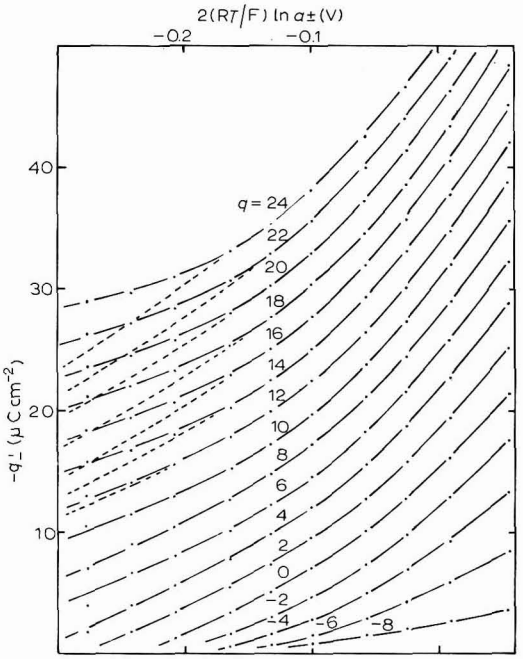

Fig. 6. Plot of charge due to specifically adsorbed Br^- (q_-^{-1}) *vs.* log activity of KBr (ln $a_\pm$). The charge on the electrode is indicated near each line. Dotted lines show data corrected as described in the text.

The adsorption isotherms of Fig. 6, even when corrected in this way, remain strongly curved like those of KCl described previously[5]. Similar behaviour is observed in work on NaCNS[22] and NaN_3[23]. If the data are plotted as log $\{a_\pm^2/|q_+^1|\}$ *vs.* q_-^{-1}, approximately straight lines are formed in the region of the point of zero charge suggesting that here the data may represented by a virial isotherm. However, at more positive charges, the lines are curved, corresponding to a decrease in the two-dimensional second virial coefficient as the amount adsorbed increases. Typically, this second virial coefficient decreases from 900 Å^2 ion^{-1} to about 400 Å^2 ion^{-1}. The lower value is comparable with that obtained for iodide ion adsorbed from aqueous solution[6]. The evidence now available suggests that the simple behaviour of iodide ion observed in aqueous[6], methanolic[24] and formamide[25] solution is not

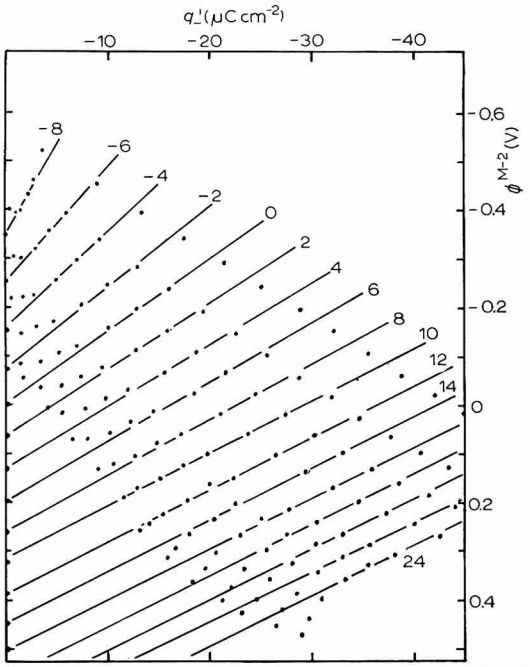

Fig. 7. Plot of potential drop across the inner region (ϕ^{M-2}) *vs.* charge due to specifically adsorbed Br^-. The charge on the electrode is indicated near each line.

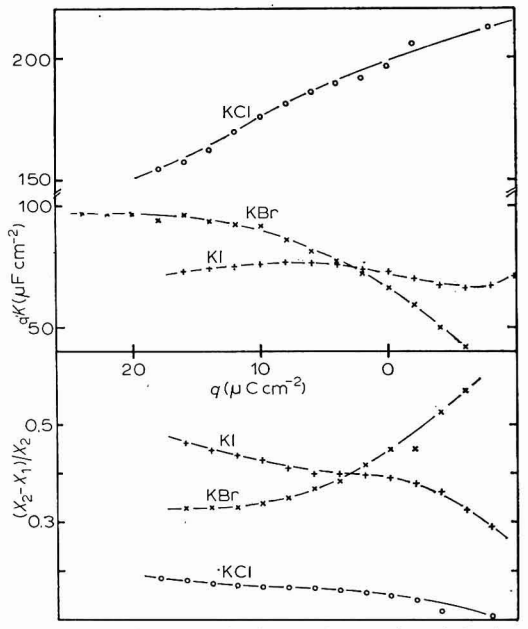

Fig. 8. Plot of the partial integral capacity of the inner layer at constant $q(_{q'}K)$ and the thickness ratio $(x_2-x_1)/x_2$ as a function of the charge on the electrode. (○), KCl; (×), KBr; (△), KI.

typical of simple inorganic ions, but is perhaps a consequence of the exceptionally strong adsorption of iodide.

It seems unlikely that the apparent decrease in the second virial coefficient in the adsorption of bromide and other more weakly adsorbed anions is due to the inadequacy of the virial adsorption isotherm itself. Other isotherms such as the Frumkin isotherm or the Zhukovitskii–Flory–Huggins isotherm cannot describe curvature of the isotherm such as that observed in these systems. Consideration of the discrete nature of the charge in the inner layer[26,27] suggests that the leading term describing the interaction between adsorbed charges may be between first-order in q_-^{-1} (as in the virial or Frumkin isotherms) for a thermally disordered layer, and $(q_-^{-1})^{\frac{3}{2}}$ for a rigid lattice. The behaviour described in Fig. 6 is outside this range. Equally, it seems unlikely that the decrease is due to the decrease in the thickness of the diffuse layer caused by the increase in bulk ionic strength, since this should occur also with iodide solutions.

It is possible that the explanation for this effect lies in the fact that chloride and bromide ions are further from the metal surface than iodide ion and nearer to the outer Helmholtz plane. In the more concentrated solutions, the cations in the outer Helmholtz plane will tend to screen the interactions between the specifically adsorbed anions. This effect will be greater at the more positive charges and higher concentrations, and would qualitatively account for the observed effect. A much more complete screening was previously invoked to account for the behaviour of the toluenesulphonate ion oriented perpendicularly to the electrode[28]. In that case the adsorbed ion behaves like a neutral molecule; the screening for a small ion like

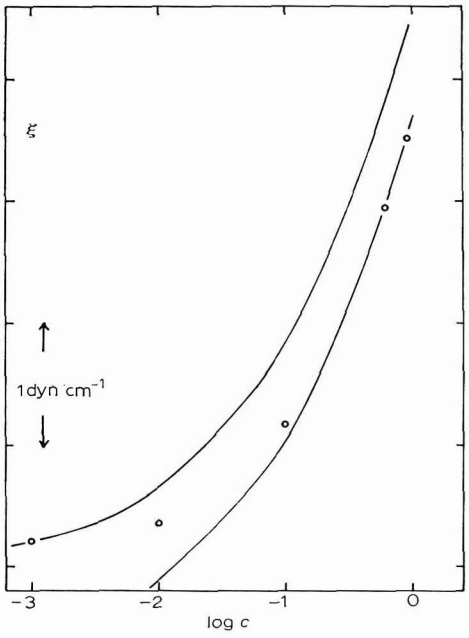

Fig. 9. Plot of ξ_- $(= \gamma + qE^-)$ for aq. NaF at 25° *vs.* log concn. of NaF. Points are from the integration of GRAHAME's capacity data[4]; lines calcd. from diffuse-layer theory.

bromide will be much less complete and the behaviour remains typical of ionic adsorbates.

(c) Specific adsorption of fluoride ion

Since GRAHAME's work, several attempts have been made[29-31] to assess the quantity of specifically adsorbed fluoride ion at a mercury electrode. The present work has relevance to this in that it shows that greater reliance must be placed on capacity measurements than on electrocapillary measurements in fluoride solutions on the positive side, especially in dilute solutions. It seemed worthwhile, therefore, to integrate GRAHAME's data[4] for NaF and to compare the concentration-dependence with that predicted from diffuse-layer theory. Integration was done with a computer as described above, using GRAHAME's values for the potential of the point of zero charge and a constant value of 42.56 μJ cm^{-2} for the interfacial tension at this point. The experimental results at $q = +10$ μC cm^{-2} are shown in Fig. 9, together with the line calculated by integrating diffuse-layer theory; this has been placed in two positions, one through the point at the lowest concentration and one through that at the highest. The latter seems more likely to be correct in view of the possible contribution of transport effects[20,21] which would lead to somewhat higher ξ-values at low concentration. Nevertheless, the discrepancies in either case are less than 1 dyn cm^{-1} and in the region above 0.1 M, the slope of the experimental curve is virtually identical with that calculated from diffuse-layer theory. Thus, measurements of precision not yet attained, combined with an improved theory of the diffuse layer, would be necessary to demonstrate the existence of specific adsorption of fluoride ion.

NOTE ADDED IN PROOF

More recently Dr. S. TRASATTI, working in Bristol, has obtained more reliable results for the drop-time curve in 0.01 M NaF. On the negative branch the drop-time curve is in excellent agreement with both the electrocapillary results and the integrated capacity, while on the positive branch it agrees only with the integrated capacity curve and this agreement is as good as that found on the negative branch. These experiments confirm the views expressed above that results from the capillary electrometer are not reliable in this particular region of potential and solution concentration. The earlier drop-time experiments reported in the text appear to be unreliable because the capillary used for them had previously been used in non-aqueous solutions.

ACKNOWLEDGEMENT

We should like to thank Dr. W. R. FAWCETT for assistance with the differentiation program, the University of Bristol Computer Unit for computing facilities, and the Somerset L.E.A. for a grant to J. L. during the course of this work.

SUMMARY

The capacity of the double layer at a mercury electrode in contact with aqueous KBr solutions was measured at 25°. These results, together with those for

other halides, are used to investigate the relation between electrocapillary and capacity measurements. Under most conditions there is no disagreement, but errors can occur in electrocapillary measurements on a positively charged surface in dilute solutions of weakly-adsorbed electrolytes, possibly due to the occurence of a finite contact angle. To obtain accurate surface excesses it is important to make measurements at closely spaced concentrations.

The adsorption isotherm of Br^-, in common with several other anions, exhibits features which do not seem to be explicable in terms of current theory. The question of specific adsorption of F^- is briefly discussed.

REFERENCES

1 M. A. V. DEVANATHAN AND S. G. CANAGARATNA, *Electrochim. Acta*, 8 (1963) 77.
2 M. A. V. DEVANATHAN AND B. V. K. S. R. A. TILAK, *Chem. Rev.*, 65 (1965) 635.
3 J. O'M. BOCKRIS, K. MÜLLER, H. WROBLOVA AND Z. KOVAC, *J. Electroanal. Chem.*, 10 (1965) 416.
4 D. C. GRAHAME, *J. Am. Chem. Soc.*, 76 (1954) 4819.
5 D. C. GRAHAME AND R. PARSONS, *J. Am. Chem. Soc.*, 83 (1961) 1291.
6 D. C. GRAHAME, *J. Am. Chem. Soc.*, 80 (1958) 4201.
7 G. GOUY, *Ann. Chim. Phys.*, (7) 29 (1903) 145.
8 O. A. ESIN AND B. MARKOV, *Acta Physiochim. URSS*, 10 (1939) 373.
9 M. A. V. DEVANATHAN AND P. PERIES, *Trans. Faraday Soc.*, 50 (1954) 1236.
10 W. ANDERSON AND R. PARSONS, *Proc. 2nd Intern. Congress Surface Activity*, Butterworths, London, 1957.
11 G. J. HILLS AND R. PAYNE, *Trans. Faraday Soc.*, 61 (1965) 316.
12 D. C. GRAHAME, R. P. LARSEN AND M. A. POTH, *J. Am. Chem. Soc.*, 71 (1949) 2978.
13 G. A. HULETT AND H. D. MINCHIN, *Phys. Rev.*, 31 (1950) 388.
14 R. PARSONS AND F. G. R. ZOBEL, *J. Electroanal. Chem.*, 9 (1965) 333.
15 R. PARSONS, *Trans. Faraday Soc.*, 51 (1955) 1518.
16 D. C. GRAHAME, *Chem. Rev.*, 41 (1947) 441.
17 H. WROBLOVA, Z. KOVAC AND J. O'M. BOCKRIS, *Trans. Faraday Soc.*, 61 (1965) 1523.
18 D. C. GRAHAME AND B. SODERBERG, *J. Chem. Phys.*, 22 (1954) 449.
19 R. PAYNE, *J. Electrochem. Soc.*, 113 (1966) 999.
20 D. C. GRAHAME, *J. Am. Chem. Soc.*, 68 (1946) 301.
21 G. C. BARKER, *J. Electroanal. Chem.*, 12 (1966) 495.
22 R. PARSONS AND P. C. SYMONS, unpublished work.
23 C. D'ALKAINE, E. R. GONZALEZ AND R. PARSONS, unpublished work.
24 J. D. GARNISH AND R. PARSONS, *Trans. Faraday Soc.*, 63 (1967) 1754.
25 R. PAYNE, *J. Chem. Phys.*, 42 (1965) 3371.
26 C. A. BARLOW AND J. R. MACDONALD, *Advances in Electrochemistry*, edited by P. DELAHAY, Wiley/Interscience, New York, 6 (1967) 1.
27 S. LEVINE, J. MINGINS AND G. M. BELL, *J. Electroanal. Chem.*, 13 (1967) 280.
28 J. M. PARRY AND R. PARSONS, *J. Electrochem. Soc.*, 113 (1966) 992.
29 R. PAYNE, *J. Electroanal. Chem.*, 7 (1964) 343.
30 B. B. DAMASKIN, N. V. NIKOLAEVA-FEDOROVICH AND A. N. FRUMKIN, *Dokl. Akad. Nauk, SSSR*, 121 (1958) 129.
31 R. D. ARMSTRONG, W. P. RACE AND H. R. THIRSK, *J. Electroanal. Chem.*, 14 (1967) 143.

ELECTROANALYTICAL CHEMISTRY AND INTERFACIAL ELECTROCHEMISTRY
Elsevier Sequoia S.A., Lausanne – Printed in The Netherlands

THE CORRECTION FOR ELECTRODE OXIDATION DURING THE ANODIC ESTIMATION OF ADSORBATE COVERAGE ON SMOOTH Pt ELECTRODES

S. B. BRUMMER AND KATHLEEN CAHILL
Tyco Laboratories, Inc., Waltham, Mass. (U.S.A)
(Received April 21st, 1967)

INTRODUCTION

In recent years there has been considerable interest in the estimation of adsorbed layers on Pt. This interest has been stimulated by a desire to correlate oxidation rates of organic materials with their coverages. Such studies have been attempted for MeOH[1–3], HCOOH[1,4–7], CO[8–10] and recently for hydrocarbons[11–13], and the probability is that interest in this field will expand. The purpose of this paper is to examine the principal experimental method that is being used.

The first serious attempt to estimate θ (= coverage) on Pt electrodes appears to have been made by PAVELA[14] although his priority has been disputed (see ref. 5). PAVELA adsorbed onto Pt electrodes from MeOH solutions and then removed the electrodes from solution and washed them. Then he anodically stripped the adsorbate in fresh base electrolyte. Since he had no adsorbate in solution, he had no problem with more adsorbate diffusing to the electrode during the stripping and hence he could strip the adsorbate slowly. Because of this, he did not push the oxidation of the adsorbate into the region of electrode oxidation and no correction for such oxidation was necessary. This method has been used extensively by the Russian school[2,5,15]. It has the major advantage of eliminating electrode oxidation corrections but has the major disadvantages that it is tedious and not responsive to the presence of labile adsorbates likely to be lost on washing.

Attempts have therefore been made to develop *in situ* anodic stripping techniques for use particularly with smooth Pt electrodes. The usual approach is to strip the adsorbate rapidly enough to avoid serious problems with diffusional processes. This invariably pushes the adsorbate oxidation into the region of electrode oxidation*. Electrode oxidation is allowed for by assuming that it is identical as for the base electrolyte at the same stripping current density (or same sweep rate for a linear anodic sweep). This approach was pioneered by BREITER AND GILMAN[3] and has been used extensively since (*e.g.* refs. 4, 8, 11–13 and others).

The application of the method is as follows: In the presence of the adsorbate the total charge passed to O_2-evolution, Q_A, is

$$Q_A = Q_{ads.} + Q_{elect.}{}^A + Q_{dl}{}^A + Q_{soln.} \quad (1)$$

* The oxidation of most organic molecules tends to "passivate" in the region of electrode oxidation, probably because fresh material will not adsorb in this region. As a result, the contribution of charge from material in solution during stripping is usually inconsequential—even slower than diffusion.

Here, Q_{ads} is the (required) charge to oxidize the adsorbate, $Q_{elect.}{}^{A}$ the charge to oxidize the electrode in presence of the adsorbate, $Q_{dl}{}^{A}$ the double-layer charge passed in presence of the adsorbate, and $Q_{soln.}$ the charge passed in oxidizing material from solution during the stripping. In the base electrolyte, with no adsorbate present, the charge Q_B is

$$Q_B = Q_{elect.}{}^{B} + Q_{dl}{}^{B}. \quad (2)$$

Then

$$Q_A - Q_B = Q_{ads.} + (Q_{elect.}{}^{A} - Q_{elect.}{}^{B}) + (Q_{dl}{}^{A} - Q_{dl}{}^{B}) + Q_{soln.}. \quad (3)$$

The double-layer term is usually assumed to be negligible* and $Q_{soln.}$ is small or can be eliminated. Then

$$Q_A - Q_B = Q_{ads.} + \Delta Q_{elect.}. \quad (4)$$

The assumption is usually made that $\Delta Q_{elect.}$ is zero and that

$$Q_A - Q_B = Q_{ads.}. \quad (5)$$

The justification for this is that $Q_A - Q_B$ is frequently found to be independent of the stripping rate over a wide range, although $Q_{elect.}{}^{B}$ itself changes substantially with stripping rate.

The completeness of elimination of electrode oxidation was questioned earlier[7] and a technique was evolved to test for it. In this technique, the adsorbate was partially stripped with an anodic galvanostatic pulse, i_a (charge density passed $= Q_a$), and the efficiency of stripping was tested by applying a rapid cathodic pulse, i_c. During i_c, two quantities could be measured, Q_o and Q_H. Q_o is the charge to reduce any oxide formed during i_a and it was assumed that $(Q_a - Q_o)$ was used in oxidizing the adsorbate. Q_H is the charge to deposit H-atoms on the bare part of the surface. When divided by the maximum charge to deposit H-atoms on the clean surface ($Q_H{}^{max}$), this gives $\theta_H{}^{c}$, the fraction of the surface available for H-atom deposition. It was argued that when $\theta_H{}^{c}$ is equal to 1, the surface must be clean and hence the extrapolation of $(Q_a - Q_o)$ to $\theta_H{}^{c} = 1$ gives $Q_{ads.}$.

In the earlier study[7] for $HCOOH_{ads.}$, quite good agreement was found using this method ($Q_{ads.} = 285\ \mu C/real\ cm^2$) with BREITER's value[4a] ($260\ \mu C/r.\ cm^2$) derived from eqn. (5). Only indifferent agreement was found for[9] CO with GILMAN's value[8,17], however. The most important difference between the HCOOH[7] and[9] CO studies was that in the former Q_o was negligible but in the latter it constituted a large part of Q_a**. BREITER[18] has argued that serious errors can arise because the charge in oxidizing Pt, $Q_{elect.}$, is greater than the charge in reducing the thus-formed oxide[19,20]. In reply[21], it was pointed out that this $Q_{elect.}/Q_o$ ratio of greater than unity probably arose from impurities in the solution in the cases considered*** and that it was therefore reasonable to assume it as equal to 1†. Also, the data of ref. 9 seemed to show that $Q_{elect.}/Q_o$ is just one. GILMAN[17] has raised a more serious objection. He pointed out that while

* A recent discussion[16] shows this to be a justifiable assumption.

**WARNER AND SCHULDINER[10] have used a somewhat different method to allow for $Q_{elect.}{}^{A}$. They assume that at high i_a the adsorbate (CO) is oxidized *before any electrode oxidation occurs at all*. This result, that Q_o is large *during the stripping* itself, shows that their assumption is not correct.

*** Recently, BAGOTSKII *et al.*[22] have reported a slow irreversible oxidation of Pt which could lead to $Q_{elect.}/Q_o > 1$. Similarly, SCHULDINER AND WARNER[23] report a similar phenomenon, "dermasorbed oxygen". Such effects are unlikely to lead to $Q_{elect.}/Q_o$ substantially greater than 1 in the experiments of refs. 7 and 9, however, because the time-scale of the experiments was much too fast.

† Other studies [24,25], particularly ref. 25, have shown that with care, $Q_{elect.}/Q_o$ is 1.

$Q_{elect.}/Q_o$ is 1, the reduction of Pt oxide is slow and can easily be pushed into the H-atom deposition region. It is clear that this would be disastrous for use of the current-reversal method since it would lead to over-estimation of $(Q_a - Q_o)$ and under-estimation of $Q_H{}^c$*. The net effect would be to over-estimate $Q_{ads.}$ which is the direction of disagreement with GILMAN's earlier data[8] for CO.

Because of its simplicity, the direct method is becoming more widely used, and a test of its validity does seem desirable. It is clear from the above, however, that there is considerable controversy about the "current-reversal" method developed earlier[7,9] and about its suitability to test eqn. (5), the basic equation of the "direct" method of allowing for electrode oxidation. In this work it was thought to use the current-reversal method in circumstances where there could be no controversy about the correction Q_o, in order to test eqn. (5). One possible way to do this is to employ small values of i_a for stripping purposes. Then, electrode oxidation during stripping can be minimized. The difficulty with this is that there is then a considerable problem with most adsorbates as $Q_{soln.}$, the oxidation of material from solution during stripping, is not negligible. To overcome this, we have worked with a system where only the adsorbed material is electro-active and the original "fuel" is inert. Then the adsorbate can be stripped as slowly as is necessary to avoid electrode oxidation without problems from $Q_{soln.}$.

A system suitable for such a study is "reduced CO_2" — an adsorbed species first reported by GINER[26]. The reduced CO_2 can be formed at low potentials, *e.g.*, below 0.35 V *vs.* R.H.E., and re-oxidized at reasonable rates ($\sim$ 100 μA/r. cm^2) before electrode oxidation. Above the potential region where it is reductively adsorbed, CO_2 is completely inert. It is therefore the perfect system for analyzing the validity of the "direct" method since, ideally, we can arrange $(Q_a - Q_o)$ to be equal to Q_a $(Q_o = 0)$. In addition, by working at higher values of i_a, where Q_o is not zero, we can decide how to allow for $Q_{elect.}$ when using the current-reversal method and decide on its range of validity.

We have thus reduced CO_2 on smooth Pt electrodes from 1 *M* H_2SO_4 solutions at 40° and have studied the adsorbate with the current-reversal technique and with the "direct" method. The major result of this work is to demonstrate that eqn. (5) does give an accurate estimate of electrode oxidation during anodic stripping. However, the direct method is not as precise in use as the current-reversal technique, particularly for small amounts of adsorbate. In addition, it is shown that the current-reversal method experiences some difficulty at high values of i_a, when $Q_o > 0$, but with care quite large amounts of Q_o can be accurately allowed for.

EXPERIMENTAL

The electrochemical cell was a Pyrex tube, capacity $\sim$ 100 ml, with two side compartments for reference and counter electrodes. The inlet of the cell was arranged so that purified solution could be admitted *via* Teflon-barrelled taps and could be discarded after use. Before passage through the cell, gases were pre-saturated with electrolyte; they were vented out *via* bubblers. The cell was thermostatted in an air oven at 40 $\pm$ 0.5°.

Electrolyte purification was carried out in a separate ($\sim$ 1 l) chamber at 60°. The

*$\theta_H{}^c$ is underestimated because this oxide increases the "double-layer" capacity which is subtracted from $Q_H{}^c$. This effect is larger than the increase in $Q_H{}^c$ from oxide reduction actually in the H-atom region. Alone, the latter is small and causes an increase in $\theta_H{}^c$.

principle of the purification technique was controlled-potential adsorption. Adsorption of possible impurities in the solution was carried out on a Teflon-bonded Pt fuel cell electrode held at 0.3 V *vs.* R.H.E. In addition, a platinized-Pt wire in the solution was held at 1.1 V to oxidize any impurities that do not adsorb. Potentials were fixed against a H_2-charged Pd foil with high current capacity potentiometers. The solution was vigorously stirred during the electrolysis (minimum of 20 h) with a magnetic stirrer.

The criterion of purity was that in the working cell at 40°, without stirring, there was no change ($< 10\ \mu C/r.\ cm^2$) in charge to oxidize the electrode at ~ 100 mA/r. cm^2 in 600 sec. Similarly, there was no change in $Q_H{}^{max}$ ($< 2\%$).

The electrolyte was prepared by diluting reagent-grade H_2SO_4 (Allied Chemical) with quadruply-distilled H_2O. N_2 was "pre-purified grade" (Matheson) and was passed through liquid N_2 traps before use. CO_2 was Coleman "instrument grade" (99.99 vol.%, Matheson) and was pre-saturated with electrolyte before use.

The reference electrode was the "polarized H_2-electrode" described by GINER[27]. Data are referred to the reversible hydrogen electrode in the working solution (R.H.E.).

The working electrode was a Pt foil (99.9%, Engelhard) of about 1 cm^2 geometric area. It was annealed in an oxidizing gas flame between each experiment. Results are given in terms of *real area* (r.cm^2); defined as corresponding to 210 μC of charge for galvanostatic cathodic H-atom deposition*.

The potential of the working electrode was changed in rapid sequence to clean it and to allow adsorption at fixed potential. This was done by modulating the input of a potentiostat, and was described in detail recently[13c]. As before[7,9], current reversal was accomplished by switching galvanostatic circuits with Hg-wetted relays. The circuitry to allow automatic switching of these relays has been described in ref 28.

Otherwise, the techniques are as described previously[6,7,13c].

RESULTS AND DISCUSSION

Direct charging method of estimating reduced CO_2

Typical anodic charging curves are shown in Fig. 1. Curve A was taken after allowing adsorption for 100 sec at 0.05 V. The background curve B was similar to that

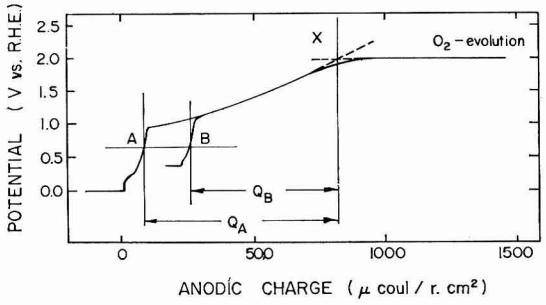

Fig. 1. Anodic charging curves on smooth Pt taken at 67 mA/r. cm^2. A taken after adsorbing reduced CO_2 for 100 sec at 0.05 V. B is similar to the curve found under N_2 (potentials include iR).

* The use of this method has been discussed in detail in ref. 7.

found under N_2 at the same current density. It was taken in the presence of CO_2, the oxide from the electrode cleaning stage having been reduced for 1 sec at 0.30 V. This treatment allows insignificant ($< 10^{-3}$ monolayers) adsorption. It can be seen that the curves coincide in the O_2-evolution region and, indeed, are parallel well before this. The method of estimating the charges, Q_A and Q_B, is indicated in the figure. The major experimental uncertainty is in the location of point X.

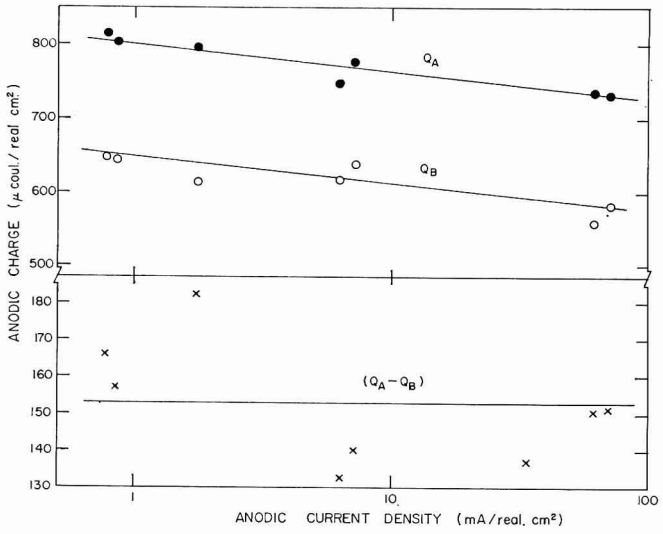

Fig. 2.

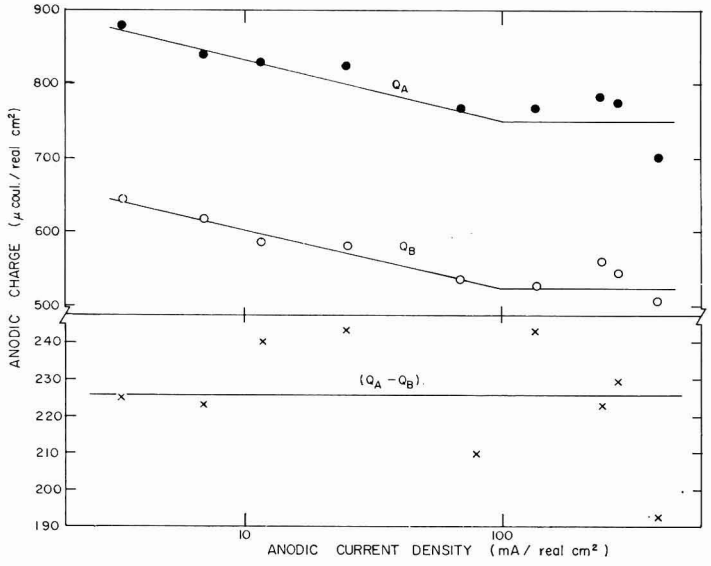

Figs. 2-3. Variation of Q_A, Q_B and $(Q_A - Q_B)$ with i_a for CO_2 adsorbed (2) for 20 sec at 0.10 V; (3) for 100 sec at 0.20 V.

Typical examples of the variation of Q_A and Q_B with i_a are shown in Figs. 2 and 3 for adsorption at 0.10 V for 20 sec and 0.20 V for 100 sec, respectively. We see that both Q-values decrease with increase in i_a but that their difference is independent of i_a over a wide range. The values for this difference are 153 ± 9 (mean deviation) and 226 ± 12 μC/r. cm^2 for the two cases.

Adsorbate estimation by current reversal without electrode oxidation

A typical chronopotentiogram for the current-reversal method is shown in Fig. 4. Here i_a is ~ 100 μA/r. cm^2 and i_c is ~ 200 mA/cm^2. As indicated, the principle of the method is to use the hydrogen charging curve to determine the efficiency of the anodic current in oxidizing the adsorbate. It is considered that when $\theta_H{}^c = 1$ (*i.e.*, $Q_H = Q_H{}^{max}$) the electrode is clean. Then, where no electrode oxidation or other reaction from solution occurs during passage of i_a, the anodic charge to $\theta_H{}^c = 1$ is the charge to oxidize the adsorbate originally present.

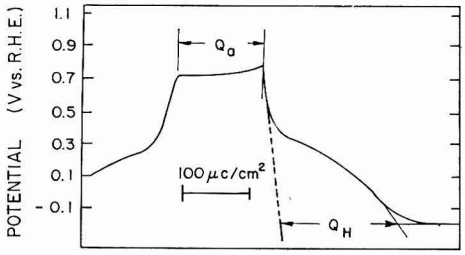

Fig. 4. Typical current-reversal chronopotentiogram taken after adsorbing CO_2 for 20 sec at 0.10 V. i_a, 100 μA/r.cm^2; i_c, 200 mA/r. cm^2.

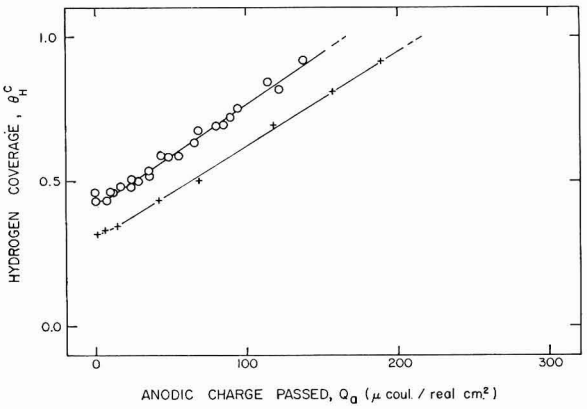

Fig. 5. Variation of electrode cleanliness ($\theta_H{}^c$) with charge passed during low current density (100 μA/r. cm^2) anodic part of current-reversal procedure (Q_a). (○), Adsorption for 20 sec at 0.10 V; (+), adsorption for 100 sec at 0.20 V.

Figure 5 shows the results for the application of this method to the two adsorption situations investigated in the previous section. We see that apart from a small inflexion near the beginning of the anodic wave ($Q_a \rightarrow 0$) $\theta_H{}^c$ increases linearly with Q_a. Eventually $\theta_H{}^c$ becomes unity. At the current density used, there is no electrode

oxidation up to this point. Then the value of Q_a for $\theta_H{}^c \rightarrow 1$ should be the charge to oxidize the adsorbate. The appropriate values for adsorption for 20 sec at 0.10 V and 100 sec at 0.20V are 164 ± 5 and 216 ± 5 μC/r. cm^2, respectively.

These values are in good agreement ($+7\%$ and -5%, respectively) with the results of the direct charging method. Since the current-reversal technique involves no electrode oxidation, this agreement can be taken as good evidence that the assumptions of eqn.(5) are correct. In short, the amount of electrode oxidation that occurs during the transient anodic galvanostatic oxidation of adsorbed CO_2 is the same as the oxidation of the clean electrode at the same current density.

Since both methods yield the same result for $Q_{ads.}$, we may ask which method is to be preferred in practice. The direct method has the advantage of rapid application, only two determinations (Q_A and Q_B) being required to analyze a given amount of adsorbate. Its disadvantage is the large correction for $Q_{elect.}$ (see Figs. 2 and 3). Thus even at 100 mA/r. cm^2, $Q_{elect.}$ is 600 μC/r. cm^2. In the present system, this correction imposes a measurement uncertainty of not less than 10 μC/r. cm^2 even at low coverages. The current-reversal technique has the disadvantage of being much more tedious, at least 8 points being required to derive a statistically meaningful Q_a–$\theta_H{}^c$ line. Also, the method cannot be used when there is significant electrochemical reaction of the "fuel" in the relatively low stripping potential region. At least it cannot where i_a is low, as it is here. The method does have the advantage of great precision, however, since no corrections need be made for electrode oxidation. The uncertainty in routine use of the method is no more than 5 μC/r. cm^2 and can readily be improved*. This method, then, is particularly applicable for examining small coverages or any coverage where high precision is required. It has the additional advantage that from the slope of the Q_a–$\theta_H{}^c$ line, information on the oxidation state and on the homogeneity of the adsorbate can also be obtained[7].

Adsorbate estimation with current reversal allowing electrode oxidation

A major disadvantage of the current-reversal technique, as described above, is its sensitivity to anodic faradaic reactions of the fuel during adsorbate stripping. This could be overcome if the anodic pulse i_a could be made larger so that the period of anodic stripping, τ_a, were shorter. The difficulty, as discussed in the introduction, is that $Q_{elect.}$ is not then zero and there is considerable controversy as to whether the cathodically-found oxide, Q_o, is equal to $Q_{elect.}$[17–25]. To investigate the limits of the current-reversal method where Q_o is not zero, we have again applied it to reduced-CO_2 oxidation. This system is particularly suitable since no complications from $Q_{soln.}$ can arise.

Figure 6 shows the kind of chronopotentiogram obtained when Q_o is significant. This was taken after adsorption for 100 sec at 0.05 V, the anodic current density is 20 mA/r. cm^2 and the cathodic current density, 147 mA/r. cm^2. The lettering of the significant points in this figure is similar to that in Fig. 2 of ref. 9. In that earlier work, Q_o was calculated by extending the line FG to the potential H. However, the slope of the line HI suggests that some oxide reduction is still occurring in this region. Therefore the previous estimates[9] of Q_o were probably too low. However, there is another problem, probably more serious. Q_H was previously estimated by extrapolating HI to the potential of K. But, if some oxide reduction is going on in the region HI, this will give

* The most important factor is careful calibration of the oscilloscope screen.

too low a value of Q_H. The net effect will be to overstate $(Q_a - Q_o)$ and to understate $\theta_H{}^c$. A systematic disagreement will then be found between this technique and the direct method. This is probably the reason for the previous disagreement[9] with GILMAN's results for CO[8,17].

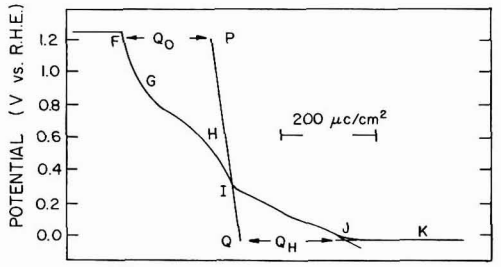

Fig. 6. Typical cathodic part of the current-reversal chrono-potentiogram taken after high anodic current density (10–20 mA/r. cm²) when electrode oxidation is significant. Cathodic current density, ~ 150 mA/r. cm² (potentials are iR-free).

The question then is how to allow for capacitative effects during oxide reduction and H-atom deposition. If we could do this, we could compare $(Q_a - Q_o)$ *vs.* $\theta_H{}^c$, with the Q–θ plots obtained with low i_a, when Q_o is zero. Then we could investigate how much $Q_{elect.}$ we can allow before some oxide reduction is pushed into the H-atom region and this is the limit of the method. The following experiment was done to find the relationship between the double-layer capacity and the coverage: CO_2 was adsorbed for various times at 0.10 V and its coverage was estimated with cathodic H-atom charging. Before H-atom deposition was applied, the potential was raised to 0.50 V for 10 msec to eliminate the adsorbed H present at 0.10 V. Similarly, the double-layer capacity was investigated as a function of adsorption time with anodic galvanostatic pulses from 0.10 V or with cathodic pulses after the 0.50-V step, there was no difference. The capacity decreased linearly from 42 μF/r. cm²* for $\theta = 0$, to 32 μF/r. cm² for $\theta \simeq 0.7$. Then, to allow for capacitance effects for a given current-reversal transient, a preliminary estimate was made of θ_H and the corresponding value of C_{dl} was obtained from the results of the above experiment. A line PQ was constructed at point I of Fig. 6 with a slope, $dE/d\tau$, of i_c/C_{dl}. This allowed a better value of θ_H to be determined and further iteration of C_{dl}. However, it was rarely necessary to iterate C_{dl} more than once.

This method of allowing for double-layer charging is accurate in the H-atom region but could lead to small errors in the oxide region because no account was taken of the variation C_{dl} with oxide coverage *per se*. However, the slope of FG was usually close enough to that of PG to suggest that this error was not greater than 10 μC/r. cm².

Figures 7 and 8 show the results obtained for adsorption for 20 sec at 0.10 V and 100 sec at 0.05 V, respectively. The crosses represent the results obtained with the low current density, current-reversal method. The lines are drawn through the crosses. The dark circles show the total anodic charge, including $Q_{elect.}$, passed at high current densities (12 mA/r.cm² in Fig. 7, 21 mA/r. cm² in Fig. 8). We see a systematic and large deviation. The open circles represent these data points corrected by subtraction of Q_o, determined as shown in Fig. 6. For adsorption at 0.10 V, the low current density

* This value is in excellent agreement with the figure of 40 μF/r. cm² reported by SCHULDINER AND ROE[29].

method gives 164 ± 5 μC/r. cm^2 for $Q_{ads.}$, the open circles yield 152 ± 7. At 0.05 V, the values are 188 ± 5 and 182 ± 5 μC/r. cm^2, respectively.

It is evident that the compensation for $Q_{elect.}$ by subtracting Q_o from Q_a is very good. In Fig. 8, for example, we can subtract up to 170 μC/r. cm^2 of oxide with an overall error of less than 6 μC/r. cm^2. The current-reversal technique can then be used with sufficiently high current densities to allow elimination of solution effects.

The limits of the current-reversal method used in this way can be gauged from Figs. 7 and 8. Thus, there is a small difference between the crosses and the open cir-

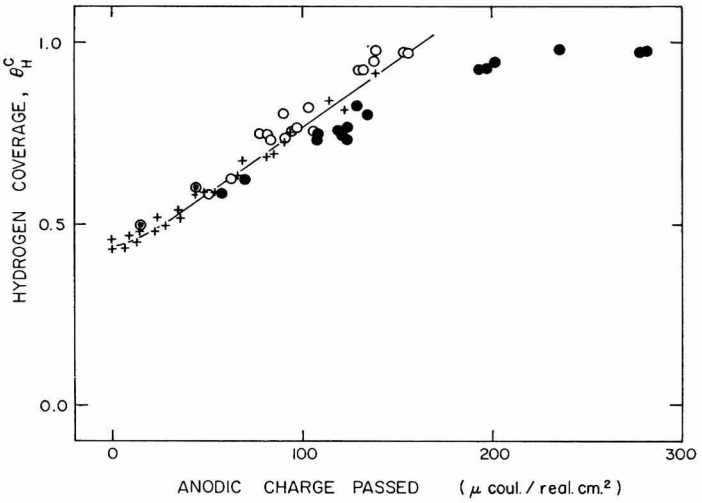

Fig. 7. Variation of electrode cleanliness ($\theta_H{}^c$) with total anodic charge Q_a, (●) and with charge corrected for electrode oxidation (○). Adsorption of CO_2, 20 sec at 0.10 V; i_a, 12 mA/r. cm^2; i_c, 147 mA/r. cm^2. The crosses show the previous data with $i_a = 100$ μA/r. cm^2 when electrode oxidation is negligible. The line is drawn through the crosses.

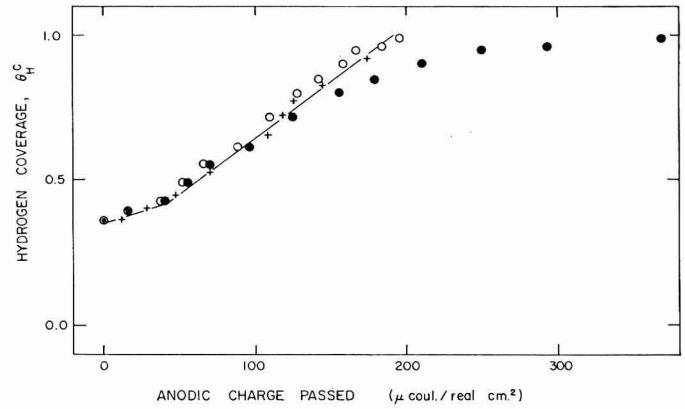

Fig. 8. Variation of electrode cleanliness ($\theta_H{}^c$) with total anodic charge, Q_a (●) and with charge corrected for electrode oxidation (○). Adsorption of CO_2 100 sec at 0.05 V; i_a, 21 mA/r. cm^2; i_c, 147 mA/r. cm^2. The crosses show data with $i_a = 78$ μA/r. cm^2 where electrode oxidation is negligible. The line is drawn through the crosses.

cles. This difference is within experimental error but is quite systematic, which suggests that it is significant. It may arise either from slight over-compensation for Q_o or from some oxide reduction being pushed into the H-atom region. In the present case, the former seems more likely from an examination of the variation of the deviations with Q_o. It probably arises from the over-simplified capacity correction made. At this juncture, a more elaborate correction does not seem worthwhile. We can conclude that whilst there may be small errors in allowing for $Q_{elect.}$ by assuming it equal to Q_o, they do not significantly lower the accuracy of the estimation of $Q_{ads.}$, particularly when compared with the direct charging method.

CONCLUSIONS

(1) The "direct" method of analyzing adsorbed layers on smooth Pt electrodes has been compared with the "current-reversal" technique using "reduced CO_2" as a model system.

(2) The charge passed to O_2-evolution during an anodic galvanostatic transient increases with decrease in current density, i_a, both in the presence (Q_A) and absence (Q_B) of an adsorbate. The difference between these two charges ($Q_A - Q_B$) at a given current density is independent of i_a. This suggests the complete elimination of electrode oxidation effects and accurate estimation of the adsorbate charge, $Q_{ads.}$.

(3) Current reversal with low i_a to oxidize the adsorbate, and high i_c to estimate the "end-point" of total electrode cleanliness from the adsorbate, is an independent method of adsorbate analysis because no electrode oxidation occurs. Use of this method with $i_a \sim 100$ μA/r. cm^2 shows that $Q_{ads.}$ is equal to $(Q_A - Q_B)$ and that the direct method is appropriate for adsorbate analysis, The current-reversal technique is more tedious but more accurate than the direct method.

(4) The current-reversal technique was also investigated for higher values of i_a (10–20 mA/r. cm^2) where electrode oxidation occurs before reversal. By using appropriate capacity data, good elimination of electrode oxidation may be made by direct subtraction of the charge found for oxide reduction. The agreement with the current-reversal method without electrode oxidation is within experimental error but there is apparently a small systematic over-correction for electrode oxidation. This is not sufficient to vitiate estimates of $Q_{ads.}$ and allows use of the current-reversal technique in the presence of complicating effects from solution reactions during the anodic stripping.

(5) The current-reversal technique is likely to find application where very accurate values of $Q_{ads.}$ are required, where θ is small, and to give information on the structure of the adsorbate.

ACKNOWLEDGEMENT

It is a pleasure to acknowledge support of this work by the Office of Naval Research.

SUMMARY

"Reduced CO_2" adsorbed on smooth Pt electrodes from 1 M H_2SO_4 solutions at

40° has been used as a model system to investigate the anodic charging methods of estimating adsorbates. Three methods have been compared: the usual "direct" method and two variations of the previously-developed current-reversal method.

In the direct method, the charge passed to O_2-evolution during an anodic galvanostatic transient increases with decrease of the current density, i_a, both in the presence of adsorbate (Q_A) and for the background electrolyte (Q_B). As is often found, the difference ($Q_A - Q_B$) is independent of i_a (1–500 mA/r. cm^2). This suggests complete elimination of electrode oxidation effects and correct estimation of the adsorbate, Q_{ads}.

Current reversal, with low i_a to oxidize the adsorbate, and high i_c to estimate the "end point" of total electrode cleanliness from the adsorbate, is an independent method of adsorbate analysis because no electrode oxidation occurs. Use of this method with $i_a \simeq 100\ \mu$A/r. cm^2 shows that Q_{ads} is equal to ($Q_A - Q_B$) and that the direct method is appropriate for adsorbate analysis. The current-reversal technique is more tedious but more accurate than the direct method.

The current-reversal technique was also investigated for higher values of i_a (10–20 mA/r. cm^2) where electrode oxidation occurs before reversal. By using appropriate capacity data, good elimination of electrode oxidation may be made by direct subtraction of the charge found for oxide reduction. The agreement with the current-reversal method without electrode oxidation is within experimental error but there is apparently a small systematic over-correction for electrode oxidation. This is not sufficient to vitiate estimates of Q_{ads}, and allows use of the current-reversal technique in the presence of complicating effects from solution reactions during the anodic stripping.

The useful ranges of experimental application of these different methods for estimating adsorbate coverage are discussed.

REFERENCES

1 J. GINER, *Electrochim. Acta*, 9 (1964) 63.
2 O. A. PETRY, B. I. PODLOVCHENKO, A. N. FRUMKIN AND HIRA LAL, *J. Electroanal. Chem.*, 10 (1965) 253.
3 M. W. BREITER AND S. GILMAN, *J. Electrochem. Soc.*, 109 (1962) 622; M. W. BREITER, *Electrochim. Acta*, 8 (1963) 973; 9 (1964) 927; *J. Phys. Chem.*, 69 (1965) 3377.
4 (a) M. W. BREITER, *Electrochim. Acta*, 8 (1963) 447; (b) *ibid.*, 8 (1963) 457; (c) *ibid.*, 10 (1965) 503.
5 B. I. PODLOVCHENKO, O. A. PETRY, A. N. FRUMKIN AND HIRA LAL, *J. Electroanal. Chem.*, 11 (1966) 12.
6 S. B. BRUMMER AND A. C. MAKRIDES, *J. Phys. Chem.*, 48 (1964) 1448.
7 S. B. BRUMMER, *J. Phys. Chem.*, 69 (1965) 562.
8 S. GILMAN, *J. Phys. Chem.*, 67 (1963) 1898; 68 (1964) 70.
9 S. B. BRUMMER AND J. I. FORD, *J. Phys. Chem.*, 69 (1965) 1355.
10 T. B. WARNER AND S. SCHULDINER, *J. Electrochem. Soc.*, 111 (1964) 992.
11 S. GILMAN, *Trans. Faraday Soc.*, 61 (1965) 2546, 2562; 62 (1966) 466, 481.
12 L. W. NIEDRACH, *J. Electrochem. Soc.*, 111 (1964) 1309; 113 (1966) 645; L. W. NIEDRACH, S. GILMAN, I. WEINSTOCK, *ibid.*, 112 (1965) 1161. L. W. NIEDRACH AND M. TOCHNER, *ibid.*, 114 (1967) 17.
13 (a) S. B. BRUMMER, J. I. FORD AND M. J. TURNER, *J. Phys. Chem.*, 69 (1965) 3424; (b) S. B. BRUMMER AND M. J. TURNER, *Hydrocarbon Fuel Cell Technology*, edited by B. S. BAKER, Academic Press, New York, 1965, p. 409; (c) S. B. BRUMMER AND M. J. TURNER, *J. Phys. Chem.*, 71 (1967) 2825; (d) S. B. BRUMMER AND M. J. TURNER, submitted to *J. Phys. Chem.*
14 T. O. PAVELA, *Ann. Acad. Sci. Fennicae, Ser. A*, (1954) 59.
15 V. S. BAGOTSKII AND YU. B. VASILEV, *Fuel Cells, Their Electrochemical Kinetics*, Consultants Bureau, New York, 1966, p. 77 *et seq.*
16 S. B. BRUMMER, *J. Phys. Chem.*, 71 (1967) 2838.

17 S. GILMAN, *J. Phys. Chem.*, 70 (1966) 2886.
18 M. W. BREITER, *J. Electrochem. Soc.* 112 (1966) 1244.
19 K. J. VETTER AND D. BERNDT, *Z. Electrochem.*, 62 (1958) 378.
20 S. W. FELDBERG, C. G. ENKE AND C. E. BRICKER, *J. Electrochem. Soc.*, 110 (1963) 826.
21 S. B. BRUMMER, *J. Electrochem. Soc.*, 113 (1966) 641.
22 V. I. LUK'YANYCHEVA AND V. S. BAGOTSKII, *Dokl. Akad. Nauk SSSR*, 155 (1964) 160; V. I. LUK'YANYCHEVA, V. I. TIKHOMIROVA AND V. S. BAGOTSKII, *Elektrokhimiya*, 1 (1965) 262.
23 S. SCHULDINER AND T. B. WARNER, *J. Electrochem. Soc.*, 112 (1965) 212.
24 W. BOLD AND M. BREITER, *Electrochim. Acta*, 5 (1961) 145.
25 S. GILMAN, *Electrochim. Acta*, 9 (1964) 1025.
26 J. GINER, *Electrochim. Acta*, 8 (1963) 857.
27 J. GINER, *J. Electrochem. Soc.*, 111 (1964) 376.
28 Tyco Laboratories, Inc. report to U. S. Army Engineer Research and Development Laboratories, Fort Belvoir, Va., on Contract DA 44-009-AMC-410(T), April, 1965.
29 S. SCHULDINER AND R. M. ROE, *J. Electrochem. Soc.*, 110 (1963) 332.

ELECTROANALYTICAL CHEMISTRY AND INTERFACIAL ELECTROCHEMISTRY
Elsevier Sequoia S.A., Lausanne – Printed in The Netherlands

THE ADSORPTION OF SULPHIDE IONS AT A MERCURY ELECTRODE

R. D. ARMSTRONG, D. F. PORTER AND H. R. THIRSK

Department of Physical Chemistry, University of Newcastle upon Tyne, Newcastle upon Tyne, 1 (England)

(Received April 28th, 1967)

NOTATION

C	Concentration of species S_1 (mole cm^{-3})
C'	Concentration of species S_2 (mole cm^{-3})
C_0	Concentration of species S_1 as $x \rightarrow \infty$ (mole cm^{-3})
C_0'	Concentration of species S_2 as $x \rightarrow \infty$ (mole cm^{-3})
C_b	Series equivalent electrode capacity in base solution ($\mu F\ cm^{-2}$)
C^i	Differential capacity of the inner layer ($\mu F\ cm^{-2}$)
C_p^*	Parallel equivalent electrode capacity ($\mu F\ cm^{-2}$)
${}_\infty C_p$	Parallel equivalent electrode capacity as $\omega \rightarrow \infty$ ($\mu F\ cm^{-2}$)
C_p^*	$= C_p - {}_\infty C_p$ ($\mu F\ cm^{-2}$)
C_s	Measured series capacity ($\mu F\ cm^{-2}$)
$C_s(f \rightarrow 0)$	Series equivalent electrode capacity at low frequencies ($\mu F\ cm^{-2}$)
D	Diffusion coefficient of species S_1 ($cm^2\ sec^{-1}$)
D'	Diffusion coefficient of species S_2 ($cm^2\ sec^{-1}$)
E	Electrode potential (volts relative to Hg/HgO in 1 *M* NaOH solution)
f	Frequency (c/sec)
F	Faraday
i	Current density ($A\ cm^{-2}$)
j	$\sqrt{-1}$
k, k'	First-order homogeneous rate constants (sec^{-1})
k_h	First-order heterogeneous rate constant ($cm\ sec^{-1}$)
P	Amplitude of sinusoidal perturbation (V)
q_m	Charge in metal electrode ($\mu C\ cm^{-2}$)
q_1	Specifically adsorbed charge ($\mu C\ cm^{-2}$)
R_p	Parallel equivalent electrode resistance ($\Omega\ cm^2$)
R_s	Measured series resistance ($\Omega\ cm^2$)
R_{so}	Series equivalent solution resistance (Ω)
t	Time (sec)
V	Rate of interfacial reaction (mole $cm^{-2}\ sec^{-1}$)
x	Distance into solution from electrode (cm)

Z	Electrode impedance (Ω cm^2)
Γ	Concentration of ions adsorbed on electrode (mole cm^{-2})
$\tan \delta$	Loss tangent ($=\omega C_s[R_s - R_{so}]$)
$\tan \delta^*$	Loss tangent ($=[\omega C_p{}^* R_p]^{-1}$)
μ	Reaction zone thickness (cm)
τ	Life time of species S_1 (sec)
ϕ, ϕ_m	Potential of metal electrode relative to bulk solution (V)
ϕ_{m-2}	Potential of metal electrode relative to outer Helmholtz plane (V)
ϕ_0	D.c. component of ϕ (V)
ϕ_1	Potential of inner Helmholtz plane relative to bulk solution (V)
ω	Angular frequency (sec^{-1})
ω^*	Angular frequency at $(\tan \delta^*)^{-1} = 1$ (sec^{-1})

INTRODUCTION

The electrocapillary curve for mercury in 0.5 *M* K_2S solution, reported by GOUY[1], shows a very sharp maximum at a negative potential (−0.81 V on Hg/HgO). This behaviour has previously been interpreted in terms of the strong specific adsorption of S^{2-} or HS^- ions[2]. A recent investigation[3] showed that in the potential region in question, mercury dissolves as the complex ion $HgS_2{}^{2-}$ and no evidence for specific anion adsorption was found in 0.5 *M* Na_2S solution at potentials < -0.86 V (Hg/HgO). The question was also raised as to what extent the shape of the electrocapillary curve at potentials > -0.86 V was attributable to the faradaic dissolution process and it appeared that the latter was insufficient to account for the sharp maximum.

It seems likely, therefore, that specific anion adsorption occurs to some extent and it is desirable to measure the differential capacity of the electrode in a solution in which the dissolution reaction is unimportant, to eliminate the contribution of the faradaic pseudocapacity. Since the dissolving species is[3] $HgS_2{}^{2-}$, the sulphide ion concentration must be reduced in order to allow an investigation of the double layer, Hg/S^{2-}, HS^-. In the present work, this was achieved by using a solution of NaHS, the pH of which was controlled by a carbonate–bicarbonate buffer.

EXPERIMENTAL

Electrode impedance measurements have been made with both a potentiostat (at frequencies of 15–2000 c/sec) and an a.c. bridge (at frequencies of 0.2–50 kc/sec), in the manner described previously[3,4]. In addition, drop-time measurements were made using a conventional three-electrode polarographic cell and dropping mercury electrode. In all cases potentials were measured with respect to a Hg/HgO reference electrode in 1 *M* NaOH solution.

The electrolyte used in this work was 0.5 *M* $Na_2S + 1$ *M* $NaHCO_3$ solution, which is self-buffered at a pH that is approximately the p*K* of the aqueous carbonate–

bicarbonate system and which was measured as ~9.5. If a value of $1 \cdot 10^{-14}$ mole l^{-1} is assumed[5] for the dissociation constant, K_{HS^-}, the ionic concentrations of the sulphide species present are $[HS^-]=0.5$ *M* and $[S^{2-}]=1.5 \times 10^{-5}$ *M*. The reversible potential for black HgS in this solution was measured as -0.692 V (Hg/HgO) and at this potential the thermodynamic concentration of HgS_2^{2-} was calculated as 8.7×10^{-5} *M*, assuming[3] an equilibrium constant of $1 \cdot 10^{54}$ mole^{-2} l^2 for the reaction, $Hg^{2+} + 2\,S^{2-} \rightleftharpoons HgS_2^{2-}$.

A solution of 0.5 *M* NaOH + 1 *M* $NaHCO_3$, having the same pH as the buffered sulphide solution, was used as a "base" electrolyte to obtain impedance and drop-time measurements in the absence of effects due to adsorption, dissolution or solid film formation involving sulphur species.

All solutions were prepared in an atmosphere of purified nitrogen from deoxygenated triply-distilled water. AnalaR-grade reagents were used throughout and mercury was purified by chemical cleaning followed by two vacuum distillations. Measurements were made at room temperature, $24 \pm 1°$.

RESULTS

Drop-time measurements

In order to investigate the form of the electrocapillary curve, drop-time measurements were made in both the buffered sulphide solution and the base solution. Figure 1 shows the resultant curves and compares them with GOUY's result in 0.5 *M* K_2S solution, plotted on the same potential scale. The same general features are

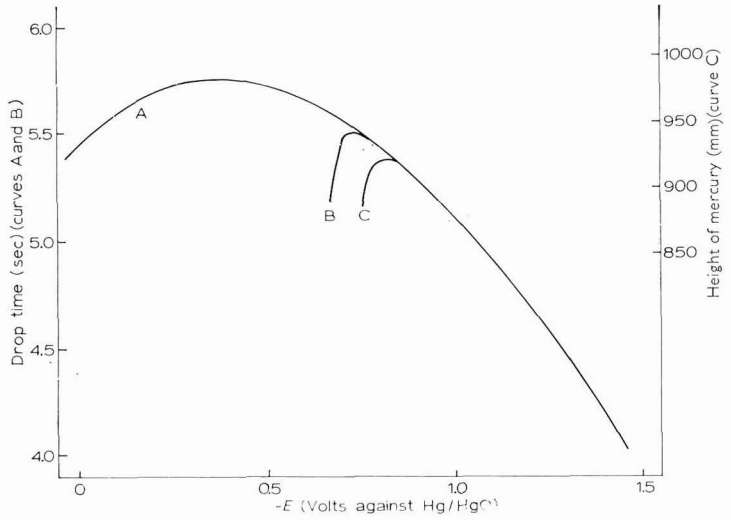

Fig. 1. Electrocapillary curves for mercury in sulphide solns. (A), drop-time measurements in 0.5 *M* NaOH + 1 *M* $NaHCO_3$; (B), drop-time measurements in 0.5 *M* Na_2S + 1 *M* $NaHCO_3$; (C), surface tension measurements in 0.5 *M* K_2S by GOUY[1].

observed, with the e.c.m. in the buffered solution displaced ~ 0.11 V positive to the e.c.m. in the alkaline solution. Since the concentration of HS^- ion is slightly higher in the solution of lower pH and that of the S^{2-} ion is reduced from 0.38 *M* in 0.5 *M* K_2S solution to 1.5×10^{-5} *M* at the lower pH, any adsorption effects must be due to S^{2-} ions rather than HS^- ions.

Drop-times at potentials > -0.68 V (Hg/HgO) were irreproducible and could not be measured owing to the presence of a solid phase on the electrode. Subsequent measurements[6] have shown this phase to be HgS formed initially by the growth of two successive monomolecular layers.

Impedance measurements

The frequency-dependence of the electrode impedance in the buffered solution was measured using the a.c. bridge at fixed potentials in the potential region where the electrocapillary curve deviated from that of the base electrolyte, and the results are shown in Figs. 2 and 3. At more negative potentials, the electrode impedance was identical with that of the base solution and showed no frequency dispersion.

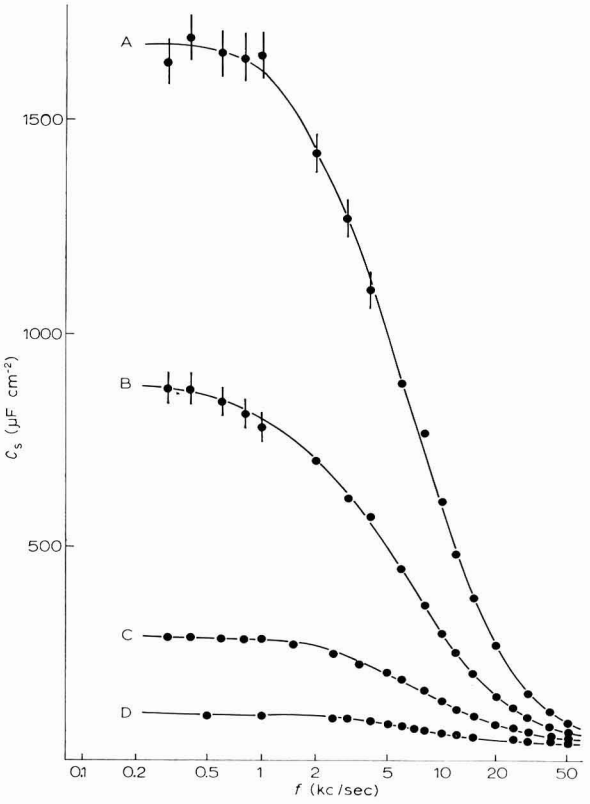

Fig. 2. Frequency-dependence of the electrode capacity, C_s, at fixed potentials in 0.5 *M* Na_2S + 1 *M* $NaHCO_3$ soln. (A), — 0.71; (B), — 0.72; (C), — 0.73; (D), — 0.74 V (Hg/HgO).

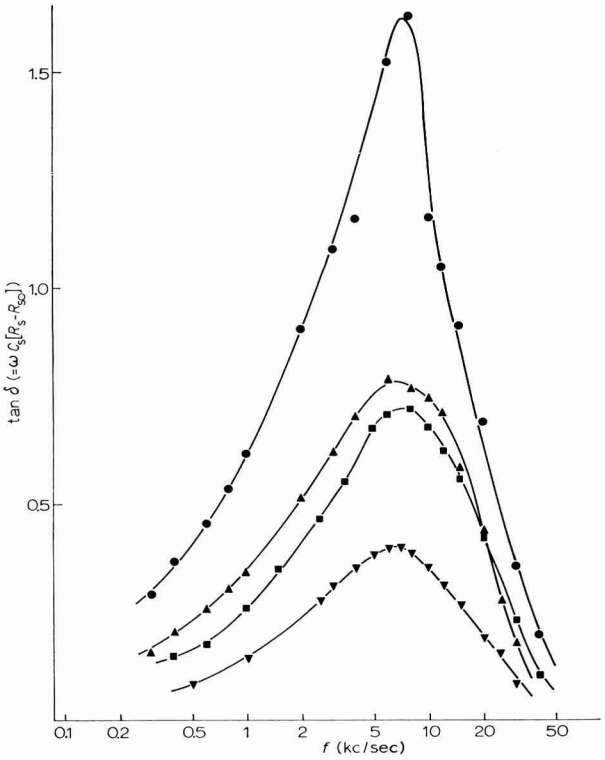

Fig. 3. Frequency-dependence of the loss tangent, tan δ, at fixed potentials in 0.5 M Na_2S + 1 M $NaHCO_3$ soln. (●), — 0.71; (▲), — 0.72; (■), — 0.73; (▼), — 0.74 V (Hg/HgO).

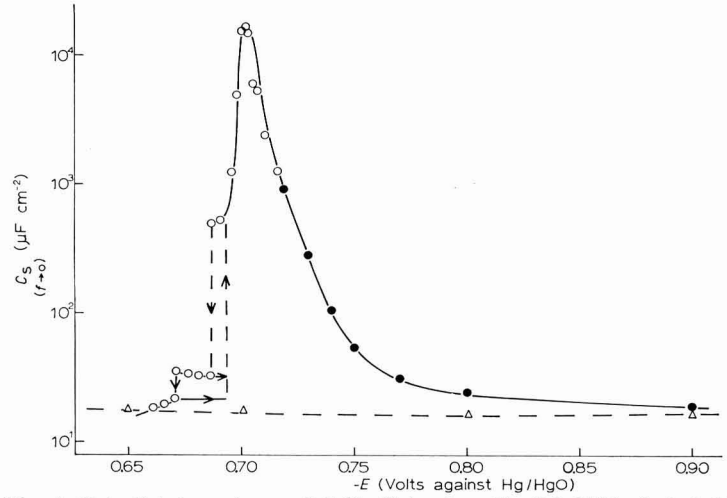

Fig. 4. Potential-dependence of $C_s(f \to 0)$ in: (○, ●); 0.5 M Na_2S + 1 M $NaHCO_3$; (△), 0.5 M NaOH + 1 M $NaHCO_3$. Open points, potentiostatic measurements; solid points, a.c. bridge measurements.

The capacity–frequency relationship at each potential (Fig. 2) showed that the capacity, C_s, was frequency independent at low frequencies (<1 kc/sec). At higher frequencies, the capacity decreased, showing an inflection at ~ 7 kc/sec and a corresponding maximum was observed in the frequency-dependence of the loss tangent, tan δ ($=\omega C_s[R_s - R_{so}]$ where ω is the angular frequency, C_s and R_s are, respectively, the measured capacity and measured resistance and R_{so} is the solution resistance) (Fig. 3). These features are characteristic of a relaxation process of some nature and will be discussed in the next section.

Instrumental limitations prevented the determination of the capacity at frequencies where the relaxation was complete. However, a series of low frequency capacities, $C_s(f \rightarrow 0)$, prior to relaxation, were obtained.

Figure 4 shows the potential dependence of $C_s(f \rightarrow 0)$ both for the base solution and the buffered sulphide solution. For the latter, it is a composite graph of points obtained by different techniques. The negative section up to the rising side of the peak was obtained from a.c. bridge measurements described above. For the capacity peak, very accurate control of potential was required since (i) the potential-dependence in this region is very high indeed and (ii) the HgS monolayer grows in the surface with some irreversibility if the potential is allowed to drift too positive. These measurements were therefore made using the potentiostatic method with low amplitude a.c. signals (1 or 2 mV) at low frequencies (down to 15 c/sec).

The impedance was purely capacitative (phase angle $= -90°$) at low frequencies at all potentials in the adsorption region, except in the potential region of the highest capacities where a small resistive component was found and was attributed to the solution resistance between the end of the Luggin probe and the working electrode. This becomes comparable with the electrode impedance, even at the lowest frequencies, when the electrode admittance is high.

On the anodic side of the peak, the capacity decreased rapidly and reversibly to a short plateau and then fell discontinuously to a much lower value. This discontinuity, which corresponded to the growth of the first HgS monolayer, exhibited a hysteresis with potential and was followed by a second discontinuity at ~ 15 mV more positive, corresponding to the growth of a second monolayer.

The double-layer capacities in the solid phase monolayer regions were obtained potentiostatically and are approximate only, as in these potential regions the impedance showed a genuine faradaic pseudocapacity, since the double layer capacitance was no longer so high as to render the faradaic admittance negligible. In fact, these points were obtained at a frequency of 1 kc/sec, to minimise the effect of the pseudocapacity.

Integration of the low frequency capacity–potential relationship yields the charge on the metal electrode, q_m. Figure 5 shows the potential dependence of q_m for this system, values of q_m being calculated on the assumption that there is no specific adsorption[3] at -0.90 V (Hg/HgO) and that the value of q_m at this potential is -12.1 μC cm^{-2}, as found for the base solution by integration of the capacity from the potential of the e.c.m. in this solution up to -0.90 V (Hg/HgO). The results in Fig. 5

show that $q_m = 0$ at a potential of -0.72 V (Hg/HgO), in fair agreement with the potential of the e.c.m. in Fig. 1 (potentials in this system are subject to rather large errors of correlation between experiments, owing to poor reproducibility of the liquid junction with 1 *M* NaOH, since this has a calculated potential of -20 mV).

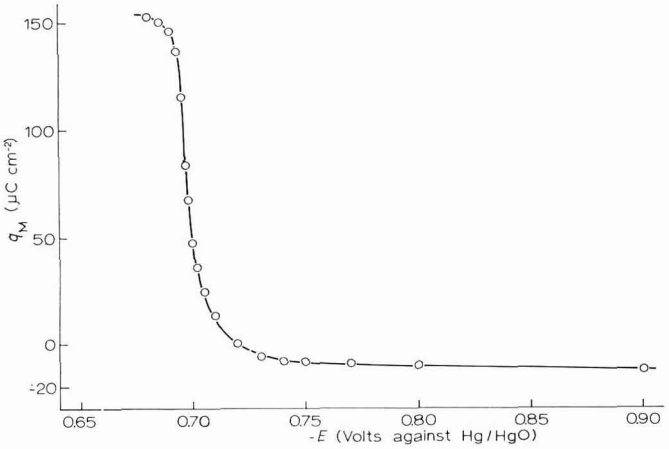

Fig. 5. Potential-dependence of the charge on the electrode, q_m, in 0.5 *M* Na_2S + 1 *M* $NaHCO_3$ soln.

DISCUSSION

Thermodynamic double-layer capacity

The maxima obtained in the electrocapillary curves by GOUY[1] and ourselves can be attributed to the adsorption of S^{2-} ions at the mercury electrode. Although it is not possible to obtain the thermodynamically-equivalent double-layer capacities, $C_s(f \rightarrow 0)$, in the alkaline (pH $\sim$13) sulphide solution, at potentials around the e.c.m., such measurements have been obtained at pH $\sim$9.5, as described above. That these are the thermodynamic double-layer values is confirmed by the following observations: (i) the potential of the e.c.m. obtained from drop-time measurements coincides, within experimental error with that obtained by integration of $C_s(f \rightarrow 0)$; (ii) the frequency-dependence of C_s and tan δ shows the absence of a faradaic pseudocapacity which would otherwise cause both these quantities to increase monotonically with decreasing frequency; (iii) the calculated thermodynamic equilibrium concentration of the HgS_2^{2-} ion is only $\sim 5 \cdot 10^{-5}$ *M* at a potential of -0.70 V (Hg/HgO); (iv) a pseudocapacity is observed at low frequencies only when the HgS monolayer is present on the electrode surface, since this reduces the double-layer capacity to a value at which its impedance is comparable with the faradaic impedance.

As GOUY pointed out, the very sharp maximum in the electrocapillary curve leads to a very high double-layer capacity ($\sim$15,000 μF cm^{-2}).

Concentration-dependence of the potential region of adsorption

It has been observed in a number of systems[7] that a region of strong adsorption immediately precedes the potential at which a solid phase forms on the electrode. If this feature is to be invariant with changes in concentration of the electroactive anion, the potential region of adsorption must show the same concentration-dependence as the reversible potential of the solid phase, *i.e.*, $60/n$ mV decade^{-1}, where n = ionic charge.

In the case of the S^{2-} ion, the e.c.m. lies in this region and thus shows a dependence of $\sim +30$ mV decade^{-1} decrease in concentration (comparing the results of GOUY[1] with our own). (The complete concentration-dependence of the electrode impedance was not attempted since the limited accuracy of measurement of such large capacities results in very large errors after the processes of graphical integration with respect to potential, followed by differentiation with respect to concentration. However it is worthwhile making a comparison with the results of GOUY[1] to obtain the approximate concentration-dependence.) This is contrary to the usual experimental finding that the potential of the e.c.m. shows a greater concentration-dependence than might be expected (the Esin and Markov[8] effect), and the observed dependence appears to correspond to that of adsorbed ions behaving as a uniform ("smeared out") sheet of charge. This may arise when the specifically adsorbed charge is appreciably near that associated with saturation coverage, since the linear potential gradient model of the double layer is then no longer appropriate[9,10].

Throughout the present work, the double layer is treated on the basis of the model proposed by BARLOW AND MACDONALD[11] in which both the metal electrode and the solution behave as perfect conductors (*i.e.*, the effects of the diffuse double layer have been neglected). However, the deviation from the constant field approximation calculated by these authors is insufficient in this case to account for the shift in the potential of the e.c.m. This may be due to the error in the potential measurements of GOUY as a result of concentration changes at the electrode surface occurring with the copious dissolution reaction[3]. Alternatively, the hexagonal array of adsorbed ions used in the model of BARLOW AND MACDONALD may be inappropriate in the present case.

Potential-dependence of the adsorption

The most important feature of the capacity–potential relationship is perhaps the observation of a maximum. This feature is frequently observed in the adsorption of organic substances[12] at a mercury electrode, but not in the adsorption of an inorganic anion. It has previously been observed[9] that when inorganic anions are specifically adsorbed, both the charge on the electrode, q_m and, the capacity of the inner layer, $dq_m/d\phi_{m-2}$ (where ϕ_{m-2} is the potential of the metal electrode relative to the potential of the diffuse layer), increase without limit as ϕ_{m-2} increases anodically. This cannot be the case if adsorption is restricted to a monolayer, as is demonstrated below.

Let

$$q_m = f(q_1, \phi_{m-2}) \tag{1}$$

where q_1 is the specifically adsorbed charge and ϕ_{m-2} is the potential of the metal electrode with respect to that at the outer Helmholtz plane.

Then

$$dq_m = \left(\frac{\partial q_m}{\partial q_1}\right)_{\phi_{m-2}} dq_1 + \left(\frac{\partial q_m}{\partial_{\phi_{m-2}}}\right)_{q_1} d\phi_{m-2} \tag{2}$$

and

$$C^i = \frac{dq_m}{d\phi_{m-2}} = \left(\frac{\partial q_m}{\partial q_1}\right)_{\phi_{m-2}} \left(\frac{dq_1}{d\phi_{m-2}}\right) + \left(\frac{\partial q_m}{\partial \phi_{m-2}}\right)_{q_1} \tag{3}$$

where C^i is the differential inner-layer capacity.

Since $(\partial q_m/\partial \phi_{m-2})_{q_1} \sim$ constant and, to a good approximation, may be equated with the capacity of the base electrolyte, C_b,

$$C^i = C_b + \left(\frac{\partial q_m}{\partial q_1}\right)_{\phi_{m-2}} \left(\frac{dq_1}{d\phi_{m-2}}\right) \tag{4}$$

The partial derivative $(\partial q_m/\partial q_1)_{\phi_{m-2}}$ [which is not to be confused with $(\partial q_m/\partial q_1)_\mu$] can be written as

$$-\left(\frac{\partial q_m}{\partial \phi_{m-2}}\right)_{q_1} \Big/ \left(\frac{\partial q_1}{\partial \phi_{m-2}}\right)_{q_m}$$

and since these quantities can be experimentally determined, values of $(\partial q_m/\partial q_1)_{\phi_{m-2}}$ are known for a number of systems and are tabulated in Table 1.

TABLE 1

VALUES OF $(\partial q_m/\partial q_1)_{\phi_{m-2}}$ FOR SEVERAL ANIONS

Anion	$(\partial q_m/\partial q_1)_{\phi_{m-2}}$	*Range of* q_m ($\mu C\ cm^{-2}$)	*Authors*
I^- (aq.)	0.40 ± 0.02	-6 to $+18$	GRAHAME[13]
I^- (in formamide)	$0.40 \rightarrow 0.65$	$-7 \rightarrow +20$	PAYNE[14]
Cl^-	0.16 ± 0.02	0 to $+18$	GRAHAME AND PARSONS[15]
NO_3^-	0.24 ± 0.02	0 to $+18$	PAYNE[16]
Benzene-*m*-disulphonate	~ 0.25	-8 to $+16$	PARRY AND PARSONS[10]
$H_2PO_4^-$	0.15 ± 0.04	$+4$ to $+18$	PARSONS AND ZOBEL[17]

If q_1 has a finite limit (corresponding to monolayer coverage), and if $(\partial q_m/\partial q_1)_{\phi_{m-2}}$ is $\sim$ constant, C_s will not increase indefinitely with anodic potential but will show a maximum near the maximum in $(dq_1/d\phi_{m-2})$ which we would expect to be associated with approximately[10] half-coverage of the electrode with adsorbed anions. Therefore, the failure to observe capacity maxima associated with inorganic anion adsorption* (as opposed to maxima associated with C_b) in other systems is probably

* Maxima have been observed in the case of organic anions, *e.g.*, benzene-*m*-disulphonate[10].

due to the restriction of the investigations to low coverages, which is unavoidable in a number of cases since solid phases are formed before the maximum can be attained (*e.g.*, in the adsorption of phosphate anions[18]).

The specifically adsorbed charge, q_1, may be approximately evaluated if we neglect the potential drop in the diffuse double layer, as follows:

$$q_1 = \int_0^{q_1} \mathrm{d}q_1 = \int_{-\infty}^{\phi_m} \left(\frac{\mathrm{d}q_1}{\mathrm{d}\phi_m}\right) \mathrm{d}\phi_m$$

$$= \int_{-\infty}^{\phi_m} \left(\frac{\partial q_1}{\partial q_m}\right)_{\phi_m} \left(C_s - C_b\right)_{(f\to 0)} \mathrm{d}\phi_m \qquad (5)$$

where ϕ_m is the potential of the metal electrode relative to the bulk solution.

If $(\partial q_1/\partial q_m)_{\phi_m}$ is independent of ϕ_m (for experimental evidence of this assumption see Table 1),

$$q_1 = \left(\frac{\partial q_1}{\partial q_m}\right)_{\phi_m} \int_{-\infty}^{\phi_m} \left(C_s - C_b\right)_{(f\to 0)} \mathrm{d}\phi_m \qquad (6)$$

Thus, a charge which is proportional to the adsorbed charge may be obtained by evaluating the integral of eqn. (6), and this is shown for the present work in Fig. 6 as a function of the electrode potential, E.

The value of $(\partial q_1/\partial q_m)_{\phi_m}$ must now be considered. For the infinite imaging treatment of the compact double layer[11], with the constant field approximation (neglect of the discrete ion potential) and assuming a constant dielectric constant, this quantity has the value $(x_2 - x_1)/x_2$ where x_1 and x_2 are the distances from the electrode surface to the inner and outer Helmholtz planes, respectively. Then, in the present case, for $x_1 = 1.84$ Å, $x_2 = 4$ Å, this would lead to a saturation coverage of adsorbed charge of $\sim 295\ \mu\mathrm{C\ cm^{-2}}$, which compares with a value of $\sim 270\ \mu\mathrm{C\ cm^{-2}}$, calculated for a hexagonal close packed array of spheres of radius 1.84 Å.

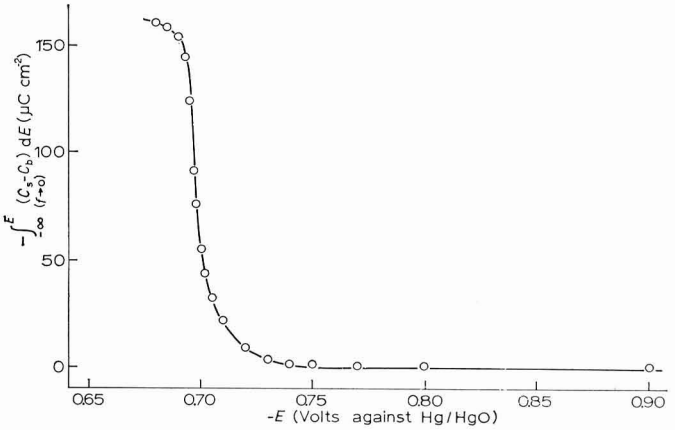

Fig. 6. Potential-dependence of $\int_{-\infty}^{E} (C_s(f\to 0) - C_b)\, \mathrm{d}E$ in 0.5 M Na_2S + 1 M $NaHCO_3$ soln.

The potential-dependence of the adsorption isotherm would be ideally tested by investigating the dependence of q_1 on ϕ_1, the micropotential at an anion adsorption site. Unfortunately, the electrode potential, E, must be used instead of ϕ_1 since the latter is not known. This will only give a good approximation if (a) there is a constant field in the inner layer and (b) there is a relatively small potential drop in the diffuse layer.

The potential-dependence of q_1 is plotted semi-logarithmically in Fig. 7 and shows an approximate linear dependence at low values of q_1 of ~ 30 mV decade^{-1}. Since in the constant field approximation ($\Delta\phi_1 = \{(x_2 - x_1)/x_2\}\Delta E$) a slope of ~ 55 mV decade^{-1} would be anticipated, the experimentally obtained value is a measure of the many partially justified assumptions that have been made.

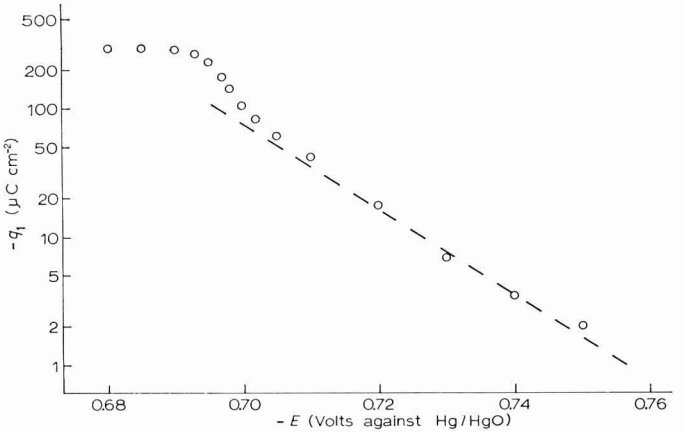

Fig. 7. Potential-dependence of the estimated adsorbed charge, q_1, in 0.5 M Na_2S + 1 M $NaHCO_3$ soln. Dashed line is drawn to slope of (30 mV)$^{-1}$.

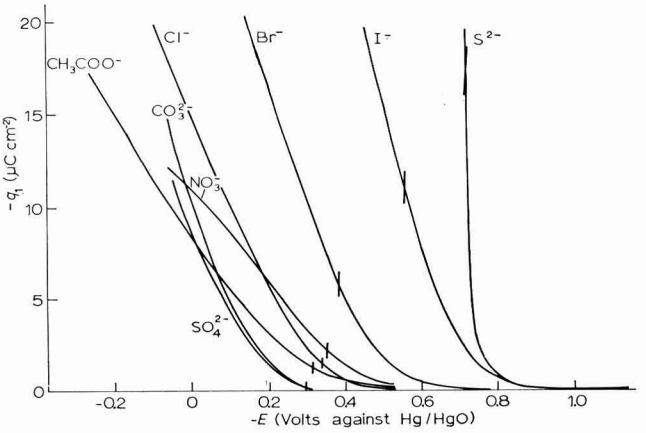

Fig. 8. Potential-dependence of q_1 for various anions, as published by MOTT and WATTS-TOBIN[9]. Concn. 0.1 M except for S^{2-} (1.5×10^{-5} M). Vertical lines indicate point of zero charge.

Comparison of sulphide with other adsorbed anions

Unfortunately it is not possible to compare the adsorption of sulphide ions in the present experiments directly with corresponding data for other ions. MOTT AND WATTS-TOBIN[9] have published a plot of q_1 against E for a number of anions adsorbed at a mercury electrode from 0.1 M solutions. This is reproduced in Fig. 8 together with the present results for sulphide ions where the bulk concentration is only $\sim 1.5 \times 10^{-5}$ M.

Hence, whilst a direct comparison is not afforded, it is clear that sulphide ions are adsorbed more at more negative potentials than any other anions previously investigated. Such behaviour is presumably associated with the small size and double charge of the sulphide ion, although one might expect these properties to hinder the adsorption process insofar as they give rise to strong ionic hydration[19,20], (CONWAY AND BOCKRIS[21] have reported a primary hydration number of 8 for S^{2-}).

The two other strongly hydrated, doubly charged anions for which data are shown in Fig. 8, *i.e.*, carbonate and sulphate, are considerably larger and the charge on these ions is likely to be of a more distributed nature than in the case of the S^{2-} ion. These factors will affect the degree to which adsorbed ions interact with one another and may constitute the explanation for the attainment of such a high coverage in the case of S^{2-} ions.

Relaxation process

It was observed earlier that the capacity of the mercury electrode in the buffered sulphide solution at fixed potentials shows a frequency-dependence (Fig. 2) which, in the region prior to the formation of a monolayer of solid HgS, is not attributable to a faradaic process and shows features characteristic of a relaxation process. We may define the relaxation frequency as that at which the maximum occurs in the loss tangent, tan δ, (Fig. 3) by analogy with similar observations in Debye relaxation phenomena. In this case, the maximum is at $\sim 7 \pm 2$ kc/sec corresponding to a relaxation time of $\sim 25 \pm 7$ μsec, and it appears to be independent of electrode potential within the limits of experimental error. The inflections in the plots of C_s *vs.* log f occur in the same frequency range as the maximum in tan δ.

In an attempt to determine the nature of the process responsible for these observations, the experimental data were treated by the method of LORENZ AND MÖCKEL[22] by plotting $(\tan \delta^*)^{-1}$ as a function of $\omega^{-\frac{1}{2}}$ at fixed potentials, and an example is shown in Fig. 9. The quantity, tan δ^*, is given by

$$\tan \delta^* = (\omega C_p^* R_p)^{-1}$$

with

$$C_p^* = C_p - {}_\infty C_p$$

where C_p is the parallel equivalent electrode capacity, ${}_\infty C_p$ the value of C_p as $f \to \infty$ (*i.e.*, the parallel equivalent capacity after relaxation) and R_p the parallel equivalent electrode resistance. The value of ${}_\infty C_p$ was estimated from the graph of C_s *vs.* log f at

approximately 25 μF cm^{-2} (it was found that (tan δ^*)$^{-1}$ was not a sensitive function of $_{\infty}C_p$ in the potential region of high adsorption).

The present results are unfortunately subject to instrumental limitations at high frequencies, which give rise to errors in the determination of the solution

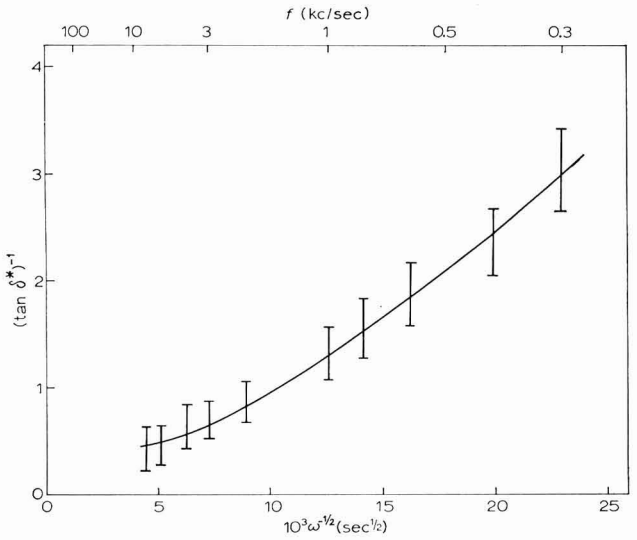

Fig. 9. Experimental dependence of (tan δ^*)$^{-1}$ on $\omega^{-\frac{1}{2}}$ at $E = -0.71$ V (Hg/HgO) in 0.5 M Na_2S + 1 M $NaHCO_3$ soln.

resistance, R_{so}. Since (tan δ^*)$^{-1}$ is extremely sensitive to this quantity at high frequencies, the graph cannot be reliably plotted at values of $\omega^{-\frac{1}{2}} \lesssim 0.005$ sec$^{\frac{1}{2}}$. An error bar is shown for each experimental value and indicates the error in (tan δ^*)$^{-1}$ due to the uncertainty in R_{so}. The true value of R_{so} is considered to lie between the value of R_s measured at high frequencies (50 kc/sec) at potentials negative to the adsorption region, and the value of R_s at $\omega = \infty$, extrapolated from a graph of R_s *vs.* $\omega^{-\frac{1}{2}}$, after the method suggested by LORENZ[23].

LORENZ AND MÖCKEL[22] have shown that the dependence of (tan δ^*)$^{-1}$ on $\omega^{-\frac{1}{2}}$ is characteristic of the slow step involved in the overall process of adsorption at the electrode and have obtained curves for the case of pure diffusion-control of the adsorbing species and the case of diffusion coupled with a slow adsorption step. An example is shown in the Appendix (Fig. A2), where the treatment is further extended for the case of diffusion coupled with a slow homogeneous reaction in solution, and the dependence of (tan δ^*)$^{-1}$ on $\omega^{-\frac{1}{2}}$ in this case is shown in Fig. A1.

The manner in which sulphide ions are adsorbed at the electrode most probably follows one of the following two schemes:

$$\left.\begin{aligned} HS^- &\rightleftharpoons S^{2-} + H^+ \\ S^{2-} &\rightleftharpoons S^{2-}_{ads} \end{aligned}\right\} \qquad \text{I}$$

$$HS^- \rightleftharpoons H^+ + S^{2-}_{ads.} \qquad II$$

Owing to the appreciable buffer capacity of the carbonate–bicarbonate system and the low concentration of sulphide ion, the hydrogen ion concentration is, to a good approximation, constant and the first reaction in scheme I may be regarded as pseudo-first-order in S^{2-}.

The results of Fig. 9 indicate that the slow step of the adsorption process is not solely a diffusion process, since this would require a straight line[22] with intercept $(\tan \delta^*)^{-1} = 1$ at $\omega^{-\frac{1}{2}} = 0$. The fact that $(\tan \delta^*)^{-1}$ falls below unity indicates that one of the processes in either scheme I or scheme II is the slow step. It is considered unlikely that the heterogeneous adsorption step of scheme I is the slow step, in view of the results obtained by LORENZ[24] for the adsorption of I^-, Br^-, SCN^- and N_3^- ions at a mercury electrode.

It is shown in the Appendix, that if the homogeneous step of scheme I is to be rate-determining, then the plot of $(\tan \delta^*)^{-1}$ *vs.* $\omega^{-\frac{1}{2}}$ should show a minimum, whereas scheme II would lead to values of $(\tan \delta^*)^{-1}$ increasing monotonically with $\omega^{-\frac{1}{2}}$. In view of the experimental error, it cannot be reasonably ascertained whether or not a minimum is present and the data were therefore analysed for both cases in the manner described in the Appendix, *i.e.*, by estimating $d(\tan \delta^*)^{-1}/d(\omega^{-\frac{1}{2}})$ as $\omega \rightarrow 0$ and the frequency, ω^*, at which $(\tan \delta^*)^{-1} = 1$.

Hence, approximate values have been calculated for the pseudo-first-order homogeneous rate constant, k, (scheme I) and, assuming a Langmuir isotherm to be obeyed, for the interfacial reaction rate, V (scheme II). It was found that $k \sim 10^{13}$ sec^{-1}; such a high value is in serious disagreement with the value that would be expected on the basis of the results of EIGEN *et al.*[25], from which the rate constant for such a proton recombination process is $\sim 10^{10}$ $mole^{-1}$ sec^{-1}. Thus, in the sulphide solution of pH ~ 9.5, the pseudo-first-order rate constant, k, for the conversion of S^{2-} to HS^- is ~ 0.3 sec^{-1} and we should therefore expect the relaxation to occur at about the same angular frequency, which is considerably lower than the observed value of $\sim 4 \cdot 10^5$ sec^{-1}. It appears unlikely, therefore, that reaction scheme I is responsible for the observed phenomena.

If the data for the heterogeneous case (scheme II) are treated, the calculated value of V is $\sim 10^{-4}$ mole cm^{-2} sec^{-1} and it seems likely therefore that the reaction is a heterogeneous one and that the relaxation effects observed are attributable to a process of dissociative adsorption in which HS^- ions are simultaneously dissociated at the electrode and adsorbed as S^{2-} ions.

ACKNOWLEDGEMENTS

R.D.A. thanks Imperial Chemical Industries Limited for the provision of a Research Fellowship, and D.F.P. thanks the Science Research Council for the provision of a Research Studentship, during the tenure of which this work was carried out.

APPENDIX. ADSORPTION AT AN ELECTRODE COUPLED WITH A HOMOGENEOUS REACTION IN SOLUTION

In this Appendix, we derive the impedance of an electrode at which a species S_1 (concentration C_0) is adsorbed when this species S_1 undergoes a homogeneous reaction with a species S_2 (concentration C_0').

$$S_1 \underset{k'}{\overset{k}{\rightleftharpoons}} S_2 \tag{A1}$$

We shall treat the case where S_1 at the electrode surface ($x=0$) is always in equilibrium with the adsorbed material and where $C_0' \gg C_0$. The derivation is similar to that used by LORENZ AND MÖCKEL[22].

On subjecting the electrode potential to a sinusoidal perturbation

$$\phi = \phi_0 + P \exp(j\omega t) \tag{A2}$$

the diffusion equation for S_1 is

$$\frac{\partial C}{\partial t} = D \frac{\partial^2 C}{\partial x^2} + k'C' - kC \tag{A3}$$

with the boundary conditions

$$C \to C_0, \qquad x \to \infty \tag{A4}$$

$$\frac{\mathrm{d}\Gamma}{\mathrm{d}t} = D\left(\frac{\partial C}{\partial x}\right)_{x=0} = \left(\frac{\partial \Gamma}{\partial C_0}\right)_{\phi}\left(\frac{\partial C}{\partial t}\right)_{x=0} + \left(\frac{\partial \Gamma}{\partial \phi}\right)_{C_0}\frac{\mathrm{d}\phi}{\mathrm{d}t} \tag{A5}$$

With the assumption that $C'(x, t) = C_0'$, since $C_0' \gg C_0$ the solution of (A3) with (A4) and (A5) is

$$C = C_0 + C_2 \exp(j\omega t) \exp\left[-\left(\frac{k+j\omega}{D}\right)^{\frac{1}{2}} x\right] \tag{A6}$$

where

$$C_2 = -\frac{\left(\frac{\partial \Gamma}{\partial \phi}\right)_{C_0} P j\omega}{D^{\frac{1}{2}}(k+j\omega)^{\frac{1}{2}} + \left(\frac{\partial \Gamma}{\partial C_0}\right)_{\phi} j\omega} \tag{A7}$$

Thus we find

$$\frac{\mathrm{d}\Gamma}{\mathrm{d}t} = \frac{Nj\omega D^{\frac{1}{2}}(\alpha+\beta j)\exp(j\omega t)}{D^{\frac{1}{2}}(\alpha+\beta j)+jM\omega} \tag{A8}$$

where

$$M = \left(\frac{\partial \Gamma}{\partial C_0}\right)_{\phi}, \qquad N = \left(\frac{\partial \Gamma}{\partial \phi}\right)_{c_0} P,$$

$$\alpha = (k^2+\omega^2)^{\frac{1}{4}} \frac{\omega}{2^{\frac{1}{2}}(k^2+\omega^2-k\sqrt{k^2+\omega^2})^{\frac{1}{2}}},$$

and

$$\beta = (k^2+\omega^2)^{\frac{1}{4}} \frac{(k^2+\omega^2)^{\frac{1}{2}}-k}{2^{\frac{1}{2}}(k^2+\omega^2-k\sqrt{k^2+\omega^2})^{\frac{1}{2}}}$$

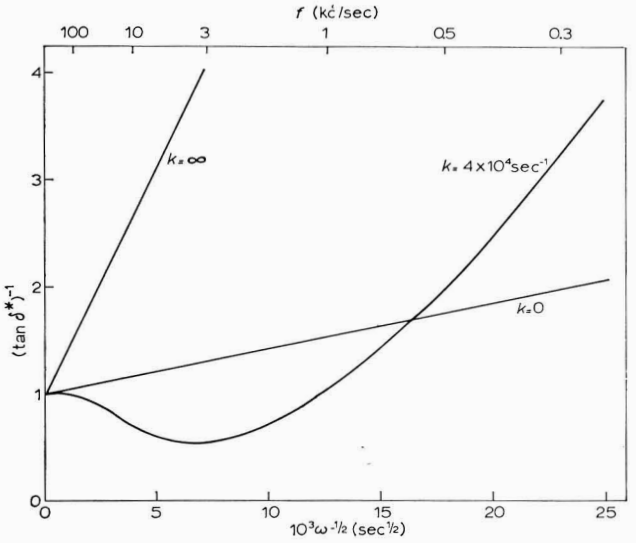

Fig. A1. Predicted dependence of $(\tan \delta^*)^{-1}$ on $\omega^{-\frac{1}{2}}$ for the case of adsorption coupled with a homogeneous reaction. Curves obtained from eqns. (A14), (A15) and (A17) with the conditions: $D = D' = 10^{-5}$ cm² sec^{-1}, $(\partial\Gamma/\partial C_0) = 10^{-4}$ cm, $C_0'/C_0 = 10$.

The interfacial impedance is measured as a parallel combination, C_p and R_p. Thus the admittance

$$\frac{1}{Z} = j\omega C_p + \frac{1}{R_p} = \frac{i}{P \exp(j\omega t)} \tag{A9}$$

Now

$$i = \frac{dq_m}{dt} = \left(\frac{\partial q_m}{\partial \phi}\right)_{\Gamma} \frac{d\phi}{dt} + \left(\frac{\partial q_m}{\partial \Gamma}\right)_{\phi} \frac{d\Gamma}{dt} \tag{A10}$$

Therefore

$$\frac{1}{Z} = \frac{i}{P\exp(j\omega t)} = j\omega\left(\frac{\partial q_m}{\partial \phi}\right)_\Gamma + \left(\frac{\partial q_m}{\partial \Gamma}\right)_\phi \frac{d\Gamma}{dt} \cdot \frac{1}{P\exp(j\omega t)}$$

$$= j\omega\, {}_\infty C_p + \left(\frac{\partial q_m}{\partial \Gamma}\right)_\phi \frac{d\Gamma}{dt} \cdot \frac{1}{P\exp(j\omega t)} \tag{A11}$$

where

$${}_\infty C_p = \left(\frac{\partial q_m}{\partial \phi}\right)_\Gamma$$

is the infinite frequency capacity.

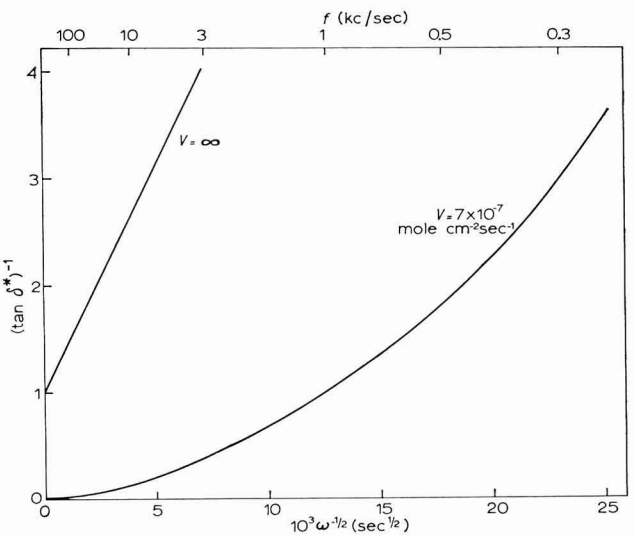

Fig. A2. Predicted dependence of $(\tan \delta^*)^{-1}$ on $\omega^{-\frac{1}{2}}$ for the case of adsorption coupled with a slow heterogeneous reaction. Curves obtained from eqn. (28) of LORENZ AND MÖCKEL[22], using the same conditions as for Fig. A1, with $C_0' = 10^{-2}$ M and the assumption that a Langmuir isotherm is obeyed.

This leads to

$$R_p = \left(\frac{\partial \phi}{\partial \Gamma}\right)_{c_0}\left(\frac{\partial \Gamma}{\partial q_m}\right)_\phi \left[\frac{(\alpha^2+\beta^2)D + 2M\beta\omega D^{\frac{1}{2}} + M^2\omega^2}{\alpha M\omega^2 D^{\frac{1}{2}}}\right] \tag{A12}$$

$$C_p = {}_\infty C_p + \left(\frac{\partial q_m}{\partial \Gamma}\right)_\phi \left(\frac{\partial \Gamma}{\partial \phi}\right)_{c_0}\left[\frac{(\alpha^2+\beta^2)D + M\beta\omega D^{\frac{1}{2}}}{(\alpha^2+\beta^2)D + 2M\beta\omega D^{\frac{1}{2}} + M^2\omega^2}\right] \tag{A13}$$

Following LORENZ AND MÖCKEL[22], we evaluate the phase angle remaining after the subtraction of the infinite frequency capacity,

$$\tan \delta^* = \frac{1}{\omega R_p C({}_p - {}_\infty C_p)}$$

Thus

$$\tan \delta^* = \frac{\alpha M \omega}{D^{\frac{1}{2}} \alpha^2 + M\beta\omega + D^{\frac{1}{2}} \beta^2} \tag{A14}$$

In the limit $\omega \gg k$

$$\frac{1}{\tan \delta^*} = 1 + \left(\frac{2D}{\omega}\right)^{\frac{1}{2}} \cdot \frac{1}{M} \tag{A15}$$

and when $\omega \ll k$

$$1/\tan \delta^* = (Dk)^{\frac{1}{2}}/M\omega \tag{A16}$$

For $k \to \infty$, eqn. (A14) is no longer applicable and

$$1/\tan \delta^* = 1 + (2D'/\omega)^{\frac{1}{2}}/M' \tag{A17}$$

where

$$M' = \left(\frac{\partial \Gamma}{\partial C_0'}\right)_\phi = \left(\frac{\partial \Gamma}{\partial C_0}\right)_\phi \frac{dC_0}{\partial C_0'} = \left(\frac{\partial \Gamma}{\partial C_0}\right)_\phi \frac{C_0}{C_0'}$$

and for all cases in the limit $\omega \to 0$,

$$\frac{d(\tan \delta^*)^{-1}}{d(\omega^{-\frac{1}{2}})} = \frac{(2D')^{\frac{1}{2}}}{\left(\frac{\partial \Gamma}{\partial C_0}\right)_\phi} \cdot \frac{C_0'}{C_0} \tag{A18}$$

With the use of these relationships, the curve $(\tan \delta^*)^{-1}$ *vs.* $\omega^{-\frac{1}{2}}$ may be constructed (Fig. A1). This should be compared with that expected for a slow heterogeneous reaction (Fig. A2).

Finally, it is interesting to note the connection between a fast homogeneous reaction and a heterogeneous reaction. If reaction (A1) occurs in a reaction zone of thickness μ, then the rate of the reaction (V moles cm^{-2} sec^{-1}) is given by

$$V = k' C_0' \mu \tag{A19}$$

Now the thickness, μ, may be evaluated from the Einstein relation
$\mu = (D\tau)^{\frac{1}{2}} = (D/k)^{\frac{1}{2}}$

Hence

$$V = k' C_0' (D/k)^{\frac{1}{2}} = C_0 (kD)^{\frac{1}{2}} \tag{A20}$$

The equivalent heterogeneous rate constant, k_h, would lead to a rate

$$V = k_h C_0'$$

so that

$$k_h = \{(k\,D)^{\frac{1}{2}}/C_0'\}\,C_0 \tag{A21}$$

In the analysis of a $(\tan\delta^*)^{-1}$ *vs.* $\omega^{-\frac{1}{2}}$ curve, we evaluate the rate constants by observing the angular frequency, ω^*, at which $(\tan\delta^*)^{-1}=1$. Interpreting this as due to a heterogeneous reaction we obtain (assuming a Langmuir isotherm to be obeyed)

$$\omega^* = \frac{k_h}{\left(\frac{\partial\Gamma}{\partial C_0'}\right)_\phi} = \frac{k_h}{\left(\frac{\partial\Gamma}{\partial C_0}\right)_\phi \frac{C_0}{C_0'}} \tag{A22}$$

whereas interpreting this as a homogeneous reaction

$$\omega^* \approx (kD)^{\frac{1}{2}} / \left(\frac{\partial\Gamma}{\partial C_0}\right)_\phi \tag{A23}$$

so that the rate constants derived on either interpretation have the equivalence expressed in eqn. (A21).

SUMMARY

The impedance of a mercury electrode in sulphide ion solution of pH 9.5 has been studied using a.c. impedance techniques. Sulphide ions are very strongly specifically adsorbed at the electrode over a short potential range in the region of the e.c.m., leading to very high double-layer capacities. The potential-dependence of the capacity exhibits a maximum, followed at more anodic potentials by a discontinuity corresponding to the formation of a solid phase monolayer of HgS on the electrode. The frequency-dependence of the impedance in the potential region of adsorption indicates a relaxation process at a frequency of ~ 7 kc/sec, and this is attributed to the slow dissociative adsorption of the HS^- species according to the reaction scheme $HS^- \rightleftharpoons H^+ + S^{2-}$.

REFERENCES

1 G. GOUY, *Ann. Chim. Phys.*, 29 (1903) 145.
2 A. N. FRUMKIN, *Kinetics of Electrode Processes*, University Press, Moscow, 1952.
3 R. D. ARMSTRONG, D. F. PORTER AND H. R. THIRSK, *J. Electroanal. Chem.*, 14 (1967) 17.*
4 R. D. ARMSTRONG, W. P. RACE AND H. R. THIRSK, *J. Electroanal. Chem.*, 14 (1967) 143.
5 A. J. ELLIS AND R. M. GOLDING, *J. Chem. Soc.*, (1959) 127.
6 R. D. ARMSTRONG, D. F. PORTER AND H. R. THIRSK, to be published.
7 R. D. ARMSTRONG AND M. FLEISCHMANN, *J. Polarog. Soc.*, 11 (1965) 31.
8 O. A. ESIN AND B. F. MARKOV, *Acta Physicochem. URSS*, 10 (1939) 353.
9 N. F. MOTT AND R. J. WATTS-TOBIN, *Electrochim. Acta*, 4 (1961) 79.
10 J. M. PARRY AND R. PARSONS, *Trans. Faraday Soc.*, 59 (1963) 24.
11 C. A. BARLOW AND J. R. MACDONALD, *J. Chem. Phys.*, 40 (1964) 1535.
12 A. N. FRUMKIN, *Modern Aspects of Electrochemistry*, No. 3, edited by J. O'M. BOCKRIS AND B. E. CONWAY, Butterworths, London, 1964, chap. 3.
13 D. C. GRAHAME, *J. Am. Chem. Soc.*, 80 (1958) 4201.
14 R. PAYNE, *J. Chem. Phys.*, 42 (1965) 3371.

* In Figs. 8 and 9 the values of R_s shown are too great by 0.4 Ω cm^2.

15 D. C. GRAHAME AND R. PARSONS, *J. Am. Chem. Soc.*, 83 (1961) 1291.
16 R. PAYNE, *J. Electrochem. Soc.*, 113 (1966) 999.
17 R. PARSONS AND F. G. R. ZOBEL, *J. Electroanal. Chem.*, 9 (1965) 333.
18 R. D. ARMSTRONG, M. FLEISCHMANN AND J. W. OLDFIELD, *J. Electroanal. Chem.*, 14 (1967) 235.
19 J. O'M. BOCKRIS, M. A. V. DEVANATHAN AND K. MÜLLER, *Proc. Roy. Soc. London*, 274A (1963) 55.
20 T. N. ANDERSEN AND J. O'M. BOCKRIS, *Electrochim. Acta*, 9 (1964) 374.
21 B. E. CONWAY AND J. O'M. BOCKRIS, *Modern Aspects of Electrochemistry*, No. 1, Butterworths, London, 1954, p. 65.
22 W. LORENZ AND F. MÖCKEL, *Z. Elektrochem.*, 60 (1956) 507.
23 W. LORENZ, *Z. Phys. Chem. (Leipzig)*, 224 (1963) 145.
24 W. LORENZ, *Z. Phys. Chem. (Leipzig)*, 232 (1966) 176.
25 M. EIGEN, W. KRUSE, G. MAASS AND L. DE MAEYER, *Progress in Reaction Kinetics*, Vol. 2, edited by G. PORTER, Pergamon Press, 1964, p. 285.

ELECTROANALYTICAL CHEMISTRY AND INTERFACIAL ELECTROCHEMISTRY
Elsevier Sequoia S.A., Lausanne – Printed in The Netherlands

ELECTROSTATIC STREAMING CURRENT DEVELOPED IN THE TURBULENT FLOW THROUGH A PIPE

E. T. HIGNETT* AND J. C. GIBBINGS
Fluid Mechanics Division, Department of Mechanical Engineering, University of Liverpool (England)
(Received April 3rd, 1967)

INTRODUCTION

Two dissimilar phases or two dissimilar substances are frequently observed to acquire electrostatic charges of equal magnitude but of opposite sign after contact and subsequent separation. When the phases brought into contact are a solid and a liquid, then small charge densities in low-conductivity liquids can result in high values of the electric field. When the separated charges in the liquid are convected away by a fluid motion, then a rate of transport of charge occurs. This has been called a streaming current.

The charges occurring upon insulating surfaces have been postulated as the origin of the dust patterns found to result from the flow of gases. These patterns can be related to the nature of the flow at the surface and in particular to the value of the skin friction[1]. This suggests that the charging is related to the skin friction of the gas flow.

Experimental and analytical studies have been made of the special case of the streaming current developed in liquids flowing through circular pipes[2,3]. These studies have helped to distinguish some of the variables that control the phenomena.

The principles of dimensional analysis have been applied to determine the non-dimensional groups that arise in a general description of the occurrence of a streaming current[4,5]. One of these non-dimensional groups, for the specific case of turbulent flow through circular pipes, is the length–diameter ratio of the pipe. The effect of this group, which has been experimentally determined, has already been described[6].

This paper describes an experiment to determine the effects of three more non-dimensional groups that form independent variables.

2. DIMENSIONLESS GROUPS GOVERNING THE ELECTROSTATIC STREAMING CURRENT

The following three dimensionless groups of variables that arise in the streaming current phenomena have been derived[4,5];

(a) a streaming current group:

$$i_s^2/(\varrho u^4 \varepsilon l^2) \qquad (1)$$

* Now at Central Electricity Generating Board, Leeds.

where i_s is the streaming current,
l is a typical length,
U is a reference fluid velocity,
ε is the dielectric coefficient,
and ϱ is the fluid density
(b) a conductivity group:

$$(\varepsilon U)/(\lambda l) \tag{2}$$

where λ is the liquid electric conductivity.
(c) a Reynolds number group:

$$R_e \equiv (\varrho U l)/\mu \tag{3}$$

where μ is the liquid viscosity.

For turbulent flow in a pipe, it has been shown[6] that the effect of pipe length upon the streaming current can be expressed as

$$i_s = i_\infty[1 - \exp\{-(J_L - J_{L_0})\}] \tag{4}$$

where i_∞ is the current corresponding to $L = \infty$,
L is the pipe length,
L_0 is the pipe length entry correction,

$$\left.\begin{aligned} J_L &= (\lambda L)/(\bar{u}\varepsilon) \\ J_{L_0} &= (\lambda L_0)/(\bar{u}\varepsilon) \end{aligned}\right\} \tag{5}$$

and $\bar{u}$ is the mass flow rate mean velocity in the pipe.

Using $\bar{u}$ as the reference velocity and the pipe diameter, d, as the reference length, the above non-dimensional groups can be written as

$$i_\infty^2/\varrho\bar{u}^4\varepsilon d^2, \quad \varepsilon\bar{u}/\lambda d, \quad \varrho\bar{u}d/\mu \tag{6}$$

By cross-multiplication these groups can be rearranged to give,

$$i_\infty^2/\lambda d^3\varrho\bar{u}^3 = f[\varepsilon\mu/\lambda\varrho d^2, \quad \varrho\bar{u}d/\mu] \tag{7}$$

and it becomes easier to perform experiments in which the effect of each of the independent groups is separately assessed, because the group, $(\varepsilon\mu/\lambda\varrho d^2)$, is a constant for a particular liquid in a particular pipe.

An experimental investigation of this relation is now described.

3. EXPERIMENTAL METHOD

The apparatus used in these experiments consisted of a reservoir from which the liquid was allowed to flow through a capillary tube before discharging into an insulated receiver. The reservoir, capillary tube, and receiver were all of stainless steel. The head of liquid was controlled by rotating the reservoir and capillary tube about an axis through the lower end of the tube (Fig. 1).

The reservoir and capillary tube were electrically earthed and the current flowing into the receiver was measured by allowing it to discharge to earth through a very high resistance and measuring the potential across the resistance with a Trub: Tauber electrostatic voltmeter (range, 0–150 V). Resistances in the range 10^9–10^{13} Ω were used to enable the measurements to cover a range of streaming current from 10^{-7} A to 10^{-12} A.

The flow rate was calibrated against the head of liquid by weighing the liquid discharged in a known time. The coefficient of skin friction, determined from the energy loss in flowing through the tube, is compared in Fig. 2, with the theoretical value for laminar flow and with the well established experimental Blasius relation for low Reynolds number turbulent flow in smooth pipes. The latter is

$$C_f = AR_e^{-0.25} \tag{8}$$

where A has the value 0.3164.

The agreement is seen to be satisfactory.

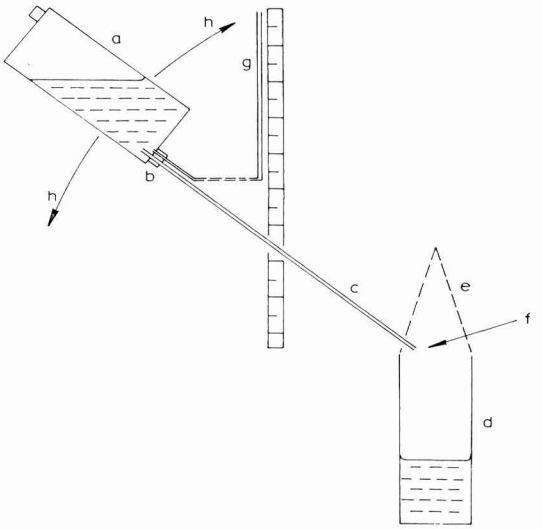

Fig. 1. General arrangement of the apparatus. Liquid flow charging apparatus: (a), reservoir; (b), polythene plug; (c), stainless-steel tube; (d), receiver; (e), P.T.F.E. suspension; (f), axis of rotation through end of tube; (g), manometer; (h), direction of rotation.

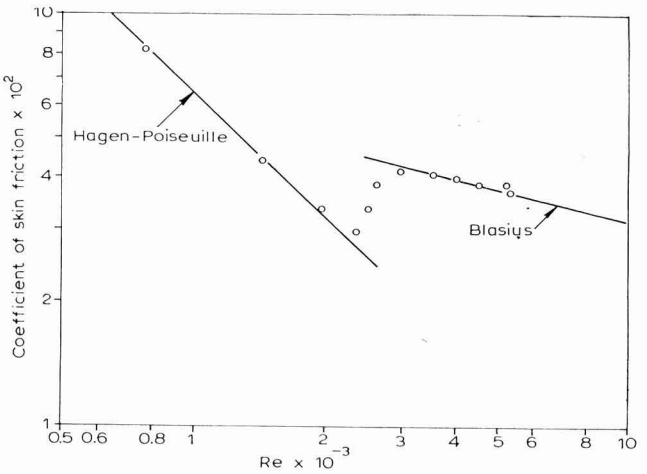

Fig. 2. Measured skin friction coefficient.

The surface roughness of the tubes was measured by a Talley-Surf apparatus. The roughness was of two groups corresponding to the respective manufacturers. Typical records are shown in Fig. 3.

Tubes of Group 1 were the smoothest having a roughness of about $\pm 0.6 \times 10^{-6}$ m superimposed upon a surface waviness of $\pm 4 \cdot 10^{-6}$ m with a wavelength of $5 \cdot 10^{-3}$ m. Tubes of Group 2 were the roughest and they had a roughness of about $\pm 15 \cdot 10^{-6}$ m. All these figures are approximate guides as can be seen in Fig. 3.

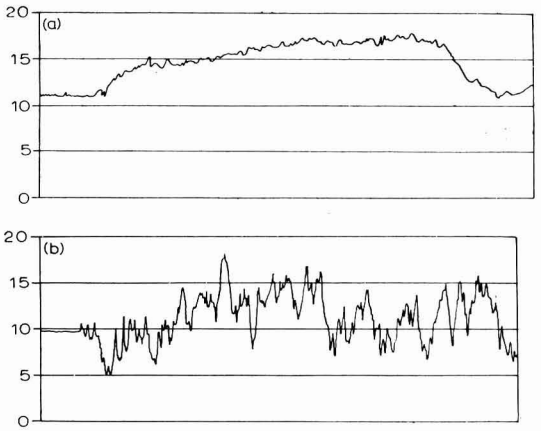

Fig. 3. Surface roughness of the tubes of: (a), group 1: vertical magnification, 2000, 1 div. $\equiv$ 1.25×10^{-6} m; horizontal magnification, 20, 1 div. $\equiv 2.5 \times 10^{-4}$ m; (b), group 2: vertical magnification, 1000, 1 div. $\equiv 2.5 \times 10^{-6}$ m; horizontal magnification, 20, 1 div. $\equiv 2.5 \times 10^{-4}$ m.

Liquids of high electrical insulation were chosen for the experiments. Samples of kerosene and a kerosene–benzene mixture were mainly used, a few measurements being made with carbon tetrachloride. The conductivities of the samples were in the range 10^{-12}–10^{-10} mho m^{-1}.

The experiments were carried out at a temperature of $20° \pm 0.5°$ in a temperature-controlled room. The air supply to the room was filtered to avoid dust settling on the apparatus and changing the insulation.

4. THE EFFECT OF THE REYNOLDS NUMBER

Results of an experiment on a particular liquid in one pipe of Group 1 are shown in Fig. 4. The points joined by the solid line are plots of the non-dimensional current group of eqn. (7) without the entry length correction incorporated, so that eqn. (4) was used in the form

$$i_s = i_\infty [1 - e^{-J}]$$

On writing the current group as,

$$I_\infty \equiv i_\infty^2 / \lambda d^3 \varrho \bar{u}^3$$

the values of I_∞ are seen to increase markedly by an order of 10^2 through the transition range from laminar to turbulent flow. Comparison with Fig. 2 shows that

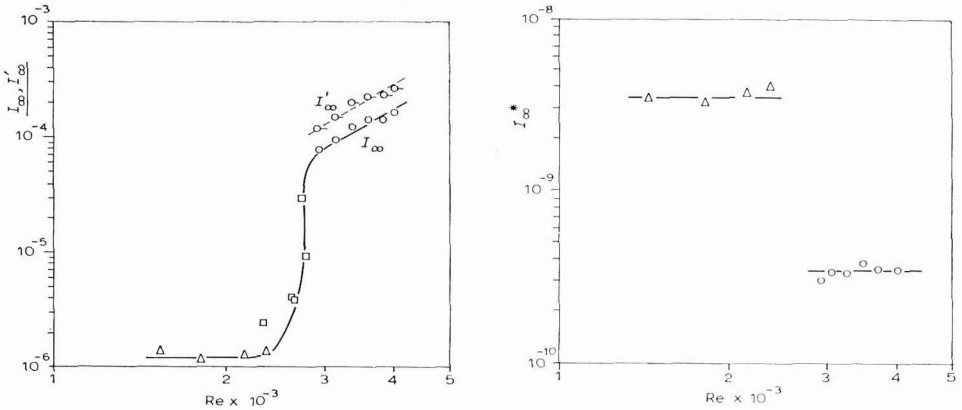

Fig. 4. Non-dimensional streaming current as a function of Reynolds number. (△), laminar flow I_∞; (□), transitional flow I_∞; (○), turbulent flow I_∞; (○-), turbulent flow I_∞'.

Fig. 5. Non-dimensional streaming current based upon the wall velocity gradient. (△), laminar flow; (○), turbulent flow.

although this increase in streaming current is associated with the similar increase of skin friction, the latter increase is of much smaller degree.

The entry correction length previously determined for turbulent flow had the value

$$L_0/d = 54.4$$

Assuming that this value applies to the flow described by Fig. 4, then values of the non-dimensional current group, embodying this correction to i_∞ and denoted by I_∞', are shown as the flagged points in Fig. 4. The correction is seen in this case to be of the order of 75%.

The entry length correction is not expected to have the same value, or even the same form for laminar flow, and so the results for this flow regime are uncorrected here.

The values for the transition regime shown in Fig. 4 are mean values of electrical measurements which fluctuated greatly in accord with the well known flow fluctuations in this regime.

In view of the similarity between the functional relationship between I_∞ and R_e, and that between the coefficient of skin friction and R_e, it is suggested that the velocity gradient at the pipe wall, du/dy, may be a more significant parameter than the pipe mean velocity, $\bar{u}$. The non-dimensional current group is thus written,

$$I_\infty^* \equiv i_\infty^2/\lambda d^6 \varrho (du/dy)^3 \tag{9}$$

The results shown in Fig. 4 have been recalculated on this basis and are shown plotted in Fig. 5. The change through the transition region is now reduced from an order of 10^2 to a reversed order of 10. Thus, although the rise in the velocity gradient through the transition range explains the rise in the streaming current, it does so only partially. However, it is interesting that separately in both flow regimes, I_∞^* has a constant value. This point is referred to again later.

5. THE EFFECT OF THE ε-GROUP

Values of I_∞' for turbulent flow, as a function of R_e, were determined for a range of values of the group $(\varepsilon\mu)/(\varrho\lambda d^2)$ in a series of pipes of Group 1 and with a series of liquids. Values are shown plotted in Fig. 6.

All results show a uniform rise in I_∞' with the Reynolds number. Clear of the transition regions, all the results fit reasonably the straight lines shown, all of which have a slope of 2.50.

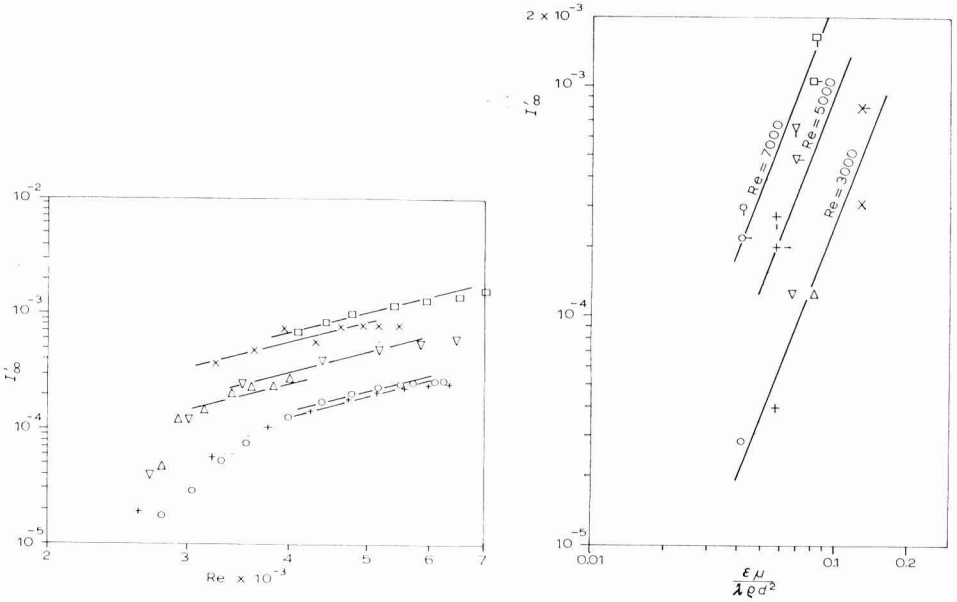

Fig. 6. Non-dimensional streaming current as a function of Reynolds number, Group 1 tubes. $\varepsilon\mu/\lambda\varrho d^2$: (○), 0.042; (+), 0.058; (▽), 0.068; (△), 0.081; (□), 0.082; (×), 0.13.

Fig. 7. Non-dimensional streaming current as a function of the conductivity group, Group 1 tubes.

The family of curves indicate a general increase in I_∞' with increase in the group $(\varepsilon\mu/\varrho\lambda d^2)$.

Values, cross-plotted from the results of Fig. 6, are shown in Fig. 7 as plots of I_∞' *vs.* $(\varepsilon\mu/\varrho\lambda d^2)$for three values of the Reynolds number. The three straight lines that are drawn to fit the points all have a slope of 2.75.

Thus, these experiments suggest the relation,

$$I_\infty'/[\varepsilon\mu/\varrho\lambda d^2]^{2.75} = f(R_e)$$

Corresponding values are shown plotted in Fig. 8. Correlation is only partly successful and this corresponds to the scatter seen in Fig. 7. Again, as in Fig. 6, a mean curve is drawn having a slope of 2.50, so that

$$I_\infty' \propto (\varepsilon\mu/\lambda\varrho d^2)^{2.75} R_e^{2.50} \qquad (10)$$

It is possible that the two lowest sets of results are associated with a smaller tube

diameter than that used for the others. This could be connected with the fact that the entry length correction, L_0/d was determined using a tube of Group 2 and could have a different value for the smoother tubes of Group 1. Another possibility, that the surface roughness may be significant, is discussed later.

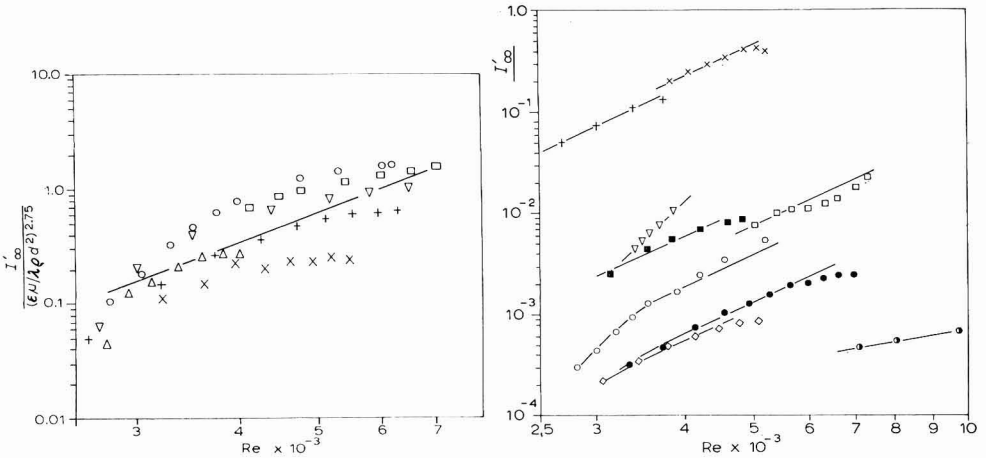

Fig. 8. Correlation for tubes of Group 1. Set: (○), 8; (□), 9; (△), 10; (×), 11; (+), 14; (▽), 15.

Fig. 9. Non-dimensional streaming current as a function of Reynolds number, Group 2 tubes. $\varepsilon\mu/\lambda\varrho d^2$: (◑), 0.039; (○), 0.064; (△), 0.075; (◇), 0.083; (●), 0.087; (□), 0.14; (■), 0.15; (▽), 0.32; (×), 0.39; (+), 0.51.

6. THE EFFECT OF TUBE SURFACE ROUGHNESS

The tubes of Group 2 had a higher degree of surface roughness than those of Group 1. Results for the turbulent flow in the tubes of Group 2 are shown plotted in Fig. 9 (I_∞' as a function of R_e). Values are cross-plotted in Fig. 10 as I_∞' *vs.* $(\varepsilon\mu/\lambda\varrho d^2)$ for three values of the Reynolds number. The three straight lines fitted to the experimental points are all drawn with a slope of 3.50. This then implies that

$$I_\infty'/[\varepsilon\mu/\lambda\varrho d^2]^{3.5} = f(R_e) \tag{11}$$

A comparison of Figs. 7 and 10 shows that the value of I_∞' for the rougher tubes of Group 2 is about twice that for the smoother ones of Group 1. In contrast, the results shown in Fig. 2 indicate that the roughness of the tubes of Group 2 was such that they can be regarded as smooth for the fluid motion whereas they are seen to be rough for the electrical phenomena.

As the roughness shape was not controlled and as, basically, only two roughness heights were used in the experiments, a correlation for the roughness effect cannot be determined.

The form of the functional relationship of eqn. (11) for the tubes of Group 2 is shown in Fig. 11 where a straight line is fitted to the results. The slope of this line is 3.25.

Two sets of the results plotted in Fig. 11 do not correlate satisfactorily.

There seems to be no explanation for the discrepancy in the upper set. The lower set was obtained for the flow of carbon tetrachloride, and the conductivity of this liquid varied so much with time that it was difficult to get the conductivity values to agree before and after a run. Excluding these two sets, the others are seen to lie within a band width somewhat smaller than that shown in Fig. 8 for the tubes of Group 1.

Thus the mean line of Fig. 11 represents

$$I_\infty' \propto (\varepsilon\mu/\lambda\varrho d^2)^{3.5} Re^{3.25} \tag{12}$$

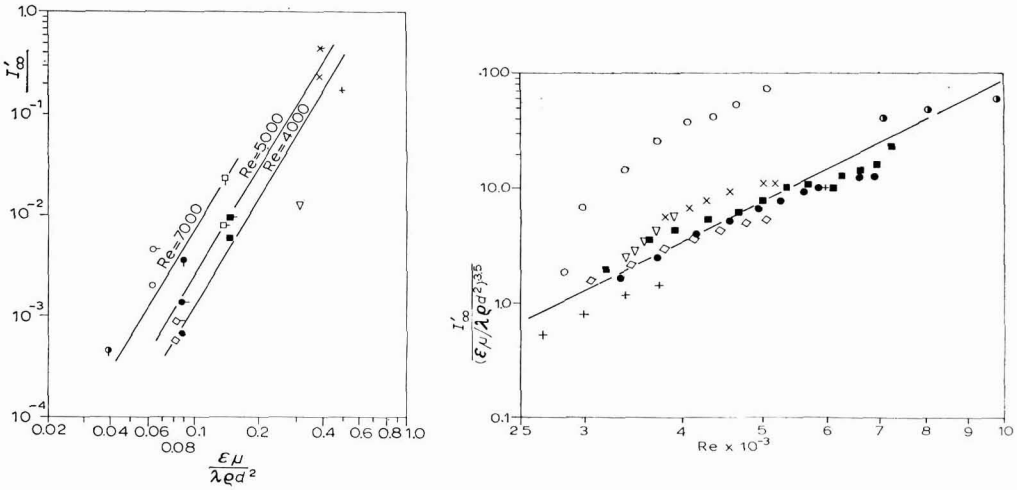

Fig. 10. Non-dimensional streaming current as a function of the conductivity group, Group 2 tubes.

Fig. 11. Correlation for tubes of Group 2. Set: (○), 1; (×), 4; (+), 4; (▽), 7; (◇), 12; (□), 13; (□), 2; (◑), 3.

7. EFFECT OF THE INDEPENDENT VARIABLES UPON THE STREAMING CURRENT

The experimental results represented by eqns. (10) and (12) for the tubes of Groups 1 and 2, respectively, can be written in the form,

$$I_\infty' \propto (\varepsilon\mu/\lambda\varrho d^2)^{m_1} Re^{m_2} \tag{13}$$

Converting this from the form of eqn. (7) to that of eqn. (6) by cross-multiplying, results in

$$i_\infty'^2/\varrho\bar{u}^4\varepsilon d^2 \propto (\varepsilon\bar{u}/\lambda d)^{-n_1} Re^{n_2} \tag{14}$$

Using the notation of eqn. (5) and writing,

$$J_d \equiv \lambda d/\varepsilon\bar{u}$$

then,

$$i_\infty'^2/\varrho\bar{u}^4\varepsilon d^2 \propto J_d^{n_1} Re^{n_2} \tag{15}$$

where now

$$n_1 = 1 - m_1$$

$$n_2 = m_2 - m_1$$

For tubes of Group 1,

$$n_1 = -1.75$$

$$n_2 = -0.25$$

and for tubes of Group 2,

$$n_1 = -2.5$$

$$n_2 = -0.25$$

Although there is appreciable scatter of the present experimental results after the application of the correlations, it is significant that the streaming current group is dependent upon the same power of the Reynolds number as is the friction coefficient as given by eqn. (8)*.

Equations (13) and (15) can be expanded into the form,

$$i_\infty' \propto \mu^{o_1} \cdot \bar{u}^{o_2} \cdot \lambda^{o_3} \cdot d^{o_4} \cdot \varepsilon^{o_5} \cdot \varrho^{o_6}$$

so that,

$$o_1 = -\tfrac{1}{2} n_2$$

$$o_2 = \tfrac{1}{2}(4 - n_1 + n_2)$$

$$o_3 = +\tfrac{1}{2} n_1$$

$$o_4 = \tfrac{1}{2}(2 + n_1 + n_2)$$

$$o_5 = \tfrac{1}{2}(1 - n_1)$$

$$o_6 = \tfrac{1}{2}(n_2 + 1)$$

The values of all the indices are given in Table 1. In the first two columns are the results for tubes of Group 1 (the smoother tubes), and for the rougher ones of

TABLE 1

Parameter	*Index*	*Index value*				
		Present results			*Gavis & Koszman*	*Gavis & Koszman derived*
		Group 1	*Group 2*	*Group 1* $L_0 = o$		
$\varepsilon\mu/\lambda\varrho d^2$	m_1	2.75	3.5	2.5		
R_e	m_2	2.5	3.25	2.25		
Ja	n_1	−1.75	−2.5	−1.5		0.0
R_e	n_2	−0.25	−0.25	−0.25		−0.25
μ	o_1	0.125	0.125	0.125	−0.625	0.125
$\bar{u}$	o_2	2.75	3.125	2.625	1.875	1.875
λ	o_3	−0.875	−1.25	−0.75	0.0	0.0
d	o_4	0.0	−0.325	0.125	0.875	0.875
ε	o_5	1.375	1.75	1.25	1.00	0.5
ϱ	o_6	0.375	0.375	0.375	0.625	0.375
R_e	p_2			0.0		

* Recent experiments in the laminar flow regime (to be the subject of another paper) have given the same result.

Group 2. As already mentioned, despite the different values of m_1 and m_2 for the smoother and rougher tubes, the value of n_2 for both is the same as the corresponding index for the skin friction coefficient.

The effect of the increase of surface roughness from the tubes of Group 1 to those of Group 2 is seen to change the correlation so that n_1 becomes more negative. Obviously, the present correlation is inadequate to provide a measure of the roughness effects, because if the roughnesses were of one shape, then these effects should be represented by a further non-dimensional group such as either h/d or $J_h \equiv (\lambda h/\varepsilon \bar{u})$, where h is a measure of the roughness height. Such a group cannot be added to the right-hand side of eqn. (12) as a simple multiplier, because this would make $i_\infty = 0$ when $h = 0$. A more extended range of experiments is required to determine the effects of roughness.

The results in Table 1 also show that the index for the diameter, d, *i.e.*, o_4, is zero for the smoother tubes. This raises the possibility that the phenomena is strongly controlled by what happens in a region very close to the wall so that the thickness of this region is very small compared to d and the behaviour is the same as would occur along a plane wall. This suggestion is consistent with the very small thicknesses of electrical boundary layers, as represented by double-layer thicknesses that occur in stationary liquids*. For the rougher tubes, o_4 is no longer zero and this is consistent with an effect due to the group, h/d. This suggests that the tubes of Group 1 might be behaving as smooth tubes.

A correlation was also obtained for the tubes of Group 1 by neglecting the pipe entry effect; *i.e.*, values of I_∞ were correlated in the form of eqn. (13). The results for the various indices are given in the third column of Table 1. The values of m_1 and m_2 are seen to differ from those in the first column resulting in a difference in n_1, but the value of n_2 remains at the skin friction index of -0.25.

KOSZMAN AND GAVIS have also given results for the turbulent flow in tubes[7]. These were for values of i_∞, *i.e.*, with L_0 taken as zero, and the flow conditions were different from the present experiments as indicated by a comparison of their measured frictional coefficients with the present ones. The indices for their results are given in the fourth column of Table 1. Again, as with columns 2 and 3, there are divergences from column 1 due probably to the differences just mentioned. The indices given do not all fit into a correlation of the form of eqn. (13). However, their main experimental support was for the values of o_2, o_4 and o_3 giving the variations with $\bar{u}$, d and λ. If the first two of these values and the relation of eqn. (13) are accepted, then the other indices follow and are given in column 5 of Table 1. Two points of interest emerge. First, the value of o_3 as determined experimentally by KOSZMAN AND GAVIS is confirmed. Second, the value of n_2 is again the skin friction index of -0.25.

The wall velocity gradient is given by,

$$\frac{du}{dy} = \frac{C_f \varrho \bar{u}^2}{8\mu}$$

Then for turbulent flow, substitution of eqn. (8) gives,

$$\frac{du}{dy} = \frac{A \varrho \bar{u}^2}{8\mu R_e^{0.25}}$$

* This is supported by the recent laminar flow experiments already mentioned.

The non-dimensional group of eqn. (9) becomes

$$I_\infty^* = I_\infty \bar{u}^3/d^3(\mathrm{d}u/\mathrm{d}y)^3$$
$$= I_\infty (8/A)^3(1/R_e^{2.25})$$

Writing

$$I_\infty^* \propto (\varepsilon\mu/\lambda\varrho d^2)^{p_1} R_e^{p_2}$$

a comparison with eqn. (13) gives,

$$p_1 = m_1$$

and

$$p_2 = m_2 - 2.25$$

From the results in the third column of Table 1, $p_2 = 0.0$; the corresponding horizontal line is drawn in Fig. 5.

8. CONCLUSIONS

A modestly satisfactory correlation of the streaming current measurements was obtained in the form,

$$I_\infty' \propto (\varepsilon\mu/\lambda\varrho d^2)^{m_1} R_e^{m_2}$$

The non-dimensional group, $i_\infty'^2/(\varrho\bar{u}^4\varepsilon d^2)$, was then proportional to the same power of the Reynolds number as is the skin friction coefficient. This same index was obtained for tubes of increased roughness and for results computed taking no account of the entry length correction.

The velocity gradient at the wall, $\mathrm{d}u/\mathrm{d}y$, is significant in an explanation of the large increase in streaming current through the transition region. The streaming current in the smoothest tubes was independent of tube diameter suggesting that the charging phenomena was closely linked with the flow region very close to the wall and that these tubes were behaving as smooth tubes.

SUMMARY

The results of measurement of electrostatic streaming currents in turbulent flow through round pipes have been correlated in terms of non-dimensional groups. A non-dimensional current group is found to vary with the same power of the Reynolds number as does the skin friction coefficient. A surface roughness that is too small to affect the skin friction coefficient is found to affect markedly the streaming current.

REFERENCES

1 E. T. HIGNETT, *Aero. Res. Conn. Current Papers*, 631, 1963.
2 A. KLINKENBERG AND J. L. VAN DER MINNE, *Electrostatics in the Petroleum Industry*, Elsevier, Amsterdam, 1958.
3 J. GAVIS AND I. KOSZMAN, *J. Colloid. Sci.*, 16 (1961) 375.
4 J. C. GIBBINGS AND E. T. HIGNETT, *Electrochim. Acta*, 11 (1966) 815.
5 J. C. GIBBINGS, *Electrochim. Acta*, 12 (1967) 106.
6 E. T. HIGNETT AND J. C. GIBBINGS, *J. Electroanal. Chem.*, 9 (1965) 260.
7 I. KOSZMAN AND J. GAVIS, *Chem. Eng. Sci.*, 17 (1962) 1023.

ELECTROANALYTICAL CHEMISTRY AND INTERFACIAL ELECTROCHEMISTRY
Elsevier Sequoia S.A., Lausanne – Printed in The Netherlands

PHOTOCHEMIE ANOMALER NUCLEINSÄUREBAUSTEINE. II. ELEKTRONENAKZEPTOR-EIGENSCHAFTEN VON AZAANALOGEN DER PYRIMIDIN- UND PURINREIHE AUS POLAROGRAPHISCHEN MESSUNGEN*

L. KITTLER UND H. BERG

Deutsche Akademie der Wissenschaften zu Berlin, Institut für Mikrobiologie und experimentelle Therapie, Abteilung Biophysikochemie, Jena (DDR).

(Eingegangen am 3. April 1967)

EINLEITUNG

Seit Ende der fünfziger Jahre hat die polarographische Methode in der Nucleinsäureforschung in drei Richtungen Bedeutung erlangt:

1) Nachweis von Konformationsänderungen[1]

2) Ermittlung von Adduktgleichgewichten[2]

3) Bestimmung der Elektronenakzeptor–Donator-Stärke[3] der Basen-Bausteine.

Letztere erfolgt an der reaktivsten Stelle im Molekül, und die bisherigen Halbstufenpotential-Ergebnisse haben quantenchemische Vorausberechnungen der Elektronendichten überraschend gut bestätigen können. Während die natürlichen Basen auf diese Weise schon ausreichend charakterisiert worden sind, fehlen entsprechende Daten bei den anomalen, inkorporierbaren Derivaten, insbesondere der Azaanalogen. Um deren Eigenschaften vergleichen zu können, müssen zunächst die polarographischen Ergebnisse der natürlichen Basen vorangestellt werden.

1952 fanden CAVALIERI UND LOWY[4], dass im sauren pH-Bereich von 25 untersuchten Pyrimidinen nur 9 Depolarisatoreigenschaften haben. Für die polarographische Reduktion ist die $-\overset{3}{N}=\overset{4}{C}-\overset{5}{C}=\overset{6}{C}-$Anordnung unbedingt erforderlich. Wird darin die $-\overset{3}{N}=\overset{4}{C}-$Doppelbindung durch Tautomerie oder Substitution verändert, so wird die Elektronenaufnahme in den meisten Fällen erschwert oder verhindert. ELVING UND SMITH[5–7] stellten 1962 Reduktionsmechanismen auf. Danach spalten die protonierten Pyrimidine Ammoniak ab, sofern sie in C_4-Position eine Aminogruppe tragen. Uracil und Thymin verursachen nur Oxydationsstufen nach Salzbildung an der Quecksilberelektrodenoberfläche[8,9]. Beim Cytosin kann sowohl eine Oxydationsstufe als auch eine Reduktionsstufe ausgebildet werden. Letztere liegt sehr nahe am Leitsalzanstieg, so dass ihre Höhe schwer zu bestimmen ist. Nach JANIK UND PALEČEK[10] sollen dabei 4 Elektronen verbraucht werden.

Auffallend ist, dass nur in saurem Medium Reduktionsstufen mit Diffusionscharakter ausgebildet werden, während zum neutralen pH-Bereich eine kinetische Begrenzung registriert wird und nach höheren pH-Werten die Stufe auf Null absinkt. Dieses Verhalten begründet die Annahme, dass protonierte Formen die Voraussetzung für den Reduktionsprozess bilden.

* I. Mitteilung: *Photochem. Photobiol.*, 6 (1967) 199.

In jüngster Vergangenheit häufen sich die Mitteilungen, wonach die basischen Grundbausteine der Nucleinsäuren durch entsprechende Azaanaloge in der DNS und RNS ersetzt werden[11,12].

Diese Inkorporation verändert die Stabilität der Doppelhelix und ermöglicht die Lenkung metabolischer[13] und cancerostatischer[14] Eigenschaften. Die Ursache für diese bedeutsamen Wirkungen der Azaverbindungen liegt in ihrer elektronischen Struktur, zu deren Aufklärung die Polarographie einen Beitrag zu leisten vermag. Weiterhin konnte mit dieser Methode die Photostabilität gemessen werden.

Aus diesen Gründen soll aus vorliegender Mitteilung ein möglichst geschlossenes Bild des polarographischen Verhaltens der Azapyrimidine und Azapurine gegeben werden, woraus die wichtigsten Aspekte für ihre Anwendung in der Molekularbiologie deutlich werden.

Allgemein ist gegenüber den natürlichen Nucleinsäurepyrimidinen in der Azapyrimidinreihe eine Positivierung der Halbstufenpotentiale zu beobachten, was die elektrochemische Analyse bedeutend erleichtert[15]. Im Gegensatz dazu ändern sich die Reduktionspotentiale in der Purinreihe im Vergleich zu den entsprechenden 8-Azaderivaten geringfügig. Es werden nur solche Verbindungen reduziert, die in C_6-Stellung nicht substituiert sind oder eine Aminogruppe bzw. NHR oder NR_1R_2 tragen. Befindet sich an dieser Stelle eine Ketogruppierung, so ist eine elektrochemische Reduktion bis -2.0 V nicht möglich.

EXPERIMENTELLES

Für die Registrierung der polarographischen Strom–Spannungs-Kurven diente ein ungarischer Tintenschreiber-Polarograph vom Typ OH-102. Die Halbstufenpotentiale beziehen sich auf die 1*N*-Kalomelelektrode. Die Konzentration der untersuchten Substanzen betrug $5 \cdot 10^{-4}$ *M*. Ausser bei pH-Abhängigkeiten (Britton–Robinson-Puffer 0.1 *M*) wurde Phosphat-Puffer pH 7 (0.1 *M*) verwendet. Alle Messungen wurden bei 25° durchgeführt.

ERGEBNISSE UND DISKUSSION

Wie Tabelle 1 zeigt, werden die Azapyrimidine in einem für polarographische Untersuchungen sehr günstigem Bereich reduziert, so dass die molekularbiologisch wichtigsten Substanzen einer eingehenden polarographischen Analyse unterzogen werden konnten.

Lediglich für das 6-Azauracil (6-AU) lagen schon Messungen von KRUPIČKA UND GUT vor[16]. Abb. 1 zeigt die pH-Abhängigkeit des 6-AU in Britton–Robinson-Puffer. Auffällig ist die Verminderung der Kurvensteilheit zwischen pH 3 und 6, was diese Autoren auf das Vorhandensein verschieden protonierter Formen zurückführten. Ausserdem kann die Komplexbildungstendenz der Borsäure des Puffers Komplikationen hervorrufen. Durch vollständige N-Methylierung des 6-AU wurde die Diketoform mit der C=N-Doppelbindung als Elektronenakzeptor-Gruppe im Molekül angegeben. Als Reduktionsprodukt wurde das entsprechende 5,6-Dihydro-6-AU vermutet.

Dieses Problem wurde von uns auf anderem Wege geklärt, in dem die Photohydratation studiert wurde[17]. Die UV-Bestrahlung führte zu den 5-Hydroxy-6-Hydro-

TABELLE 1

HALBSTUFENPOTENTIALE ($\pi_{\frac{1}{2}}$) UND ELEKTRONENAUFNAHME (v) VON AZAANALOGEN DER PYRIMIDIN UND PURINREIHE

(Phosphatpuffer pH 7, 0.1 *M*, gegen 1 *N* KCl-Elektrode, 25°)

	Substanz	$\pi_{\frac{1}{2}}$(*V*)	v
1	6-Azauracil	−1.30	2
2	6-Azauridin	−1.36	2
3	5-Azauracil	−1.52	2
4	1,3-Dimethyl-6-Azauracil	−1.35	2
5	5-Chlor-6-Azauracil	−1.34	4
6	5-Brom-6-Azauracil	−1.28	4
7	5-Jod-6-Azauracil	−0.84, −1.30	4*
8	5,6-Dihydro-6-Azauracil	—	—
9	5-Amino-6-Azauracil	−1.55	4
10	5-Amyl-6-Azauracil	−1.39	2
11	5-Azaorotsäure	−1.30	2
12	2-Thio-6-Azauracil	−1.09, −1.30	2
13	6-Azacytosin	−1.17, −1.40	4*
14	5-Azacytosin	−1.40, −1.80	4*
15	5-Azacytidin	−1.35, −1.68	4*
16	2-Amino-4-Methylamino--5-carboxy-6-Azapyrimidin	−1.02, −1.55	4*
17	8-Azaadenin	−1.40	4
18	8-Azaguanin	—	—
19	8-Azaxanthin	—	—
20	8-Azahypoxanthin	—	—

* Doppelstufe bestehend aus 2 zweielektronigen Reduktionsstufen.

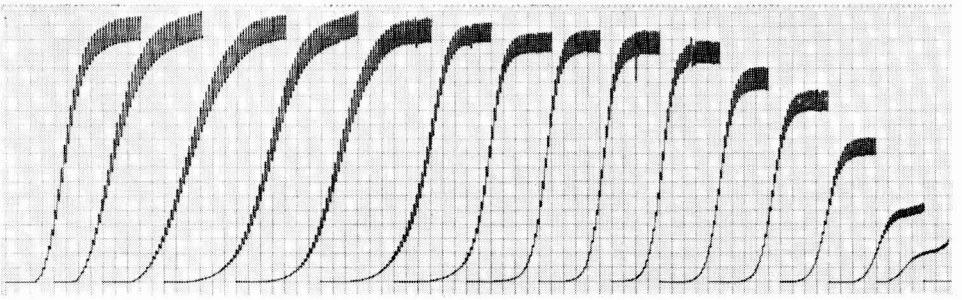

Abb. 1. 6-Azauracil: pH-Abhängigkeit. $c = 5 \cdot 10^{-4}$ *M* in Britton–Robinson-Puffer (0.1 *M*); $s = 6 \cdot 10^{-8}$ A D^{-1}, 50 mV/Abszisse, Kapazitätsstromkompensation 0.4 μA V^{-1}, $t = 25°$, gegen 1 *N* KCl-Elektrode Potentialbeginne: pH 1.0 (0.1 *N* H_2SO_4), −0.4 V; pH 2.2 und 3.0, −0.5 V; pH 4.1, −0.6 V; pH 5.3, −0.7 V; pH 6.3, −0.8 V; pH 7.0, −0.9 V; pH 7.7, −1.0 V; pH 8.3, −1.1 V; pH 9.0, 9.8 und 10.3, −1.2 V; pH 10.6 und 10.8, −1.3 V; pH 11.2, −1.4 V; pH 12.0, −1.5 V.

6-AU. Dieser Reaktionsverlauf kann spektrophotometrisch aus der Abnahme der Absorptionsbande bei 260 nm und polarographisch aus dem Abfall der Reduktionsstufenhöhe verfolgt werden (Abb. 2). Diese Reaktion ist in stark saurem pH-Bereich (~pH 1.5) und bei erhöhter Temperatur (~100°) teilweise reversibel (~40%). Das bedeutet eine Rückbildung der 5:6-Doppelbindung, wodurch die Absorption bei 260 nm wieder auftritt. Daraus kann mit Sicherheit geschlossen werden, dass für die polarographische Elektronenaufnahme die 5:6-C=N-Doppelbindung verantwortlich ist, was ebenfalls für das 6-Azathymin (6-AT) zutrifft (Abb. 3).

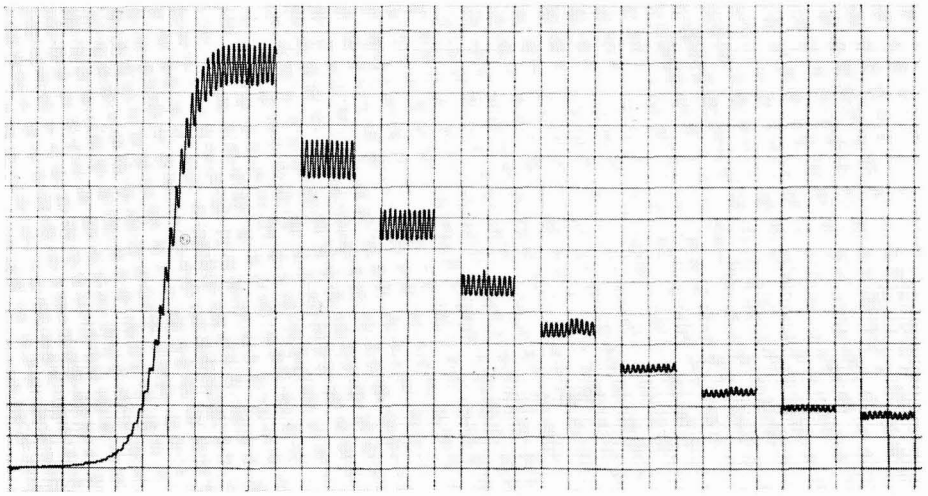

Abb. 2. 6-Azauracil: Photoreaktion. $c = 2 \cdot 10^{-4}$ *M* in Phosphatpuffer pH 7 (0.1 *M*), ab −1.0 V, 50 mV/Absz., Kapazitätsstromkompensation 0.3 μA V^{-1}, t = 25°, Potential auf −1.45 V festgestellt. hν: 0′, 5′, 10′, 15′, 20′, 25′, 30′, 35′, 40′. Lichtintensität in der Bestrahlungszelle $6.7 \cdot 10^{-6}$ Einstein cm^{-2} min^{-1}.

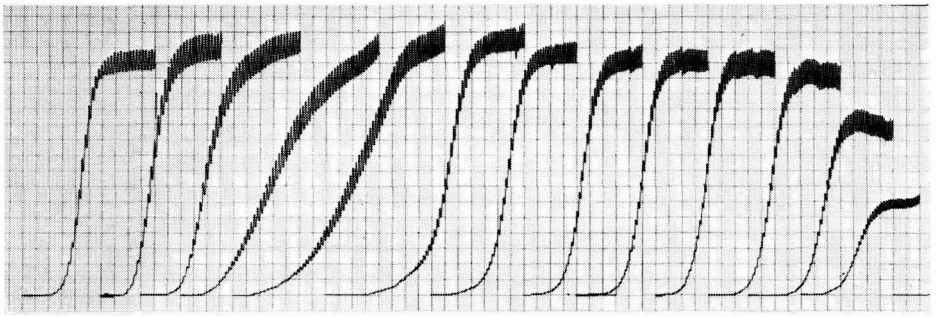

Abb. 3. 6-Azathymin: pH-Abhängigkeit. $c = 5 \cdot 10^{-4}$ *M* in Britton–Robinson-Puffer (0.1 *M*); $s = 6 \cdot 10^{-8} A D^{-1}$, 50 mV/Abszisse, Kapazitätsstromkompensation 0.4 μA V^{-1}, $t = 25°$, gegen 1 *N* KCl-Elektrode. Potentialbeginne: pH 1.0 (0.1 *N* H_2SO_4), −0.5 V; pH 2.2 und 3.0, −0.6 V; pH 4.1, −0.7 V; pH 5.3, −0.8 V; pH 6.3, −0.9 V; pH 7.0, −1.1 V; pH 7.7 und 8.3, −1.2 V; pH 9.0, 9.8 und 10.6, −1.3 V; pH 11.2, −1.4 V; pH 12.0, −1.5 V.

Weitere Aufschlüsse über den Elektronenakzeptor (EA)-Prozess vermitteln die Abbildungen 4 und 5 mit den Abhängigkeiten des Halbstufenpotentials ($\pi_{\frac{1}{2}}$) vom pH-Wert. Bei pH-Werten >6 beträgt der Anstieg dieser Kurven 60 mV/pH. Diesem entspricht bei Zweielektronenmechanismus die Addition von zwei Protonen. Der Elektrodenprozess verläuft unter diesen Bedingungen nach folgendem Schema:

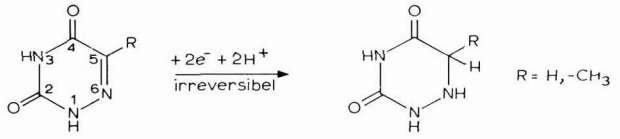

Die grössere Steilheit der $\Delta\pi_{\frac{1}{2}}/\Delta$pH-Kurven für pH-Werte <6 lässt auf eine stärkere Protonierung des Gesamtmoleküls schliessen.

Im stärker alkalischen Bereich (pH 9) gehen die Diffusionsgrenzströme in kinetisch begrenzte über, was auch aus der Abnahme ihrer Höhe sichtbar wird. In diesem Bereich liegen die Gleichgewichte der konjugierten Basen mit Protonen. (Die pK-Werte für 6-AU betragen 7.0 bzw. 12.9)[18].

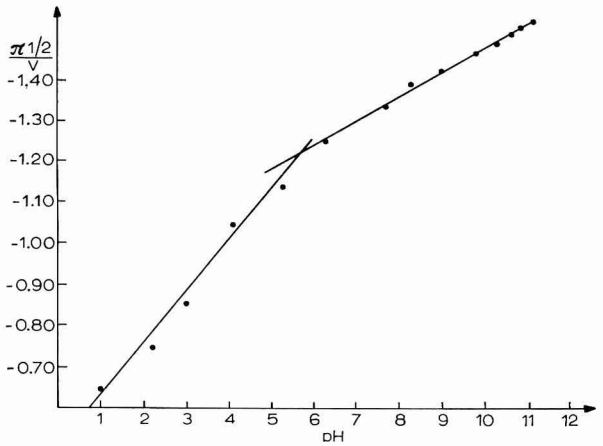

Abb. 4. Abhängigkeit des Halbstufenpotentials ($\pi_{\frac{1}{2}}$) vom pH-Wert für 6-Azauracil.

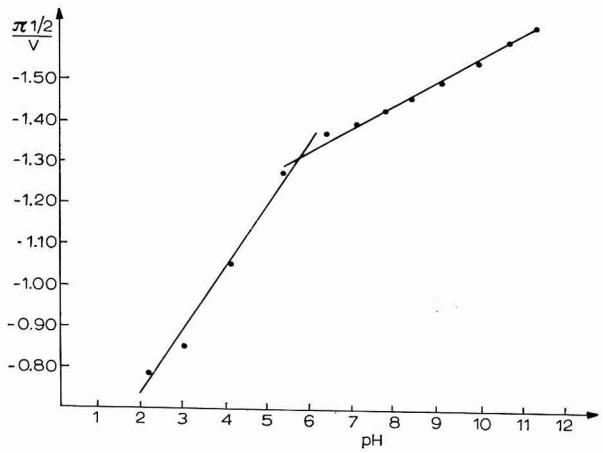

Abb. 5. Abhängigkeit des Halbstufenpotentials ($\pi_{\frac{1}{2}}$) vom pH-Wert für 6-Azathymin.

Allgemein gilt, dass die symmetrischen Triazine im Vergleich zu den asymmetrischen Triazinen trotz eines analogen Mechanismus schwerer reduziert werden (s.Tabelle 1). Diese Eigenschaft lässt sich damit begründen, dass die symmetrischen Verbindungen eine geringere Polarität besitzen. Dieser Effekt spiegelt sich auch im photochemischen Verhalten wieder, wonach diese Verbindungen sehr stabil gegen UV-Strahlung sind[19].

6-Azacytosin (6-AC) wird in einem vierelektronigen Reduktionsprozess irreversibel reduziert, wobei eine Doppelstufe registriert wird (Abb. 6). Im sauren pH-Bereich bildet sich auf der 2. Reduktionsstufe eine katalytische Wasserstoffwelle aus. Dieses Phänomen ist für Stickstoffheterocyclen zu erwarten, sofern am N-Atom noch ein freies Elektronenpaar vorhanden ist[20], wodurch die Reduktion des gebundenen Wasserstoffions erleichtert wird.

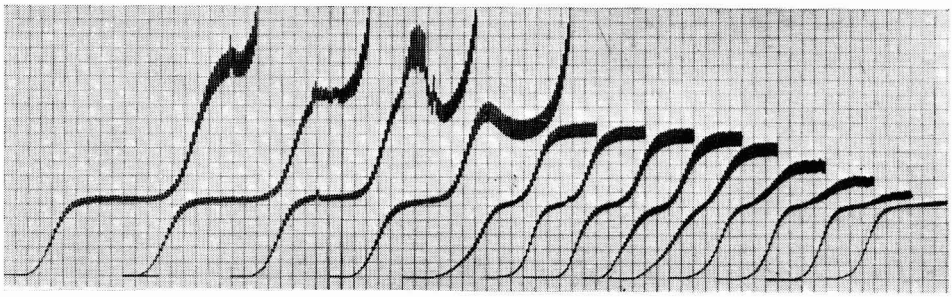

Abb. 6. 6-Azacytosin: pH-Abhängigkeit. $c = 5 \cdot 10^{-4}$ M in Britton–Robinson-Puffer (0.1 M); $s = 2 \cdot 10^{-7} A D^{-1}$, 50 mV/Abszisse; Kapazitätsstromkompensation 0.4 μA V^{-1}, $t = 25°$; gegen 1N KCl-Elektrode. Potentialbeginne: pH 2.2, −0.4 V; pH 3.0, −0.5 V; pH 4.1, −0.6 V; pH 5.3, −0.7 V; pH 6.3, −0.8 V; pH 7.0 und 7.7, −1.0 V; pH 8.3 und 9.0, −1.1 V; pH 9.8, 10.3 und 10.8, −1.2 V; pH 11.2, −1.3 V.

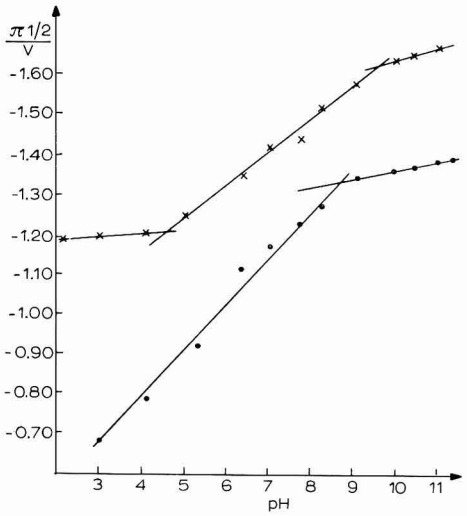

Abb. 7. Abhängigkeit des Halbstufenpotentials ($\pi_{\frac{1}{2}}$) vom pH-Wert für 6-Azacytosin.

Die positivere Stufenhöhe ist unabhängig vom pH-Wert, während die negativere bei pH-Werten >9 kontinuierlich abnimmt, was die gleichen Ursachen hat, die schon beim 6-AU und 6-AT erläutert wurden. Die erste Reduktionswelle entspricht der Desaminierung und erst danach erfolgt die Aufspaltung der 5:6-Doppelbindung. Um diese Reaktionsfolge zu begründen, wurde eine $1 \cdot 10^{-3}$ M 6-AC-Lösung elektrolysiert. Dabei wurde das Potential auf den Diffusionsstrom der 1. Stufe eingestellt. Während der Abnahme dieser Stufenhöhe (die negativere blieb unverändert) konnte

TABELLE 2

ABHÄNGIGKEIT DES HALBSTUFENPOTENTIALS ($\pi_{\frac{1}{2}}$) VOM pH-WERT FÜR 6-AC

Milieu	*Stufe*	$\pi_{\frac{1}{2}}/pH$,(mV)
pH < 8.5	1. Stufe	115
	2. Stufe	26
pH > 8.5	1. Stufe	85
	2. Stufe	30

erwartungsgemäss freies Ammoniak mit Nesslers Reagenz nachgewiesen werden. Abb. 7 zeigt die Abhängigkeit des Halbstufenpotentials ($\pi_{\frac{1}{2}}$) vom pH-Wert für 6-AC. In Tabelle 2 sind diese Werte zusammengestellt. Der Reduktionsmechanismus wäre demnach wie folgt zu formulieren:

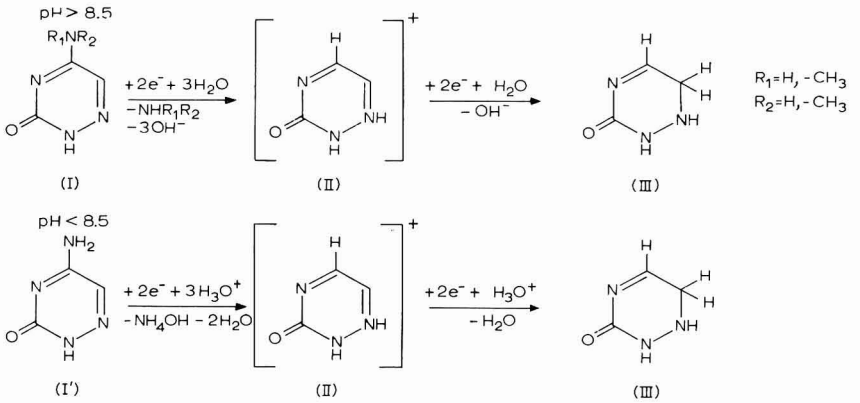

Die Existenz von (II) ist hypothetisch. Im alkalischen Bereich wird ebenfalls unter NH_3-Abspaltung die 3:4-Doppelbindung zurückgebildet, wogegen im sauren pH-Bereich die bereits protonierte $-NH_3$-Gruppe als NH_4OH abgespalten werden kann. Die Existenz von (III) stützt sich auf spektrophotometrische Daten und auf Ergebnisse der Photohydratation[19]. Während der UV-Bestrahlung (bei pH 7) sinkt das Absorptionsmaximum bei 258 nm ab, was auf das Verschwinden der 5:6-Doppelbindung zurückzuführen ist und gleichzeitig wird es nach kürzeren Wellenlängen verschoben (239 nm). SHUGAR UND JANION[21] haben das Maximum bei 239 nm der in Konjugation stehenden Doppelbindungen O=C—N=C— zugeordnet.

Die 5-Halogenderivate des 6-AU werden in vierelektronigen Prozessen reduziert, wobei im Falle des 5-Jod-Derivates eine Doppelstufe (je 2 Elektronen in zwei Stufen) auftritt. Während der Photolyse (Abb. 8) wird das Molekül zunächst zum 6-AU dehalogeniert (1. Stufe nimmt schneller ab als die 2.). Das dehalogenierte Produkt unterliegt wiederum der photochemischen Hydratation (2.Stufe). Der Ablauf beider Prozesse kann aus Verminderung beider Reduktionsstufen verfolgt werden, wodurch auch die Reaktionsfolge des Elektrodenprozesses gesichert wird (I = Cl, Br, I).

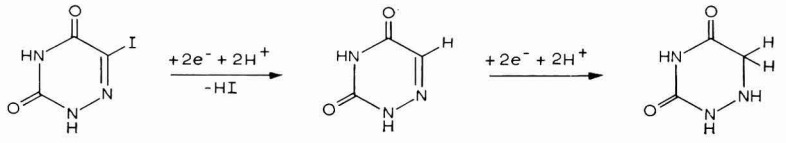

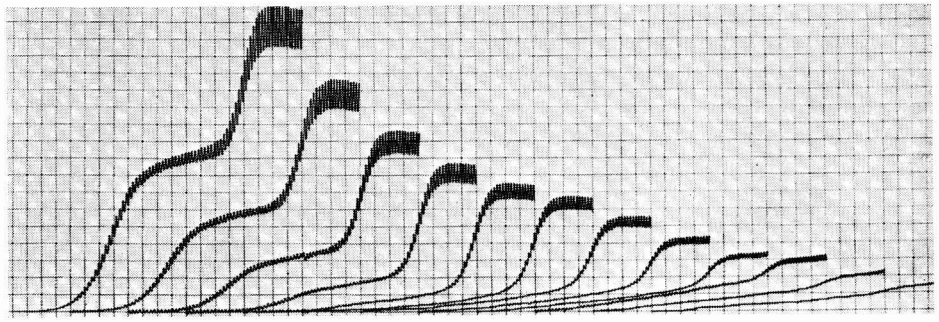

Abb. 8. 6-Jod-6-Azauracil: Photoreaktion. $c = 2 \cdot 10^{-4}$ *M* in Phosphatpuffer pH 7 (0.1 *M*); ab −0.5 V, 50 mV/Abszisse, Kapazitätsstromkompensation 0.55 μA V^{-1}, $t = 25°$.
$h\nu$: 0″, 20″, 60″, 120″, 180″, 300″. Lichtintensität in der Bestrahlungszelle $6.7 \cdot 10^{-6}$ Einstein cm^{-2} min^{-1}.

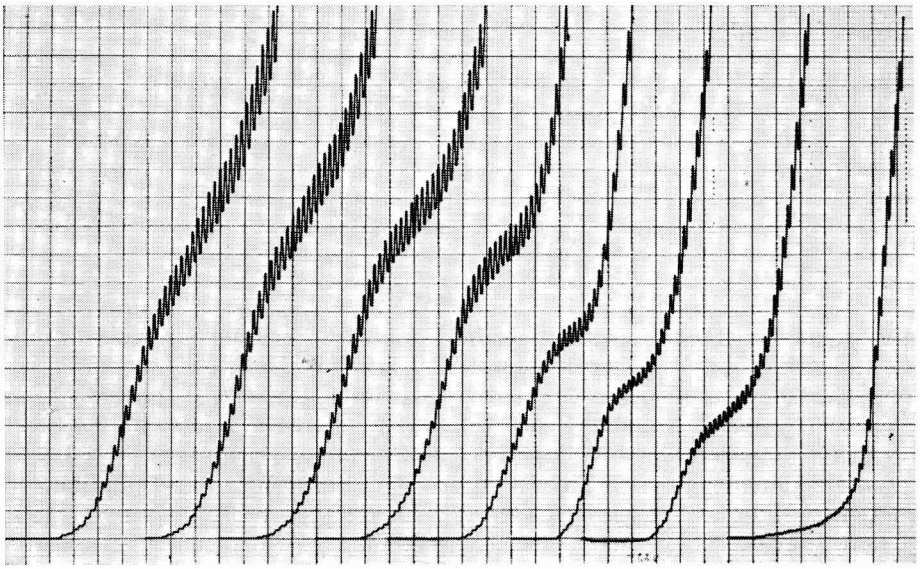

Abb. 9. 8-Azaadenin: pH-Abhängigkeit. $c = 5 \cdot 10^{-4}$ *M* in Britton–Robinson-Puffer (0.1 *M*); $s = 16 \cdot 10^{-8} AD^{-1}$, 50 mV/Abszisse; Kapazitätsstromkompensation 0.4 μA V^{-1}, $t = 25°$ gegen 1 *N* KCl-Elektrode. Potentialbeginne: pH 1.0 (0.1 *N* H_2SO_4), −0.7 V; pH 2.1 und 3.0, −0.8 V; pH 4.0, −0.9 V; pH 5.3, −1.0 V; pH 6.3 und 7.0, −1.2 V; pH 7.7, −1.4 V.

Die Unterschiede im polarographischen Verhalten der 8-Azapurine zu den entsprechenden Purinen sind nicht wesentlich. Dieses hängt damit zusammen, dass die Substitution im Ring und das Reduktionszentrum nicht im unmittelbaren Zusammenhang stehen.

8-Azaadenin wird in einem 4-elektronigen Vorgang reduziert (Abb.9). Auffällig ist, dass die Stufenhöhe—im Gegensatz zu den 6-Azapyrimidinen—im sauren pH-Bereich kinetisch begrenzt ist (Abb.10). Aus der Halbstufenpotentialabhängigkeit (Abb. 11) geht die Beteiligung von 5 Protonen beim Reduktionsprozess hervor. In

Analogie zum 6-AC steht daher folgendes Schema mit den experimentellen Ergebnissen in Einklang (die Lage der Doppelbindung in Sechsring ist unsicher):

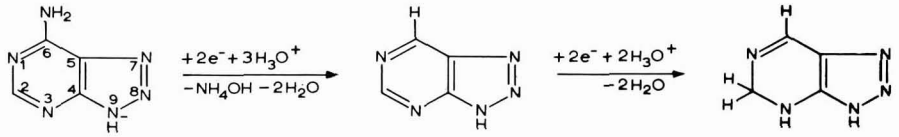

Alle 8-Azapurine, die in 6-Stellung eine Keto-Gruppe tragen, sind bis -2.0 V an der Quecksilbertropfelektrode nicht reduzierbar. Aus vorliegenden Ergebnissen geht hervor, dass die Einführung der Azagruppierung eine beträchtliche Steigerung der EA-Stärke des Moleküls nur bei den Pyrimidinen verursacht.

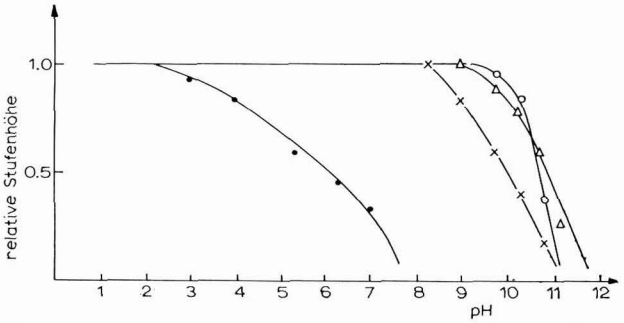

Abb. 10. Abhängigkeit der Stufenhöhe vom pH-Wert, (●) 8-Azaadenin; (○) 6-Azathymin; (×) 6-Azacytosin (2.Stufe); (△) 6-Azauracil.

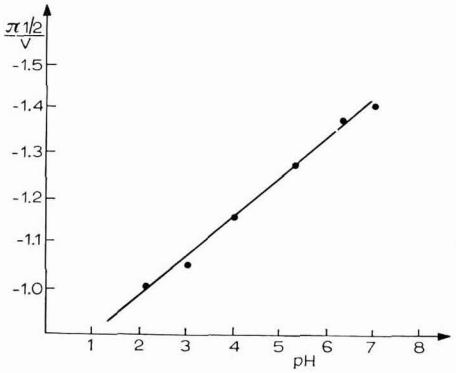

Abb. 11. Abhängigkeit des Halbstufenpotentials ($\pi_{\frac{1}{2}}$) vom pH-Wert für 8-Azaadenin.

ZUSAMMENFASSUNG

Es wurde das polarographische Verhalten von 6- bzw. 5-Azapyrimidinen und 8-Azapurinen untersucht. In der Azapyrimidinreihe unterliegt die 5:6-Doppelbindung einer 2-elektronigen Reduktion. Ist dieser Grundkörper in 4- oder 5-Position durch andere reduktionsfähige Gruppen substituiert, so handelt es sich immer um einen vierelektronigen Reduktionsprozess. In einigen Fällen werden diese Stufen aufgespal-

ten, was die Untersuchung des Reduktionsmechanismus erleichtert. Dabei wird zuerst die exocyclische Gruppe reduziert, dann erfolgt die Reduktion des Ringsystems.

In der 8-Azapurinreihe sind die Unterschiede zu den normalen Purinen nicht so gross.

Dieses Verhalten wird damit begründet, dass der Fünfring in beiden Fällen in den Reduktionsprozess nicht einbezogen wird.

Frau Dr. P. K. CHANG, New Haven (Conn.) und den Herrn Dr. J. GUT, Dr. V. FUČIK und Dr. A. PISKALA, Prag sei für die Überlassung wichtiger Substanzen gedankt.

SUMMARY

Azapyrimidines and azapurines incorporated in nucleic acids are most important in molecular biological research. To evaluate the electron donor–acceptor strength the electrochemical reduction of 5- or 6-azapyrimidines and 8-azapurines has been investigated by polarography and the reduction products were examined chemically, polarographically, spectrophotometrically, and photochemically. Azapyrimidines were reduced at their 5:6 double bond in a two-electron process. A four-electron process takes place, if the 4- or 5-position is substituted by a reducible group. The polarographic properties of 8-azapurines are very similar to these of purines in consequence to the fact that in this case substitution and reduction do not occur at equal position in the molecule.

LITERATUR

1 H. BERG, H. BÄR UND F. A. GOLLMICK, *Biopolymers*, 5 (1967) 61.
2 H. BERG UND F. A. GOLLMICK, *III. Jena. Symp., 1965, Elektrochemische Methoden und Prinzipien in der Molekular-Biologie*, Akad. Verlag, Berlin, 1966, S. 533.
3 L. KITTLER UND H. BERG, *III. Jena. Symp., 1965, Electrochemische Methoden und Prinzipien in der Molekular-Biologie*, Akad. Verlag, Berlin, 1966, S. 547.
4 L. F. CAVALIERI UND B. A. LOWY, *Arch. Biochem. Biophys.*, 35 (1952) 83.
5 D. L. SMITH UND P. J. ELVING, *J. Am. Chem., Soc.*, 84 (1962) 2741.
6 D. L. SMITH UND P. J. ELVING, *J. Am. Chem. Soc.*, 84 (1962) 1412.
7 D. L. SMITH UND P. J. ELVING, *Anal Chem.*, 34 (1962) 930.
8 O. MANOUSEK UND P. ZUMAN, *Collection Czech. Chem. Commun.*, 20 (1955) 1340.
9 G. HORN UND P. ZUMAN, *Collection Czech. Chem. Commun.*, 25 (1960) 3401.
10 B. JANIK UND E. PALEČEK, *Arch. Biochem. Biophys.*, 105 (1964) 225.
11 D. GRÜNBERGER, R. N. MASLOVO UND F. ŠORM, *Collection Czech. Chem. Commun.*, 29 (1964) 152.
12 H. L. GÜNTHER UND W. H. PRUSOFF, *Biochim. Biophys. Acta*, 55 (1962) 778.
13 F. ŠORM, Z. ŠORMOVA, K. RAŠKA UND M. JUROVCIK, *Rev. Roumaine Biochim.*, 3 (1966) 139.
14 F. ŠORM UND J. VESSELY, *Neoplasma*, 11 (1964) 123.
15 J. KRUPIČKA UND J. GUT, *Collection Czech. Chem. Commun.*, 25 (1960) 592.
16 J. KRUPIČKA UND J. GUT, *Collection Czech. Chem. Commun.*, 27 (1962) 547.
17 L. KITTLER UND H. BERG, *Photochem. Photobiol.*, 6 (1967) 199.
18 J. JONAŠ UND J. GUT, *Collection Czech. Chem. Commun.*, 27 (1962) 716.
19 L. KITTLER, unveröffentlichte Ergebnisse.
20 J. VOLKE, *Talanta*, 12 (1965) 1081.
21 C. JANION UND P. SHUGAR, *Acta Biochim. Polonica*, 8 (1960) 309.

ELECTROANALYTICAL CHEMISTRY AND INTERFACIAL ELECTROCHEMISTRY
Elsevier Sequoia S.A., Lausanne – Printed in The Netherlands

THE ELECTROCHEMICAL REDUCTION OF THE TRIPHENYLSULFONIUM ION

P. S. MCKINNEY AND SUSAN ROSENTHAL*
Harvard University, Cambridge, Mass. (U.S.A.)
(Received January 9th, 1967; in revised form July 27th, 1967)

An investigation of the electroreduction of "onium" compounds of Group-Va and -VIa elements was prompted by the polarographic data reported by MATSUO, for several "phenyl-onium" compounds[1]. These data indicated that, though the tetraphenylarsonium and -phosphonium compounds were reduced in a single apparently two-electron step in aqueous solution, the analogous compounds of antimony, sulfur, selenium and tellurium exhibited two polarographic waves and reduced *via* step-wise mechanisms. A complete electrochemical study of the tetraphenylstibonium ion confirmed the two-step reduction process and demonstrated that the mercury electrode was involved chemically in the first reduction step[2]. In fact, diphenylmercury could be obtained quantitatively by controlled-potential electrolysis at potentials prior to the second wave. The triphenylsulfonium ion has now been studied to determine whether its mechanism parallels that of the antimony compound. This communication presents the results of that investigation.

Several other studies of sulfonium compounds have been reported. Mixed aryl- and alkylphenacylsulfonium compounds reduce polarographically in three steps[3–4]. The first, a two-electron wave, involves the rupture of the C–S bond while the second and third waves are due to the reduction of acetophenone produced during the first reduction step. The trimethylsulfonium ion is reported to reduce in a single two-electron step[5]. The electrolysis of several triphenylsulfonium salts at aluminum cathodes in dimethylformamide and in water has been reported[6]. The electrolyses were performed without potential control and an estimate for the number of faradays (n-value) involved in the reduction process could not be made directly. However, indirect evidence, based on excellent product analysis, seemed to favor a two-electron reduction mechanism. Finally, as indicated above, a polarographic study of triphenylsulfonium chloride has been carried out by SHINAGAWA *et al.*[7]. They report a two-step reduction in which both waves appear to be of equal height. They suggest a reaction scheme, based on polarographic evidence alone, which is not supported by the findings of the present investigation.

Polarographic data

The polarographic behavior of the triphenylsulfonium ion is complicated and displays peculiarities often associated with reactions in which the adsorption of reactants and products plays an important role. At concentrations from 3×10^{-5} to 5×10^{-3} M a wave similar to that shown in Fig. 1B is obtained. It appears to be a

* Present Address: Harvard Medical School, 25 Shattuck Street, Boston, Mass.

single wave with a large maximum and an estimated half-wave potential of -1.2 V *vs.* SCE. At concentrations $\geqslant mM$, the maximum can be substantially reduced but not eliminated by the addition of Triton X-100 even in amounts up to several percent. From 5×10^{-5} to 5×10^{-4} M, the addition of 0.008% Triton X-100 essentially eliminates the maximum and permits the recording of a polarogram with two waves as shown in Fig. 1A. The first wave is slightly more positive than the original wave and the second substantially negative with respect to the original. The magnitude of the maximum precludes an accurate description of the effect of very small concentrations of Triton X-100 on the half-wave potentials. However, the first wave shifts approximately 20 mV anodic and the second wave shifts about 40 mV cathodic

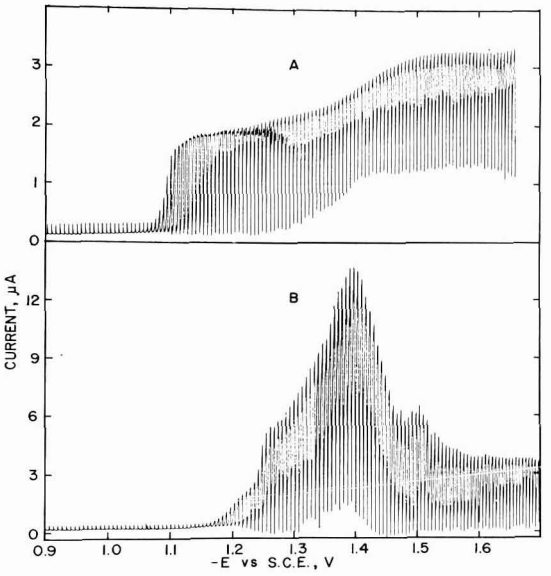

Fig. 1. Polarograms of 2.9×10^{-4} M triphenylsulfonium bromide at a pH of 11.5. (A) recorded in the presence of 0.008% Triton X-100; (B) recorded with no maximum suppressor.

when the suppressor concentration is increased from 0.004% to 0.008%. It is interesting to note that when gelatin is used as a maximum suppressor in place of Triton X-100, the results are quite different. In this case, the maximum is eliminated over the entire concentration range from 3×10^{-5} to 5×10^{-3} M, but only a single wave with a half-wave potential of approximately -1.2 V is obtained. The final limiting current in this case is depressed by about 10% by the presence of the gelatin.

Table 1 lists the diffusion current constant, I, as a function of concentration in the absence of maximum suppressor. Maximum currents were measured at a potential of -1.6 V. The value of I remains essentially constant down to a concentration of about 5×10^{-4} M. Below this value I increases to some extent due presumably to an increase in the net "n-value" for the reaction. This is in agreement with controlled-potential coulometric data (vide infra). In the presence of maximum suppressor when two waves are evident, though the data are somewhat irreproducible, i_d/C values are constant for both waves. However, the first wave is larger than the

second by a factor of 1.6 on the average. This observation is contrary to that reported by SHINAGAWA who recorded waves of equal height[7].

The variation of limiting current with the height of the mercury-head (h) indicates diffusion control for the total wave both in the presence and absence of Triton X-100. However, a slight curvature, concave upward, in a plot of the limiting current of the first wave as a function of $h^{\frac{1}{2}}$, corrected for back pressure, suggests either some adsorption character for the first wave or a latent influence of the maximum.

TABLE 1

DIFFUSION CURRENT CONSTANT, I, AS A FUNCTION OF CONCENTRATION

Capillary characteristics: $m = 1.56$ mg sec^{-1}, $t = 4.1$ sec at -1.6 V *vs.* SCE

Conc. (mM)	$i_d/Cm^{\frac{2}{3}}t^{\frac{1}{6}}$*	*Conc. (mM)*	$i_d/Cm^{\frac{2}{3}}t^{\frac{1}{6}}$*
0.032	5.0	1.0	4.1
0.06	4.5	3.0	4.1
0.10	4.3	5.0	4.0
0.50	4.2		

* Diffusion currents were measured at a potential of -1.6 V *vs.* SCE without maximum suppressor.

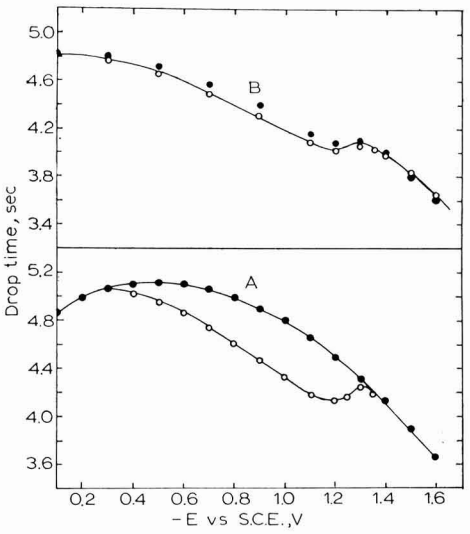

Fig. 2. Drop-time curves for solutions of triphenylsulfonium bromide at pH 10.5. (A) ● supporting electrolyte alone, ○ 2.9×10^{-4} M triphenylsulfonium bromide; (B) 2.9×10^{-4} M triphenylsulfonium bromide: ○ with 0.008% Triton X-100, ● with 0.008% gelatin.

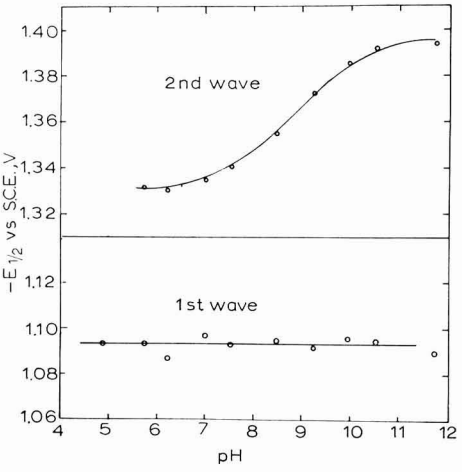

Fig. 3. Half-wave potentials as a function of pH for solutions containing 2.9×10^{-4} M triphenylsulfonium bromide and 0.008% Triton X-100.

That adsorption is an important factor in the overall reaction process is emphasized by the drop-time *vs.* potential curves shown in Fig. 2. It is clear that the triphenylsulfonium ion is adsorbed at the electrode surface. The fact that there is a change in the curve following the first half-wave potential and that desorption does

not take place until -1.35 V *vs.* SCE suggests that a product of the first reduction step is also adsorbed. At very low concentrations of the electroactive species, 3×10^{-5} M, adsorption of Ph_3S^+ is still evident as indicated by the deviation of the drop-time curve from that for supporting electrolyte alone. Finally, a comparison of drop-time curves for solutions containing gelatin and Triton X-100 is shown in Fig. 2b. There does not appear to be any significant difference in the adsorption properties of the two solutions in-so-far as such properties are indicated by drop-time curves, and hence no clue to the different polarographic properties of the solutions cited above can be obtained from these data.

The dependence of the half-wave potentials on various solution parameters is important in the understanding of the reaction process. Fig. 3 indicates the pH dependence of both waves. The first wave is independent of pH while the second shows a slight non-linear dependence reminiscent, in form, of the tetraphenylstibonium ion[2], and similar to the reported behavior of the phenylmercury cation[8,9]. Such non-linear curves are not uncommon in irreversible reductions involving organic species and the magnitude of the shift, which is quite small, is not without precedent[10]. Both half-wave potentials are linear functions of the concentration of triphenylsulfonium bromide. The first shifts anodic with a slope of about 50 mV per ten-fold change in concentration. The second wave shifts cathodic with a slope of approximately 60 mV per decade change in concentration. The first wave shows a positive half-wave potential dependence on the drop-time while the second is independent of this parameter.

Based on the usual polarographic wave analysis, the second wave is irreversible while the first has an abnormally steep slope for a wave which appears to involve a single electron.

Controlled-potential electrolysis data

The most striking feature of the electrolysis data is that the n-value is concentration dependent. Table 2 lists such data obtained in the absence of Triton X-100 at a control potential of -1.6 V *vs.* SCE, that is, at a potential on the limiting current

TABLE 2

APPARENT n-VALUE AS A FUNCTION OF CONCENTRATION

Conc. (mM)	n_{app}	*Conc. (mM)*	n_{app}
0.46	2.0	3.5	1.8
0.79	2.0	4.7	1.7
1.2	1.95	8.4	1.6
2.6	1.8		

plateau well beyond the second polarographic wave. At low concentrations, the reduction appears to procede *via* a two electron process. As the concentration of the electroactive species is increased the "n-value" decreases. Solubility limitations preclude the investigation of solutions more concentrated than 8–9 mM and hence it is not clear whether the apparent value of n would eventually approach 1 or level off at an intermediate value. (The significance of these alternatives is discussed below.) Electrolysis at potentials beyond the second wave does not appear to be

influenced by the presence of Triton X-100. If, in the presence of Triton X-100, an electrolysis is performed at -1.25 V, on the plateau of the first wave, an apparent n-value of 1.1 ± 0.1 is obtained regardless of concentration.

Electrolysis at potentials on the first wave produced two products which could be separated by thick-layer chromatography and which were identified as diphenylsulfide and diphenylmercury. The yield of these products was in excellent agreement with the amounts expected assuming the stoichiometric conversion of the triphenylsulfonium ion into these two compounds. Neither benzene nor biphenyl were identified as components of the electrolysis mixture. In addition to diphenylsulfide and diphenylmercury, benzene was produced by electrolysis at potentials beyond the second wave. The ratio of benzene to diphenylmercury was dependent upon the initial concentration of the electroactive species. As expected, when the apparent n-value was two, no diphenylmercury was produced and as the n-value decreased, the quantity of diphenylmercury produced increased. Theoretical calculations of expected amounts of diphenylsulfide and diphenylmercury based on the observed n-value of the electrolysis were in excellent agreement with the experimental yields of the two products for values of n from 1.6–2.0.

Finally, an electrolysis was carried out at -1.6 V *vs.* SCE of a 3.5×10^{-3} M solution of triphenylsulfonium ion containing 0.01% gelatin. The apparent n-value for this process was 2.0 compared to a value of 1.7 for an electrolysis under the same conditions but containing Triton X-100 as a maximum suppressor. The products were identified as benzene and diphenylsulfide.

Reaction scheme for triphenylsulfonium ion reduction

The following reaction scheme is proposed to account for the electrochemical data outlined above. The first electron transfer, responsible for the initial polarographic wave is:

$$(C_6H_5)_3S^+ \ldots Hg + e^- \rightarrow [(C_6H_5)_3S \ldots Hg^{\cdot}] \quad (1)$$

The radical produced can either decay *via* a disproportionation reaction

$$2[(C_6H_5)_3S \ldots Hg^{\cdot}] \rightarrow (C_6H_5)_2S + (C_6H_5)_2Hg + Hg \quad (2)$$

or, at potentials on or beyond the second wave, the radical can accept another electron and a proton

$$[(C_6H_5)_3S \ldots Hg^{\cdot}] + e^- + H^+ \rightarrow (C_6H_5)_2S + C_6H_6 + Hg \quad (3)$$

The involvement of the mercury electrode both as a reactant and as an adsorption surface is emphasized by its inclusion as a part of the initial reacting species. It seems clear that strong adsorption at the electrode surface is a necessary prerequisite for the eventual arylation of the mercury electrode as demonstrated in the present instance, in the case of the tetraphenylstibonium ion[2] and in some recent work on the diphenylthallium cation[11].

The reaction scheme detailed above seems to account for the observed electrochemical behavior. The relation between half-wave potential and pH indicates that protons are not involved in the first step but are involved prior to the rate-determining step of the second electron transfer, at least at intermediate pH values. It may be that in strongly alkaline solution protonation occurs after the second electron transfer as suggested by MAIRANOVSKII[12]. The concentration dependence

of the second half-wave potential is due to the competition of the second-order disproportionation reaction for the reducible species. Furthermore, the positive shift of the first half-wave potential with concentration is also attributable to the disproportionation reaction if the first reduction process is reversible or quasireversible. In such a case, with deactivation of the product by a rapid chemical reaction, a drop time dependence, as noted experimentally, is also expected[13]. Both of these factors indicate a reversible process even though the slope of the first polarographic wave is abnormally sharp for a one-electron transfer. It seems probable that this is due to the influence of the maximum which is difficult to suppress. It is also likely that the maximum is responsible for the slight non-linearity in the limiting current *vs.* $h^{\frac{1}{2}}$ plot since other features usually associated with adsorption waves are not evident in the present case.

If the first wave does involve, at least formally, the production of a radical in what is apparently a reversible process, it is of interest to determine the stability of the intermediate. Cyclic voltammetric studies were performed in an effort to detect the reoxidation of the radical, but no anodic wave was observed even at the fastest possible scan rates and oscillographic detection of the current–time curve. This placed an upper limit of approximately 10 msec on the lifetime of the radical. Relatively slow scan studies however did provide an interesting picture of the competing adsorption processes in the system. Fig. 4 shows a steady-state triangular-

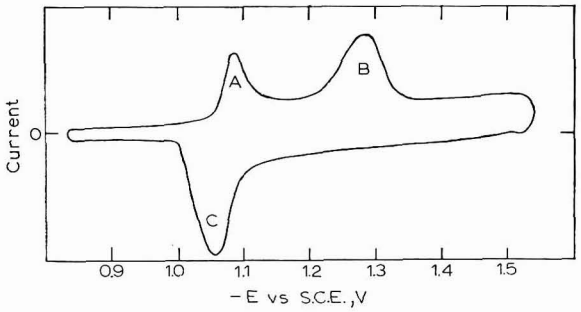

Fig. 4. Steady-state triangular wave voltammogram obtained at a HMD electrode for a solution of 6×10^{-5} *M* triphenylsulfonium bromide at pH 11.5. Scan rate, 500 mV sec^{-1}.

wave polarogram for a 6×10^{-5} *M* solution of triphenylsulfonium bromide containing no maximum suppressor. Initially, peak B is very large, C is quite small and A is missing. As B decreases, peaks A and C increase to steady values as shown. A and C are non-faradaic, adsorption peaks as evidenced by their direct proportionality to the scan rate and it was established, by comparison with authentic material, that they are due to the adsorption and desorption of diphenylsulfide. Initially, when little diphenylsulfide has been produced, and because it is competing with the triphenylsulfonium ion for electrode sites, peak C is small and A missing. As its concconcentration builds up at the electrode surface, diphenylsulfide becomes the predominantly adsorbed species, replacing the sulfonium ion and causing a further decrease in peak B. At slower scan rates, peak C decreases, A disappears and B decreases only slightly. In this case, following the desorption of diphenylsulfide at C, diffusion of the sulfonium ion from the bulk of the solution and of the sulfide away

from the electrode shift the adsorption equilibrium in favor of the sulfonium compound once more thus eliminating A and reinforcing B. The same behavior is noted at higher concentrations of the sulfonium ion. In the presence of Triton X-100, the triangular-wave polarogram is as expected for a two-step reduction process in which there are no reoxidizable species. The diphenylsulfide peaks are also gone, no doubt, because of the adsorption of the surfactant at the electrode surface.

One of the most interesting aspects of the reaction process is the competition of the disproportionation reaction (2) and the second electron transfer reaction (3). The reactions remain competitive even when the electrode is maintained at a potential well out on the second wave. This is indicated by the non-integral and concentration-dependent n-values cited in Table 2 and by the unequal heights of the polarographic waves. MEITES has developed equations which permit the calculations of the rate constant of such a second-order reaction in such an e.c.e. mechanism[14]. Two parameters must be experimentally evaluated in order to make the calculation. β, which is dependent upon cell geometry, stirring rate, diffusion coefficient, etc., can be evaluated from the final slope of a plot of the log of the electrolysis current *vs.* time, and π which is defined by

$$\pi = (n_1 + n_2 - n_{\text{apparent}})/n_2$$

where in the present case $n_1 = n_2 = 1$, and n_{apparent} is experimentally determined. The average value of the rate constant calculated for a series of electrolyses with apparent n-values from 1.6–1.8 was $2.9 \pm 0.3\ M^{-1}\ 1\ \text{sec}^{-1}$. This value is valid, however, only if it can be assumed that the intermediate species is distributed homogeneously throughout the solution. If the reaction takes place at or near the electrode surface,

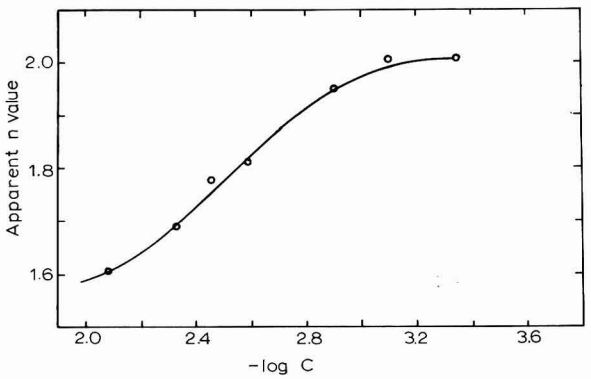

Fig. 5. Apparent n-values as a function of concentration for the electrolysis of triphenylsulfonium bromide.

the calculated rate constant will be too small. There is, in fact, evidence which suggests that the reaction takes place at the electrode surface. The apparent tendency of the diffusion current constant, I, listed in Table 1, to become constant at higher concentrations and the leveling off of a plot of apparent n-value *vs.* log C as shown in Fig. 5 both, if real, could be explained by assuming that the disproportionation is a surface reaction. The present data do not permit an unambiguous identification of the process to be made and the calculated rate constant must be considered as a lower limit.

The pronounced effect of gelatin on the reduction process is not easily explained. It is found generally, that Triton X-100 and gelatin can be used interchangeably as maximum suppressors and their effects on polarographic behavior are usually quite similar. The apparent shift of the second wave toward more positive potentials implies that the second electron transfer has been greatly facilitated by the presence of gelatin and, in fact, is so facile that there is no longer any one-electron intermediate species. Though inhibition of electron transfer is a more usual consequence of the addition of surfactants, there are instances in which reactions are facilitated[15]. It might also be argued that the presence of gelatin prevents the reactant from adsorbing in an orientation which favors the arylation of the mercury surface. However, the similarity of the drop-time curves of solutions containing gelatin and Triton X-100 appears to refute this.

It is clear that the reduction mechanism of the triphenylsulfonium ion differs in certain basic ways from that of the tetraphenylstibonium ion reported previously[2], though there are definite similarities. Both processes show two-step polarographic behavior, involve chemical and adsorption involvement of the electrode and can be described by reactions which are stoichiometrically analogous. The important difference, of course, lies in the fact that the disproportionation reaction of the product of the first electron transfer process remains competitive with the second electron transfer in the case of the sulfonium compound. A complete two-electron reduction is affected at potentials on the second wave of the stibonium ion. In this respect, the stibonium ion reduction parallels the reduction of the phenylmercuric cation[8,9]. It was, in fact, suggested that the first reduction step of the antimony compound involved the formation of phenylmercury radicals as one of the products and that the remainder of the reduction process was identical to that of a phenylmercury compound[2]. In the case of the sulfonium compound it would be possible to argue that the first step is identical to that described above for the stibonium ion but that the presence of adsorbed diphenylsulfide inhibits the further reduction of the phenylmercury radical but not its disproportionation. It seems more likely, however, that the first step involves the formation of a triphenylsulfonium radical which disproportionates very rapidly at the electrode to diphenylmercury and diphenylsulfide bypassing the phenylmercury radical intermediate. Further, it must be assumed that this disproportionation reaction is much more rapid than that of the phenylmercuric species and that the second electron transfer, or the preceding protonation step, is greatly inhibited in the sulfonium case. The concentration dependence of the first half-wave potential in the present case, which is not noted in either the stibonium or phenylmercury reduction processes is an additional argument in favor of a different initial deactivating reaction in the case of the sulfonium ion reduction.

Though it is tempting to speculate on the geometrical configuration and the nature of the bonding in the initial reacting species at the electrode surface, it seems premature to do so at the present time. It is evident that adsorption plays an important role in the processes where transarylation of the electrode takes place and it seems likely that the reacting species must be able to adopt a configuration at the electrode which favors the formation of phenylmercury bonds. Furthermore, this is probably most likely if the central atom can readily utilize its *d* orbitals as sulfur often does. Satisfactory explanations of differences in the reduction processes and subsequent

non-electrochemical reactions of analogous compounds must await further studies of the "onium" compounds and attempts, perhaps by molecular orbital arguments, to assign configurations and relative stabilities to possible intermediate and adsorbed species. Such studies are at present underway in this laboratory.

EXPERIMENTAL

Triphenylsulfonium bromide was prepared according to the method of WILDI *et al. via* a Grignard reaction on diphenylsulfoxide[16]. The purified product had m.p. 294.5° (Fisher block). WILDI *et al.* report m.p. 285–286° presumably in a capillary tube while BONNER reports m.p. 292.5° on a Fisher block[17]. Triphenylsulfonium chloride was prepared by the method of BONNER and had m.p. 297–298° in good agreement with the literature value. Both compounds displayed identical electrochemical properties. Mass spectra obtained for both compounds confirmed their identity.

All polarograms were run at a constant ionic strength of 1 F by the addition of the required amount of KCl to the buffered solution. Clark and Lubs buffers were used up to pH 10 and above this value solutions as described by BATES AND BOWER were used[18].

Polarograms were performed using a controlled-potential polarograph of conventional design. The response of the amplifiers was adequate for use in cyclic voltometric studies. Polarograms and slow scan triangular wave curves were recorded on a Mosely Model 2-D X–Y recorder with a slewing rate of $\frac{1}{2}$ sec for full scale deflection, which was deemed adequate for the recording of maximum current polarograms. Higher frequency curves were displayed on a Tektronix Model-502 oscilloscope. The triangular wave was obtained from a Hewlett-Packard Model-202A low-frequency function generator. Controlled-potential electrolyses were performed using a Wenking Model 61RS potentiostat. Current–time curves were recorded and current integration was done graphically. The electrolysis was carried out at a mercury pool in a cell of conventional design.

Diphenylsulfide and diphenylmercury produced during electrolysis were removed from solution by extraction with carbon tetrachloride. Separation of the two components was affected by thick-layer chromatography using silica gel P_{254} distributed by Brinkman Instruments. The compounds were extracted from the silica gel and weighed. Blank experiments using authentic samples indicated that a 98% recovery of diphenylsulfide and a 95% recovery of diphenylmercury was possible by this method if the separation was done quickly. If it was not done rapidly, diphenylmercury was lost by decomposition from the thick-layer plate. This rather unusual decomposition of the normally stable compound is readily observable under UV light. Identification of diphenylmercury and diphenylsulfide was made on the basis of their IR spectra and thin-layer chromatographic behavior as compared to authentic samples of the compounds. Benzene was identified by its characteristic UV absorption after separation from diphenylsulfide by distillation.

ACKNOWLEDGEMENTS

The authors are grateful to the National Science Foundation for a grant

(GP-6664) in support of this work. The authors wish to thank Dr. E. C. WOODBURY for valuable discussions concerning the preparation and separation of various compounds involved in this research.

SUMMARY

A reaction scheme based on polarographic, controlled-potential electrolysis and cyclic voltammetric data has been proposed for the electrochemical reduction of the triphenylsulfonium ion in aqueous solution. Comparison of the reduction process with those of other analogus "onium" compounds of Group Va indicates that there are both similarities and interesting differences in their reaction paths. The role of adsorption appears to be an important one in the overall process.

REFERENCES

1 H. MATSUO, *J. Sci. Hiroshima Univ., Sec. A.*, 22 (1958) 281.
2 M. D. MORRIS, P. S. MCKINNEY AND E. C. WOODBURY, *J. Electroanal. Chem.*, 10 (1965) 85.
3 P. ZUMAN AND S.-Y. TANG, *Collection Czech. Chem. Commun.*, 28 (1963) 829; S.-Y. TANG AND P. ZUMAN, *ibid.*, 28 (1963) 1524.
4 J. E. SAVEANT, *Compt. Rend.*, 257 (1963) 448; 258 (1964) 585.
5 E. L. COLICHMAN AND D. L. LOVE, *J. Org. Chem.*, 18 (1953) 40.
6 M. FINKELSTEIN, R. C. PETERSON AND S. D. ROSS, *J. Electrochem. Soc.*, 110 (1963) 422.
7 M. SHINAGAWA, H. MATSUO AND N. MAKI, *Bunseki Kagaku*, 5 (1956) 80.
8 V. VOJIR, *Collection Czech. Chem. Commun.*, 16 (1951) 488.
9 R. E. BENESCH AND R. BENESCH, *J. Am. Chem. Soc.*, 73 (1951) 3391; *J. Phys. Chem.*, 56 (1952) 648.
10 P. J. ELVING, *Pure Appl. Chem.*, 7 (1963) 123.
11 Private communication from M. D. MORRIS, The Pennsylvania State University, University Park, Pa.
12 S. G. MAIRANOVSKII, *J. Electroanal. Chem.*, 4 (1962) 166.
13 J. HEYROVSKÝ AND J. KŮTA, *Principles of Polarography*, Academic Press, New York, 1966, p. 396.
14 L. MEITES, *J. Electroanal. Chem.*, 5 (1963) 270.
15 Reference 13, p. 303 ff.
16 B. S. WILDI, S. W. TAYLOR AND H. A. POTRATZ, *J. Am. Chem. Soc.*, 73 (1951) 1965.
17 W. A. BONNER, *Ibid.*, 74 (1952) 5078.
18 L. MEITES, *Handbook of Analytical Chemistry*, McGraw-Hill, New York, 1963, chapter 11.

Elsevier Sequoia S.A., Lausanne – Printed in The Netherlands

SHORT COMMUNICATIONS

Temperature coefficient of e.m.f. of the cell Cu | Cu-soap(s), K-soap, Ag-soap(s) | Ag and the entropy of reactions

Although most of the heavy-metal salts of the higher fatty acids are insoluble in water, metal–metal soap electrodes have been little studied. KOLTHOFF AND JOHNSON[1] used a silver–silver laurate electrode for measuring the laurate ion activity in aqueous solutions of potassium laurate. We have carried out systematic studies on a number of metal–metal soap electrode systems using electropositive metals like copper, nickel, cobalt, etc. In recent communications we have reported on the suitability of cobalt–cobalt soap[2] and copper–copper soap electrodes[3] for studying the detergent anion activity variation in aqueous solutions of potassium salts of the higher fatty acids. This communication is a further study of the metal–metal soap electrode systems and reports on the values of ΔG, ΔH and ΔS, calculated from e.m.f. measurements of the cell $Cu|CuD_2(s)$, KD, $AgD(s)|Ag$, for the reaction $Cu + 2\,AgD \rightleftharpoons CuD_2 + 2\,Ag$ (D = laurate, myristate, palmitate and stearate).

Experimental

Reagents: Lauric, myristic, palmitic and stearic acids were reagent-grade (B.D.H.) products purified by repeated crystallization from alcohol.

Potassium laurate, myristate, palmitate and stearate. These were obtained by refluxing equivalent amounts of fatty acids and potassium hydroxide in alcohol for 10–12 h on a water bath. The soaps were further purified in a soxhlet by acetone and finally, recrystallised from alcohol.

Copper and silver soaps. Copper and silver soaps were prepared by direct methathesis at 50–55° from the corresponding potassium soaps and an aqueous solution of copper sulphate or silver nitrate. The precipitated metal soaps were washed with distilled water and then with ethanol to remove free precipitant.

Preparation of copper and silver electrodes. Copper electrodes were prepared by depositing copper on platinum wires by the electrolysis of a solution containing 8% $CuSO_4$ and 4.6% H_2SO_4. The electrodes were connected to a 2-V battery and a current of 15 mA was passed for 4 h.

Silver electrodes were prepared by the method described by KOLTHOFF AND JOHNSON[1].

E.m.f. measurements. E.m.f. measurements of the cell,

$$Cu|CuD_2(s),\ KD(C),\ AgD(s)|Ag$$

were carried out at different temperatures in a thermostat. The two limbs of an H-type cell were provided with silver and copper electrodes, respectively. The cell contained aqueous solutions of potassium soap saturated with silver and copper soap.

The reaction taking place in the cell for the passage of 2F of electricity is:

TABLE 1

E.M.F. OF THE CELL, TEMPERATURE COEFFICIENT OF E.M.F., AND ΔG, ΔH AND ΔS FOR THE CELL REACTIONS

Cell reaction	*E.m.f. of cell at 303°K, E (V)*	$\frac{dE}{dT}$ *(V deg^{-1}.)*	$\Delta G_{303\,°K}$ *(Cal)*	$\Delta S_{303\,°K}$ *(Cal deg.$^{-1}$)*	$\Delta H_{303\,°K}$ *(Cal)*
$Cu + 2C_{11}H_{23}COOAg \rightleftharpoons (C_{11}H_{23}COO)_2Cu + 2Ag$	0.290	0.001	−13380	46.13	590
$Cu + 2C_{13}H_{27}COOAg \rightleftharpoons (C_{13}H_{27}COO)_2Cu + 2Ag$	0.270	0.00095	−12460	43.81	810
$Cu + 2C_{15}H_{31}COOAg \rightleftharpoons (C_{15}H_{31}COO)_2Cu + 2Ag$	0.241	0.0009	−11110	41.51	1460
$Cu + 2C_{17}H_{35}COOAg \rightleftharpoons (C_{17}H_{35}COO)_2Cu + 2Ag$	0.210	0.000816	−9685	37.62	1695

$$2\,AgD + 2\,e \rightleftharpoons 2\,Ag + 2\,D^-$$
$$Cu + 2\,D^- \rightleftharpoons CuD_2 + 2\,e$$
$$Cu + 2\,AgD \rightleftharpoons CuD_2 + 2\,Ag$$

Results and discussion

The e.m.f. of the cells were found to be independent of the concentration of the potassium soap solution. ΔG, ΔH and ΔS have been calculated (at 303°K) using the following equations:

$$\Delta G = -nEF \tag{1}$$

$$\Delta G - \Delta H = T\left(\frac{d(\Delta G)}{dT}\right)$$

Or

$$-nEF = \Delta H - nFT\left(\frac{dE}{dT}\right) \tag{2}$$

$$\Delta S = nF\left(\frac{dE}{dT}\right) \tag{3}$$

Table 1 gives the values of the e.m.f. of the cell at 303°K, the temperature coefficient of the e.m.f. and the values of ΔG, ΔH and ΔS for the cell reactions.

Chemical Laboratories,
University of Roorkee,
Roorkee (India)

WAHID U. MALIK
AJAY K. JAIN

1 I. M. KOLTHOFF AND W. F. JOHNSON, *J. Phys. Colloid Chem.*, 52 (1948) 22.
2 W. U. MALIK AND A. K. JAIN, *J. Electroanal. Chem.*, 14 (1967) 37–41.
3 W. U. MALIK, S. I. AHMAD AND A. K. JAIN, *Kolloid-Z.*, 218 (1967) 155.

Received May 31st, 1967

Spurious faradaic process and determination of the point of zero charge of mercury

In their thorough study of experimental methods for the determination of the point of zero charge (E_z) of mercury in various electrolytes, GRAHAME *et al.*[1] noted that the classical method (his method V) employing a streaming mercury electrode (SME) gave, for 0.1 *M* KCl, a value of E_z, 3 mV less negative than other methods. He considers this method to be the most reliable for dilute solutions with the reservation that it would be desirable to understand its source of error.

The main source of error in this method is the occurrence of a spurious faradaic process in the range of potentials near E_z. Since the electrode is at open circuit, the faradaic current must be compensated by the charging current of the double layer. The potential E_m at open circuit is then shifted positively with respect to the true E_z for a cathodic faradaic process, and negatively for an anodic process. This effect was noted by LAITINEN *et al.*[2] for the dropping mercury electrode and was applied to the analysis of oxygen traces. The treatment of the shift of potential of a SME at open circuit, which was recently developed[3] for kinetic studies in media of low conductivity, will be transposed to the present problem. GRAHAME's observations[1] will be discussed, and the possibility of *serious* error on E_z for systems for which the double-layer capacity near E_z is low (*i.e.*, below 10 μF cm^{-2}) will be pointed out.

We assume hydrodynamic conditions for which eqn. (1) below applies as a first approximation. This is not the case in many instances, but the treatment points out the essential factors. We further assume that the potential is in the limiting current range for the reduction or oxidation of the impurity involved in the faradaic process. This is the case for O_2-reduction for which E_z for most electrolytes is in the plateau of the first wave (reduction to hydrogen peroxide). The shift of potential, obtained by equating the capacity and limiting currents is then

$$|E_m - E_z| = 2nF\delta^{\frac{1}{3}}D^{\frac{1}{3}}\frac{1}{C}r(l/m)^{\frac{1}{3}}c^s \qquad (1)$$

where n is the number of electrons in the faradaic process, F the faraday, δ the mercury density, D the diffusion coefficient of the species being reduced or oxidized, C the integral capacity of the double layer (assumed to be potential-independent in the interval $E_m - E_z$), r the radius of the mercury-jet, l its length, m the flow rate of mercury, and c^s the bulk concentration of the reducible or oxidized species. One has $E_m - E_z \gtrless 0$ for a cathodic or anodic process, respectively.

Equation (1) shows that $E_m - E_z$ is proportional to the bulk concentration, c^s, and to $(l/m)^{\frac{1}{3}}$. Typical data for a conventional SME are: $r = 5 \cdot 10^{-3}$ cm, $l = 1$ cm, $m = 1$ g sec^{-1}, $C = 20$ μF cm^2. The shift of potential is then approximately 16 mV for $n = 2$ and $c^s = 10^{-5}$ mole l^{-1}, *i.e.*, for a not particularly strenuous removal of dissolved oxygen from an aqueous solution. Assuming that the electrode characteristics in GRAHAME's experiments[1] were similar to those of this calculation, one estimates a residual oxygen concentration of $2 \cdot 10^{-6}$ mole l^{-1} in this author's careful work. It does not appear easy, to say the least, to lower this residual concentration by conventional techniques[4].

The foregoing analysis shows that a serious error can be expected when the capacity C is much lower than the value of 20 μF cm^{-2} used in the above numerical

example. This is the case in dilute (*e.g.*, 10^{-3} *M*) aqueous solutions or in non-aqueous solvents of low dielectric constant ($C = 1$ μF cm^{-2} in some instances). The shift of potential can easily be 0.1 V, unless residual oxygen is very carefully removed. This is often harder to achieve with non-aqueous solvents than with aqueous solutions because of the higher oxygen solubility in many of these solvents than in water. Application of this method to potassium acetate solution in glacial acetic acid gave E_m-values which disagreed significantly (0.1 V or more) with E_z as determined by the minimum in the differential capacity–potential curve[5] (adsorption could also be invoked to account for the discrepancy or part of it).

Equation (1) suggests a method for the extrapolation of E_m back to E_z. Thus, a plot of E_m *vs.* $(l/m)^{\frac{1}{2}}$ should yield E_z as intercept for $(l/m)^{\frac{1}{2}} = 0$. This relationship seems to be obeyed (Fig. 1) for an essentially air-saturated solution. However, this procedure is not particularly recommended unless the hydrodynamic conditions justify the application of eqn. (1). Moreover, the range of l/m over which a SME operates properly is rather limited, and extrapolation is uncertain.

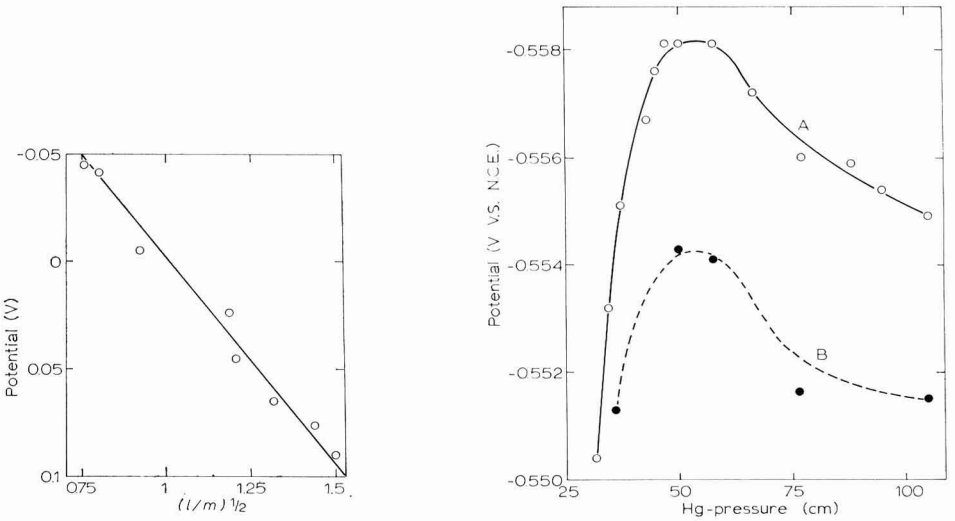

Fig. 1. Potential at open circuit *vs.* $(l/m)^{\frac{1}{2}}$ for air-saturated 1.014 *M* $HClO_4$. Potential referred to H_2-electrode at 1 atm. in soln. Extrapolation to $(l/m)^{\frac{1}{2}} = 0$, yields $E = -0.18$ V in this scale, *i.e.*, -0.43 V *vs.* SCE (not too far off for *extremely poor* conditions).

Fig. 2. Potential at open circuit *vs.* mercury pressure for 1 *M* KNO_3 + 0.1 *M* KCl: (A), after de-aeration; (B), after introduction of oxygen trace following de-aeration. The value of E_z thus obtained was to be used in an analysis of SLUYTERS' data[6] on this electrolyte mixture. This accounts for the selection of this solution in this work.

Some caution is also in order in the application of GRAHAME's recommendation to regard as valid, values of E_z corresponding to the plateau in a plot of potential *vs.* mercury-pressure. A maximum in the curve, rather than a plateau, may indeed be observed (Fig. 2). The shape of the curve in Fig. 2 can be explained tentatively by assuming the proper variations of l and m as the pressure increases. Even when a plateau is observed, one cannot assume with certainty, as GRAHAME suggested, that $E_m = E_z$. A constant error may well prevail.

In conclusion, the only way errors in values of E_z determined by this method can be prevented, seems to be the complete removal of reducible or oxidizable impurities. The error resulting from a spurious faradaic process can be roughly estimated by means of eqn. (1) provided the bulk concentration of impurity is known (*cf.* above reservation). This concentration could be determined *in situ* by means of a coulostatic method with a hanging mercury drop[4].

Acknowledgement

This work was supported by the National Science Foundation. The experimental part of this work was done at Louisiana State University, also with support from the National Science Foundation. One of the authors (G.T.) is indebted to the Consiglio Nazionale delle Ricerche for a travel grant.

Department of Chemistry,
New York University,
New York, N.Y. 10003 (U.S.A.)

P. DELAHAY
G. TESSARI*

1 D. C. GRAHAME, R. P. LARSEN AND M. A. POTH, *J. Am. Chem. Soc.*, 71 (1949) 2978.
2 H. A. LAITINEN, T. HIGUCHI AND H. CZUHA, *ibid.*, 70 (1948) 561.
3 P. DELAHAY, *J. Electroanal. Chem.*, 10 (1965) 1.
4 F. R. SMITH AND P. DELAHAY, *ibid.*, 10 (1965) 435.
5 P. DELAHAY AND H. LAUER, unpublished investigation.
6 M. SLUYTERS-REHBACH, B. TIMMER AND J. H. SLUYTERS, *Rec. Trav. Chim.*, 82 (1963) 553.

Received May 29th, 1967.

* Present address: Istituto di Chimica Analitica della Universita di Bari, Via Amendola, 173, Bari, Italy.

Electrochemical reduction of perrhenate in sulfuric acid solution

Although the products of Re(VII) reduction in acid solutions have been thoroughly examined in recent years, the results of the many investigations present a confusing picture[1–6]. The assignment of valence changes for the first polarographic wave in acid media, for instance, ranges from one to seven electrons depending on the investigator consulted. It has been generally conceded, however, that this wave corresponds to the three-electron reduction to the Re(IV) state[4]. Attempts to verify valence changes by coulometric measurements on mercury pool electrodes have met with small success owing to the apparent ability of a rhenium species to depolarize the hydrogen evolution reaction on mercury[2]. This communication presents some observations on the reduction of perrhenate in sulfuric acid solution on platinum and mercury electrodes and attempts to eliminate some of the past difficulty in interpreting the nature of the first reduction wave.

Materials and apparatus

Re(VII) was obtained as high purity rhenium heptoxide* and used without further purification. A standard sulfuric acid solution of 3.7 M (30 wt.%) was

* From Professor Melaven, University of Tennessee, Knoxville 16, Tenn.

prepared from reagent-grade concentrated H_2SO_4 and deionized water of conductivity $<10^{-6}$ Ω^{-1} cm^{-1}. Potentiostatic measurements were made using a Duffers Model 600 potentiostat with current–time traces recorded on an Esterline-Angus graphic ammeter with appropriate shunt. Cell voltages were measured with respect to saturated calomel electrodes (SCE). Luggin capillaries containing 3.7 *M* H_2SO_4 were used to avoid chloride contamination of the solutions. Owing to the significant liquid junction potential, the measured value of the SCE *vs.* a hydrogen electrode in the same 3.7 *M* H_2SO_4 solution is 0.194 V at 25°.

Chronopotentiometric transients were obtained using a manually pulsed constant current obtained from a 30-V regulated d.c. supply and a high series resistance. The transients were displayed on a Tektronix 545-A oscilloscope with Type-D plug-in preamplifier and photographed with a Dumont 453 A Polaroid attachment. A 0.25-cm^2 platinized-platinum microelectrode was used for the chronopotentiometry. Other studies were carried out with a platinized-platinum basket electrode or a purified mercury pool. All experiments were conducted at $25\pm1°$.

Reduction on platinum

Initial observations on a platinum-black electrode in 0.025 *M* Re_2O_7 in 3.7 *M* H_2SO_4 indicated the presence of a small ill-defined reduction wave beginning at about +0.2 V *vs.* SCE. Potentiostatic reduction at the foot of this wave at about 0.0 V (SCE) produced a brown-black cathode deposit in addition to the formation of an opaque colloidal suspension of the brown-black material in the acid solution. This observation agrees with that of WEHNER AND HINDMAN[6] who suggested a +4 valence for the material formed. An electrolysis cell was therefore assembled with a potentiostatted platinum basket cathode to determine the valence change in this process. Reduction was carried out at 0.0 V (SCE) at 25° under a helium atmosphere, and the full current–time trace integrated from the recorder. The valence of the species produced by this technique was found to be 3.98, in agreement with WEHNER's observations. It should be noted that the colloidal suspension of brown-black material formed is very finely dispersed and shows no appreciable separation on centrifugation.

During the course of this electrolysis a reference platinum microelectrode was suspended in the solution. This electrode assumed a rest potential of about +0.2 V (SCE) during the electrolysis. From time to time, anodic chronopotentiograms were recorded from this electrode. These chronopotentiograms showed a well defined anodic wave with quarter wave potential, $E_{\frac{1}{4}} \simeq +0.4$ V. A typical example is shown in Fig. 1. Subsequent electrochemical oxidation on the platinum basket at potentials

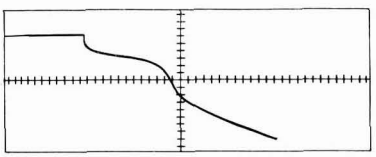

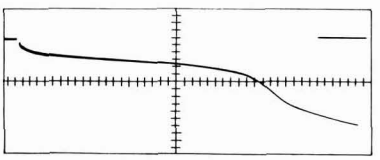

Fig. 1. Anodic chronopotentiogram on reference platinized-platinum microelectrode during reduction of perrhenate on auxiliary platinum basket. Top 0.0 V SCE, 60 mV/div. (+ = downward) 0.2 sec/div., left to right, 40 mA/cm^2, 25°.

Fig. 2. Anodic chronopotentiogram on reference microelectrode in violet-red rhenium solution after reduction on mercury. Same conditions as Fig. 1, except 0.1 sec/div., left to right.

TABLE 1

Expt. No.	*Half-wave slope, (mV/unit t/τ)*	*Calcd. αn*
(Fig. 1)	118	0.53
II	135	0.46
III	127	0.49
IV	111	0.56
V	132	0.47
		Av. 0.50

corresponding to this wave (+0.4–0.7 V) under a helium atmosphere indicated that the solution returned to its original colorless condition. The excellent definition of these traces prompted their analysis in terms of the expected potential–time dependence for an irreversible diffusion controlled process. It can be shown[7] that for such a wave:

$$\left(\frac{\partial \Delta E}{\partial t/\tau}\right)_{t=\tau/2} = 2.41 \frac{RT}{\alpha n F}$$

where τ is the transition time and all other symbols have their usual significance. Analysis of five such transients is shown in Table 1, with the values for the trace in Fig. 1 included. The average value of $\alpha n = 0.50$ derived from these slopes, is in agreement with that for a one-electron charge-transfer limited process.

Reduction on mercury

An electrolysis arrangement similar to that already described was assembled with substitution of a mercury pool (~ 25 cm^2) for the platinum basket cathode. It was found that, after a few moments of electrolysis at potentials negative to SCE, the primary cathodic process was evolution of hydrogen gas commencing at about -0.3 V (in the absence of Re_2O_7, the hydrogen evolution potential is > -2.0 V SCE). This catalytic enhancement of the hydrogen evolution is apparently a relatively efficient process since currents of about 1 A could be sustained indefinitely at -0.8 V. Continued electrolysis at about -0.3 V indicated that the hydrogen evolution process was less than 100% efficient, however, and was accompanied by slow formation of a violet-red species in solution. The colored species was first observed at the electrode surface and is not believed to arise from reduction of perrhenate in solution by dissolved hydrogen gas. Overnight electrolysis produced an intensely colored solution (violet-red) with no indication of the black-brown precipitated material found in electrolysis on platinum.

A reference platinum microelectrode placed in this solution, however, showed a rest potential essentially equal to that found in the platinum electrolysis system where a valence change of three was found. Moreover, anodic chronopotentiograms taken on this electrode (which was never moved to a potential negative to its rest potential) indicated an anodic wave identical with that found in the platinum electrolysis system as shown in Fig. 2 (note that the time base is different from that in Fig. 1). It was concluded on this evidence, that the brown-black suspensions and the violet-red solutions contained the same electroactive rhenium species, and that the apparent differences were caused by a chemical disproportionation during the electrolysis on platinum electrodes.

Discussion

While the combined data on mercury and platinum indicate the existence of a disproportionation reaction in the system, the valence of the electroactive species (V or VI) is not definitively shown. The observation of a one-electron charge-transfer slope suggests the electroactive species to be Re(VI). This observation is supported by the known disproportionation of solid ReO_3 to the (IV)- and (VII)-states[8] (further evidence for an initial univalent change has been presented in a previous paper on perrhenate reduction under capillary flow conditions[9]). The observed differences in initial reduction on platinum and mercury can then be explained by the reaction

$$3\ \mathrm{Re(VI)} \leftrightarrows \mathrm{Re(IV)} + 2\ \mathrm{Re(VII)}$$

to produce the insoluble dioxide or equivalent acid form in equilibrium with Re(VI). This reaction is apparently catalyzed by the platinum surface and not by the mercury surface, and proceeds readily on platinum at ambient temperature. This disproportionation undoubtedly can explain the wide variety of observed color variations. The expected high activation energy for the chemical process can likewise be expected to produce an indicated valence change on polarographic reduction anywhere between one and three electrons, depending on the temperature and electrode material. Thus, on an electrode and at a temperature that allows rapid equilibration of the chemical reaction, the full three-electron change will be evidenced. As catalytic activity for the disproportionation decreases, the observed "*n*"-value will likewise decrease. In an analogous manner, since the Re(IV) represents a reservoir of electroactive Re(VI), a treatment of the anodic transition time data in terms of diffusion considerations for Re(VI) is not meaningful.

Acknowledgements

This work was made possible by the support of the Advanced Research Projects Agency under Order No. 247 through the U.S. Army Electronics Laboratories (Contract No. DA 36-039 SC-89156). Permission to publish is gratefully acknowledged. The author wishes to thank H. E. FREW for carrying out much of the experimental work.

Government Research Laboratory, J. A. SHROPSHIRE
Esso Research and Engineering Company,
Linden, New Jersey (U.S.A.)

1 J. J. LINGANE, *J. Am. Chem. Soc.*, 64 (1942) 1001, 1005, 2182.
2 C. L. RULFS AND P. J. ELVING, *J. Am. Chem. Soc.*, 73 (1951) 3284, 3287.
3 J. P. KING AND J. W. COBBLE, *J. Am. Chem. Soc.*, 79 (1957) 1559.
4 I. M. KOLTHOFF AND J. J. LINGANE, *Polarography*, Vol. 2, Interscience Publishers Inc., New York, 2nd ed., 1952, p. 472.
5 J. C. HINDMAN AND P. WEHNER, *J. Am. Chem. Soc.*, 75 (1953) 2869.
6 P. WEHNER AND J. C. HINDMAN, *J. Am. Chem. Soc.*, 75 (1953) 2873.
7 P. DELAHAY, *New Instrumental Methods in Electrochemistry*, Interscience Publishers Inc., New York, 1954, p. 179.
8 N. V. SIDGWICK, *Chemical Elements and Their Compounds*, Vol. II, Oxford University Press, London, 1950, p. 1300.
9 J. A. SHROPSHIRE, *J. Electroanal. Chem.*, 9 (1965) 90.

Received March 15th, 1967

Polarography with controlled current density or chronopotentiometry with current density sweep at a dropping mercury electrode

From its inception, polarographic procedure has consisted of an essentially discontinuous, but in practice continuous, change of potential of a dropping mercury electrode and the measurement of the corresponding current.

In the fifties, the reverse procedure was tried[1,2]. This was followed by criticism[3] and more detailed exposition[4,5]. The further lack of interest may be ascribed to a serious drawback inherent in the proposed method, *viz.* the high current density during the first stage of drop life. This results in the starting of a secondary electrolysis process at a more negative electrode potential followed by a reverse reaction in the case of rapid (reversible) systems, because of the increase of electrode potential. The interpretation and quantitative evaluation of the graph suffer from this secondary effect.

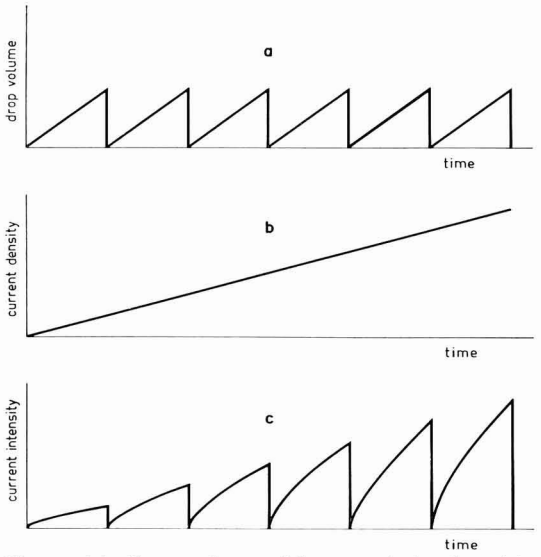

Fig. 1. (a), Drop volume; (b), current density; (c), current intensity as functions of time in arbitrary units (schematized).

The use of a circuit with controlled current *density* overcomes this difficulty. Automation as in normal polarography brings about a slowly increasing current density in such a way that during drop life it may be considered as constant. The impressed current *intensity* requires a special form and synchronization with the drop fall by means of a drop-life timer (Fig. 1).

The procedure may be considered essentially as chronopotentiometry at a mercury drop expanding at the normal rate, an idea not yet elaborated in the literature but only perhaps suggested[6]. The special feature lies in the application of a slow current density sweep.

When the apparatus has just been started, the transition time is too long to be contained within the drop life, and consequently only a small part of the chronopotentiogram is covered by the recorder. The increasing current density involves a

lowering of the transition time and a moment comes at which drop time and transition time coincide.

From this time on, the electrode potential undergoes a considerable shift in the negative direction during the last period of the drop life. This indicates that a second process (reduction of a second component or decomposition of the supporting electrolyte) starts during this period.

In contrast to the constant current intensity method, where the left branch of the envelope of the recorded diagram resembles the classical polarogram, here it is the *right* branch (Fig. 2).

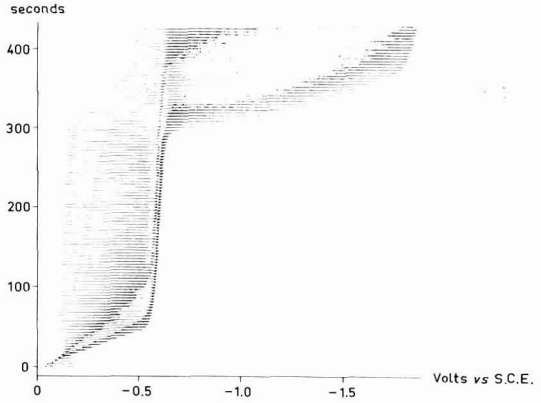

Fig. 2. Polarogram for a $5 \cdot 10^{-4}$ *M* Cd^{2+} soln. in 0.1 *M* KCl.

By analogy with the term "limiting current" in ordinary polarography, "limiting time" may be used for the moment when a considerable change of the course of the envelope is observed. It is also possible to apply the same construction for the determination of its value. The reproducibility appears to be very good.

The results obtained thus far indicate that the limiting current is proportional to the concentration (this holds also for a second component), to the two-thirds power of the head of mercury, and to the one-sixth power of the drop-time. The limiting time is inversely proportional to the gradient of the current density sweep.

Compared with classical polarography, this procedure allows the ohmic voltage drop in the circuit to be more easily eliminated. The apparently additional advantage of the absence of a maximum in the time *vs.* potential curve loses much of its interest because the value of the limiting time is strongly affected by the absence of a capillary-active substance. This is in conformity with the swirling around the mercury drop observed in the constant intensity method[3].

It will be possible to reduce, by electronic means, the recorded diagram to the neighbourhood of the envelope and thus to reduce the paper consumption.

It is hoped in the future to analyse the theoretical basis of the proposed method and give more detailed results.

Laboratory of Analytical Chemistry,
Technological University,
Delft (Netherlands)

H. L. KIES

1 M. ISHIBASHI AND T. FUJINAGA, *Anal. Chim. Acta*, 18 (1958) 112.
2 M. SENDA, T. KAMBARA AND Y. TAKEMORI, *J. Phys. Chem.*, 61 (1957) 965.
3 I. M. KOLTHOFF AND Y. OKINAKA, *J. Am. Chem. Soc.*, 80 (1958) 4452.
4 T. FUJINAGA, *Progress in Polarography*, Vol. 1, edited by P. ZUMAN AND I. M. KOLTHOFF, Interscience Publishers Inc., New York, 1962, p. 201.
5 T. FUJINAGA AND K. IZUTSU, *J. Electroanal. Chem.*, 4 (1962) 287.
6 R. W. MURRAY, *Anal. Chem.*, 35 (1963) 1785.

Received August 9th, 1967

BOOK REVIEWS

Transactions of the Third International Vacuum Congress, Stuttgart, Germany, 1965, Vol. 2, Parts I, II & III, edited by H. ADAM, Pergamon Press, Oxford, 1967, xxx + 776 pages, £20.

These 3 handsome books, totalling 800 pages and 3.7 kg weight contain the 122 papers that were presented at the 3rd International Vacuum Congress held in Stuttgart, Germany, in June 1965. They constitute Volume 2; Volume 1, containing the plenary lectures, was published earlier (reviewed in *J. Electroanal. Chem.*, 14 (1967) 371). The Congress attracted 750 participants and the immediate impression one gains (apart from the explosive growth of science, to which we are now attuned) is that vacuum science and technology has come to reach into a surprising number of subjects. Only a few years ago a vacuum system would mean that basic surface phenomena were being investigated in the absence of most of the air. Now we are sputtering, gettering, cryopumping and measuring routinely to the 10^{-10} torr range; we are studying gas flow forms and vacuum metallurgy, producing microcircuits and testing space vehicles.

At a world forum of this nature one might reasonably expect a cross-section of world effort. Certainly, a nice balance is struck between industry on the one hand and government and university laboratories on the other, and 19 countries are ostensibly represented. There are, however, disappointments. Only one Russian laboratory is represented and there is still nothing from China, where a sophisticated vacuum science and technology exists (when will they burst upon us?). Again, there are 31 papers from the United States, but the General Electric Research Laboratory with its continued eminence from LANGMUIR and DUSHMAN to the present, has made no contribution; I.B.M. and Edwards High Vacuum each have 6. The shadow of Professor ALPERT (the Bayard-Alpert gauge, the first ultrahigh vacuum tap) rightly falls across many of the pages but his active laboratory at the University of Illinois is only responsible for one paper *via* Spain. The United States and Germany (host country) together account for exactly half of all the papers. The official languages were English, French and German but English is the popular choice—70 of the papers, including 3 from Germany, are in English. Only 11 are in French.

Every reviewer of the publication of a conference must be aware of having seen something like some of it somewhere else. Indeed, previous or future details are often disclosed, and in this way science develops, but the fact remains that the best conferences are also the unique ones. Judged on this basis, the Vacuum Congress presents a substantial body of new material. It would be unfair to pick out exceptions; suffice it to say that readers of *Vacuum* and the *Journal of Vacuum Science and Technology* will not be surprised by a small number of the contributions, and may even recognise certain blocks.

Three highlights have been picked out. Electrochemists will be especially interested in E. KANSKY's electrochemical vacuum gauge (pp. 535–541). A logarithmic indication of pressure is taken from the electromotive force of a galvanic cell in which one reaction component is a gas and the electrolyte is a vacuum-tight membrane of "special glass". Partial-pressure measurements for alkali-metal vapours covering the range 10^{2}–10^{-20} torr can be made by this novel method. E. W. MÜLLER and his co-workers have collected together a set of 8 magnificent field ion micrographs for iron, nickel, cobalt and niobium (pp. 431–439). These pictures, which show atomic detail, were made possible by lowering both the shaping and ionisation fields through the presence of a partial pressure of hydrogen. With laser welding upon the scene, it is opportune to have electron beam welding *in air* reported (W. DIETRICH, pp. 595–600). The beam reaches the atmosphere through chambers which are separately maintained at intermediate pressures, and it emerges as a diverging jet which terminates in a blue ball of ionised air. Weld depth-to-width ratios of 6:1 are reported for a 3-kW, 160-kV beam.

Relatively little of the conference was devoted to ultrahigh vacuum gauges. There does not yet seem to be a general awareness that readings from presently available gauges are in considerable error at 10^{-13} torr; gauges have not kept pace with the capabilities of systems in the last few years. This is likely to be remedied at the 1968 Congress.

Papers have been split into 13 sessions although 4 of the session titles are repeated. Apart from the listing of the entire collection in this way in each book, there is neither an author nor a subject index—one has to delve despite the £20 cost. A feature of the production is the way each paper starts on a new leaf (easy reprints?). This leads to one-seventh of the book as unused glossy paper, 75 pages that are totally blank. To summarize, the books are beautiful, they provide a central depository of current information, but accessibility should have been greater.

DEREK F. KLEMPERER, Department of Physical Chemistry, University of Bristol

Progress in Nuclear Energy, Series IX. Analytical Chemistry, Vol. 7, edited by H. A. ELION AND D. C. STEWART, Pergamon Press, Oxford, 1966, 288 pages, 90s.

This volume comprises five chapters devoted to a range of analytical techniques which either have or could have application in the chemistry of nuclear energy production. The subjects and style of the contributions differ to an extent that makes any collective observations valueless.

Electron diffraction techniques and their applications to the study of surface structure (R. K. HART, 18 pages) is a brief introduction to the use of electron diffraction methods from 100 eV to 1200 keV. The potentialities of these methods are reviewed, and the application of electron microscopes in the range 50–100 keV is presented in some detail.

Liquid scintillator solutions in nuclear physics and nuclear chemistry (D. L. HORROCKS, 88 pages) is a comprehensive review of the mechanism of scintillation, the optical design of containers, and the application of scintillation counting methods to different ionising radiations. Photomultipliers are considered very briefly, but their associated electronics have been omitted.

In-line analytical instrumentation of nuclear fuel reprocessing plants (C. R. MCGOWAN AND J. K. FOREMAN, 65 pages) presents, very briefly, accounts of analytical methods that have found application or have been proposed for the control of plant operations without interruption. Methods depending upon radiation monitoring have been excluded. Clearly, an account of polarography in four pages or of oxidation–reduction potentiometry in a further four, will be of limited interest to an electrochemist, but the article indicates the ingenious way in which accepted analytical methods have been adapted to the requirements of automation.

A table of coefficients for the microprobe analyst (R. D. DEWEY; with tables of X-ray data prepared by R. D. DEWEY, R. S. MAPES AND T. W. REYNOLDS, 65 pages) gives the details of a method for calculating the results, which combines the corrections for mass absorption, fluorescent enhancement and electronic (alpha) functions into a single function (f_δ). Tables are given for f_δ for the elements 1–92 for the common analytical K- and L-lines from $\lambda = 17.6$–0.127, and ancillary tables for $g_1(x)$, $g_2(x)$, computed wavelength and interference. This contribution is for the practitioner alone, who will find no inconvenience from the scant reference to units, but who may disapprove of finding every table in two halves on obverse and reverse sides of the paper, a situation which the publishers might have remedied by using the blank page 178.

The ion-microprobe mass spectrometer (A. E. BARRINGTON, R. F. K. HERZOG AND W. P. POSCHENRIEDER, 30 pages) is an introductory article to a relatively new development in mass-spectrometry. The method of stripping material from solid surfaces, monolayer by monolayer and ionising it for mass-spectrometric analysis, using a 10-kV beam of inert gas ions, is described in detail and its potentialities are compared with such techniques as X-ray and electron diffraction, and X-ray fluorescence.

The book is well-presented and adequate author and subject indexes have been provided.

A. COUPER, University of Bristol

International Series of Monographs in Electromagnetic Waves, Vol. 12, *The Plane Wave Spectrum Representation of Electromagnetic Fields*, by P. C. CLEMMOW, Pergamon Press, London, 1966, vii+185 pages, 50s.

This book explains how general electromagnetic fields can be represented by the super-position of plane waves, and illustrates how this representation can be used in treating problems in the classical theories of radiation, diffraction and propagation. Its aim is to "furnish the student of electromagnetic theory with a useful technical tool and a comparatively compact account of some interesting aspects of his discipline". As this implies, it is a book for the specialist in electromagnetic theory.

The applications include diffraction by a plane screen, propagation over plane surfaces (*e.g.*, radio propagation over a homogeneous earth) and the field of a moving charge. Most of the book deals only with isotropic media, but anisotropic media are discussed briefly in a final chapter.

T. H. K. BARRON, Department of Theoretical Chemistry, University of Bristol.

ERRATA

B. EPSTEIN AND T. KUWANA, Electrooxidation of phthalhydrazides, *J. Electroanal. Chem.*, 15 (1967) 389–397.

The last reaction on p. 395 should read: (b) $R + O_1 \rightarrow Z$ (non-electroactive).

S. ROFFIA AND E. VIANELLO, Potential-sweep voltammetry—Adsorption of chloranilic acid on a mercury electrode, *J. Electroanal. Chem.*, 15 (1967) 405–413. Table 1, the headings of the 2nd and 3rd columns should read:

$$\left(\frac{\partial Q_{tot}}{\partial v^{-\frac{1}{2}}}\right) \text{ and } \left(\frac{\partial Q_{tot}}{\partial v^{-\frac{1}{2}}}\right)_c \left(\frac{1}{C}\right) \quad (\cdot 10^{-4})$$

CALENDAR OF FUTURE SCIENTIFIC MEETINGS

Date	*Place*	*Subject*	*Secretary*
19–21 February, 1968	Department of Chemistry, City University, St. John Street London, E.C. 1	Materials Science Club: Materials for fuel celss and high-energy batteries (electro-catalysts, electrode structure, current collection, economic factors)	Dr. A. A. C. TSEUNG at the University

Vol. 16 No. 2 JOURNAL OF ELECTROANALYTICAL CHEMISTRY AND INTERFACIAL ELECTROCHEMISTRY FEBRUARY 1968

CONTENTS

Elsevier Titles in Chemistry

INORGANIC CHEMISTRY

A Guide to Advanced Study

Third, completely revised edition

by **R. B. Heslop** and **P. L. Robinson**

6×9″, viii+774 pages, 155 tables, 400 illus., 227 lit. refs., 1967, Dfl. 32.50, US$11.00

Contents: Modern inorganic chemistry. The atomic nucleus: genesis of the elements. Radiochemistry. Electronic structures of atoms. The periodic table. Valency; nature and classification of chemical bonding. Structure and shape of molecules. Bonding and structure in compounds of non-transition elements. Bonding in transition-metal complexes. The solid state. Oxidation-reduction: redox reactions. Acids and bases. Hydrogen. The hydrides. The noble gases. The alkali metals. Beryllium, magnesium and the alkaline earth metals. Boron and aluminium. Gallium, indium and thallium. Carbon and silicon. Organometallic compounds. Germanium, tin and lead. Nitrogen and phosphorus. Arsenic, antimony and bismuth. Oxygen, sulphur, selenium, tellurium and polonium. The oxides. Peroxides and peroxo-compounds. The halogens. The halides and pseudohalides. The transition metals. Complex or co-ordination compounds and ions. Substitution reactions of metal complexes. The lanthanides, scandium and yttrium. The actinides. Titanium, zirconium and hafnium. Vanadium, niobium and tantalum. Chromium, molybdenum and tungsten. Manganese, technetium and rhenium. Iron, cobalt and nickel. The platinum metals. Copper, silver and gold. Zinc, cadmium and mercury. Index.

INTRODUCTION TO THE ATOMIC NUCLEUS

Volume 3 in a collection of monographs on "*Topics in Inorganic and General Chemistry*" edited by P. L. Robinson

by **J. G. Cuninghame**

5½×8½, xi+220 pages, 3 tables, 58 illus., 170 lit. refs., 1964, Dfl. 15.00, US$4.75

Contents: Historical introduction. General definitions and properties. Nuclear forces. Stable nuclides. Radioactivity. Nuclear models. Nuclear reactions. Fission. Alpha-decay. Beta-decay. Gamma-emission. Interaction of particles and rays with matter. Index.

INTRODUCTION TO NUCLEAR CHEMISTRY

by **D. J. Carswell**

5½×8½″, ix+279 pages, 23 tables, 69 illus., 1967, Dfl. 32.50, US$11.00

Contents: The development of nuclear chemistry. Fundamental particles and nuclear structure. Nuclear reactions and radioactivity. Properties of nuclear radiations. The detection and measurement of nuclear radiation. Nuclear instrumentation. Radiation chemistry. Isotope measurement and separation methods. Charged particle accelerators, neutron sources, production and properties of the actinide elements. Uses of isotopes. Experimental nuclear chemistry. Index.

RADIOCHEMICAL SURVEY OF THE ELEMENTS

Principal Characteristics and Applications of the Elements and their Isotopes

by **M. Haïssinsky** and **J.-P. Adloff**

6×9″, ix+177 pages, 1965, Dfl. 32.50, US$12.00

Contents: Introduction. The elements in alphabetical order. Element 102. Element 104.

THE STRUCTURE OF INORGANIC RADICALS

An Application of Electron Spin Resonance to the Study of Molecular Structure

by **P. W. Atkins** and **M. C. R. Symons**

6×9″, x+280 pages, 57 tables, 74 illus., 357 lit. refs., 1967, Dfl. 60.00, US$21.75

Contents: Introduction. An introduction to electron spin resonance. Formation and trapping of radicals. Trapped and solvated electrons. Atoms and monatomic ions. Diatomic radicals. Triatomic radicals. Tetra-atomic radicals. Penta-atomic radicals. Summary and conclusions.
Appendices: The language of group theory. The spin hamiltonian. Calculation of *g*-values. Determination of spin-density distribution and bond angles. Analysis of electron spin resonance spectra. Index.

ELSEVIER PUBLISHING COMPANY

P. O. BOX 211, JAN VAN GALENSTRAAT 335, AMSTERDAM, THE NETHERLANDS

341 E